Inhaled Particles

INTERFACE SCIENCE AND TECHNOLOGY
Series Editor: ARTHUR HUBBARD

In this series:

Inhaled Particles

Chiu-sen Wang

Professor Emeritus
College of Public Health
National Taiwan University
Taipei, Taiwan

For Aidan with love

This page is intentionally left blank

CONTENTS

Preface

Smoke exposure has been a health hazard ever since humans began to use fire. Particles discovered on cave ceilings attest to the smokiness of ancient cave environments. It is likely that cavemen inhaled a considerable amount of smoke particles when fire was used for cooking. Although not as old as smoke exposure, aerosol therapy was described in Ayurvedic medicine over four millennia ago. Despite these early experiences, scientific inquiries on inhaled particles came much later. It was not until 1700 when the first clear description about fatal dust diseases was given in Ramazzini's ground-breaking book on occupational medicine. And all our understanding of quantitative relationships between dust exposure and biological responses is derived from studies undertaken only in the last century. During past decades, increasing applications in health risk assessment, diagnosis, and therapy has led to intense scientific interest in inhaled particles.

Particle transport in the respiratory tract represents a problem of multiphase flow at the interface between physical and biological systems. The respiratory tract consists of three distinct regions: the extrathoracic airways, tracheobronchial tree, and alveolar region. These three regions differ in morphology, airflow pattern, deposition characteristics, and clearance pathway. The ability to predict local dose is of central importance in health risk assessment of inhaled toxic particles and efficacy evaluation of therapeutic aerosols. Much progress has been made in past decades, but many basic problems of great importance remain unsolved in this field.

Intensive studies in recent decades have generated a large number of research papers and books on this subject. However, it appears that there is no specialized book that integrates all is known about inhaled particles in a unified treatment. This book represents an attempt to fill this gap. It aims to provide a scientific framework essential to a reasonable understanding of inhaled particles. The emphasis is placed on demonstrating the key roles of lung morphology on airflow and particle transport as well as identifying physical and biological factors that influence deposition. Special attention is paid to maintaining consistency of treatment and a balance between theoretical modeling and experimental measurements.

The book covers all important aspects of inhaled particles including inhalability, aerosol dispersion, particle deposition, and clearance. It reviews concisely the basic background of lung morphology, respiratory physiology, aerodynamics, and aerosol science pertinent to the subject. Essential aspects of health effects and applications are also included. However, the focus has been placed on deposition, reflecting my own research interest.

One of the goals I have set for the book is to discuss the important concepts and methods employed in the field, rather than cover all the results of previous studies reported in the literature. My own view of the development of the field has therefore been a major factor in selecting the topics and materials. It is inevitable that the selection is biased. I wish to acknowledge the contributions of all researchers in this field and offer my apologies to those whose important contributions have been omitted.

The materials in this book are suitable for a graduate course in environmental health science, occupational hygiene, health physics, and biomedical engineering. It has the primary objective of providing newcomers with terminology and methodology in this field, with the hope that the readers will acquire sufficient background to better understand the current research papers and embark on a research endeavor of their own. The problems listed at the end of each chapter are intended for those readers with an inquiring mind who wish to apply the principles discussed in the text to different types of situations. Furthermore, this book attempts to clarify some incorrect views, provide a source of updated materials, and point out some future directions. It should be of use to practitioners and research scientists as well.

Preparation of this book proceeded in three stages during the past decade. The first draft evolved from the class notes I used in teaching a one-semester graduate course on inhaled particles in the College of Public Health, National Taiwan University. The writing began in 1994 but was interrupted by administrative duties when I served as Chairman of Public Health Department and Dean of the College of Public Health. The second stage of writing was carried out during my sabbatical leave in 2001. I began the final revision after Arthur Hubbard invited me to contribute this book to the series Interface Science and Technology, which he has been editing. I am grateful to him for giving me this opportunity. I wish to thank Sheldon K. Friedlander, Morton Lippmann, and James H. Vincent for their suggestions and encouragement when I began the final stage of revision. My thanks also go to Susan L. Wang for reviewing the whole text and providing me with valuable comments and suggestions, to Wan-ching Grace Chen for her assistance in organizing the materials when my writing began in 1994, and to Deling Liu, Kenneth K. Wang, and Kehsing Hwang for their help in preparing illustrations. Finally, I thank my wife Yoshiko for her unreserved support during these years.

Santa Monica, California   Chiu-sen Wang
August 2004

Glossary

Absorption (into bloodstreams): the process wherein a substance enters into bloodstreams, usually referring to absorption of a soluble substance that has dissolved from a deposited particle.

Acinus: a lung structural unit deriving from a single transitional bronchiole and comprising all the airways distal to it.

Aerodynamic diameter: the diameter of a standard density sphere that has the same settling velocity as the particle under consideration of whatever shape and density.

Aerosol: a suspension of liquid or solid particles in a gas.

Aerosol bolus: a bolus of aerosol that is usually inspired by a subject for study of dispersion and deposition of inhaled particles.

Aerosol diagnosis: identification of diseased conditions with aerosols.

Aerosol dispersion: the process wherein particles are spread out while they remain airborne.

Aerosol therapy: medication through inhalation of an aerosolized drug.

Airway: a passageway for air in the lungs.

Allergen: a substance capable of sensitizing tissue so that the tissue will respond with enhanced sensitivity when challenged by the same substance later.

Alveoli: air cells of the lungs that provide surfaces for gas exchange.

Anatomical dead space: volume of the respiratory tract in which no gas exchange occurs, excluding those alveoli that do not take part in gas exchange.

Antagonism: an interaction between two or more agents that results in a reduction in adverse effect of each agent.

Aspiration efficiency: fraction of ambient particles entering an inlet such as the nose or mouth.

Axial velocity: velocity in the axial direction.

Bifurcation: division of an airway into two branches.

Bifurcation plane: the plane containing a daughter branch and her parent tube in a bifurcation.

Boltzmann equilibrium charge distribution: the distribution of charges on particles when it has reached the equilibrium after exposure to bipolar ions.

Branching angle: the angle between the axes of a daughter branch and her parent tube in a bifurcation.

Breathing frequency: the number of breaths taken in a unit time.

Bronchi: larger airways in the tracheobronchial region.

Bronchioles: smaller airways in the tracheobronchial region.

Bronchitis: inflammation of the lining of bronchial airways

Bronchoconstriction: constriction in bronchial airways due to contraction of airway walls.

Bronchodilation: dilation of bronchial airways usually by a chemical spray.

Brownian diffusion: the net transport of particles by Brownian motion in the presence of a concentration gradient.

Brownian motion: random motion of particles due to bombardment by surrounding gas molecules.

Carcinogen: an agent that is capable of producing cancer.

Carina: a ridge-like structure formed by the bifurcation of an airway.

Ciliated cell: a type of cell having hair-like structure on its upper surface.

Clearance: the process by which deposited particles are removed from the respiratory tract.

Compartments-in-series model (for respiratory deposition): a deposition model that

considers the respiratory tract as a series of compartments.

Continuous model (for respiratory deposition): a deposition model that considers the respiratory tract as a continuous conduit of variable cross section.

Convective Brownian Diffusion: transport by Brownian diffusion taking place in flowing fluids.

Count median diameter (CMD): the particle diameter that divides, according to particle size, an aerosol into two portions of equal particle numbers.

Deposition: the process wherein an airborne particle during its transit or pause in an airway comes into contact with a wall surface and attaches there.

Deposition density: the number or mass of particles deposited over a unit surface area.

Deposition efficiency: the fraction of entering particles that have deposited in an airway segment.

Deposition flux: the rate of deposition per unit surface area.

Deposition fraction: the fraction of inhaled particles that have deposited in a respiratory region or the entire respiratory tract in a breath.

Deposition rate: the number or mass of particles deposited on a given surface area per unit time.

Deposition velocity: the ratio of deposition flux to the mainstream concentration.

Diffusion coefficient: the ratio of diffusion flux to concentration gradient.

Dissolution rate: the rate at which molecules of a solid enter into a liquid solution.

Dose-response relationship: the relationship between the dose an individual receives and the response to that dose.

Drag force: the resistance force experienced by a particle moving in a fluid.

Dry powder inhaler: a device for delivering therapeutic agents in the form of dry powder.

Dynamic shape factor: the ratio of the drag force on the particle under consideration to that on a sphere of equivalent volume diameter.

Electrostatic attraction: the attraction between two electric charges of opposite signs.

Emphysema: over-inflation of structures arising from a breakdown of alveolar walls.

Epiglottis: a plate of flexible cartilage that folds back to cover the glottis during swallowing.

Epithelium: a membranous cellular tissue that covers a surface or lines a tube in a body.

Equivalent diffusion diameter: diameter of a sphere having the same diffusion coefficient as the particle under consideration.

Equivalent volume diameter: diameter of a sphere having the same volume as the particle under consideration.

Esophagus: a muscular tube passing from the pharynx to the stomach.

Expiratory reserve volume (ERV): the maximum volume of air that can be exhaled from the functional residual capacity.

Extrathoracic region: region of the respiratory tract extending from the nose and mouth to the larynx.

Fibrogenic dust: particles that is capable of causing gradual scarring or fibrosis of the alveolar region.

Fibrosis: a condition characterized by increase of interstitial fibrous tissue.

Fick's first law of diffusion: a relationship first derived by Fick stating that the flux of a diffusing species is equal to the diffusion coefficient multiplied by the negative concentration gradient of the species.

Flow separation: detachment of the primary flow from the wall creating a "separated" region with slowly swirling flow.

Friction coefficient: the ratio of drag force to particle velocity.

Functional residual capacity (FRC): the volume of air in the lungs at end-exhalation of a

normal breath.

Gas exchange: the process by which inspired air supplies oxygen to the body and exhaled air transports carbon dioxide out of the body.

Geometric mean diameter: the exponential of the mean for a distribution of the logarithms of particle diameter. In a lognormally distributed aerosol, the geometric mean diameter is equal to the count median diameter.

Geometric standard deviation: the exponential of the standard deviation for a distribution of the logarithms of a variable such as particle diameter.

Gravitational settling velocity: velocity of a particle after the drag and gravitational force have reached an equilibrium.

Head airways region: region of the respiratory tract extending from the nose and mouth to the larynx.

Hot-wire anemometer: a device for determining gas velocity by measuring the change in electrical resistance of a heated wire.

Hygroscopic particle: a particle that is capable of absorbing moisture.

ICRP model: a mathematical model for deposition, retention and dosimetry of inhaled radioactive substances developed by the International Commission on Radiological Protection.

Image force: attractive force between a charge and the image charge it induces in a nearby surface.

Inertial deposition: deposition of a particle due to its inertia.

Inertial impaction: impaction of a particle onto a surface due to its inertia when the flow in which the particle is suspended makes a sudden turn.

Inhalable fraction: the fraction of ambient particles that can enter the nose or mouth.

Inhalable particulate mass (IPM): the mass fraction of ambient particles that can enter the nose or mouth.

Inspiratory capacity (IC): the maximum volume of air that can be inspired from the functional residual capacity.

Interception: the mechanism by which an aerosol particle is captured when it passes by a surface within a particle radius.

Interstitium: interstitial tissue.

Jet (flow): a stream of fluid discharged from a narrow opening.

Kelvin effect: increase in vapor pressure of a solvent in a droplet relative to that above a pianar surface.

Kinematic viscosity: the ratio of the viscosity to density of a fluid.

Knudsen number: mean free path of gas molecules divided by particle radius.

Laminar flow: the type of fluid flow characterized by streamlines that do not mix with each other.

Larynx: the part of airways that contains the vocal cords.

Lipophilicity: affinity for lipids.

Local deposition: deposition over a small surface area of airway walls.

Lognormal distribution: a form of distribution in which the distribution density is normally distributed with respect to the logarithms of a variable.

Lymphatic system: a part of the immune system consisting of lymph nodes and lymphatics (the small vessels that link the lymph nodes).

Macrophage: a wandering cell that is capable of engulfing particles or other materials.

Magnetic resonance imaging (MRI): a noninvasive imaging technique based on nuclear magnetic resonance of atoms in body tissues induced by the application of radio waves.

Mass median aerodynamic diameter (MMAD): the aerodynamic diameter that divides,

according to particle size, an aerosol into two portions of equal particle masses.

Mass median diameter (MMD): the particle diameter that divides, according to particle size, an aerosol into two portions of equal particle masses.

Mean free path of gas molecules: the average distance that a gas molecule travels between two successive collisions.

Mechanical mobility: the ratio between the velocity of a particle and the force producing that velocity. It is equal to the inverse of the Stokes friction coefficient.

Metal fume fever: a fever caused by inhalation of fumes from molten metals.

Metered-dose inhaler: a device for delivering exact doses of therapeutic agents with a metering valve.

Minute volume: the total volume of air inspired in one minute.

Molecular diffusion: the process by which fluid molecules move from a region of higher to one of lower concentration as a result of thermal motion.

Monodisperse aerosol: an aerosol in which all particles are of the same size.

Mouth inhalability: the fraction of ambient particles that can enter the mouth.

Mucociliary escalator: mucus flow that moves up tracheobronchial airways as a result of beating by underlying cilia.

Nasal augmenters: normal nose breathers.

Nasal septum: wall between the two nasal cavities.

Nasal turbinates: three scroll-like cartilaginous plates on the lateral walls in the main nasal cavity.

Nasal valve: the part of nasal airways located about 1.5 cm downstream of the nostrils.

Nasopharynx: the portion of the respiratory tract between anterior nares and epiglottis.

NCRP model: a mathematical model for deposition, retention and dosimetry of inhaled radioactive substances developed by the National Council on Radiation Protection and Measurements.

Nebulizer: an atomizer that generates droplets from a liquid kept in a small container.

Nose inhalability: the fraction of ambient particles that can enter the nose.

Orientation angle: the angle between the normal of the bifurcation plane of the tube under consideration and the normal of the bifurcation plane of the parent tube.

Particle Reynolds number: the Reynolds number based on particle diameter.

Péclet number: the ratio of convective mass transfer to diffusional mass transfer.

Phagocytosis: the process by which a cell engulfs a solid particle.

Pharynx: the part of airways between the nasal cavity and the larynx. It is also the passageway for food from the mouth to the esophagus.

Physiological dead space: volume of the respiratory tract in which no gas exchange occurs, including those alveoli that do not take part in gas exchange.

Poiseuille flow: laminar flow in a circular tube with a parabolic velocity profile.

Polydisperse aerosol: an aerosol in which particles have various sizes.

Pneumoconiosis: disease characterized by scars due to increase in interstitial fibrous tissue resulting from retention of certain types of mineral particles in the alveolar region.

Projected area diameter: diameter of a circle that has the same area as the projected area of the particle under consideration.

Pulmonary region: gas exchange region of the lungs.

Recirculation (flow): flow that recirculates in a small region.

Regional deposition: deposition in a single region of the respiratory tract.

Relaxation time: the time a particle takes to adjust its velocity when it is subject to a new set of forces.

Residual volume: the lung volume at the maximum expiratory level.

Respirable fraction: fraction of ambient particles that can reach the alveolar region.

Respiratory tract: the entire airway system extending from the nose and mouth to the pulmonary region.

Retention: the amount of deposited particles remaining in the respiratory tract.

Reynolds number: a dimensionless number related to the ratio of inertial to viscous forces in a fluid flow.

Schmidt number: the ratio of kinematic viscosity to diffusion coefficient.

Secondary flow: a small flow superimposed on the primary flow.

Sherwood number: the ratio of total mass transfer to diffusional mass transfer.

Slip correction factor: a correction to Stokes law to account for deviation from the assumption that the gas velocity is zero on the particle surface.

Stokes law: a relationship first derived by Stokes that describes the drag force on a sphere moving at a constant velocity relative to fluid.

Stokes number: a dimensionless number defined as the ratio of the stop distance of a particle to a characteristic length of the system under consideration.

Stop distance: the distance a particle continues to travel in the absence of external forces before coming to a stop by the resistance of air.

Synergism: the interaction of two or more agents that produces an adverse effect greater than the sum of the effects resulting from exposure to each agent separately.

Targeting (in aerosol therapy): delivering therapeutic agents to specific parts of the lungs.

Terminal settling velocity: the steady velocity acquired by a particle settling in the gravitational field.

Thermodynamic particle diameter: diameter of a sphere having the same diffusion coefficient as the particle under consideration.

Thoracic regions: the part of respiratory tract comprising the tracheobronchial and alveolar regions.

Tidal volume (TV): the volume of air inhaled and exhaled during a breath.

Total deposition: deposition in the entire respiratory tract.

Total lung capacity (TLC): the volume of air in the lungs at maximum inspiration.

Trachea: the part of airways between the larynx and main bronchi.

Tracheobronchial region: the part of airways extending from the trachea to terminal bronchioles.

Transition zone: the region between the outlet of the parent tube and the inlets of daughter branches in a bifurcation.

Turbulent flow: the type of fluid flow characterized by random eddy motion.

Typical path lung model: a lung model using a single typical pathway to represent the entire lungs or a lobe.

Ultrafine particles: particles smaller than 0.1 μm in diameter.

Vital capacity (VC): the maximum volume of air that can be exhaled from the lungs after maximum inspiration.

Womersley number: ratio of the magnitude of oscillatory disturbance in the boundary layer to the magnitude of the steady flow boundary layer.

Acronyms

ABD	Aerosol bolus dispersion
ACGIH	American Conference of Governmental Industrial Hygienists
ADAM	Aerosol-derived airway morphometry
COPD	Chronic obstructive pulmonary disease

ERV	Expiratory reserve volume
FRC	Functional residual capacity
IC	Inspiratory capacity
ICRP	International Commission on Radiological Protection
IPM	Inhalable particulate mass
IRV	Inspiratory reserve volume
NCRP	National Council on Radiation Protection and Measurements
PM	Particulate matter
PM_{10}	Particulate matter smaller than 10 μm in aerodynamic diameter
$PM_{2.5}$	Particulate matter smaller than 2.5 μm in aerodynamic diameter
ROS	Reactive oxygen species
RV	Residual volume
SARS	Severe acute respiratory syndrome
TGLD	Task Group on Lung Dynamics (an ICRP task group)
TLC	Total lung capacity
VC	Vital capacity

List of Principal Symbols

A	surface area or cross-sectional area
A_m	minimum cross-sectional area of nasal airways
B	particle mobility
$\mathbf{c}$	particle velocity resulting from the external force
C_c	slip correction factor
d_a	aerodynamic diameter
d_d	equivalent diffusion diameter
d_e	equivalent volume diameter
d_f	fiber diameter
d_{fg}	geometric mean of the fiber diameter distribution
d_g	geometric mean of the particle diameter distribution
d_p	particle diameter
d_p^*	Kelvin diameter
d_t	tube diameter
D	particle diffusion coefficient or molecular diffusion coefficient
D_e	effective axial diffusion coefficient
D_v	diffusion coefficient of water vapor molecules in air
Dn	Dean number
e	elementary charge
E	fractional deposition
E_a	fractional deposition in the alveolar region in one breath
E_{Ei}	fractional deposition in Compartment i during exhalation
$E_{Ei,i+1}$	fractional deposition in Compartment i during exhalation of the particles remaining airborne in Compartment $i+1$ at end inhalation
E_h	fractional deposition in the head airways region in one breath
E_i	fractional deposition in Compartment i in one breath
E_{Ii}	fractional deposition in Compartment i during inhalation
E_{nn}	total deposition fraction for nose-in nose-out breathing
E_{no}	total deposition fraction for nose-in mouth-out breathing
E_{on}	total deposition fraction for mouth-in nose-out breathing
E_{oo}	total deposition fraction for mouth-in mouth-out breathing
E_t	fractional deposition in the tracheobronchial region in one breath
f	Fanning friction factor or frequency of oscillation
f_e	enhancement factor for diffusional deposition in the NCRP model
f_n	fraction of particles carrying n units of elementary charge
$f(t)$	a time-dependent function representing the breathing pattern or fraction of deposited particles cleared per day
F	force
F_d	drag force

g	acceleration of gravity
H	latent heat of vaporization or width of aerosol bolus
H_{50C}	corrected half-width of aerosol bolus
H_{50E}	volumetric half-width of exhaled aerosol bolus
H_{50I}	volumetric half-width of inhaled aerosol bolus
I_n	nose inhalability
I_o	mouth inhalability
J_x	diffusion flux in the x-direction
k	Boltzmann constant
k_v	thermal conductivity of air
Kn	Knudsen number
l	length
l_e	entrance length for development of flow in a tube
l_f	fiber length
l_{fg}	geometric mean of the fiber length distribution
l_m	mean airway diameters in the tracheobronchial region or mean chord length in the alveolar region
l_t	tube length
L_d	deposition rate per unit length of airway
m	mass of a water vapor molecule
m_p	mass of particle
m_s	mass of the dissolved salt
M	molecular weight of water
M_s	molecular weight of the dissolved salt
n	particle number concentration or number of airways per generation
n^*	dimensionless number concentration of particles
n_i	number of ions each molecule of salt forms when it dissolves
n_0	initial or mainstream number concentration of particles
N_a	Avogadro's number
p	pressure
p_d	saturation vapor pressure of a droplet
p_s	saturation vapor pressure of water with a planar surface
p_∞	vapor pressure far away from a droplet
P	penetration
Pe	Péclet number
q	charge carried by a particle
q_c	threshold charge level for electrostatic deposition
Q	flow rate
r	radial coordinate
r_b	radius of bend
r_t	radius of tube
r_{12}	distance between two point charges

R	interception parameter or gas constant
R_a	fraction of particles recovered after a pause between inhalation and exhalation
R_0	curvature ratio of a curved tube
Re	flow Reynolds number
Re_p	particle Reynolds number
s	stop distance
S	dimensionless parameter for gravitational settling from laminar flow
S_f	average airway shape factor of the turbinate region
Stk	Stokes number
Stk_f	Stokes number for fibers moving in a bifurcation
Stk_n	Stokes number for particles moving in nasal airways
t	time
t^*	dimensionless time
t_h	duration of breath-holding or pause between inhalation and exhalation
T	absolute temperature
T_d	droplet temperature
T_∞	air temperature far away from a droplet
u	gas velocity
u_f	friction velocity
u_p	velocity of particle relative to gas velocity
u_x	axial flow velocity
u_0	axial flow velocity at the tube axis
$\mathbf{u}$	flow velocity vector
$\mathbf{u}^*$	dimensionless flow velocity vector
$\mathbf{u}_p$	particle velocity vector
$\mathbf{u}_p^*$	dimensionless particle velocity vector
U	average flow velocity in a tube
U_0	ambient air velocity
v_d	deposition velocity
v_e	electrical migration velocity
v_s	terminal settling velocity
v_0	initial velocity of particle
V	volume
$\tilde{V}_f$	the volume of tidal air that arrives in the final compartment
V_{FRC}	functional residual capacity
V_i	volume of Compartment i
V_L	lung volume
V_m	minute volume
V_p	volumetric lung depth

V_t	tidal volume
Wo	Womersley number
x,y,z	Cartesian coordinates
z	generation number
α_c	accommodation coefficient
α_E	fraction of air expired through the nose
α_{Ei}	a weighting factor depending on the residence time of particles in Compartment i during exhalation
α_I	fraction of air inspired through the nose
α_{Ii}	a weighting factor depending on the residence time of particles in Compartment i during inhalation
β	enhancement factor for diffusional deposition in the ICRP model
γ	surface tension of water
δ	thickness of boundary layer
ε_0	permittivity of a vacuum
η	deposition efficiency
η_a	deposition efficiency due to aerodynamic processes
η_d	deposition efficiency due to diffusional processes
η_e	enhanced deposition efficiency of a bifurcation due to convective Brownian diffusion
η_{Ei}	deposition efficiency of Compartment i during exhalation
η_{En}	deposition efficiency of nasal airways during exhalation
η_{Eno}	deposition efficiency of nasal and oral airways during exhalation
η_{Eo}	deposition efficiency of oral airways during exhalation
η_i	deposition efficiency due to inertial impaction
η_{Ii}	deposition efficiency of Compartment i during inhalation
η_{In}	deposition efficiency of nasal airways during inhalation
η_{Ino}	deposition efficiency of nasal and oral airways during inhalation
η_{Io}	deposition efficiency of oral airways during inhalation
η_{Id}	deposition efficiency due to convective Brownian diffusion
η_n	deposition efficiency of nasal airways during either inhalation or exhalation
η_o	deposition efficiency of oral airways during either inhalation or exhalation
η_s	deposition efficiency due to gravitational settling
η_{td}	deposition efficiency due to diffusion from turbulent flow
θ	branching angle of a daughter tube
θ_b	angle subtended at the center of curvature by a curved tube
μ	gas viscosity
μ_t	dimensionless parameter for convective diffusion

ν	kinematic viscosity
ρ	particle density
ρ_g	gas density
ρ_w	water density
ρ_0	standard density, 1 g/cm^3
σ_g	geometric standard deviation of the particle diameter distribution
σ_{gd}	geometric standard deviation of the fiber diameter distribution
σ_{gl}	geometric standard deviation of the fiber length distribution
τ	relaxation time
τ_{dl}	the correlation between ln l_f and ln d_f
ϕ	inclination angle relative to gravity ($\phi = 90°$ for horizontal tube)
$\varPhi$	correction factor for droplet growth
χ	dynamic shape factor
ω	angular velocity

This page is intentionally left blank

Chapter 1

Introduction

The human respiratory tract has a total surface area of about 75 m^2 for the exchange of oxygen and carbon dioxide, an essential life-supporting process. As an interface between the body and the environment, the huge surface area has also become the target for deposition of inhaled particles. For a healthy adult at rest, the lungs pump in and out almost effortlessly about 11 m^3 of air in a day. One cubic meter of ambient air contains tens to hundreds of micrograms of aerosol particles. A considerable fraction of the particles in inspired air deposits on airway surfaces. Naturally not all particles are harmful. While inhalation of particulate pollutants in ambient air and at workplaces is to be avoided, the surfaces of lung airways have been the intended target for delivery of medicinal aerosols used in topical or systemic therapy. In addition, intentional deposition of radioactive or non-radioactive particles in various regions of the lungs can provide useful information in diagnostic procedures.

Understanding of particle deposition is important in assessment of the health risk of particulate air pollutants as well as in evaluation of the efficacy of therapeutic aerosols. The respiratory tract consists of three distinct regions: the extrathoracic airways, tracheobronchial tree, and alveolar region. These three regions differ in structure and clear deposited particles by different pathways. In consequence particles deposit at different rates and have different retention times in different respiratory regions. The site of deposition and the dose at a specific site both have marked influences on the effects of deposited particles. Thus, assessment of potential health effects of inhaled particles and evaluation of the efficacy of aerosol therapy require data on doses in various regions of the respiratory system and, in some cases, detailed information on local deposition over a small surface area.

Particle transport in the respiratory tract is a problem involving interfaces between physical and biological systems. During a respiration cycle, inhaled particles take a passageway that is surrounded by surfaces of biological nature. The factors that influence particle deposition include lung morphometry, respiratory physiology, air flow, and particle properties. Particle deposition in the human respiratory tract has been a subject of intensive studies in past decades. Hatch and Gross (1964) gave the first comprehensive review of the subject forty years ago. Since then, significant advances have been made in both experimental and theoretical studies on lung morphometry, flow patterns in airways, aerosol dispersion, inhalability, particle deposition, and mechanisms of particle clearance.

Studies have revealed that the spatial distribution of deposited particles in the respiratory tract is highly uneven. This is a result primarily arising from the

complex structure of lung airways and respiratory flow patterns. The respiratory tract is a system of repeatedly bifurcating tubes. This repeated bifurcation structure of airways has profound effects on motion of inspired air, which in turn affects the trajectories of inhaled particles. Owing to the complexity of airway structure, description of the respiratory tract has relied on anatomical models that incorporate important structural features of bifurcating airways. Several lung models have been proposed. Based on measurements of five normal human lungs of various ages and sizes, Weibel (1963) has developed a symmetrical lung model consisting of 23 generations of bifurcating airways. The model, known as Weibel's lung model A, has since been widely used in studies of particle deposition. Another important factor influencing air flow in lung airways is breathing pattern. The cyclic and unsteady nature of respiratory flow imparts additional degrees of complexity to air flow. Furthermore, expansion and contraction of alveoli as air enters and exits during a respiration cycle give rise to changes in alveolar dimensions, thereby making the alveolar wall a moving boundary. Both the tidal volume and breathing frequency vary with the intensity of physical activity of an individual. Flow patterns in lung airways are very complex even at quiet breathing, ranging from turbulent flow in the trachea and larger bronchi to laminar flow in peripheral airways. At higher respiratory rates, the flow becomes turbulent in more generations of larger airways. A good understanding of the morphology of lung airways and airflow patterns in the respiratory system is therefore essential to studies of inhaled particles. Chapters 2 and 3 cover these two topics respectively.

Inhaled particles deposit on airway surfaces by a number of mechanisms, including inertial impaction, gravitational settling, Brownian motion, turbulent deposition, interception, and electrostatic attraction. The relative contributions of these mechanisms depend mainly on particle properties, especially on particle size and density. Hygroscopic particles tend to grow as inspired air is humidified. Changes in particle size during transit in lung airways clearly have effects on deposition rate and site. This is especially important for therapeutic agents that generally contain hygroscopic substances. Chapter 4 summarizes the basic principles of aerosol behavior pertinent to studies of particle deposition in the respiratory tract.

Chapter 5 describes the dispersion of aerosol particles in the respiratory tract arising from airflow and intrinsic particle motion. In a respiration cycle, inhaled particles reach various depths of the lungs during inhalation and, if they remain airborne, return to the nose during exhalation. Convective mixing and intrinsic motion of particles take place during transport of particles in lung airways. These processes give rise to mixing between incoming air and reserve air, especially in the first few generations of lung airways where the flow is normally turbulent. The particles that move into reserve air have a higher probability to penetrate into the deepest part of the lung and deposit there in

subsequent breaths. Aerosol dispersion therefore has profound effects on the spatial distribution of deposited particles.

The nose is the normal port of entry taken by inhaled air for an individual at rest. Under heavy working conditions, part of inspired air enters through the mouth to avoid excessive increase in resistance to airflow in the nose. Although the nose and mouth have the primary function of serving as ports of entry for air, they also provide the first line of defense against the intrusion of ambient particles. These two ports of entry, similar to an aerosol sampling device with a blunt inlet, block off nearly half of the particles larger than 50 μm in aerodynamic diameter. The probability for particles in ambient air to enter the nose or mouth depends on particle size and ambient air velocity. Chapter 6 discusses the inhalability of particles as it applies to these ports of entry to the respiratory system.

Chapter 7 describes the characteristics and patterns of particle deposition in lung airways. Topics covered include deposition in the entire respiratory tract, deposition in each respiratory region, and deposition in airway bifurcations. Both physical and biological factors that influence deposition are considered. Particle size, shape and density are the most important physical factors, while the biological factors include anatomical and physiological parameters. Another important aspect in particle transport is the sequential nature of the three airway regions. It is evident that only those particles that pass through an upstream region have a chance to reach the downstream regions. As a consequence, the amount of particles deposited in any region depends not only on the influencing parameters in the region itself but also on those in the upstream regions. For example, the nasal passages have small cross sections and sharp turns, and therefore can effectively remove particles larger than 10 μm in aerodynamic diameter. In consequence no particles larger than 10 μm can reach the tracheobronchial and alveolar regions. Our understanding of particle deposition has derived from theoretical studies and experiments using human subjects, laboratory animals, idealized physical models, and hollow casts of extrathoracic and bronchial airways. In recent years, significant advances have been made in numerical analyses of the flow field and particle trajectory in three-dimensional models of the respiratory tract. Results of these theoretical studies for the spatial distribution of particle deposits appear to be in general agreement with some experimental observations. Theoretical and experimental studies on local deposition have proved useful in locating deposition hot spots.

Because of the complexity of deposition processes, an accurate prediction of respiratory deposition from basic theory is still impossible. Advances in our understanding of inhaled particles have relied to a great extent on experimental studies. In deposition experiments using human subjects, the physical factors are generally under good control. On the other hand, biological differences between human subjects give rise to a corresponding intersubject variability in

deposition. Nonetheless, experiments using human subjects have yielded valuable data on deposition in the entire respiratory tract and in each respiratory region. In addition to improving our understanding of inhaled particles, these experimental results are useful for derivation of empirical equations and development of theoretical models. Chapter 8 surveys existing deposition data and reviews empirically derived equations.

Although theoretical models are not yet capable of accurately predicting local deposition, they do help improve our understanding of the effects of various parameters. They are especially useful in estimating total deposition for a wide range of particle diameters, airway sizes, tidal volumes, and breathing frequencies. There are two basic types of deposition models: continuous and compartments-in-series models. Since Findeisen (1935) proposed a compartments-in-series model for estimating total and regional deposition, many modified versions have been proposed in past decades. All models make simplifying assumptions on the anatomy of lung airways and use theoretical or empirical equations for deposition efficiency of straight or curved tubes. These models have different degrees of complexity and give somewhat different estimates. Among them, the recent ICRP and NCRP models (ICRP, 1994; NCRP, 1997) are two widely used compartments-in-series models. Chapter 9 describes existing deposition models and their applications.

Chapter 10 briefly summarizes the interactions between deposited particles and the host. Particles deposited in different regions of the respiratory tract meet different fates. Over the surfaces of airways from the nose to terminal bronchioles, a layer of mucus carries deposited particles within hours or days to the pharynx, where the mucus and particles are swallowed into the gastrointestinal tract. This mode of particle transport, a result of the action of cilia, is known as mucociliary escalator. Coughing is another mechanism to remove deposited particles from the upper respiratory tract. In the alveolar region, which have no mucus layer on the walls, macrophages engulf deposited particles and transport them to lymph nodes or the mucociliary escalator in the upper respiratory tract. Soluble particles may dissolve and then pass through alveolar membranes into bloodstreams before macrophages have a chance to engulf them. Some insoluble particles may enter epithelial or dendritic cells, or penetrate into interstitial space.

The effects of inhaled particles are discussed in Chapter 11. As noted earlier, there are beneficial as well as harmful aerosols. Harmful aerosols have received greater attention in the past because of concerns in the potential hazards arising from inhalation of particulate pollutants in ambient air, toxic particles at workplaces, radioactive particles, bacteria, and viruses. In recent years, therapeutic aerosols have become a subject of intensive studies because of their potentials in topical and systemic therapy.

Chapter 12 describes some applications of inhaled particles. Particle transport in the respiratory tract has been a subject of intensive studies, because it has applications in assessment of the health risk of toxic particles, development of diagnostic procedures, and design of respiratory delivery of therapeutic agents. Experimental data and theoretical predictions for regional deposition provide the basis for calculating tissue doses of inhaled particles. Because the site of deposition has marked influence on toxic effects, information on deposition hotspots is useful for evaluating health risk. Aerosols have found applications in a variety of diagnostic tests. These applications include use of aerosols in assessment of ventilation, airway obstruction, airway responses to pharmaceutical agents, epithelial permeability, mucociliary transport, and airway responsiveness to sensitizing and non-sensitizing stimuli. Aerosolized drugs have been used in treatment of respiratory and systemic diseases. In the medication of certain respiratory diseases, delivery of aerosolized drug through inhalation offers the advantages of minimizing systemic side effects and the time of delivery to the site of action. Regional distribution of deposited particles is a major factor determining the efficacy of therapeutic aerosols. A good understanding of regional deposition is useful for developing techniques to target specific lung regions.

PROBLEMS

1.1 You may have heard the statement that some of the dust particles in air are so small that once they are inhaled into the lungs they cannot be exhaled. Is the statement true? You will gain a better understanding of the problem as you read on.

1.2 Discuss the underlying causes for uneven distribution of particle deposits in human lungs.

1.3 Is it reasonable to assume uniform respiratory deposition in assessing the health risk of particulate pollutants?

1.4 Do you expect humans and dogs to have similar respiratory deposition patterns?

REFERENCES

Findeisen, W. (1935). Über das absetzen kleiner, in der luft suspendierter teilchen in der menschlichen lunge bei der atmung. Pflügers Archiv für gesamte Physiologie des Menschen und der Tiere 236, 367-379.

Hatch, T. F. and Gross, P. (1964). Pulmonary Deposition and Retention of Inhaled Particles. Academic Press, New York.

International Commission on Radiological Protection (1994). Human Respiratory Tract Model for Radiological Protection. Annals of the ICRP, Publication 66. Elsevier Science, Tarrytown, NY.

National Council on Radiation Protection and Measurements (1997). Deposition, Retention and Dosimetry of Inhaled Radioactive Substances, Report 125. NCRP, Bethesda, MD.

Weibel, E.R. (1963). Morphometry of the Human Lung. Academic Press, NY.

Chapter 2

Morphometry of the human respiratory system

The lungs perform two vital functions: ventilation and perfusion. Ventilation refers to the delivery of oxygen to the alveolar region of the lungs. Perfusion is the flow of blood through the pulmonary vascular trees and alveolar capillaries. To perform these two functions, the lungs have a compact three-dimensional structure consisting of a network of airways and a network of blood vessels. The two networks closely match each other in design and have a huge interface between them. It is the network of airways that is of primary concerns in our discussion of inhaled particles.

The airway network in the lungs is a very efficient system for delivery of air. During a normal breath of an average adult, the lungs pump in and out approximately 450 cm³ of air in about 4 seconds. As inspired air arrives in the alveolar region, oxygen in air and carbon dioxide in bloodstreams rapidly exchange with each other over a surface area of about 75 m² (estimates ranging from 60 to 160 m²). To deliver air quickly to such a huge surface area, the network relies on a repeatedly bifurcating system that consists of over 20 generations of airways extending from the trachea to alveolar sacs. It is of interest to note that the distance between the inlet of the trachea and the end of the respiratory tract is only about 27 cm.

There are two structurally distinct regions in the airway network in the lungs: the tracheobronchial airway tree and the alveolar region. The first region covers the airway tree from the trachea to terminal bronchioles. They are called conducting airways because they serves the function of transporting air to and from the alveolar region. The second region, also known as the pulmonary region, includes the respiratory bronchioles, alveolar ducts, alveolar sacs, and alveoli. As noted above, it is the pulmonary region that carries out the function of gas exchange.

Fig. 2.1 gives a morphological overview of the human respiratory tract. In addition to the tracheobronchial and alveolar regions in the lungs, the respiratory tract includes extrathoracic airways. Also termed the head airways region, the extrathoracic airways consist of the nose, mouth, pharynx, and larynx. The three regions of the respiratory tract differ in many aspects including structural characteristics, surface features, and physiological functions.

The term lung represents, in a restricted sense, the bronchi, bronchioles, alveolar ducts, alveolar sacs, and alveoli. In a broad sense, it includes the entire respiratory tract. In this book, we use it mostly in the restricted sense.
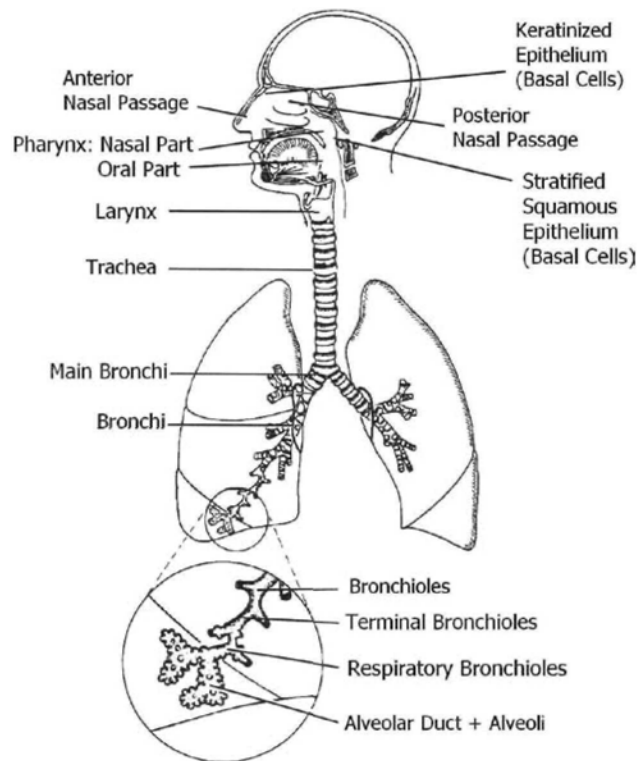
Fig. 2.1 Morphological overview of the human respiratory tract. A pulmonary acinus is enlarged to show details of respiratory bronchioles, alveolar ducts, alveolar sacs, and alveoli. Reprinted with permission from The International Commission on Radiological Protection (1994).

2.1. THE HEAD AIRWAYS REGION

The structural arrangement of the head airways is best understood by following the flow of inspired air. During nose breathing, air enters in the upward direction through anterior nares into the nasal vestibule for an individual standing upright. Beyond the vestibule, the air stream bends and moves horizontally through the slit-like passages formed by the turbinates and nasal septum. At the end of these winding passages, the air stream leaves the nasal cavity through posterior nares. It then turns downward into the nasopharynx, pharynx, larynx, and trachea. Fig. 2.2 shows various parts of the head airways region.
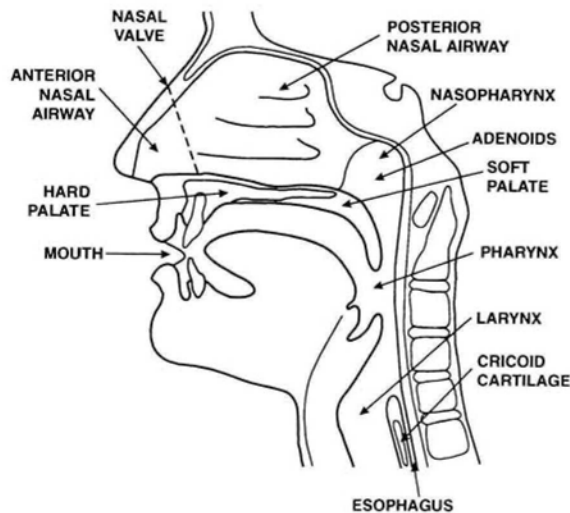
Fig. 2.2 The head airways region. Reprinted with permission from National Council on Radiation Protection and Measurements (NCRP, 1997).

Except the entrance area, the epithelium of nasal airways is ciliated and covered with a layer of mucus, which has the primary function of bringing the temperature and relative humidity of incoming air to the levels of residual air in lungs. Because of repeated beating by underlying cilia, the mucus continuously moves towards the pharynx, thereby providing a pathway for clearing deposited particles. In the non-ciliated part of anterior nares, mucus moves outwards and deposited particles can be removed by wiping, sneezing or nose blowing. The hairs at the entrance of nasal canal are capable of capturing large particles from inspired air.

The cross-sectional area varies markedly along the nasal passages. The internal ostium (nasal valve), about 1.5 cm downstream of the nostrils, is the narrowest cross section in the entire respiratory tract (see Fig. 2.3). It has a cross-sectional area of 0.3 cm^2 on each side of the nasal septum. The turbinate has a larger surface area. The dimensions of the nasal channel can vary quite considerably depending on the thickness of the mucus layer on wall surfaces and the amount of blood perfusion in surrounding tissues.

Under sedentary and light exercise conditions, the nose is the normal pathway taken by inspired air. To avoid excessive increase in resistance to airflow, part of inspired air enters through the mouth during heavy exercise. While both of these two portals have complicated structure, the nasal passages have smaller cross sections and sharper turns than the oral cavity.
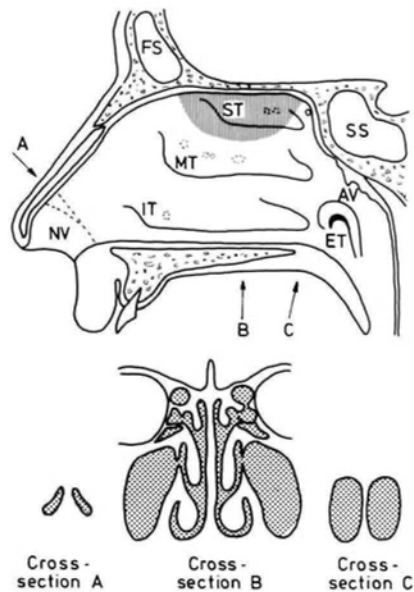
Fig. 2.3 Lateral wall of the nasal cavity and cross sections through (A) the internal ostium, (B) the middle of the nasal cavity, and (C) the choanae. Hatched area in the upper figure: olfactory region; NV: nasal vestibule; IT: inferior turbinate and orifice of the nasolacrimal duct; MT: middle turbinate and orifices of frontal sinus, anterior ethmoidal sinuses and maxillary sinus; ST: superior turbinate and orifices of posterior ethmoidal sinuses; FS: frontal sinus; SS: sphenoidal sinus; AV: adenoid vegetations; ET: orifice of Eustachian tube. Reprinted from Mygind (1979), with permission of Blackwell Publishing Ltd.

As an auxiliary port of entry for inspired air, the mouth includes the slit-like vestibule (the outer and smaller portion of the mouth) and the oral cavity proper (the inner and larger portion of the mouth). In its side view, the entire oral airway has the shape of a curved tube with variable cross sections. Air inhaled through mouth flows into the pharynx via the oropharyngeal isthmus.

In the larynx, which is about 4.4 cm in length, the ventricular folds and the vocal folds impose two consecutive constrictions on airflow. The shape of the glottal aperture, defined by the geometry of vocal folds, is elliptical at low flow rates but changes to quasi-circular at higher flow rates. During swallowing, the epiglottis covers the laryngeal tube to prevent food from entering the trachea.

Using measurements from computed tomography scans and data reported in the literature, Stapleton et al. (2000) have proposed an idealized model of the extrathoracic airways with simple geometric shapes. The model consists of the mouth, pharynx, larynx, and trachea. The upper and lower teeth each form a

semi-circle with a diameter of 2.5 cm at the front end of the mouth and extend 5 cm from the lips to the back end where the two sides of the upper and lower teeth are 4.5 cm apart. The upper and lower teeth are 1 cm apart and the hard palate has a radius of 1.25 cm. The tongue, modeled as a flat plate, begins with its tip at a level of 0.5 cm below the lower teeth and crosses the level of the upper teeth at 4 cm from the front end of the mouth. The pharynx, idealized as an elliptical cylinder, has an anterior-posterior dimension of 1.3 cm and a transverse dimension of 3.25 cm. The average cross-sectional area of the pharynx is 2.98 cm^2. The superior tip of the epiglottis is located about 2 cm above the floor of the pharynx and has an angle of about 30° with the posterior wall of the pharynx. The ventricular folds are modeled as a circular tube with a diameter of 1.6 cm. The glottis, idealized as an elliptical tube, has an anterior-posterior dimension of 1.2 cm and a transverse dimension of 1 cm. The cross-sectional area of the glottal aperture is 0.95 cm^2, which is approximately half way between the maximum opening during inhalation and the maximum opening during exhalation.

In an anatomical model proposed by Katz and Martonen (1996), the larynx is idealized as a cylinder, 6 cm in length, with the ventricular folds at 2.5 cm from the inlet and the vocal folds 2.1 cm further downstream. The inlet and outlet cross sections of the larynx are circular in shape, with a diameter of 1.8 cm. The cross section of the ventricular folds, modeled as an ellipse, has major and minor axes of 1.8 and 1.0 cm respectively. The cross section of the vocal folds, also idealized as an ellipse, has one fixed and one variable axis. The fixed axis is 1.6 cm long and the other axis is 0.70, 1.11, and 1.93 cm long for inspiratory flow rates of 15, 30, and 60 L/min, respectively. The major axis of the ventricular folds and the fixed axis of the vocal folds are normal to each other.

In a cast of oral airways used by Cheng et al. (1999) for deposition studies, the oral cavity has a length of 7.2 cm. The cross-sectional areas are 4.14 and 1.69 cm^2, respectively, at the lips and the end of the oral cavity. It increases and decreases several times along the passage, with a maximum of 9.46 cm^2 at 5.7 cm from the lips.

2.2. THE TRACHEOBRONCHIAL REGION

The tracheobronchial region includes the airways extending from the trachea to terminal bronchioles. Also known as conducting airways, this region of the respiratory tract has the primary function of transporting inspired air to the pulmonary region. The airways in this region are considerably rigid, especially the trachea and bronchi. The trachea and main bronchi have U-shaped cartilage rings in the walls, thereby giving rise to a D-shaped cross section for these

airways. The smaller bronchi have irregularly shaped cartilage plates. There is no cartilage in the walls of bronchioles.

As in head airways, the wall surfaces of tracheobronchial airways are covered with a layer of mucus, which moves constantly towards the pharynx as a result of repeated beating by underlying cilia. No exchange of oxygen and carbon dioxide between inspired air and circulating blood takes place in this region, although small amounts of soluble gases in inspired air can be absorbed into mucus and subsequently transported to bloodstreams through the epithelium. The physiological term for the tracheobronchial tree is the anatomical dead space, in contrast to the physiological dead space, which includes the anatomical dead space and those alveoli that do not take part in gas exchange.

The tracheobronchial tree has a three-dimensional compact structure of repeatedly bifurcating tubes. Although the airway structure has been frequently compared to an inverted tree, it is of some interest to note that actually very few kinds of botanical trees branch in a dichotomous pattern.

The bifurcation pattern of human lung airways is quite regular, but not symmetrical. In general, a parent airway segment divides into two daughter branches of different diameters. An obvious example of asymmetry in bifurcation occurs at lobar bronchi. To accommodate the heart, the left lung has only 45% of the total lung volume while the right lung has 55%. The right main bronchus divides into three lobar bronchi but the left main bronchus divides into only two.

Regular dichotomy is, in fact, just one type of airway multiplication in mammals. Other patterns of multiplication include monopody and trichotomy. In a monopodial airway tree, as in a dog's lungs, the daughter branches appear like offshoots from a main trunk. A bifurcation of extreme asymmetry, with its major daughter almost undistinguishable from the parent, is very close to a monopodial formation. On the other hand, an asymmetric bifurcation approaches a trichotomy pattern if it has a daughter branch so short that the two daughters of this short branch are almost comparable in size to the other daughter.

Fig. 2.4 shows the first few generations of tracheobronchial airways. As a result of repeated bifurcation, the respiratory tract provides numerous pathways for inhaled air and particles to move along. Even though the pattern of airway bifurcation is relatively regular, the division of airways terminates earlier in some pathways, thereby leading to a distribution of the number of generations among various paths. Some pathways have more generations of airways than others. Furthermore, the airway segments in the same generation vary in diameter and length from path to path. Most airway segments are relatively straight, but there are some curved airways.
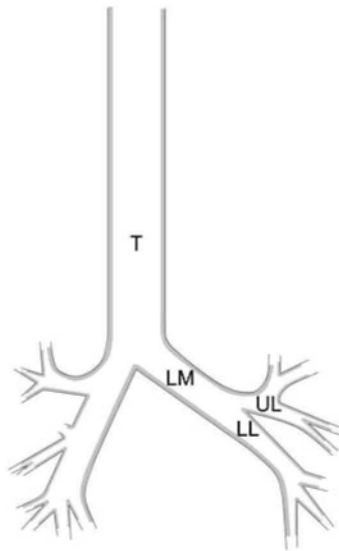
Fig. 2.4 The first few generations of tracheobronchial airways: trachea (T), left main bronchus (LM), upper lobe bronchus (UL), and lower lobe bronchus (LL).

An airway bifurcation consists of a parent tube and two daughter branches. It represents a basic building block of the tracheobronchial tree. To analyze airflow and particle transport, it is useful to consider the airway tree as a system consisting of successive bifurcations, instead of tubes connected in series. Such a viewpoint enables us to focus on the transition zone of bifurcation where airflow changes direction sharply and enhanced deposition of particles take place.

A complete specification of an airway bifurcation should include the following geometric parameters (see Fig. 2.5 for terminology):

(1) The length and diameter of the parent airway segment
(2) The length and diameter of each daughter tube
(3) The branching angle of each daughter tube (the angle between the axis of the daughter tube and the axis of the parent tube)
(4) The angle between two successive bifurcation planes (to be defined in Section 2.3)
(5) The variation in cross section of the airway in transition zone extending from the outlet of parent tube to the inlets of daughter branches
(6) The radius of curvature at the centerline of each daughter tube in the transition zone
(7) The shape of carinal ridge
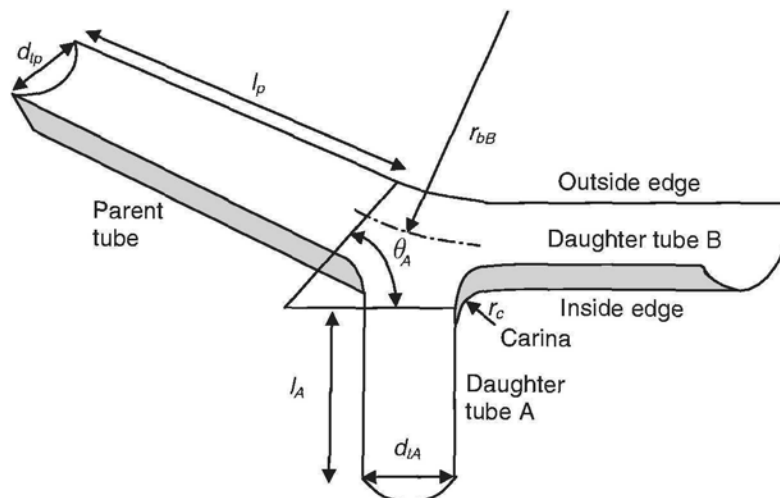
Fig. 2.5 An airway bifurcation; d_{tp}: diameter of parent tube; d_{tA}: diameter of daughter tube A; l_p: length of parent tube; l_A: length of daughter tube A; θ_A: branching angle of daughter tube A; r_{bB}: radius of curvature at the centerline of daughter tube B; r_c: radius of carinal ridge.

Even though the respiratory tract is similar in structure among individuals, the dimensions of airways vary with body size. There are only a few comprehensive morphometric studies on limited number of human lungs. Most studies focused on the diameter and length of airway segments. Some measurements on branching angle and the angle of inclination to gravity of airway segments have been reported.

In an asymmetric bifurcation, the daughter tube with the larger diameter (the major daughter) tends to continue the direction of parent tube, while the minor daughter tube branches out at a larger angle. Measurements show that the minor daughter tube has a branching angle between 30° and 65°, and the branching angle of the major daughter tube is about 20° smaller (Phalen et al., 1978). One notable exception is the first bifurcation of the tracheobronchial tree: the branching angle is 35° for the right main bronchus and 73° for the left main bronchus (Horsfield et al., 1971). The branching angles of the five lobar bronchi reported by Horsfield et al. are respectively 15, 15, 44, 48, and 63 degrees, which are well within the ranges of branching angles for the major and minor branches mentioned above.

The transition zone of a bifurcation begins at about 80% of the length of parent tube, where the cross section (normal to the axis of parent tube) gradually changes in shape, first from a circle to an ellipse and subsequently to two tangent circles. The cross-sectional area remains nearly constant in the first half of the transition zone but rapidly increases in the second half. In small

airway bifurcations, essentially no change in cross-sectional area occurs in the daughter tubes distal (in the direction of inspiratory flow) to the carinal ridge (Horsfield et al., 1971; Hammersley and Olson, 1992).

The carinal ridge has a large variety of shapes, including sharp wedge, blunt edge, asymmetric edge, saddle, and parabola (Martonen et al., 1994). Shown in Fig. 2.5 is an example of blunt carinal ridge. The carinal curvature, defined as the radius of curvature at the center of the spur divided by the radius of the daughter tube, has an average value of about 0.2, but can be as large as 2 for a very blunt carinal ridge (Horsfield et al., 1971). It is to be noted that the definition of curvature ratio used here differs by a factor of 2 from the one used by Horsfield et al. The thickness of the leading edge of the carinal ridge is less than 5-10% of the daughter diameter for smaller airways (Hammersley and Olson, 1992).

The outer wall of each daughter tube curves gradually from the direction of the parent axis to that of the daughter axis (see Fig. 2.5). The ratio of the radius of curvature at the centerline to the radius of daughter tube differs among airways of different diameters. The smaller airways have smaller curvature ratios. It is in the range of 2-6 for airways with diameters below 1.5 mm, in the range of 4-10 for airways with diameters between 1.5 and 3 mm, in the range of 7-14 for the bronchi with diameters larger than 3 mm (except the 32 large airways in the central part of the lungs), and in the range of 1-36 for the 32 central airways (Horsfield et al., 1971). At a curvature ratio of 1, the outer wall sharply bends at one point. Again it is to be noted that the definition of curvature ratio used here differs by a factor of 2 from the one used by Horsfield et al.

2.3. ANATOMICAL MODELS OF LUNGS

The human respiratory tract has over 16 million airway segments. It is impractical to specify the geometric parameters of each segment and the sequential relationship between successive segments for the entire tract. For analyses of gas flow and particle transport, a number of simplified anatomical models have been proposed to represent the human respiratory tract (Findeisen, 1935; Landahl, 1950; Davies, 1961; Weibel, 1963, 1991; Horsfield and Cumming, 1968a, b; Hansen and Ampaya, 1975; Yeh and Schum, 1980; Phalen et al., 1978). These anatomical models all take into consideration the bifurcating pattern of the respiratory tract. However, they differ to some extent in airway dimensions and the number of airway generations. Both symmetrical and asymmetrical models are available. Even though the asymmetrical models provide more realistic representations of the respiratory tract, the simpler

symmetrical models have proved to be more convenient in calculations of particle deposition and other applications.

Several different concepts have been employed in developing lung models. Weibel's lung model A (Weibel, 1963), a widely used symmetric model of the respiratory tract, uses the concept of descending generation as in a pedigree to specify the sequential relationship between successive airways. The model designates the trachea as Generation 0. On the other hand, Horsfield et al. (1971) have developed a model of the human bronchial tree using the order of airway dimension. The airways are ordered in the upward direction. The smallest airways have order 1 and the trachea has the highest order. Because the order number reflects the airway dimensions, it is useful for developing asymmetric lung models in which airways of the same generation may have very different diameters and lengths. The lung models proposed by Yeh and Schum (1980) use one typical pathway to represent an individual lobe or the entire respiratory tract. They have also employed the concept of descending generation.
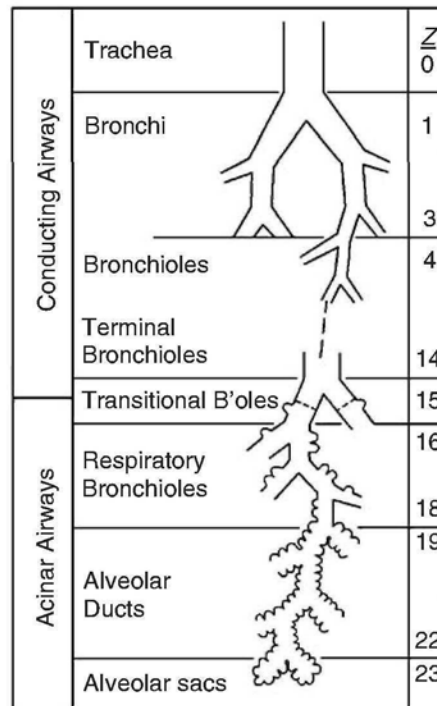
Fig. 2.6 A typical path in Weibel's lung model A showing the generation numbers (Z) of the repeatedly bifurcating airways. Adapted from Weibel (1991).

Weibel's lung model A represents the respiratory tract of an average adult with a lung volume of 0.0048 m^3 (4.8 L) at 75% maximal inflation (Weibel, 1963, 1991). Fig. 2.6 displays a typical path in this lung model. The conducting airways contain Generations 0 through 14. The airways in Generation 15 are the transitional bronchioles, which begin to have a few alveoli attached on the wall. The acinar airways will be discussed in Section 2.5.

Table 2.1 summarizes the airway dimensions and other relevant parameter values of Weibel's lung model A. The diameter ratio of the parent and daughter tubes is approximately proportional to the cube root of 2. A repeatedly bifurcating system with such a diameter ratio between the airway segments of successive generations appears to provide an optimal design that minimizes the entropy production for alveolar ventilation (Wilson, 1967). The distance from the first carina to the end of the respiratory tract is only 14.98 cm. By comparison, the trachea alone has a length of about 12 cm and the distance from the nostrils to the nasal part of the pharynx is about 12-14 cm.

As noted earlier, the airways in each generation have various diameters and lengths. For simplicity, the symmetric model uses average values to represent the diameter and length of an airway segment in each generation. The trachea has a diameter of 1.8 cm and a length of 12 cm, while a terminal bronchiole (the airway of Generation 14) has a diameter of 0.074 cm and a length of 0.16 cm. In an airway tree of regular dichotomy, the number of airways doubles in each successive generation. In consequence the total number of terminal bronchioles is 16,384, giving rise to a total cross section of 69.4 cm^2, which is about 27 times that of the trachea. The marked increase in total cross-sectional area enables inspired air to reach the huge surface area for gas exchange in a short time.

For comparison, Tables 2.2 and 2.3 give respectively the dimensions of two other lung models, one proposed by Yeh and Schum (1980) and the other by ICRP (1994). The typical path lung model developed by Yeh and Schum is based on measurements from a silicone rubber cast of the human tracheobronchial tree, while the ICRP anatomical model is a composite airway structure adapted from several lung models. In these two symmetrical models, the geometrical parameters include tube diameter, tube length, branching angle, and inclination angle relative to the gravity.

The ICRP anatomical model consists of two extrathoracic regions and three thoracic regions. The extrathoracic airways are divided into two regions: (1) the anterior nose and (2) the posterior nasal passages, larynx, pharynx, and mouth. The thoracic part of the respiratory tract is composed of the bronchial, bronchiolar, and alveolar regions. Furthermore, the ICRP model has adopted its own numbering system for airway generations, which differ to some extent from Weibel's lung model A.

Table 2.1

Characteristics of Lung Model A representing the respiratory tract of an average adult with a lung volume of 4800 cm³ at about 75% total lung capacity (based on Weibel, 1991).

Gener-ation Number	Number of Airways per Gener-ation	Airway Diameter	Airway Length	Distance from First Carina to End of Airway	Total Cross Section per Gener-ation	Total Airway Volume per Gener-ation	Cumula-tive Airway Volume
z	$n(z)$	$d_i(z)$	$l_i(z)$		$A(z)$	$V(z)$	$\sum_{i=0}^{z} V(i)$
		(cm)	(cm)	(cm)	(cm²)	(cm³)	(cm³)
0	1	1.80	12.0	-	2.54	30.5	30.5
1	2	1.22	4.76	4.76	2.33	11.1	41.7
2	4	0.83	1.90	6.66	2.13	4.11	45.8
3	8	0.56	0.76	7.42	2.00	1.50	47.3
4	16	0.45	1.27	8.69	2.48	3.23	50.5
5	32	0.35	1.07	9.76	3.11	3.29	53.8
6	64	0.28	0.90	10.66	3.96	3.55	57.4
7	128	0.23	0.76	11.42	5.10	4.04	61.4
8	256	0.186	0.64	12.06	6.95	4.45	65.8
9	512	0.154	0.54	12.60	9.56	5.15	71.0
10	1,024	0.130	0.46	13.06	13.4	6.25	77.2
11	2,048	0.109	0.39	13.45	19.6	7.45	84.7
12	4,096	0.095	0.33	13.78	28.8	9.58	94.3
13	8,192	0.082	0.27	14.05	44.5	11.7	106.0
14	16,384	0.074	0.16	14.21	69.4	11.3	117.2
15	32,768	0.050	0.133	14.34	117	8.56	125.8
16	65,536	0.049	0.112	14.46	225	13.8	139.6
17	131,072	0.040	0.093	14.55	300	15.3	155.0
18	262,144	0.038	0.083	14.63	543	24.7	179.6
19	524,288	0.036	0.070	14.70	978	37.4	217.0
20	1,048,576	0.034	0.070	14.77	1,743	66.6	283.6
21	2,097,152	0.031	0.070	14.84	2,733	110.8	394.4
22	4,194,304	0.029	0.067	14.91	5,070	185.6	580.0
23	8,388,608	0.025	0.075	14.98	7,530	308.8	888.9

Table 2.2

Characteristics of the human respiratory tract for a total lung capacity of 5,600 cm^3, with 3×10^8 alveoli, each of which having a length of 250 μm and a diameter of 300 μm (based on Yeh and Schum, 1980).

Gener-ation Number[a]	Number of Airways per Gener-ation	Airway Diameter	Airway Length	Branch-ing Angle	Incli-nation Angle Relative to Gravity[b]
z	$n(z)$	$d_t(z)$	$l_t(z)$		
		(cm)	(cm)	degrees	degrees
0	1	2.01	10.0	-	0
1	2	1.56	4.36	33	20
2	4	1.13	1.78	34	31
3	8	0.827	0.965	22	43
4	16	0.651	0.995	20	39
5	32	0.574	1.010	18	39
6	64	0.435	0.890	19	40
7	128	0.373	0.962	22	36
8	256	0.322	0.867	28	39
9	512	0.257	0.667	22	45
10	1,024	0.198	0.556	33	43
11	2,048	0.156	0.446	34	45
12	4,096	0.118	0.359	37	45
13	8,192	0.092	0.275	39	60
14	16,384	0.073	0.212	39	60
15[a]	32,768	0.060	0.168	51	60
16	65,536	0.054	0.134	45	60
17	131,072	0.050	0.120	45	60
18	262,144	0.047	0.092	45	60
19	524,288	0.045	0.080	45	60
20	1,048,576	0.044	0.070	45	60
21	2,097,152	0.044	0.063	45	60
22	4,194,304	0.043	0.057	45	60
23	8,388,608	0.043	0.053	45	60

[a] Yeh and Schum designated the trachea as Generation 1. For comparison with Weibel's lung model A, the generation number in this table starts from 0.

[b] A horizontal tube has a gravitational inclination angle of 90°.

Table 2.3

Characteristics of the respiratory tract at a functional residual capacity of 3,300 cm³ for the reference man used in ICRP model (1994).

Gener-ation Number[a]	Number of Airways per Gener-ation	Airway Diameter	Airway Length	Branch-ing Angle	Incli-nation Angle Relative to Gravity[b]
z	$n(z)$	$d_t(z)$	$l_t(z)$		
		(cm)	(cm)	degrees	degrees
0	1	1.65	9.10	-	0
1	2	1.20	3.80	36	20
2	4	0.850	1.50	35	31
3	8	0.610	0.830	28	43
4	16	0.440	0.900	35	39
5	32	0.360	0.810	39	39
6	64	0.290	0.660	34	40
7	128	0.240	0.600	48	36
8	256	0.200	0.530	53	39
9	512	0.165	0.437	54	45
10	1,024	0.135	0.362	51	45
11	2,048	0.109	0.301	46	45
12	4,096	0.088	0.250	47	45
13	8,192	0.072	0.207	48	45
14	16,384	0.060	0.170	52	45
15	32,768	0.053	0.138	45	45
16	65,536	0.051	0.110		
17	131,072	0.046	0.092		
18	262,144	0.041	0.076		
19	622,592	0.038	0.063		
20	1,474,560	0.035	0.052		
21	3,538,944	0.033	0.043		
22	8,323,072	0.031	0.036		
23	12,255,232	0.030	0.030		
24	11,993,088	0.029	0.021		
25	4,784,128	0.028	0.021		
26	1,900,544	0.028	0.017		

[a] The bronchial region consists of Generations 0 to 8; the bronchiolar region consists of Generations 9 to 15; there are three generations of respiratory bronchioles (Generations 16 to 18) and eight generations of alveolar ducts (Generations 19 to 26).

[b] A horizontal tube has a gravitational inclination angle of 90°.

Table 2.3 gives the dimensions of the three thoracic regions in the reference man used in the ICRP model. The bronchial region includes the trachea (Generation 0) and eight generations of bronchi (Generations 1-8). There are seven generations of bronchioles (Generations 9-15) in the bronchiolar region. The alveolar region contains three generations of respiratory bronchioles (Generations 16-18) and eight generations of alveolar ducts. The diameter and length of the airways in each generation of the bronchial and bronchiolar regions are values obtained from averaging the dimensions given by Weibel (1963), Yeh and Schum (1980), and Phalen et al. (1985), after the original measurements have been adjusted to a functional residual capacity of 3.3 L. The branching angle and the angle of inclination relative to gravity are identical to the values given by Phalen et al. (1985). The diameters and lengths of respiratory bronchioles and alveolar ducts are calculated from Hansen and Ampaya (1975).

As mentioned earlier, the lung model developed by Horsfield and Cumming (1968a, b) considers the respiratory tract as a convergent system. It classifies the airways by order of airway dimension instead of generation of airway division. The order starts from an end branch such as the airways of diameter 0.06 cm (order 0) and continues up to the trachea (order 25).

The model developed by Horsfield and Cumming includes both symmetric and asymmetric junctions. A junction is equivalent to a bifurcation in the lung models based on the concept of generation. A symmetric junction contains two branches of the same order that meet to form an airway of the next higher order. In an asymmetric junction, two branches of different orders join to form an airway of an order that is one higher than the higher of the two joining branches. This scheme of construction makes it possible to generate a relatively realistic model of the respiratory tract. The use of order also enables classification of airway segments in accordance with their function; an airway segment of higher order has a larger diameter and receives more inspired air. However, the asymmetrical model is considerably more complicated than a symmetrical model. While the number of generations is identical for any pathway from the trachea to the end branch in a symmetrical model, the number of orders can differ significantly from pathway to pathway in an asymmetrical model.

Because of irregularity in branching pattern, individual airway paths differ in number of generations. The path length distribution is important for a complete description of the respiratory tract. It has been given in some models of the respiratory acinus (Hansen et al., 1975; Hansen and Ampaya, 1975; Haefeli-Bleuer and Weibel, 1988).

To account for the three-dimensional nature of bronchial airways, Chen et al. (1980) have proposed a model that includes the orientation angle of each

tube in a system of repeatedly bifurcating airways. The orientation angle is defined as the angle between the normal (OM in Fig. 2.7) of the bifurcation plane (DEPO) of the tube under consideration and the normal (ON) of the bifurcation plane (PORQ) of the parent tube. It is measured in the positive sense (clockwise) about the vector (PO) representing the parent tube, which points in the flow direction during inhalation. The direction of the normal (OM) is defined so that the parent tube vector (PO), the daughter tube vector (OD), and the normal (OM) of the bifurcation plane follow the right-handed screw rule. In other words, the normal points in the direction that a right-handed screw advances when it is turned from the parent tube towards the daughter tube by the shortest route.

It is to be noted that the three-dimensional airway model permits each daughter tube to form a bifurcation plane with the parent tube. This represents a general configuration.

The orientation angle is a basic geometric parameter of an airway tree. It can be used together with branching angle to uniquely determine the gravitational inclination of a tube in an airway tree with the trachea placed in an arbitrary gravitational inclination (not necessary to be in the upright position). Measurements of gravitational inclination have been carried out for each airway segment in the human tracheobronchial tree with the trachea in the upright position (Phalen et al., 1978; Yeh and Schum, 1980). However, when these data on gravitational inclination are used with branching angle to calculate the orientation angle, it generally gives two solutions. To avoid such an uncertainty, it would be more useful to measure the orientation angle instead of the gravitational inclination.
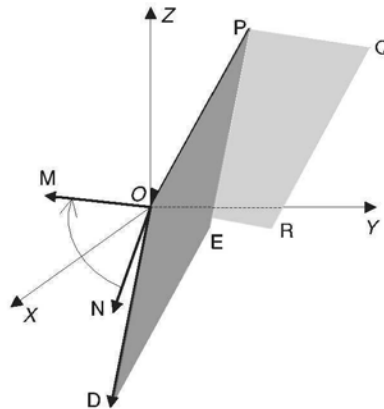
Fig. 2.7. The definition of orientation angle. PO and OD represent the parent and daughter tubes, respectively.

Chen et al. (1980) have also made use of the relative magnitude of orientation angles of the two daughter tubes in each bifurcation to construct a binary coding system for identifying individual tubes in an airway tree. The two daughter tubes in a bifurcation are assigned the binary bits 0 and 1, the tube with the smaller orientation angle being designated as 0 and the other as 1. If the two daughter tubes happen to have identical orientation angle, the one with a smaller branching angle is given the number 0. For convenience, the trachea is labeled Tube 1. The identification number for each tube in a lower generation is a sequence of binary bits obtained by arranging in descending order all the binary bits for the tube and its ancestral tubes. For example, the left main bronchus (LM), lower lobe bronchus (LL), and upper lobe bronchus (UL) in Fig. 2.4 are Tubes 11, 110, and 111, respectively. Because the identification number of each tube contains the identification numbers of all the ancestral tubes in descending order, the binary coding system automatically provides information on connectivity in the line of descent from the first airway in a repeatedly bifurcating system. Connectivity between airways of successive generations is important in the description of an airway tree. The binary coding system has another advantage that the decimal number corresponding to the binary number for each tube can be easily found. Again taking the three tubes LM, LL, and UL in Fig. 2.4 as examples, they are respectively Tubes 3, 6, and 7 in decimal number.

To account for the variations in tube diameter and length in each generation of lung airways, Soong et al. (1979) have used morphometric data in the literature and Weibel's lung model A to develop a statistical model. In their model, the lung geometry is described in terms of probability distributions for the lengths and diameters of airway segments and for the number and volume of alveoli. Subsequently, Koblinger and Hofmann (1985, 1990) have conducted comprehensive analyses on the distributions of various geometric parameters of lung airways using morphometric data of the bronchial tree (Raabe et al., 1976) and those of the pulmonary acinus (Haefeli-Bleuer and Weibel, 1988). They have derived the probability distributions for the diameter, length, branching angle, and gravitational inclination of airway segments in each generation. The correlations between daughter and parent tubes and the correlations between major and minor daughter tubes have also been reported.

An alternative way to deal with the variations in tube diameter and length in each generation of lung airways is to use the frequency distribution of airway path length. Such an anatomical model contains a large number of airway paths that have different numbers of airway generations. Each airway path of a specified length is given a complete specification on diameter, length, branching angle, and orientation angle of airway segments in each generation.

Lung models become more complex as additional features of the airways are taken into consideration. Simple lung models are sufficiently realistic to provide a basic framework for studies of inhaled particles. On the other hand, more complex models have proved useful for examining the effects of various airway features.

2.4 ANATOMICAL MODELS OF AIRWAY BIFURCATIONS

As a basic building block of the tracheobronchial tree, the airway bifurcation has been used widely in theoretical and experimental studies of air flow and particle deposition. The models of airway bifurcations employed in these studies generally differ in structure and many of them do not give specifications for the transition zone.

To take the structure of transition zone into consideration, Baláshazy and Hofmann (1993) have used 11 geometric parameters to describe a three-dimensional asymmetric bifurcation model. The two daughter tubes of the model have different lengths, diameters, and branching angles. The parent and daughter tubes, each being a circular cylinder, do not lie on the same plane. The transition zone is delimited by two parallel cross sections normal to the axis of the parent tube, the beginning section placed before or at the outlet of the parent tube and the end section placed upstream (referring to inspiratory flow) of the carinal ridge. The walls of the transition zone consist of straight line segments connecting the points on the perimeter of beginning section (BB' in Fig. 2.8) and the corresponding points on the end section (EE'). If the beginning section is placed upstream of the outlet of the parent tube, the resulting transition zone has larger cross sections (the wide bifurcation model). Shifting the beginning section downstream (say from BB' to CC') reduces the cross-sectional areas of the transition zone (the narrow bifurcation model).
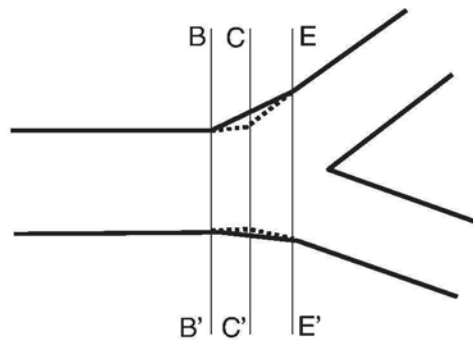
Fig. 2.8. A wide bifurcation and a narrow bifurcation.

Subsequently, Heistracher and Hofmann (1995) have presented a mathematical method for generating physiologically realistic models of airway bifurcation. The method is capable of generating a three-dimensional asymmetric bifurcation model formed by a single smooth surface. The parent tube is a straight circular cylinder, but each of the two daughter branches consists of a straight portion and a curved portion. The transition zone, which contains the two curved portions of daughter tubes, has three delimiting cross sections, one at the outlet of the parent tube and the other two at the outlets of the two curved portions of daughter tubes. The model also defines the radius of curvature at the carinal ridge.

2.5 THE ALVEOLAR REGION

Also known as acinar airways, the alveolated airways extend from transitional bronchioles to alveolar sacs. Each pulmonary acinus represents a unit of alveolated airways. It consists of a transitional bronchiole and all the airways distal to it. The alveolar region consists of over 30,000 acini.

In Weibel's lung model A, the tubes of Generation 15 are the transitional bronchioles. The respiratory bronchioles begin at Generation 16 and ends at Generation 18. The number of alveoli carried by each bronchiole increases with generation number in these three generations. Each bronchiole in Generations 16 and 17 has only a few alveoli apposed to its walls. The airways in Generations 19 to 23 are completely covered with alveoli and are called alveolar ducts (Generations 19 and 22) and alveolar sacs (Generation 23). Airway dimensions do not change much in this region. For the airways from Generations 15 to 23, the diameter decreases from 0.050 to 0.025 cm, and the length falls from 0.133 to 0.075 cm. The total number of alveolar sacs is over 8 millions, giving a total cross section of 0.753 m^2.

In the alveolar region, the alveoli attached on airway walls provide a total of approximately 60-160 m^2 of surface area for exchange of gases across the alveolar-capillary membrane, which is only about 2 μm in thickness. Closely packed alveoli form a sleeve around an alveolar duct. They appear like bubbles in soap foam. Fig. 2.9 shows a slice of human lung parenchyma at two different magnifications.

There are several ways to describe the geometry of an alveolus. One commonly used approximation is to represent an alveolus as 5/6 of a sphere with a diameter of 300 μm. The lungs of a healthy adult have about 300 million alveoli. But only those alveoli that receive adequate ventilation (supply of freshly inspired air) and perfusion (supply of blood to the capillary) participate in gas exchange. The percentage of alveoli taking part in gas exchange decreases with age. It is at least 70% for a healthy young adult.
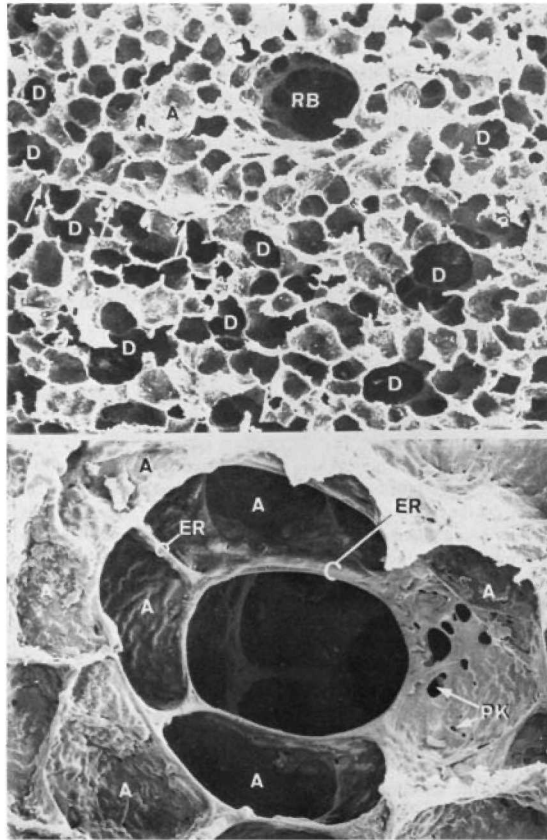
Fig. 2.9. Top panel: scanning electron micrograph of a slice of human lung parenchyma, showing a small respiratory bronchiole (RB), several alveolar ducts (D), and interlobular septum (indicated by arrows). Bottom panel: gas exchange parenchyma at a higher magnification, showing an alveolar duct (D) with several adjacent alveoli (A), entrance rings (ER), and inter-alveolar pores of Kohn (PK). Reprinted from Gehr et al. (1978) with permission of Elsevier Science Publishers.

2.6 VARIATIONS IN AIRWAY DIMENSIONS

The structure and dimensions of the respiratory tract discussed earlier in this chapter represent the airways of an average healthy adult. The volume of the respiratory tract varies with body size, gender, and age.

The dimensions of the trachea and bronchi are related to body height (Phalen et al., 1985). The ICRP model (1994) has included the scaling factors

for calculating airway dimensions of an individual from those of the reference adult male.

Airway dimensions vary slightly with gender. The size of the respiratory tract is smaller in women than in men, especially in the pharynx, larynx and large conducting airways. Measurements of airway area in 26 male and 28 female healthy nonsmoking adults show that tracheal areas in males are significantly larger than those of females even after controlling for total lung capacity (Martin et al., 1987).

Age is an important influencing factor of airway structure and dimensions. The branching structure of the lungs is developed at birth, but multiplication of alveoli is not complete until about age 2 (Zeltner et al., 1987). The airway dimensions increase by a factor of about 3 from birth to adulthood. Alveoli, 50-100 μm in diameter at birth, grow to 300 μm in adult lungs.

Other factors that can modify airway dimensions include chemical irritants and diseases. Respiratory diseases such as tumors, emphysema, and chronic bronchitis can markedly alter airway dimensions.

2.7 CHANGES IN AIRWAY DIMENSIONS DURING RESPIRATION

During a cycle of respiration, the volume of respiratory tract varies with time as air goes in and out. The change in volume differs from region to region. The head airways are quite rigid in structure and therefore very little variation in volume takes place in this region except the vocal folds. In the tracheobronchial region, the change in volume is mainly a result of expansion in cross section. For acinar airways, both the length and cross section vary during a breathing cycle.

In calculations of particle deposition, the volume of respiratory tract is generally assumed to be the average of the volume before inhalation and the volume at the end of inhalation. If a breath begins from the functional residual capacity, V_{FRC}, then the average lung volume V_L during inhalation is the sum of V_{FRC} and one half of the tidal volume, V_t:

$$V_L = V_{FRC} + \frac{1}{2} V_t \tag{2.1}$$

An alternative approach is to assume that the airway length remains constant while the cross-sectional area of the airways varies with time during a respiration cycle:

$$A(x,t) = A(x)f(t) \tag{2.2}$$

Here $A(x,t)$ is the sum of the cross-sectional area of all airways at distance x from the inlet of the trachea at time t, $A(x)$ the mean value of $A(x,t)$, and $f(t)$ a time-dependent function representing the breathing pattern.

A similar function, $A_T(x,t)$, that includes the additional cross-sectional area due to the alveolar volume associated with an airway generation in the pulmonary region can be defined as

$$A_T(x,t) = A(x,t) + \frac{V}{l_t} \tag{2.3}$$

Here V is the alveolar volume associated with an airway generation of length l_t. The function $A_T(x,t)$ also changes with time as described in Eq. (2.2).

PROBLEMS

2.1 Statistical models can be developed for lung airways using frequency distributions either for airway dimensions in each generation or for airway path lengths. Discuss the differences between these two approaches.

2.2 What are the differences between the concepts of generation and order in modeling lung airways?

2.3 Why is connectivity important in the description of an airway tree?

REFERENCES

Balásházy, I. and Hofmann, W. (1993). Particle deposition in airway bifurcations – I. Inspiratory flow. J. Aerosol Sci. 24, 745-772.

Chen, W.J.R, Shiah, D.S.P. and Wang, C.S. (1980). A three-dimensional model of the upper tracheobronchial tree. Bull. Math. Biol. 42, 847-859.

Cheng, Y.S., Zhou, Y. and Chen, B.T. (1999). Particle deposition in a cast of human airways. Aerosol Sci. Technol. 31, 286-300.

Davies, C.N. (1961). A formalized anatomy of the human respiratory tract. In: Inhaled Particles and Vapors, p.82 (Ed. Davies, C.N.). Pergamon Press, London.

Findeisen, W. (1935). Über das absetzen kleiner, in der luft suspendierter teilchen in der menschlichen lunge bei der atmung. Pflügers Archiv für gesamte Physiologie des Menschen und der Tiere 236, 367-379.

Gehr, P., Bachofen, M. and Weibel, E.R. (1978). The normal human lung: Ultrastructure and morphometric estimation of diffusion capacity. Respir. Physiol. 32, 121-140.

Haefeli-Bleuer, B. and Weibel, E.R. (1988). Morphometry of the human pulmonary acinus. Anat. Rec. 220, 401-414.

Hammersley, J.R. and Olson, D.E. (1992). Physical models of the smaller pulmonary airways. J. Appl. Physiol. 72, 2402-2414.

Hansen, J.E. and Ampaya, E.P. (1975). Human air space shapes, sizes, and volumes. J. Appl. Physiol., 38, 990-995.

Hansen, J.E., Ampaya, E.P., Bryant, G.H. and Navin, J.J. (1975). Branching pattern of airways and air spaces on a single human terminal bronchiole. J. Appl. Physiol., 38, 983-989.

Heistracher, T. and Hofmann, W. (1995). Physiologically realistic models of bronchial airway bifurcations. J. Aerosol Sci. 26, 497-509.

Horsfield, K. and Cumming, G. (1968a). Morphology of the bronchial tree in man. J. Appl. Physiol. 24, 373-383.

Horsfield, K. and Cumming, G. (1968b). Functional consequences of airways morphology. J. Appl. Physiol. 24, 384-390.

Horsfield, K., Dart, G., Olson, D.E., Filley, G.F. and Cumming, G. (1971). Models of the human bronchial tree. J. Appl. Physiol. 31, 207-217.

International Commission on Radiological Protection (1994). Human Respiratory Tract Model for Radiological Protection, Annals of the ICRP, Publication 66. Elsevier Science, Tarrytown, NY.

Katz, I.M. and Martonen, T.B. (1996). Flow patterns in three-dimensional laryngeal models. J. Aerosol Med. 9, 501-511.

Koblinger, L. and Hofmann, W. (1985). Analysis of human lung morphometric data for stochastic aerosol deposition calculations. Phys. Med. Biol. 30, 541-556.

Koblinger, L. and Hofmann, W. (1990). Monte Carlo modeling of aerosol deposition in human lungs. Part I: Simulation of particle transport in a stochastic lung structure. J. Aerosol Sci. 21, 661-674.

Landahl, H. D. (1950). On the removal of air-borne droplets by the human respiratory tract: 1. The lung. Bull. Math. Biophys. 12, 43-56.

Martin, T.R., Castile, R.G., Fredberg, J.J., Wohl, M.E. and Mead, J. (1987). Airway size is related to sex but not lung size in normal adults. J. Appl. Physiol. 63, 2042-2047.

Martonen, T.B., Yang, Y. and Xue, Z.Q. (1994). Effects of carinal ridge shapes on lung airstreams. Aerosol Sci. Technol. 21, 119-136.

Mygind, N. (1979). Nasal Allergy, Second Edition. Blackwell Scientific, Oxford.

National Council on Radiation Protection and Measurements (1997). Deposition, Retention and Dosimetry of Inhaled Radioactive Substances, NCRP Report 125. NCRP, Bethesda, Maryland.

Phalen, R.F., Yeh, H.C., Schum, G.M. and Raabe, O.G. (1978). Application of an idealized model to morphometry of the mammalian tracheobronchial tree. Anat. Rec. 190, 167-176.

Phalen, R.F., Oldham, M.J., Beaucage, C.B., Crocker, T.T. and Mortensen, J.D. (1985). Postnatal enlargement of human tracheobronchial airways and implications for particle deposition. Anat. Rec. 212, 368-380.

Raabe, O.G., Yeh, H.C., Schum, G.M. and Phalen, R.F. (1976). Tracheobronchial Geometry: Human, Dog, Rat, Hamster. Lovelace Foundation Report LF-53, Albuquerque, New Mexico.

Soong, T.T., Nicolaides, P., Yu, C.P. and Soong, S.C. (1979). A statistical description of the human tracheobronchial tree geometry. Respir Physiol. 37, 161-72.

Stapleton, K.W., Guentsch, E., Hoskinson, M.K. and Finlay, W.H. (2000). On the suitability of k-ε turbulence modeling for aerosol deposition in the mouth and throat: A comparison with experiment. J. Aerosol Sci. 31, 739-749.

Weibel, E.R. (1963). Morphometry of the Human Lung. Springer Verlag, Heidelberg.

Weibel, E.R. (1991). Design of airways and blood vessels considered as branching trees. In: The Lung: Scientific Foundations, Volume 1, pp. 711-720 (Eds-in-Chief, Crystal, R.G. and West, J.B.). Raven Press, New York.

Wilson, T.A. (1967). Design of the bronchial tree. Nature 2, 668-669.

Yeh, H.C. and Schum, G.M. (1980). Models of human lung airways and their application to inhaled particle deposition. Bull. Math. Biol. 42, 461-480.

Zeltner, T.B., Caduff, J.H., Gehr, P., Pfenninger, J. and Burri, P.H. (1987). The postnatal development and growth of the human lung. I. Morphometry. Respir. Physiol. 67, 247-268.

Chapter 3

Airflow in the respiratory system

A particle suspended in laminar flow closely follows an air streamline, except for some departure resulting from its intrinsic motion due to inertia, gravity, thermal forces, or electrostatic forces. A good understanding of airflow characteristics in the respiratory tract is therefore essential to studies of particle deposition.

Both macroscopic aspects of airflow and local aerodynamic characteristics have marked influences on the motion of an inhaled particle. The macroscopic aspects include distribution of inspired air to various lobes and individual airways, which are determined primarily by the relative resistance and compliance of each pathway. Local aerodynamic characteristics, such as velocity profiles of airflow at various cross sections of the respiratory tract, depend mainly on the structures of the airway segment under consideration and upstream airways.

As discussed in Chapter 2, there are several types of airway geometry in the respiratory tract, including bends, bifurcations, orifices, conduits with variable cross sections, expandable alveolated ducts, and wall surfaces with various features. Because of these complex airway structures, flow characteristics in the respiratory tract encompass a large variety of patterns. In addition, there is a wide range of inspiratory flow rates depending on the intensity of physical activity. Another complication arises from constantly moving boundaries of expanding and contracting airways. Although changes in lung volume during a cycle of respiration take place mostly in the alveolar region, the diameter of each airway segment in the tracheobronchial region also varies to some extent. Even the length and branching angle can change slightly during a breathing cycle.

Our understanding of the local aerodynamic characteristics derives mainly from experimental studies and numerical calculations using physical models of lung airways. No complete theoretical solution is currently available for airflow fields in the respiratory tract.

3.1 BREATHING DYNAMICS AND RESPIRATORY VOLUMES

The lungs have no skeletal muscle. The driving force for respiration is the movement of the thoracic cage, which consists of the ribs, sternum, thoracic vertebrae, diaphragm, and intercostal muscles. The diaphragm is the principal muscle of inspiration. Contraction of the diaphragm leads to enlargement of the

thoracic cage and lungs. In response air pressure drops in the alveolar region, thereby drawing ambient air into the respiratory tract. Relaxation of respiratory muscles at the end of inhalation allows to the lungs to recoil to the functional residual capacity.

Figure 3.1 illustrates the changes in lung volume during a complete cycle of breathing. The lung volume at the maximum inspiratory level is the total lung capacity (TLC). It is about 6-7 L for an average healthy adult. The residual volume (RV) represents the lung volume at the maximum expiratory level. It is about 20-30% of the total lung capacity for a healthy young adult but gradually increases with age. The difference between the total lung capacity and the residual volume is the vital capacity (VC).
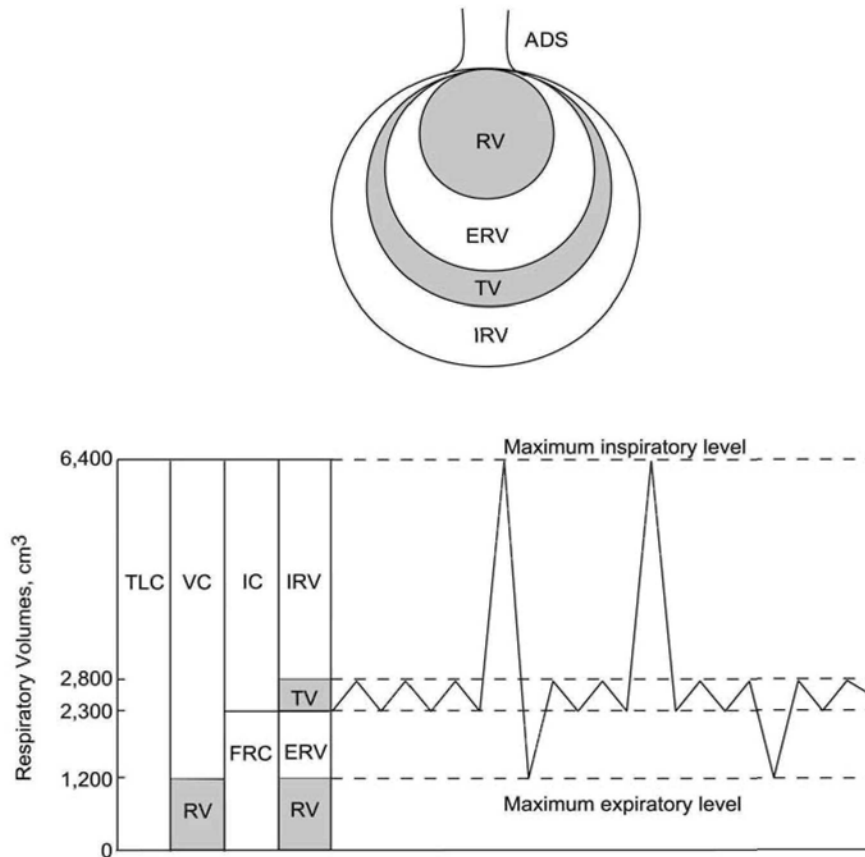
Fig. 3.1 Typical values of respiratory volumes in cm^3. ADS: anatomical dead space, RV: residual volume, ERV: expiratory reserve volume, TV: tidal volume, IRV: inspiratory reserve volume, TLC: total lung capacity, VC: vital capacity, IC: inspiratory capacity, FRC: functional residual capacity.

The volume of air inspired in a normal breath, termed tidal volume (TV or V_T), is about 0.45-0.60 L for a healthy adult at rest. During heavy work, the tidal volume may exceed 1.5 L. The lung volume at end-exhalation of a normal breath represents the functional residual capacity (FRC). It is determined by a balance between the inward recoil of the lungs and the outward recoil of the chest wall. The functional residual capacity is about 2.7 L for a female and 3.3 L for a male.

The inspiratory capacity (IC) is the difference between the total lung capacity and the functional residual capacity. The difference between the functional residual capacity and the residual volume is called the expiratory reserve volume (ERV), while the difference between the inspiratory capacity and the tidal volume is termed the inspiratory reserve volume (IRV).

The respiratory volumes can differ considerably between a normal adult and a patient with lung disease.

3.2 RESPIRATORY PHYSIOLOGY

An important parameter of respiratory physiology is minute ventilation. Also known as minute volume, it represents the volume of air inhaled per minute. If breathing frequency is expressed in number of breaths per minute, the minute volume is equal to the product of breathing frequency and tidal volume.

The minute ventilation varies with age and body mass. For an individual, the factors affecting minute ventilation include physical activity and state of health. Environmental factors such as ambient temperature, oxygen concentration in ambient air, irritants, and toxicants also have marked effects on minute ventilation.

The minute volume has a wide range of values. At low physical activities, it varies from about 1.5 L for a baby under one year old to about 10 L for an adult. Under the conditions of heavy exertion, an adult can have a minute volume of about 60 L. To adapt to low levels of atmospheric oxygen at high altitudes, the Tibetans have larger minute volumes.

For an individual, the physical activity level influences both the tidal volume and breathing frequency. Listed in Table 3.1 are the values of ventilation parameters used in the ICRP model (ICRP, 1994). A healthy adult male at rest breathes about 12 times a minute with a tidal volume of 0.75 L. During heavy work, the breathing frequency and tidal volume increase to about 26 breaths/min and 1.92 L, respectively.

Compared with adults, children have higher breathing frequencies and lower tidal volumes. The breathing frequency and tidal volume are about 20 breaths per minute and 0.18 L respectively for a 7-year old child, and about 30 breaths per minute and 0.07 L respectively for a 1-year old baby.

Table 3.1
Ventilation parameters used in the ICRP model (ICRP, 1994)

	Functional Residual Capacity (L)	Breathing Frequency (breaths/min)	Tidal Volume (L)
Male			
Sitting	3.30	12	0.75
Light Exercise	3.30	20	1.25
Heavy Exercise	3.30	26	1.92
Female			
Sitting	2.68	14	0.46
Light Exercise	2.68	21	0.99
Heavy Exercise	2.68	33	1.36

3.3 MACROSCOPIC ASPECTS OF AIRFLOW IN LUNG AIRWAYS

The network of lung airways consists of many parallel paths, each of which includes a large number of generations of airway segments connected in series. An important aspect of airflow in lungs is the distribution of inspired air among these parallel paths.

The flow rate and distribution of inspired air depend on airway resistance and parenchymal compliance, which are determined by the elastic properties of airway walls. Compliance represents the ratio of the change in volume to the change in pressure. The resistance to airflow, which is determined primarily by airway geometry and dimensions, occurs mainly in the nasal cavity and segmental bronchi (Generations 2 to 6). The nasal cavity contributes about 50% of the total airway resistance during normal nose breathing, while the trachea and larynx together contribute almost 70% of the total resistance during mouth breathing.

Because of variations in airway resistance and parenchymal compliance among different parts of the lungs, there are both spatial and temporal inequalities in ventilation distribution. Uneven airflow distribution and sequential ventilation can lead to marked differences in flow velocity in various airway segments of the same generation.

The distribution of inspired air is, in general, not proportional to the lung volume distal to any confluence point in the bronchial tree, regardless of whether the lung volume is equally divided. As a result, some parts have higher ratios of ventilation to lung volume (Milic-Emili et al., 1966). This is known as ventilation to volume inhomogeneity or ventilation asymmetry.

Experimental results suggest that the left lung tends to expand more than the right lung at higher lung volumes (Bennett et al., 1999). The experiments

use monodisperse aerosol containing ^{99m}Tc-labeled iron oxide particles with a mass median aerodynamic diameter of 3.5 μm. Healthy subjects inhale clean air to various end inspiratory lung volumes with a 40-cm³ bolus of aerosol injected near the end of inspiration (at the volumetric front depth of 70 cm³). Based on the posterior images obtained by gamma camera analysis, the ratio of particle deposition in the left and right lungs, normalized by the left-to-right ratio of lung volume, is 1.60 ± 0.45 (mean $\pm$ standard deviation) and 1.96 ± 0.72 at the end inspiratory lung volume of 70 and 85% total lung capacity, respectively. At 50% total lung capacity, the normalized deposition ratio is 1.37 ± 0.37. The results suggest that considerably more air goes to the left lung at higher lung volumes.

There is a tendency to fill and empty different parts of the lungs sequentially during a respiration cycle. The first portion of inspired air goes to the apical part of the lungs. During mid-inspiration, airflow is distributed to all parts of the lungs, but in the second half of inhalation an increasingly larger proportion goes to the basal part. The emptying of various parts of the lungs takes place in the reverse order during expiration. This pattern of sequential filling and emptying, known as the first-in last-out principle, was first hypothesized by Fowler (1949). Using boluses of ^{133}Xe to label sequential portions of inspired gas during vital-capacity inhalations by standing subjects, Dollfuss et al. (1967) have found that the hypothesis holds when inhalation begins from the residual volume. Experimental evidence of asynchronous ventilation has also been reported in other studies (Anthonisen et al., 1970; Fukuchi et al., 1980).

For inhalations beginning from functional residual capacity, Grant et al. (1974) have shown that the distribution of gas inspired at constant inspiratory flow rates (0.1-1.0 L/s) by subjects seating upright varies with flow rate over the first part of the tidal volume but becomes less dependent of flow rate in later parts of the tidal volume. At 0.1 L/s, basal ventilation exceeds apical but, at 1.0 L/s, apical ventilation exceeds basal.

Under the influence of gravity, the weight of lungs creates a pressure difference of about 0.8 kPa from the apical parts to the basal parts of the lungs of a healthy adult in the upright position. During normal breathing, the ventilation to volume ratio in the apical parts of the lungs is about 60% of that in the basal parts. In other words, the alveoli in the apical parts are well inflated but poorly ventilated, while those in the basal parts are poorly inflated but well ventilated. In addition, the regions with lower ventilation to lung volume ratios inspire more rapidly at the beginning of inspiration than at the end. Conversely, the regions with higher ventilation to lung volume ratios inspire more slowly at the beginning of a breath.

Disproportional distribution of airflow can also occur at bifurcations of smaller airways. Calculations using morphometric data show that, while the flow rate in an airway segment is on average proportional to the cross-sectional area, there are significant variations with the diameter of the parent tube and the branching angle of the major daughter (Phillips et al., 1994; Phillips and Kaye, 1997).

The discussions given above are based on experimental results obtained with healthy subjects. In patients with impaired airways, distribution of inspired air among various pathways is even less uniform, especially between normal part and damaged part of the lungs.

3.4 LOCAL AERODYNAMIC CHARACTERISTICS

In analyses of particle deposition in the respiratory tract, two distinct types of flow are of interest. One is the flow around a particle and the other the flow in a conduit. The flow around a particle, which is important in the analysis of drag force on a particle, will be discussed in Chapter 4.

3.4.1 General Concepts in Fluid Mechanics

Air flowing at sufficiently low velocities in a tube has orderly streamlines and therefore the flow is called laminar. The velocity at any point in a steady laminar flow does not change with time. At higher velocities, eddy motion appears and the flow becomes turbulent. A distinct feature of turbulent flow is that the velocity fluctuates randomly with time both in magnitude and direction.

The Reynolds number, a dimensionless parameter, is useful for describing the characteristics of fluid flow. It is proportional to the ratio of inertial forces to frictional forces acting on each small element of the fluid. The flow is laminar if frictional forces dominate (low Reynolds number) and turbulent if inertial forces dominate (high Reynolds number). The flows in two geometrically similar systems have similar flow characteristics if the Reynolds numbers are identical.

The Reynolds number for air flow in a circular tube is defined as

$$\text{Re} = \frac{d_t U}{\nu} \tag{3.1}$$

Here d_t is the tube diameter, U the average velocity in the tube, and ν the kinematic viscosity of air.

The flow in a circular tube is laminar if the Reynolds number is smaller than a critical value, about 2,300. Fully developed laminar flow in a tube has a parabolic velocity profile:

$$u_x = u_0 \left[1 - \left(\frac{r}{r_t} \right)^2 \right]$$ (3.2)

Here u_x is the axial velocity at a point with a radial distance r from the tube axis, u_0 the axial velocity at the tube axis, r the radial coordinate, and r_t the tube radius. It follows from Eq. (3.2) that u_0 is equal to $2U$.

The fully developed laminar flow in a circular tube is also known as Poiseuille flow. If the velocity profile at the inlet is not parabolic, it takes a certain length for the flow to become fully developed. The entrance length is given by

$$l_e = 0.03 d_t \, \text{Re} \qquad \text{for } 50 < \text{Re} < 2300$$ (3.3)

Here d_t is the tube diameter. For Re < 1, the ratio of the entrance length to the tube diameter is about 1.5.

Flow in a tube normally is turbulent when Re is higher than 2300. In the presence of disturbances at the inlet, the critical Reynolds number may be reduced to about 2000. The length for turbulent flow to become fully developed is about 40 tube diameters. When turbulent flow becomes fully developed, the time-averaged axial velocity has a relatively flat profile in the core but drops sharply over a thin boundary layer near the wall. The velocity at the tube axis is approximately equal to 1.2 U.

Because the outside wall of a daughter branch in an airway bifurcation curves gradually from the direction of the parent axis to that of the daughter axis, curved tubes have been used as an airway model for analyses of particle deposition in a bifurcation. In a curved tube, every element of airflow has to change its direction continuously as it proceeds downstream. In consequence a pair of secondary motions develop in the radial direction, with air moving from the core towards the outside edge of the bend and then returning to the inside edge along the wall region.

Fig. 3.2 depicts a pair of secondary flows in a cross section of a curved tube and the velocity profiles in two different planes. The axial velocity profile in plane of the bend has the shape of a distorted parabola with its peak shifted towards the outside edge. In the transverse plane, the axial velocity profile takes the shape of an M. As to be discussed in a later section, the flow pattern in a daughter tube of a bifurcation is similar to that in a curved tube depicted in Fig. 3.2.
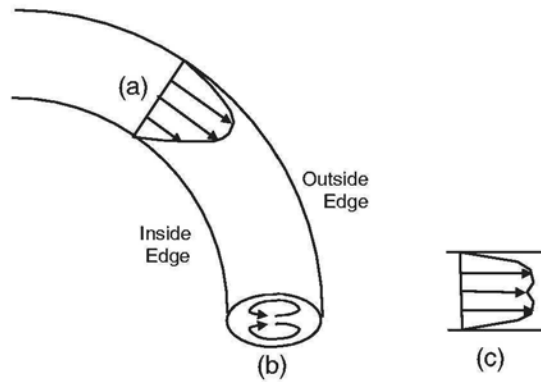
Fig. 3.2 Velocity profiles of laminar flow in a curved tube: (a) axial velocity profile in plane of bend, (b) secondary motions in a cross section, and (c) axial velocity profile in transverse plane.

The flow in a curved tube is characterized by the flow Reynolds number and the Dean number. The Dean number is defined as the ratio of the flow Reynolds number to the square root of the curvature ratio:

$$Dn = \frac{Re}{R_0^{1/2}} \tag{3.4}$$

Here the curvature ratio, R_0 ($= r_b/r_t$), is the ratio of the bend radius to the tube radius.

Flow patterns in many parts of the respiratory tract are considerably more complex than in straight or curved tubes. They have features such as jets and flow separation, which are absent in laminar and turbulent flows seen in straight and curved tubes of constant cross sections. Both experimental and theoretical methods are available for studies of flow in conduits of complex geometry. Qualitative observations of airflow patterns in physical models of lung airways can be made using smoke as a tracer. Alternatively, dye can be used as a tracer to observe patterns of water flow in airway models. Use of hot-wire anemometers provides data on velocity profiles.

In principle, the flow field in the respiratory tract can be calculated from the continuity and Navier-Stokes equations for an incompressible gas:

$$\nabla \cdot \mathbf{u} = 0 \tag{3.5}$$

$$\rho_g \frac{\partial \mathbf{u}}{\partial t} + \rho_g (\mathbf{u} \cdot \nabla)\mathbf{u} = -\nabla p + \mu \nabla^2 \mathbf{u} \qquad (3.6)$$

Here u is the gas velocity, ρ_g the gas density, p the pressure, and μ the gas viscosity.

Numerical solutions to the continuity and Navier-Stokes equations have been obtained for a number of idealized anatomical models of respiratory airways with appropriate inlet and outlet conditions. For some cases, the numerical solutions have been verified with experimental measurements using physical models of lung airways.

3.4.2 Overview of Flow Patterns in Respiratory Airways

The flow pattern varies from region to region in the respiratory tract, reflecting the marked changes in geometry of the airways. During the inspiratory phase, there is turbulence in the nasal cavity and larynx. Jets appear downstream of the ventricular and vocal folds. Flow is generally turbulent in the trachea and larger airways. In smaller airways, flow becomes laminar but the velocity profile is quite complex.

An overview on the wide variety of flow fields can be obtained from the average flow velocity and Reynolds number in each airway segment. Although the airway diameter decreases with increasing generation number, the total cross-sectional area of airways in a generation increases rapidly because the tube number doubles in each successive generation. As a consequence, the average flow velocity and Reynolds number drop sharply along a typical path of the respiratory tract.

Table 3.2 gives the average velocity and Reynolds number for constant flow with a tidal volume of 1,000 cm^3 and an inspiratory duration of 2 seconds. The Reynolds number is 2,084 in the trachea, but drops to 1.3 and 0.01 in transitional bronchioles (Generation 15) and alveolar sacs (Generation 23), respectively. With a Reynolds number higher than 2000, flow in the trachea is turbulent because of the disturbances created in the larynx.

The velocity profile at each cross section of an airway segment varies continuously during one complete cycle of respiration. It depends on many parameters, including geometry of the airway segment, flow Reynolds number, and velocity profile at the inlet cross section of the airway segment. Additional complication arises from the expansion and contraction of airways during a respiration cycle. The change in alveolar volume during a breath creates a complex flow pattern in alveolar ducts, where the airflow consists of two parts: one part moves in the axial direction and the other part goes in and out of adjacent alveoli.

Table 3.2

Characteristics of the respiratory tract of an average adult at about 75% total lung capacity (based on Weibel, 1991) and constant airflow with a tidal volume of 1,000 cm^3 and an inspiratory duration of 2 seconds. The lung volume = 4,800 cm^3. The kinematic viscosity of air at 37°C and 1 atm = 0.17 cm^2/s.

Generation Number	Number of Airways per Generation	Airway Diameter	Airway Length	Total Cross Section	Average Airflow Velocity	Average Airflow Reynolds Number
z	$n(z)$	$d_t(z)$	$l_t(z)$	$A(z)$	$u(z)$	Re
		(cm)	(cm)	(cm^2)	(cm/sec)	
0	1	1.80	12.0	2.54	197	2084
1	2	1.22	4.76	2.33	215	1540
2	4	0.83	1.90	2.13	236	1151
3	8	0.56	0.76	2.00	251	827
4	16	0.45	1.27	2.48	202	533
5	32	0.35	1.07	3.11	161	331
6	64	0.28	0.90	3.96	126	208
7	128	0.23	0.76	5.10	98	133
8	256	0.186	0.64	6.95	72	79
9	512	0.154	0.54	9.56	52	47
10	1,024	0.130	0.46	13.4	37	28
11	2,048	0.109	0.39	19.6	26	16
12	4,096	0.095	0.33	28.8	17	9.7
13	8,192	0.082	0.27	44.5	11	5.4
14	16,384	0.074	0.16	69.4	7.2	3.1
15	32,768	0.050	0.133	117	4.3	1.3
16	65,536	0.049	0.112	225	2.2	0.64
17	131,072	0.040	0.093	300	1.7	0.39
18	262,144	0.038	0.083	543	0.92	0.21
19	524,288	0.036	0.070	978	0.51	0.11
20	1,048,576	0.034	0.070	1,740	0.29	0.057
21	2,097,152	0.031	0.070	2,730	0.18	0.033
22	4,194,304	0.029	0.067	5,070	0.099	0.017
23	8,388,608	0.025	0.075	7,530	0.066	0.010

An important feature of respiratory flow is its cyclic nature. In spontaneous breathing, the expiratory phase is slightly longer than the inspiratory phase and there is usually a short pause between the two phases. The flow rate varies continuously with time during breathing. Although respiratory flow is cyclic in nature, the flow rate is not a sinusoidal function of time. During inhalation, the flow rate increases sharply at the beginning, remains at the peak rate for a major

part of the inspiratory phase, and then falls sharply to zero. The time profile of expiratory flow rate is almost identical in shape, but opposite in direction, to that of the inspiratory flow rate.

At this point it is important to note that some experiments on gas transport and particle deposition have been conducted using controlled breathing patterns in which both inspiratory and expiratory flow rates are held constant.

3.5 FLOW IN HEAD AIRWAYS

There are two inhalation routes, one through the nose and the other through the mouth. Nasal augmenters (normal nose breathers) use the nose at lower levels of physical activity, but take in about 50% of inspired air through the mouth during heavy exercise. For a mouth breather, the fraction of total inspiratory flow passing through the mouth is 30% at sleep and rest, but increases to 60 and 70% at the levels of light and heavy exercise, respectively (ICRP, 1994). These variations should be taken into consideration in calculating the flow Reynolds number for each portal of entry.

Airflow accelerates when it enters the nostrils and reaches the maximum velocity at the nasal valve. Turbulence appears downstream of the nasal valve, as a result of the sharp increase in airway cross section. At the nasopharyngeal region, the air streams from the two nasal passages merge and make a sharp turn into the pharynx. The peak axial velocity shifts towards the outside edge of the bend and secondary motions develop. Flow patterns in the pharynx depend on the position of the soft palate. The palate is forward against the tongue during nasal breathing, but moves to the middle of the airway when air is inhaled through both nose and mouth.

The oral passage extending from the mouth to larynx has the shape of a curved tube of variable cross-sectional area. As a consequence, the axial velocity profiles are skewed with the peak velocity shifted towards the outside edge of the bend. In addition, secondary flow vortices develop in the radial direction, with air moving from the core towards the outside edge of the bend and then returning to the inside edge along the wall region. The secondary flows have a pattern more complex than that shown in Fig. 3.2, because the cross-sectional area varies considerably along the oral passage. Recirculation zones appear at points where the cross section expands sharply, such as the lower part of the mouth and the inside edge of the bend near the pharynx.

Downstream of the ventricular folds are a flow separation zone and an asymmetric jet. Similar flow patterns appear in the section downstream of the vocal folds for the conditions of sedentary and light physical activity. Because of increase in the glottal aperture, flow decelerates and no jet forms in the vocal

folds during heavy breathing. Turbulence begins to appear at an inspiratory flow rate of 30 L/min. corresponding to the level of light physical activity.

There are a large number of experimental and theoretical studies on flow fields in head airways. Hahn et al. (1993) have measured velocity profiles in a physical model of the nasal cavity. Numerical simulation of airflow in the nasal passage has been made by Keyhani et al. (1995) and Sarangapani and Wexler (2000). Martonen et al. (1993) have obtained numerical solutions for laryngeal air flow in a two-dimensional model. By solving the steady-state Navier-Stokes and continuity equations numerically, Katz et al. (1997) have calculated the flow field in a three-dimensional larynx model during inhalation, taking into account the effect of glottal aperture modulation. The calculated pressure and velocity distributions show that the glottal aperture has a profound effect on laryngeal jets, recirculation zones, and circumferential flow. Li et al. (1996) has conducted numerical simulations of inspiratory flow in two- and three-dimensional models of oropharyngeal cavities.

More recently, Kleinstreuer and Zhang (2003) have employed a commercial finite-volume based program to simulate the flow field in an oral airway model extending from the mouth to trachea. A Reynolds averaged Navier-Stokes k-ω turbulence model has been used in analysis of the flow field in an idealized model of mouth (Matida et al., 2003). Zhang et al. (2004) have reported results of numerical calculations for the flow field in an upper airway model extending from the mouth to the airway segments of Generation 3. These calculations have generally given consistent results on flow patterns in extrathoracic airways.

3.6 FLOW IN TRACHEOBRONCHIAL AIRWAYS

Even under normal breathing conditions, flow separates from the wall and forms a jet downstream of the glottis. The disturbances lead to turbulent flow in the trachea and larger bronchi. The velocity profile at the entrance to the trachea is in the shape of a wedge and gradually becomes blunt as the flow proceeds downstream. Secondary flows developed in head airways persist into the inlet section of trachea.

As can be seen in Table 3.2, the Reynolds number drops sharply at each airway bifurcation. In consequence flow quickly becomes laminar as it proceeds downstream. However, flow patterns downstream of a bifurcation are quite complex because of the sharp change in flow direction.

Schroter and Sudlow (1969) have measured velocity profiles of laminar flow in symmetrical models of two successive bifurcations using a hot wire probe. In their study, the flow Reynolds number ranges from 100 to 1,500 (based on the conditions in the tube under consideration) and the velocity

profiles at the inlet of the first parent tube are either flat or parabolic. The diameters of the tubes in three successive generations are 2.54, 1.98, and 1.55 cm, respectively. The daughter tubes of the first bifurcation are 7 cm long. The parent and two daughter tubes in each bifurcation are in the same plane and the branching angle of each daughter tube is 35°. The results show that, in a daughter tube of the first bifurcation, the axial velocity profile during inhalation has the shape of a skewed parabola with the peak shifted towards the inner edge of the tube. A new velocity boundary layer develops on the inside edge downstream of the carinal ridge and, depending on the curvature of the wall surface in the transition zone, a flow separation zone may appear on the outside edge.

Fig. 3.3 shows a typical velocity profile in the plane of bifurcation in a daughter tube. The axial velocity profile in the plane normal to the bifurcation is M-shaped. Owing to sudden changes in flow direction at the bifurcation, two secondary flow streams appear downstream of the carinal ridge. The secondary flows combine with the axial flow to form a pair of helical streams in each daughter branch. Secondary flows have marked influences on particle deposition because the radial component of air velocity tends to bring particles closer to tube walls.

The flow characteristics in a parent tube during the expiratory phase are as complex as in a daughter branch during the inspiratory phase. While the flow rate during exhalation changes with time in a pattern similar to that during inhalation, the axial velocity profiles differ significantly between the two respiratory phases.
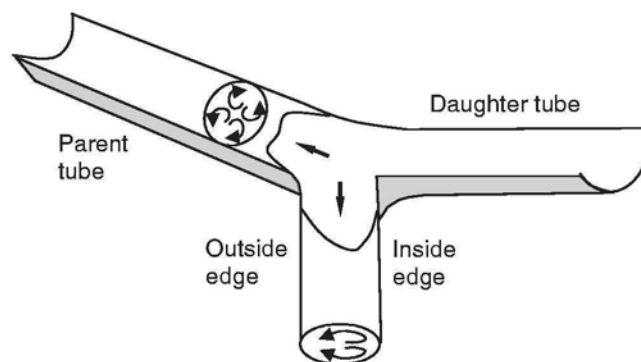
Fig. 3.3 A single bifurcation showing the axial velocity profiles in the plane of bifurcation in a daughter tube during inhalation and in the parent tube during exhalation. A pair of secondary flows is created in each daughter tube during inhalation, while two pairs are created in the parent tube during exhalation.

Schroter and Sudlow (1969) have studied flow profiles in the parent tube of single bifurcations during exhalation using a flat velocity profile at the ends of daughter tubes (the inlets for expiratory flow). The results show that, in the plane of bifurcation, the axial velocity profile in the parent tube has the shape of a flattened M when the two air streams from daughter tubes just merge, but subsequently develops into a flattened parabola. In the plane normal to the bifurcation plane, the axial velocity profile also begins with a flattened M-shape, but subsequently becomes very flat in form. Fig. 3.3 shows a typical axial velocity profile in the plane of bifurcation in the parent tube during exhalation. Secondary flows also appear downstream of a junction during exhalation, because of sudden changes in flow direction. The merging of air streams from the two daughter branches generates four helical streams in the parent tube. Clearly, the transient velocity profile at each cross-section of an airway segment during the expiratory phase is not a mirror image of that during the inspiratory phase.

Additional measurements of velocity profiles in physical models of bronchial airways have subsequently been reported by Olson et al. (1970), Pedley et al. (1971), and Chang and El Masry (1982).

3.6.1 Effects of Successive Bifurcations

In the tracheobronchial tree, the tube length is about 3 times the tube diameter for most generations (see Table 2.1). For Re > 100, the tube length to diameter ratio does not satisfy Eq. (3.3). As a result, flow in each tube downstream of a bifurcation rarely becomes fully developed before it arrives at the next bifurcation. The developing velocity profile near the end of a parent tube therefore propagates into its daughter tubes. It is evident that local aerodynamic characteristics in a repeatedly bifurcating airway are far more complex than in single bifurcations.

The velocity distribution at the inlet of a tube has significant effects on the velocity profile in the tube. Schroter and Sudlow (1969) have investigated velocity profiles of laminar flow in daughter tubes of the second bifurcation in symmetrical models of two successive bifurcations. The inlet velocity profile of a daughter tube in a second bifurcation (a bifurcation of the second generation) is far from flat and therefore the axial velocity profile in the tube is no longer a skewed parabola as in a daughter tube of the first bifurcation. The axial velocity distribution in a daughter tube of a second bifurcation depends to a great extent on the orientation of the second bifurcation relative to the first bifurcation. The profiles in plane of bifurcation and normal to plane of bifurcation both have the shape of an asymmetric M for the daughter tubes of a second bifurcation that is normal to the first bifurcation. In a daughter tube of a second bifurcation that is in plane with the first bifurcation, the axial velocity distribution is generally

asymmetric in plane of bifurcation but quite symmetric in the plane normal to the bifurcation. The two daughter tubes of a second bifurcation have somewhat different axial velocity profiles, depending on the position of the daughter tube relative to the parent tube.

Chen and Wang (1984) have solved the steady-state vorticity transport equation numerically for inspiratory flow in two-dimensional models of two successive bifurcations using a flat velocity profile at the inlet. The axial velocity profiles calculated for both symmetric and asymmetric airway models are similar in shape to the experimentally observed profiles (Schroter and Sudlow, 1969; Pedley et al., 1971; Chang and El Masry, 1982). However, the calculations using two-dimensional models could not provide information on secondary flow.

More detailed flow patterns in successive bifurcations have been obtained using computational fluid dynamics in recent years. Lee et al. (1996) have reported results of calculations for the flow fields in symmetric and asymmetric three-dimensional models of two successive bifurcations. More recently, Zhang et al. (2002) have obtained numerical solutions for cyclic flow in a three-dimensional model of three successive bifurcations.

3.6.2 Effects of the Shape of Transition Zone

Powerful computational software developed in recent years has made it possible to simulate the flow field in the complex structures of transition zone. The results of numerical calculations indicate that the shape of the transition zone has profound influences on flow field (Balásházy and Hofmann, 1993a, b; Heistracher and Hofmann, 1995; Balásházy and Hofmann, 2001). To examine the effects of transition geometry, these theoretical studies have made use of three different bifurcation models: a narrow bifurcation model, a wide bifurcation model, and a physiologically realistic model. The three bifurcation models differ mainly in the geometry of transition zone (see Chapter 2 for details). In essence, the physiologically realistic model of airway bifurcation consists entirely of smooth wall surfaces, whereas the narrow and wide bifurcation models are formed with walls containing sharp edges at surface intersections. The diameters of the parent tube and the two daughter branches are 0.56, 0.45, and 0.36 cm, respectively.

For a parabolic inspiratory flow of 1 L/s, the calculated axial velocity profiles in the daughter tubes of the physiologically realistic model are less asymmetric and the secondary flow is weaker in comparison with those in the narrow bifurcation model (Heistracher and Hofmann, 1995). The strong asymmetry in the inspiratory velocity profiles calculated using the narrow bifurcation model tends to persist through the entire lengths of the daughter branches, whereas the axial velocity profiles calculated using the

physiologically realistic model become symmetric before reaching the outlets of the daughter tubes. During both inspiratory and expiratory phases, a region of reverse flow (in the cross sections at the inlets to daughter tubes) appears in the vicinity of the carinal ridge of the physiologically realistic model. The absence of a region of reverse flow and the stronger secondary flow in the narrow bifurcation model are likely to give an overestimated deposition rate at the carinal ridge during inhalation.

3.6.3 Effects of the Shape of Carinal Ridge

Martonen et al. (1994b) have studied the effects of carinal ridge shape on flow pattern in airway bifurcations during inhalation. The parent and daughter tubes used in the calculations correspond, respectively, to the tubes of Generations 6 and 7 in Weibel's lung model A. The minute volumes are 7, 20, and 60 L, representing the conditions of sedentary, light activity, and heavy activity, respectively. The results indicate that the effects of carinal ridge shape vary with flow rate. At an inspiratory flow rate of 0.23 L/s, the effects tend to attenuate rapidly and the axial velocity profile becomes symmetric before reaching the outlets of the daughter tubes. However, the effects persist through the entire lengths of the daughter tubes and propagate to tubes of the succeeding generation at an inspiratory flow rate of 2 L/s. An asymmetric carinal ridge gives rise to an asymmetric velocity profile in the parent tube and different velocity profiles in the two daughter branches. Among the three shapes of symmetric carinal ridge studied, the saddle-shaped ridge has the highest magnitude of velocity just downstream of the ridge, followed by the blunt ridge and parabolic ridge in descending order.

3.6.4 Effects of Surface Structure

Numerical calculations for steady flow in two-dimensional models of airway segments with various configurations of cartilaginous rings show that the rings have marked effects on flow fields in tracheobronchial airways (Martonen et al., 1994a; Musante and Martonen, 2001a). Airway segments considered in the studies include Generations 2 to 5 of Weibel's lung model A. The ring diameter is one fifth of the tube diameter. The studies examined three different ring configurations: (1) contiguous rings, (2) regularly spaced rings with the first ring at the airway inlet, and (3) identical to the second configuration except that the first ring is placed at one ring diameter downstream from the inlet. The separation between neighboring rings is equal to one ring diameter in Configurations (2) and (3). The velocity profile at the airway inlet is flat. Even for the low flow rate corresponding to quiet breathing, the presence of the first ring forces the flow towards the centerline of the airway, leading to increase in velocity in the regions between the boundary

layers and the core. The resulting velocity profile in the axial direction has the shape of an M. The subsequent rings help propagate the entrance effect downstream and, as a result, the M-shaped velocity profile flattened very slowly. The effect is greater at higher flow rates. In the configurations with regularly spaced rings, the spacing between neighboring rings tends to attenuate the entrance effect faster but recirculation flow occurs in the region between rings.

Abnormal surface structures arising from airway disease also have considerable effects on flow field. Musante and Martonen (2001b) have reported results of numerical calculations for steady two-dimensional flow using two different airway configurations: (1) a semi-spherical tumor on the wall of a tube in Generation 11 of Weibel's lung model A and (2) a spherical tumor at the carinal ridge of a bifurcation consisting of tubes in Generations 7 and 8. The ratio of the tumor diameter to airway diameter is 0.8. Each daughter tube of the bifurcation has a branching angle of 35°. The velocity profile is flat at the inlet. The presence of a tumor on the wall has the effect of reducing the cross-sectional area, thereby increasing the flow velocity in the area just over the tumor. The disturbances propagate downstream, giving rise to a flattened velocity profile at the outlet. In the bifurcation studied, the presence of a tumor at the carinal ridge forces the flow to diverge just upstream of the tumor. Interestingly, the disturbances quickly die out in daughter tubes.

3.6.5 Effects of Oscillatory Flow

The velocity profile at each cross section of an airway varies with time continuously during a breathing cycle. Theoretical and experimental studies have indicated that the frequency of respiration is sufficiently low so that the flow can be considered as quasi-steady (Pedley et al., 1977; Chang and Menon, 1993). In other words, the velocity profile at any instant is identical to that in a steady flow with the same flow rate as the oscillatory flow at that instant.

For oscillatory laminar flow in a long straight tube, the Womersley number plays an important role:

$$\text{Wo} = \frac{d_t}{2}\left(\frac{\omega}{\nu}\right)^{1/2} \tag{3.7}$$

Here d_t is the tube diameter and ν the kinematic viscosity. The angular velocity ω is related to the frequency of oscillation f by $\omega = 2\pi f$. The Womersley number represents the ratio of the magnitude of oscillatory disturbance in the boundary layer to the magnitude of the steady flow boundary layer. If Wo < 1, a quasi-steady velocity profile can be assumed. It implies that the flow in the tube

responds instantaneously to the variation of the applied pressure gradient. When Wo is greater than 1, the laminar flow in the tube core have phase lags with respect to the applied pressure gradient (Womersley, 1955).

For flow with a non-parabolic velocity profile, Schroter and Sudlow (1969) have defined the Womersley number as

$$Wo = \delta \left(\frac{\omega}{\nu}\right)^{1/2} \qquad\qquad (3.8)$$

The thickness of the boundary layer δ is given by (Schlichting, 1979):

$$\delta = \left(\frac{\nu l_t}{U}\right)^{1/2} \qquad\qquad (3.9)$$

Here U is the average velocity and l_t the tube length. Combining Eqs. (3.8) and (3.9) gives

$$Wo = \left(\frac{\omega l_t}{U}\right)^{1/2} \qquad\qquad (3.10)$$

During normal breathing, the values of Wo are less than 1 for most airways in both inspiratory and expiratory phases. In the trachea and larger bronchial airways, the turbulence created at higher flow rates appears to have markedly reduced the magnitude of oscillatory disturbances (Pedley et al., 1977). Eq. (3.10) breaks down during the short pause between inhalation and exhalation, but the effect is negligible because the pause is very short. It is therefore reasonable to consider the flow in lung airways to be quasi-steady.

3.7 FLOW IN THE ALVEOLAR REGION

As shown in Table 3.2, the Reynolds number is less than 1 in tubes of Generations 16 through 23. In consequence the flow in the alveolar region is viscous. Air moves in two major directions in respiratory bronchioles and alveolar ducts. As a result of alveolar expansion during inhalation, part of inspired air moves in the axial direction to distal airways, while the remainder moves in the radial direction to surrounding alveoli. These two parts of flow reverse their direction as alveoli contract during exhalation.

Numerical calculations have been carried out by Tsuda and his associates for cyclic flow in an idealized model of expandable alveolated duct (Tsuda et

al., 1995; Otani et al., 1996). Fig. 3.4 shows a longitudinal section of the model used in their studies. The idealized model consists of a tube and a toroid. The toroid has the shape of an O-ring, which makes the three-dimensional airway axisymmetric and thereby greatly simplifies the flow field.

During a complete breathing cycle, the expansion and contraction of the tube and toroid is assumed to follow a sinusoidal function of time with the shape of the walls remaining geometrically self similar. Geometrical variables considered in the studies include the tube diameter (d_t), the toroid radius (r_a), and the width of the toroid opening (the chord length, l_a). The aperture angle, or the opening half angle (α, one half of the angle subtended by the chord), remains constant.

The results show that the flow field near the alveolar opening is very complex even in the highly simplified airway model. At low flow Reynolds number (the flow Reynolds number at peak inspiration is about 0.5), the time-dependent two-dimensional flow in the toroid is largely a function of the opening half angle and the ratio of the flow into the toroid to the flow in the tube. The flow ratio is small in the proximal part of the acinus, but increases along the axial direction.

For a given toroid geometry with a small opening half angle, there is a large region of recirculation near the proximal corner of the toroid (see Fig. 3.4) when the ratio of the flow into the toroid to the flow in the tube is small. The region of recirculation decreases in size as the flow ratio increases. When the flow ratio increases to a critical value, the recirculation disappears and the flow in the toroid becomes largely radial. For a given flow condition, the region of recirculation is larger in a toroid with a smaller opening half angle. During inspiration with recirculation in the toroid, a small portion of air flow in the tube enters the toroid from the proximal end of the toroid opening.
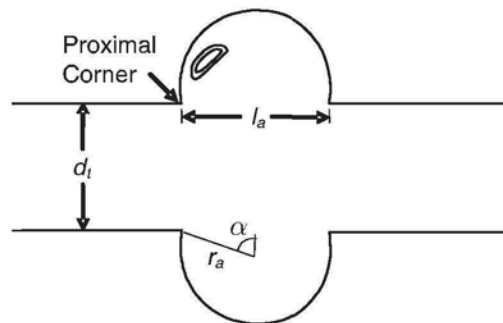
Fig. 3.4 An axisymmetric model of alveolar duct. α: aperture angle, r_a: toroid radius, l_a: chord length, d_t: tube diameter.

In the toroid, airflow approaches the walls in the direction of the wall movement, except in the middle region of the toroid where air recirculates slowly with a stagnation saddle point appearing near the proximal corner of the toroid opening. At a stagnation saddle point, two streamlines move in and two other streamlines move away at the same time. It is a characteristic structure of chaotic flow. Because the inertial effect of the fluid is negligible, the chaotic flow structure in the idealized model of an alveolated duct is primarily a result of the conduit geometry and time-dependent motion. Tsuda et al. (1995) have calculated the trajectories of two particles starting from slightly different positions near the stagnation saddle point. The separation between the two particles grows exponentially in time, making it essentially unpredictable within a short time after the two particles depart with each other. The chaotic flow clearly gives rise to a type of mixing different from turbulent flow.

The flow patterns during inspiration and expiration are nearly identical but in the opposite direction. Interestingly, the recirculation region remains in the proximal side of the toroid throughout the entire breathing cycle.

Tippe and Tsuda (1999) have conducted an experimental study on flow fields in an expandable large-scale silicone model of the alveolated duct described above. In addition to exchange of convective flow between the duct and alveolus, they have observed large recirculation flows in the expanding alveolus. The experiment has given support to the hypothesis that aerosol particles can deposit in the peripheral region of the lungs as a result of the expansion and contraction of the acinus during breathing.

Lee and Lee (2003) have solved the continuity and Navier Stokes equations for flow in an alveolated tube using a commercial program (CFX-F3D). The airway model consists of a straight circular tube surrounded by axisymmetric alveoli. There are a total of 30 identical cells in the structure. During a respiration cycle, the volume of the airway model changes linearly with time while the geometry remains self-similar. The results show that, during both respiratory phases, the axial velocity profile is flatter than the parabolic form in the distal section.

3.8 SUMMARY OF FLOW PATTERNS IN AIRWAYS

Table 3.3 summarizes the flow patterns in various subregions of the respiratory tract during a steady inspiratory flow of 500 cm³/s. The flow rate represents the level of light physical activity. At higher flow rates, turbulent flow can appear in large bronchial airways as well as the trachea. Increase in flow rate also can generate secondary flows in smaller bronchioles.

Table 3.3

Flow characteristics in various subregions of the respiratory tract during a steady inspiratory flow of 500 cm^3/s. The Reynolds numbers are calculated using the tube diameters in Weibel's lung model A listed in Table 2.1. Air is at 37°C.

Subregions	Reynolds Number	Flow Characteristics
Nose	Variable	Turbulence, secondary flow
Mouth	Variable	Turbulence, secondary flow, recirculation
Pharynx	Variable	Jet, secondary flow, recirculation, turbulence
Larynx	Variable	Jet, secondary flow, recirculation, turbulence
Trachea	2084	Jet, flow separation, turbulence
Bronchi Generations 1-3	827-1540	Mostly laminar, complex velocity profiles, strong secondary flow, flow separation
Bronchioles Generations 4-14	3.1-533	Laminar, less complex velocity profiles, secondary flow in larger bronchioles
Respiratory Bronchioles	0.21-1.30	Laminar, flow in axial and radial directions
Alveolar Ducts	0.017-0.110	Laminar, flow in axial and radial directions
Alveolar Sacs	0.01	Laminar, flow in axial and radial directions
Alveoli	Variable	Laminar, recirculation, chaotic

PROBLEMS

1.1 The location of an inhaled aerosol bolus in lungs has been expressed in terms of the distance from mouth or the depth of inhalation. Do these two terms represent the same physical concept?

1.2 The expansion and contraction of airways are dynamic in nature. They are functions of time depending on the compliance and resistance of the

airways. Discuss the effects of this dynamic behavior on the transient velocity profile in an airway.

REFERENCES

Anthonisen, N.R., Robertson, P.C. and Ross, W.R.D. (1970). Gravity-dependent sequential emptying of lung regions. J. Appl. Physiol. 28, 589.

Balásházy, I. and Hofmann, W. (1993a). Particle deposition in airway bifurcations – I. Inspiratory flow. J. Aerosol Sci. 24, 745-772.

Balásházy, I. and Hofmann, W. (1993b). Particle deposition in airway bifurcations –II. Expiratory flow. J. Aerosol Sci. 24, 773-786.

Balásházy, I. and Hofmann, W. (2001). Fluid dynamics and related particle deposition patterns in human airway bifurcations. In: Medical Applications of Computer Modeling: The Respiratory System, pp. 83-108 (Ed. Martonen, T.B.). WIT Press, Southampton, UK.

Bennett, W.D., Scheuch, G., Zeman, K.L., Brown, J.S., Kim, C., Heyder, J. and Stahlhofen, W. (1999). Regional deposition and retention of particles in shallow, inhaled boluses: Effect of lung volume. J. Appl. Physiol. 86, 168-173.

Chang, H.K. and El Masry, O.A. (1982). A model study of flow dynamics in human central airways, Part I: Axial velocity profiles. Respir. Physiol. 49, 75-95.

Chang, H.K. and Menon, A.S. (1993). Airflow dynamics in the human airways, In: Aerosols in Medicine: Principles, Diagnosis and Therapy, second revised edition, pp. 85-116 (Eds. Morén, F., Dolovich, M.B., Newhouse, M.T. and Newman, S.P.). Elsevier Science, Amsterdam.

Chen, H. and Wang, C.S. (1984). Steady laminar flow in two successive bifurcations. Chem. Eng. Commun. 31, 327-349.

Dollfuss, R.E., Milic-Emili, J and Bates, D.V. (1967). Regional ventilation of the lung, studied with boluses of ^{133}Xenon. Respir. Physiol. 2, 234-246.

Fowler, W.S. (1949). Lung function studies, III. Uneven pulmonary ventilation in normal Subjects and in patients with pulmonary disease. J. Appl. Physiol. 2, 283-299.

Fukuchi, Y., Cosio, M., Murphy, B. and Engel, L.A. (1980). Intraregional basis for sequential filling and emptying of the lung. Respir. Physiol. 41, 253.

Grant, B.J.B., Jones, H. A. and Hughes, J.M.B. (1974). Sequence of regional filling during a tidal breath of man. J. Appl. Physiol. 37, 158-165.

Hahn, I., Scherer, P.W. and Mozell, M.M. (1993). Velocity profiles measured for airflow through a large-scale model of the human nasal cavity. J. Appl. Physiol. 75, 2273-2287.

Heistracher, T. and Hofmann, W. (1995). Physiologically realistic models of bronchial airway bifurcations. J. Aerosol Sci. 26, 497-509.

International Commission on Radiological Protection (1994). Human Respiratory Tract Model for Radiological Protection, Annals of the ICRP, Publication 66. Elsevier Science, Tarrytown, NY.

Katz, I.M., Martonen, T.B. and Flaa, W. (1997). Three-dimensional computational study of inspiratory aerosol flow through the larynx: The effect of glottal aperture modulation. J. Aerosol Sci. 28, 1073-1083.

Keyhani, K., Scherer, P.W. and Mozell, M.M. (1995). Numerical simulation of airflow in the human nasal cavity. J. Biomed. Eng. 117, 429-441.

Kleinstreuer, C. and Zhang, Z. (2003). Laminar-to-turbulent fluid-particle flows in a human airway model. Int. J. Multiphase Flow 29, 271-289.

Lee, D.Y. and Lee, J.W. (2003). Characteristics of particle transport in an expanding or contracting alveolated tube. J. Aerosol Sci. 34, 1193-1215.

Lee, J.W., Goo, J.H. and Chung, M.K. (1996). Characteristics of inertial deposition in a double bifurcation. J. Aerosol Sci. 27, 119-138.

Li, W.I., Perzl, M., Heyder, J., Langer, R., Brain, J.D., Englmeier, K.-H., Niven, R.W. and Edwards, D.A. (1996). Aerodynamics and aerosol particle deaggregation phenomena in model oral-pharyngeal cavities. J. Aerosol Sci. 27, 1269-1286.

Martonen, T.B., Zhang, Z. and Lessmann, R.C. (1993). Fluid dynamics of the human larynx and upper tracheobronchial airways. Aerosol Sci. Technol. 19, 133-156.

Martonen, T.B., Yang, Y. and Xue, Z.Q. (1994a). Influences of cartilaginous rings on tracheobronchial fluid dynamics. Inhal. Toxicol. 6, 185-203.

Martonen, T.B., Yang, Y. and Xue, Z.Q. (1994b). Effects of carinal ridge shapes on lung airstreams. Aerosol Sci. Technol. 21, 119-136.

Matida, E.A., DeHaan, W.H., Finlay, W.H. and Lange, C.F. (2003). Simulation of particle deposition in an idealized mouth with different small diameter inlets. Aerosl Sci. Technol. 37, 924-932.

Milic-Emili, J, Henderson, J.A., Dolovich, M.B., Trop, D., Kaneko, K. (1966). Regional distribution of inspired gas in the lung. J Appl Physiol. 21, 749-759.

Musante, C.J. and Martonen, T.B. (2001a). Computational fluid dynamics in human lungs. I: Effects of natural airway features. In: Medical Applications of Computer Modeling: The Respiratory System, pp. 131-145 (Ed. Martonen, T.B.). WIT Press, Southampton, UK.

Musante, C.J. and Martonen, T.B. (2001b). Computational fluid dynamics in human lungs. II: Effects of airway disease. In: Medical Applications of Computer Modeling: The Respiratory System, pp. 147-164 (Ed. Martonen, T.B.). WIT Press, Southampton, UK.

Olson, D.E., Dart, G.A. and Filley, G.F. (1970). Pressure drop and fluid flow regime of air inspired into the human lung. J. Appl. Physiol. 28, 482-494.

Otani, Y., Butler, J.P., Emi, H. and Tsuda, A. (1996). Flow-induced mixing at low Reynolds number in an expanding and contracting alveolus model, In: Aerosol Inhalation: Recent Research Frontiers, Proceedings of the International Workshop on Aerosol Inhalation, Lung Transport, Deposition and the Relation to the Environment: Recent Research Frontiers, Warsaw, Poland, September 14–16, 1995, pp. 187-193. (Eds. Marijnissen, J.C.M. and Gradoń, L.). Kluwer, Dordrecht, Netherlands.

Pedley, T.J., Schroter, R.C. and Sudlow, M.F. (1971). Flow and pressure drop in systems of repeatedly branching tubes. J. Fluid Mech., 46, 365-383.

Pedley, T.J., Schroter, R.C. and Sudlow, M.F. (1977). Gas flow and mixing in the airways. In: Bioengineering aspects of the Lung, pp163-265 (Ed. West, J.B.). Marcel Dekker, New York.

Phillips, C.G., Kaye, S.R. and Schroter, R.C. (1994). A diameter-based reconstruction of the branching pattern of the human bronchial tree. Part I: Description and application. Respir. Physiol. 98, 193-217.

Phillips, C.G. and Kaye, S.R. (1997). On the asymmetry of bifurcations in the bronchial tree. Respir. Physiol. 107. 85-98.

Sarangapani, R. and Wexler, A.S. (2000). Modeling particle deposition in extrathoracic airways. Aerosol Sci. Technol. 32, 72-89.

Schlichting, H. (1979). Boundary Layer Theory. McGraw-Hill, New York.

Schroter, R.C. and Sudlow, M.F. (1969). Flow patterns in models of the human bronchial airways. Respir. Physiol. 7, 341-355.

Tippe, A. and Tsuda, A. (1999). Recirculating flow in an expanding alveolar model: Experimental evidence of flow-induced mixing of aerosols in the pulmonary acinus. J. Aerosol Sci. 31, 979-986.

Tsuda, A., Henry, F.S. and Butler, J.P. (1995). Chaotic mixing of alveolated duct flow in rhythmically expanding pulmonary acinus. J. Appl. Physiol. 79, 1055-1063.

Weibel, E.R. (1991). Design of airways and blood vessels considered as branching trees. In: The Lung: Scientific Foundations, Volume 1, pp. 711-720 (Eds-in-Chief, Crystal, R.G. and West, J.B.). Raven Press, New York.

Womersley, J.R. (1955). Oscillatory motion of a viscous liquid in a thin walled elastic tube. Phil. Mag. Ser. 7, 46, 199-221.

Zhang, Z., Kleinstreuer, C. and Kim, C.S. (2002). Cyclic micron-size particle inhalation and deposition in a triple bifurcation lung airway model. J. Aerosol Sci. 33, 257-281.

Zhang, Z., Kleinstreuer, C., Kim, C.S. and Cheng, Y.S. (2004). Vaporizing microdroplet inhalation, transport, and deposition in a human upper airway model. Aerosol Sci. Technol. 38, 36-49.

Chapter 4

Behavior of aerosol particles

An aerosol consists of a gas and the particles suspended in the gas. The particles can be either liquid or solid. While liquid droplets are normally spherical, solid particles can have a variety of shapes. For a spherical particle, the physical diameter is a natural measure of its size. To express the size of a nonspherical particle, a convenient approach is to use an equivalent diameter, which is defined as the diameter of a sphere that has the same value in a specified property as the particle under consideration. For example, a commonly used equivalent diameter is the projected area diameter, sometimes referred to as geometric diameter. It is defined as the diameter of a circle that has the same area as the projected area of the particle under consideration.

An aerosol in which all suspended particles are of the same size is called a monodisperse aerosol. Test aerosols carefully produced in the laboratory are usually monodisperse. Atmospheric aerosols are polydisperse, with a wide range of particle sizes, because they are generated by several different mechanisms.

The count median diameter and mass median diameter are two statistical quantities useful for providing a representative particle size in polydisperse aerosols. By definition, one half of the total number of particles in an aerosol is contributed by particles larger than the count median diameter. Similarly, one half of the total mass of particles is contributed by particles larger than the mass median diameter.

The probability density function, or frequency function, is a useful mathematical tool for characterizing the distribution of particle size in a polydisperse aerosol. Many polydisperse aerosols fit the lognormal distribution quite well. A lognormal count distribution has the following probability density function

$$f(d_p) = \frac{1}{\sqrt{2\pi}\, d_p \ln\sigma_g} \exp\left[-\frac{(\ln d_p - \ln d_g)^2}{2(\ln\sigma_g)^2} \right] \qquad (4.1)$$

Here d_g and σ_g are the geometric mean diameter and geometric standard deviation, respectively. In an aerosol with a lognormal distribution, the geometric mean diameter is the same as the count median diameter.

Elongated particles, such as asbestos and man-made vitreous fibers, are distributed with respect to two dimensions, diameter and length. The bivariate

lognormal distribution has been used to characterize the size distribution of man-made mineral fibers (Schneider and Holst, 1983). It has the following probability density function

$$f(d_f, l_f) = \frac{1}{2\pi d_f l_f (1 - \tau_{dl}^2)^{1/2} \ln \sigma_{gd} \ln \sigma_{gl}} \exp\left[-\frac{A^2 + B^2 - 2\tau_{dl}AB}{2(1 - \tau_{dl}^2)} \right] \qquad (4.2)$$

$$A = \frac{\ln d_f - \ln d_{fg}}{\ln \sigma_{gd}} \qquad (4.3)$$

$$B = \frac{\ln l_f - \ln l_{fg}}{\ln \sigma_{gl}} \qquad (4.4)$$

Here d_f and l_f are the fiber diameter and length, respectively; σ_{gd} and σ_{gl} are respectively the geometric standard deviations for the fiber diameter and length; τ_{dl} is the correlation between $\ln l_f$ and $\ln d_f$; d_{fg} and l_{fg} are the geometric mean diameter and length of fibers, respectively.

Particle size can undergo changes through a number of physical and chemical processes, including condensation, evaporation, chemical reactions, and coagulation. In addition, particles can deposit on surfaces at rates depending on particle size. As a result, the particle size distribution of an aerosol continuously evolves from the time it is generated. In ambient air, particles are normally in the size range of 10 nm -100 μm. Particles larger than 100 μm settle out quickly, while those smaller than 10 nm coagulate rapidly. Particles in various size intervals are given specific names: particles smaller than 0.1 μm in geometric diameter are known as ultrafine particles, and those smaller than 2.5 and 10 μm in aerodynamic diameter (an equivalent diameter to be defined later) are called $PM_{2.5}$ and PM_{10}, respectively.

Particles suspended in a flowing gas follow the flow quite closely. In laminar flow, the trajectory of a particle departs slightly from a local gas streamline as a result of particle inertia, gravitational force, thermal force, or electrostatic force. Deposition takes place when a particle comes into contact with a surface, such as airway walls in the respiratory tract. Fig. 4.1 depicts five important mechanisms of particle deposition in lung airways. These mechanisms are discussed in the sections that follow. For a more comprehensive treatment of aerosol properties and behavior, readers are referred to Friedlander (2000), Hinds (1999), Reist (1993), Vincent (1995), and Willeke and Baron (2001).
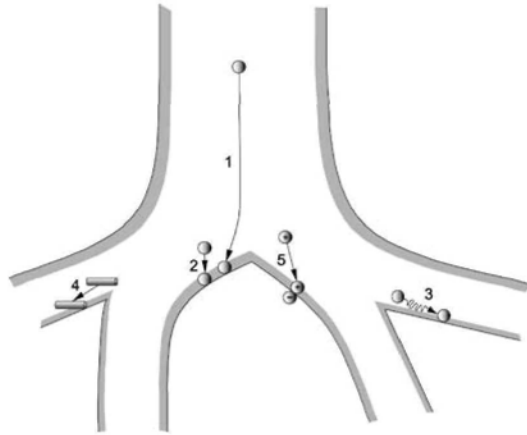
Fig. 4.1 Mechanisms of particle deposition in the respiratory tract: 1. inertial impaction, 2. gravitational settling, 3. Brownian motion, 4. interception, 5. electrostatic forces. Turbulent deposition, another important mechanism, is not shown in the figure.

4.1 DRAG FORCE

When a particle moves through a gas, the surrounding gas molecules have a tendency to resist its motion. The total resisting force, also known as drag force, for a spherical particle is proportional to its diameter d_p, relative velocity u_p, and gas viscosity μ:

$$F_d = 3\pi\mu d_p u_p$$

$$= \frac{24}{\mathrm{Re_p}}\left(\frac{\pi}{4} d_p^2\right)\left(\frac{1}{2} \rho_g u_p^2\right) \qquad \text{for } \mathrm{Re_p} < 1.0 \qquad (4.5)$$

Here $\mathrm{Re_p}$ is the particle Reynolds number and ρ_g the gas density. The particle Reynolds number is a dimensionless group related to the particle diameter, relative velocity, and kinematic viscosity of gas ν:

$$\mathrm{Re_p} = \frac{d_p u_p}{\nu} \qquad (4.6)$$

It can be seen from the above equation that the particle Reynolds number represents the ratio of inertial forces to viscous forces. The inertial forces can be neglected when $Re_p < 1$.

Eq. (4.5) is known as Stokes law. It holds for rigid spherical particles moving at constant velocity relative to gas flow. The drag calculated by Stokes law has an error of 12% at $Re_p = 1.0$. The error decreases with decreasing particle Reynolds number.

An important assumption of Stokes law is that the gas at particle surface has zero velocity relative to the particle. This assumption holds well when the particle has a diameter much larger than the mean free path of gas molecules. The mean free path is the average distance traveled by a gas molecule between two successive collisions. In analyses of the interaction between gas molecules and particles, it is convenient to use the Knudsen number Kn, a dimensionless number defined as the ratio of the mean free path to particle radius. For Kn of the order of unity or larger, the drag force is smaller than predicted by Stokes law. Conventionally this condition is described as a result of slip on the particle surface. To account for this effect, Cunningham (1910) has proposed a correction factor, (1 + 1.26Kn). When the right-hand side of Eq. (4.5) is multiplied by the Cunningham correction factor, Stokes law can be used to predict the drag force for particles with a diameter about the same as the mean free path of gas molecules. The range of applicability of Stokes law is further extended by an expression of the form:

$$C_c = 1 + Kn \left[1.257 + 0.4 \exp(-1.1/ Kn) \right] \tag{4.7}$$

This empirically developed expression, now known as the slip correction factor, agrees well with experimental data for a wide range of particle sizes (Davies, 1945). At ambient conditions, the mean free path of air molecules is proportional to the absolute temperature and inversely proportional to the pressure. As a consequence, the slip correction factor increases with increasing temperature.

4.2 GRAVITATIONAL SETTLING

A settling particle quickly reaches a constant velocity (known as the terminal velocity) as a result of balancing between the gravitational force and drag force. Equating the drag force to the force of gravity give the following equation for settling velocity:

$$v_s = \frac{\rho \, d_p^2 \, g \, C_c}{18 \, \mu} \qquad \text{for } \mathrm{Re_p} < 1.0 \qquad (4.8)$$

Here ρ is the particle density. The buoyancy force of air is neglected in derivation of the above expression.

The particle size and density are two important influencing parameters as the settling velocity is directly proportional to the particle density and the square of particle diameter. The slip correction factor also depends on particle size, but the correction is small for particles larger than one micrometer in diameter. In the range of temperature between 223 and 773 K, air viscosity is proportional to $T^{0.74}$. However, the settling velocity changes little with temperature under ambient conditions, because both the viscosity and slip correction factor increase with increasing temperature.

A nonspherical particle generally has drag higher than a spherical particle of the same volume. To account for the increase in drag force due to nonsphericity, a dynamic shape factor based on equivalent volume diameter has been introduced. The equivalent volume diameter is defined as the diameter of a sphere that has the same volume as the particle under consideration. Incorporating the dynamic shape factor and slip correction factor in Eq. (4.5) gives the following expression for drag on a nonspherical particle:

$$F_d = \frac{3 \pi \mu \, u_p \, d_e \, \chi}{C_c(d_e)} \qquad (4.9)$$

Here χ is the dynamic shape factor, d_e the equivalent volume diameter of the particle, and $C_c(d_e)$ the slip correction factor for a sphere with a diameter d_e.

The dynamic shape factor of most nonspherical particles falls in the range of 1.1 to 1.9 (Mercer, 1973). For example, the dynamic shape factor is 1.36 for quartz dust, 1.57 for sand particles, and 1.88 for talc powder. The dynamic shape factor for a long cylinder with an aspect ratio (length to diameter) of 10 is only about 1.2 when settling with the axis in the vertical direction (Hinds, 1999).

When the effect of nonsphericity is taken into consideration, the expression for the terminal settling velocity becomes

$$v_s = \frac{\rho d_e^2 \, g \, C_c(d_e)}{18 \, \mu \chi} \qquad (4.10)$$

The aerodynamic diameter is an equivalent diameter widely used in analysis of particle inertia. It is defined as the diameter of a sphere with a standard density (1,000 kg/m^3 or 1 g/cm^3) that has the same settling velocity as the particle under consideration.

An important problem in inhaled particles is deposition of particles from flow in an airway. For particles settling from fully developed laminar flow in a horizontal tube, the fraction of entering particles that deposit in the tube is given by (Thomas, 1958):

$$\eta = \frac{2}{\pi}\left[2S(1 - S^{2/3})^{1/2} - S^{1/3}(1 - S^{2/3})^{1/2} + \arcsin S^{1/3} \right] \tag{4.11}$$

The dimensionless parameter for gravitational settling from laminar flow, S, is defined by the expression

$$S = \frac{3v_s l_t}{4U d_t} \tag{4.12}$$

Here l_t is the tube length, d_t the tube diameter, and U the average flow velocity in the circular tube. The above expression for deposition efficiency was first derived by Thomas (1958) using the concept of settling pattern and subsequently by Pich (1972) using the concept of limiting trajectory. A limiting trajectory is the trajectory of a particle that just barely escapes deposition in the tube. In other words, it is the trajectory that separates the particles depositing in the tube from those penetrating through the tube.

For gravitational deposition from laminar flow in inclined channels, the deposition efficiency can be calculated using the concepts of particle trajectory function and limiting trajectory (Wang, 1975). The trajectory function used to describe particle motion is equivalent to the stream function used in fluid flow. For particles settling from laminar flow, Walton (1954) has demonstrated that the number concentration of particles, n, along a particle trajectory remains unchanged if the effect of particle inertia can be neglected. In the analysis of particle motion, it is convenient to use the concept of trajectory tube, called dust flow-tube by Walton (1954). It is defined as the surface formed by all the trajectories that pass through a closed curve. The flow rate of particles in a trajectory tube can be calculated by taking a surface integral of the product, n·u$_p$, over its cross section.

For particles settling from downhill flow in a circular tube that inclines at an angle ϕ with respect to gravity, the fraction of entering particles that deposit in the tube is given by (Wang, 1975):

$$\eta = 1 - \frac{2}{\pi}\arcsin(1 - \zeta^2)^{1/2} + \frac{(1 - \zeta^2)^{1/2}}{\pi\left(1 + \frac{v_s\cos\phi}{U}\right)}\left[4S\sin\phi - \left(2 + \frac{v_s\cos\phi}{U}\right)\zeta\right]$$

(4.13)

$$\zeta = \frac{S\sin\phi}{1 + \frac{3v_s\cos\phi}{4U}}$$

(4.14)

The parameter S is given by Eq. (4.12). In the analysis, it is assumed that the inlet and outlet cross sections of the tube are normal to the tube axis. For a horizontal tube, $\phi = 90°$, and Eq. (4.13) reduces to Eq. (4.11).

The analysis for uphill flow in an inclined circular tube is more complex because some particles fall back out of the inlet section (it is assumed that no particle falls back into the tube after leaving). Wang (1975) has given a detailed analysis of this case.

4.3 INTERCEPTION

When a particle following an air streamline comes within a particle radius from a surface, it makes contact with the surface even if its trajectory does not deviate from the streamline. This mechanism of deposition is called interception. It is a function of interception parameter, defined as the ratio of particle size to the characteristic length of the system such as an airway diameter in the respiratory tract.

Interception is the only mechanism of deposition if a particle has no intrinsic motion. Under such conditions, only those particles that are moving right next to the walls can deposit. In respiratory deposition, interception is important only for long fibers. Elongated particles tend to move with their axes parallel to the streamlines and therefore their aerodynamic diameters are much smaller than their lengths. Long fibers can sneak through numerous turns to reach airways of very small diameters, where they have a high probability to make contact with airway surfaces.

4.4 INERTIAL IMPACTION

For a particle larger than a few micrometers in diameter, its inertia plays an important role when it moves in a flow that changes direction sharply such as in the transition zone of an airway bifurcation. A large particle cannot make a

sharp turn as easily as gas molecules and therefore takes a trajectory not as curvy as the turning streamlines.

The trajectory of a particle moving relative to airflow can be analyzed using the equation of motion, which is obtained from a force balance on the particle. The drag of air on a particle obeys Stokes law when the particle Reynolds number is small. Such a particle is called a Stokesian particle.

According to Stokes law, the drag is directly proportional to the relative velocity. For Stokesian particles, it is convenient to define a mechanical mobility as follows:

$$B = \frac{C_c}{3\pi\mu d_p} \tag{4.15}$$

The mechanical mobility is the inverse of the Stokes friction coefficient.

For a Stokesian particle moving relative to airflow, a force balance gives the following equations of motion in the x direction and in vector form, respectively:

$$m_p \frac{du_{px}}{dt} = -\frac{1}{B}(u_{px} - u_x) + m_p g_x \tag{4.16}$$

$$m_p \frac{d\mathbf{u}_p}{dt} = -\frac{1}{B}(\mathbf{u}_p - \mathbf{u}) + m_p \mathbf{g} \tag{4.17}$$

Here m_p is the particle mass and g_x the gravitational acceleration in the x-direction. u_x and u_{px} are, respectively, the air velocity and particle velocity in the x direction. In the derivation of the above equations, it is assumed that Stokes law applies even though the particle does not move at constant relative velocity. The validity of this assumption has been discussed by Friedlander (2000).

In the absence of external forces, the equation of motion can be written in the following dimensionless form

$$\text{Stk} \frac{d\mathbf{u}_p^*}{dt^*} = -(\mathbf{u}_p^* - \mathbf{u}^*) \tag{4.18}$$

The Stokes number is defined by

$$\text{Stk} = \frac{\rho d_p^2\, U\, C_c}{18\,\mu l} \tag{4.19}$$

The dimensionless time, t^*, and dimensionless velocity vectors, $\mathbf{u_p}^*$ and $\mathbf{u}^*$, are obtained by scaling the time and velocity vectors, respectively, by the characteristic time l/U and the characteristic velocity U. The system under consideration has a characteristic length l. It is important to note that different characteristic lengths have been used in the literature for the same geometric system. As a result, Stokes number may differ in values depending on the definition of characteristic length.

To calculate particle trajectories from Eq. (4.18), appropriate flow field and initial conditions are needed. When the flow velocity is low compared with the speed of sound and the volume fraction of particles in the aerosol is less than a few percentage points, the presence of particles has little effect on the flow field. Under these conditions, the flow field can be obtained from the continuity and Navier-Stokes equations and then used for trajectory calculations.

Computation for a particle trajectory is started from a given position at the inlet cross section of the system, say a curved tube. A trajectory that comes within one particle radius from a wall surface represents a deposited particle. It can be seen from the dimensionless transport equations and boundary conditions that the particle trajectory depends on three dimensionless groups: the Stokes number, interception parameter and flow Reynolds number. Two geometrically similar systems with different values of physical parameters have identical solutions for inertial deposition if each of these three dimensionless groups is identical between the two systems. The similitude law is useful for theoretical analysis as well as for interpretation of experimental data.

The rate of deposition is usually expressed in terms of deposition flux or deposition efficiency. Deposition flux is the number of particles deposited over a unit area of wall surface in a unit time. Because particle trajectories do not cross each other, deposition flux at any point on a wall surface can be calculated by tracking the trajectories of deposited particles from the inlet cross section to the site of deposition. This is best done by considering a small surface element on the wall and tracking only those particles that deposit on the perimeter of that surface element. The initial positions of these deposited particles define a corresponding area element at the inlet cross section. It is evident that the particles passing through this small area element at the inlet deposit in the small surface element on the wall under consideration. The rate at which particles pass through the small area element at the inlet can be calculated using the particle concentration and flow velocity at that area element. This is also the rate at which particles deposit on the small surface element on the wall.

Deposition efficiency can be calculated using the concept of limiting trajectories. The initial positions of limiting trajectories divide the inlet cross section into two areas. The particles that enter through one of the two areas

deposit in the system, while those enter through the other area do not deposit. Integrating the product of particle concentration and flow velocity over the first area gives the rate of particle deposition in the system. Deposition efficiency is obtained by dividing the rate of deposition by the rate at which particles enter the system.

Two other parameters useful for analysis of inertial impaction are relaxation time τ and stop distance s. Relaxation time represents the time a particle takes to adjust its velocity when it is subject to a new set of forces. Stop distance is defined as the maximum distance a particle with a given initial velocity continues to travel in still air before it comes to a stop in the absence of external forces. Application of Stokes law gives the following expressions for the relaxation time and stop distance:

$$\tau = m_p B = \frac{\rho d_p^2 C_c}{18\,\mu} \qquad \text{for } Re_p < 1 \qquad (4.20)$$

$$s = v_0\,\tau \qquad \text{for } Re_p < 1 \qquad (4.21)$$

Here v_0 is the initial velocity of particle. The mechanical mobility B is given in Eq. (4.15). Eq. (4.21) states that the stop distance of a particle is equal to the product of the initial velocity and relaxation time, while Eq. (4.20) indicates that the relaxation time is proportional to the square of particle diameter. It follows that a larger particle with a higher initial velocity can continue to move a longer distance before it stops. Under ambient conditions, the relaxation time changes little with temperature, because both the slip correction factor and air viscosity increase with increasing temperature.

The Stokes number defined in Eq. (4.19) is simply the ratio of the stop distance to a characteristic length of the system. As an example, if the tube radius, d_t, is taken as the characteristic length of a curved tube, the Stokes number is

$$Stk = \frac{\tau\,U}{d_t/2} = \frac{\rho_0\,d_a^2\,U\,C_c}{9\,\mu\,d_t} \qquad (4.22)$$

Here the standard density and aerodynamic diameter are used instead of the particle density and diameter.

As mentioned in Chapter 3, curved tubes have been used as an airway model for study of inertial impaction because of similarity in flow pattern between a curved tube and a daughter tube of a bifurcation. The flow in a

curved tube with a sufficiently large curvature ratio of the bend is characterized by the Reynolds and Dean numbers.

From dimensional considerations, it can be shown that the impaction efficiency of a bend for Stokesian particles is a function of four dimensionless groups: the Stokes number, interception parameter, flow Reynolds number, and curvature ratio of the bend. For Stk $\ll$ 1 and large values of Re, the impaction efficiency can be approximated by (Cheng and Wang, 1981):

$$\eta = \left(\frac{2}{\pi} + \frac{1}{R_0} + \frac{4}{3\pi R_0^2} \right) \text{Stk} \cdot \theta_b \qquad \text{for a bend with angle } \theta_b \qquad (4.23)$$

$$\eta = \left(1 + \frac{\pi}{2R_0} + \frac{2}{3R_0^2} \right) \text{Stk} \qquad \text{for a 90° bend} \qquad (4.24)$$

Here R_0 (= r_b/r_t) is the curvature ratio of the bend, r_b the bend radius, r_t the tube radius, and θ_b the angle subtended by the bend with respect to the origin (see Fig. 4.2). These expressions are based on an idealized flow in a bend (Cheng and Wang, 1975). In the idealized flow, the secondary flow is assumed to be negligible and the axial flow velocity normalized by the average velocity, u_θ/U, is equal to the distance from the axis of the bend (the z-axis) divided by the bend radius. It is an approximation to the skewed parabolic profile normally seen in a bend. These expressions for inertial impaction have applications in calculations of inertial deposition in lung bifurcations. More recently, Cheng et al. (1999) have shown that inertial impaction in the oral airway can be modeled as deposition in a 180° bend using the idealized flow, which appears to be a good approximation for turbulent flow in the oral airway.
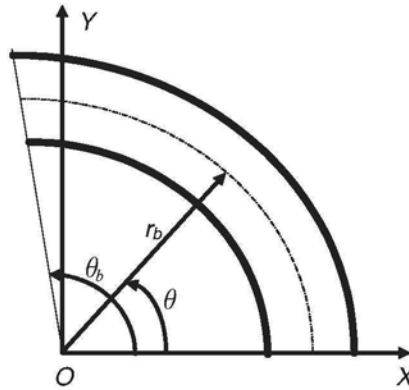
Fig. 4.2 System of x-y coordinates for a bend with angle θ_b.

4.5 BROWNIAN MOTION AND DIFFUSION

Small particles suspended in still air continuously exhibit an irregular movement, known as Brownian motion. First reported in 1827 by the British naturalist Robert Brown for pollen grains suspended in water, the motion is a result of collision with fluid molecules. It is therefore a type of thermal motion. However, Brownian motion differs considerably in pattern and magnitude from thermal motion of gas molecules. A gas molecule moves in a straight line and changes direction only when it collides with another molecule or a surface, whereas an aerosol particle changes direction of motion continuously as a result of numerous collisions with gas molecules. In addition, particles move much slower than gas molecules.

If the spatial distribution of particles is not even, Brownian motion will lead to a net transport of particles from a region of higher concentration to a region of lower concentration. The net transport is known as Brownian diffusion. The number of particles transported through a unit cross-sectional area in a unit time is given by Fick's first law of diffusion:

$$J_x = -D \frac{\partial n}{\partial x} \qquad (4.25)$$

Here J_x is the particle flux, D the diffusion coefficient, and n the particle concentration. Equation (4.25) indicates that the particle flux is proportional to the concentration gradient.

The diffusion coefficient can be calculated from the Stokes-Einstein equation:

$$D = \frac{k \, T \, C_c}{3 \, \pi \, \mu \, d_p} \qquad (4.26)$$

Here k is the Boltzmann constant and T the absolute temperature. Derivation of the above equation is based on the assumption, first made by Einstein (1905), that the translational energy of a particle undergoing Brownian motion is identical to that of fluid molecules.

According to Equation (4.26), diffusion coefficient varies with the slip correction factor and particle diameter. For large particles, the diffusion coefficient is inversely proportional to particle diameter because the slip correction is negligible. For particles much smaller than the mean free path of gas molecules, the slip correction factor is approximately proportional to the

reciprocal of particle diameter and therefore the diffusion coefficient is inversely proportional to the square of particle diameter.

The tables of aerosol properties in Appendix A5 give values of diffusion coefficient for a range of particle sizes. At ambient conditions, the diffusion coefficient is approximately proportional to the absolute temperature, because the ratio of the slip correction factor to gas viscosity changes little with temperature.

Brownian diffusion plays an important role in transport of small particles. For a nonspherical particle, it is useful to describe its size by the equivalent diffusion diameter, defined as the diameter of a sphere that has the same diffusion coefficient as the particle under consideration. Unlike gravitational settling and inertial impaction, Brownian motion is independent of particle density. In other words, very small particles have high diffusion coefficients regardless of their mass density. It is interesting to note that a 0.3-μm sphere with a density of 10,000 kg/m^3 has a relatively high diffusion coefficient as well as a high settling velocity.

In an aerosol with unit concentration gradient of particles, the rate of particle transport is directly proportional to the diffusion coefficient. According to the values of diffusion coefficient given in Appendix A5, the rate of transport by diffusion of 0.01-μm particles is more than 20,000 times that of 10-μm particles.

A useful parameter for estimating the rate of transport is the rms (root-mean-square) displacement of particles due to Brownian motion:

$$\left(\overline{x^2}\right)^{1/2} = (2D\,t)^{1/2} \tag{4.27}$$

Here x is the displacement of a particle during elapsed time t. The equation states that the rms displacement is proportional to the square root of diffusion coefficient. The rms displacement represents an average distance that a group of particles travel in a given elapsed time. It is useful for comparing the contribution of Brownian diffusion with other deposition mechanisms in analyses of inhaled particles. Eq. (4.27) can be derived using Fick's second law of diffusion:

$$\frac{\partial n}{\partial t} = D\frac{\partial^2 n}{\partial x^2} \tag{4.28}$$

Equation (4.28) is simply a mass balance for aerosol particles undergoing Brownian motion in still air. Applying the equation to the problem of diffusional deposition on a vertical plane surface gives:

$$J_x = -D \left. \frac{\partial n}{\partial x} \right|_{x=0} = -n_0 \left(\frac{D}{\pi t} \right)^{1/2} \tag{4.29}$$

Here n_0 is the initial particle concentration. The rate of transport given in the above equation assumes that the aerosol has a uniform initial concentration and the particle concentration is uniform at large distances from the surface at all times. In applications to systems of finite volumes such as a respiratory airway or alveolus, the assumption of uniform concentration at large distances from the walls no longer holds. However, Equation (4.29) is still useful for estimating the upper limit of deposition rate as long as the concentration at the center of an airway or alveolus remains unchanged.

Dividing the deposition flux by the undisturbed concentration (the concentration far away from surfaces) gives the deposition velocity. For Brownian diffusion, deposition velocity represents an effective velocity of aerosol particles arriving at the surface. This differs from gravitational deposition, in which deposition velocity is identical to settling velocity.

4.6 CONVECTIVE BROWNIAN DIFFUSION

The rate of deposition by Brownian motion from laminar or turbulent flow is higher than from still air. The increase arises from replenishment of fresh particles in the boundary layer by flow arriving from upstream, which leads to a local concentration gradient higher than when there is no flow. The transport process, known as convective Brownian diffusion, plays a key role in deposition of small particles in the respiratory tract. The equation of convective Brownian diffusion for aerosol particles is

$$\frac{\partial n}{\partial t} + \mathbf{u} \cdot \nabla n = D \nabla^2 n - \nabla \cdot \mathbf{c} n \tag{4.30}$$

Here $\mathbf{c}$ is the particle velocity resulting from the external force. Under steady state conditions and in the absence of external forces, the equation of convective Brownian diffusion can be written in the following dimensionless form

$$\mathbf{u}^* \cdot \nabla^* n^* = \frac{1}{Pe} \nabla^{*2} n^* \tag{4.31}$$

Here n^* is the particle concentration normalized by the mainstream concentration. The dimensionless velocity and operator, $\mathbf{u}^* = \mathbf{u}/U$ and $\nabla^* = l\nabla$, are defined using the average velocity U and the characteristic length of the system l. The Péclet number, $Pe = l\, U/D$, represents the ratio of convective mass transfer to diffusional mass transfer. It is equal to the product of Schmidt number (Sc) and flow Reynolds number. The Schmidt number, defined as the ratio of kinematic viscosity to particle diffusion coefficient, depends only on the nature of the gas and particles.

The equation of convective Brownian diffusion can be solved with appropriate boundary conditions to give the concentration distribution, which in turn can be used to calculate the particle flux at surfaces from Eq. (4.25). The boundary condition is given as $n = 0$ at a dimensionless distance R (the interception parameter) from the surface, because of the finite size of particle.

As in Brownian diffusion, particle flux can be used to calculate deposition velocity, v_d, due to convective Brownian diffusion. Alternatively, the particle concentrations at the inlet and outlet cross sections can be used to calculate deposition efficiency of the system.

The ratio of the total mass transfer to the diffusional mass transfer, $v_d l/D$, is known as Sherwood number (Sh). It is useful for estimating the increase in transfer due to convection. From the dimensionless transport equations and boundary conditions, it can be seen that Sherwood number is a function of Péclet number, interception parameter, and flow Reynolds number. Two geometrically similar systems with different values of physical parameters have identical solutions for convective Brownian diffusion if each of these three groups is identical between the two systems. The similitude law is useful for theoretical analysis as well as for interpretation of experimental data.

Mathematical solutions are available for deposition by convective Brownian diffusion from fully developed laminar flow in a circular tube with uniform particle concentration at the inlet. The penetration P, defined as the fraction of entering particles that exit the tube, is a function of a dimensionless parameter alone. The dimensionless parameter is defined as

$$\mu_t = \frac{D\,l_t}{Q} \tag{4.32}$$

Here D is the diffusion coefficient of particles, l_t the tube length, and Q the volumetric flow rate in the tube. Gormley and Kennedy (1949) have given the solutions in two truncated series, one for small values of μ_t and the other for large values of μ_t:

$$P = 1 - 5.46\,\mu_t^{2/3} + 3.77\,\mu_t + 0.814\,\mu_t^{4/3} \qquad \text{for } \mu_t < 0.006 \qquad (4.33)$$

$$P = 0.819\exp(-11.49\,\mu_t) + 0.0976\exp(-70.07\,\mu_t) + 0.0325\exp(-179\,\mu_t)$$

$$\text{for } \mu_t \geq 0.006 \qquad (4.34)$$

Subsequently, Ingham (1975) has derived the following expression, which is applicable for the entire range of μ_t

$$P = 0.819\exp(-11.49\,\mu_t) + 0.0976\exp(-70.07\,\mu_t) + 0.0325\exp(-179\,\mu_t)$$
$$+ 0.0509\exp(-107.2\,\mu_t^{2/3})$$

$$\text{for all values of } \mu_t \qquad (4.35)$$

4.7 DEPOSITION FROM TURBULENT FLOW

Large and small particles deposit from turbulent flow by different mechanisms. In the core of turbulent flow in a tube, eddy motion provides a good mixing so that the particle concentration is relatively uniform in the radial direction at each cross section. In a thin layer next to the wall, particles larger than about 1 µm continue to move by inertia. They may penetrate the laminar layer and deposit if they have sufficiently high velocity normal to the surface. On the other hand, the final approach for small particles to the wall relies on Brownian motion.

For particles larger than about 1 µm, correlations of experimental data give the following form for deposition velocity (Friedlander, 2000)

$$v_d = \frac{6 \times 10^{-4}\,u_f^5\,\tau^2}{\nu^2} \qquad (4.36)$$

Here u_f is the friction velocity, τ the relaxation time of particles, and ν the kinematic velocity. In turbulent pipe flow, the friction velocity is proportional to the average flow velocity and the square root of Fanning friction factor f.

$$u_f = U\left(\frac{f}{2}\right)^{1/2} \qquad (4.37)$$

Diffusional deposition velocity for small particles is given by (Wells and Chamberlain, 1967):

$$v_d = \frac{0.04U}{\text{Re}^{1/4}}\left(\frac{\rho_g D}{\mu}\right)^{2/3}$$ (4.38)

Here U is the average flow velocity in the tube, Re the flow Reynolds number, ρ_g the gas density, D the diffusion coefficient of particles, and μ the gas viscosity.

For particles moving in turbulent flow in a tube of diameter d_t and length l_t, a mass balance gives the following equation for the penetration

$$P = \exp\left(\frac{-4v_d l_t}{d_t U}\right)$$ (4.39)

4.8 ELECTROSTATIC FORCES

Particles produced by mechanical processes usually carry a significant number of charges because of static electrification. After remaining airborne for about 100 minutes, the charges on particles reach the Boltzmann equilibrium distribution as a result of attachment by positive and negative ions. These small ions are charged molecular clusters formed in air under the radiation from natural sources such as cosmic ray and radioactivity emanating from soil. Near the ground, continuous formation of ions at a rate of about 20 ions·s^{-1}·cm^{-3} (Bricard and Pradel, 1966) and continuous loss of ions due to attachment to particles and other surfaces result in an equilibrium concentration in the range of 100 to 5,000 ions·cm^{-3}, with an average of about 800 ions·cm^{-3}. Such concentration levels of small ions are sufficient to keep the electric charges on particles at the Boltzmann equilibrium distribution, which is described by the following equation (Keefe, et al., 1959):

$$f_n = \frac{\exp[-n^2 e^2 /(4\pi\varepsilon_0 d_p kT)]}{\sum_{n=-\infty}^{\infty} \exp[-n^2 e^2 /(4\pi\varepsilon_0 d_p kT)]}$$ (4.40)

Here e is the elementary charge, k the Boltzmann constant, T the absolute temperature, ε_0 the permittivity of a vacuum, and f_n the fraction of particles with diameter d_p carrying n (can be positive or negative) units of elementary charge. In the SI system of units, ε_0 is equal to 8.85 x 10^{-12} C^2/N·m^2.

For particles smaller than 0.01 μm in diameter, over 99% of the particles carry no charges when they are at the Boltzmann equilibrium charge

distribution. The percentage of uncharged particles drops to 42.6% for 0.1-μm particles, 13.5% for 1-μm particles, and 4.3% for 10-μm particles. Eq. (4.40) does not apply to radioactive particles, which are self-charging to some extent.

In the absence of an applied electric field, two types of electrical forces can move charged particles towards a surface: image force and repulsive force. A charged particle induces an image charge in a nearby surface. The electrostatic attraction between the particle charge and the image charge provides a force for the particle to move towards the surface. Repulsive forces between two particles carrying charges of like sign can also drive particles towards a surface.

The repulsive force between two point charges of like sign separated by a distance r_{12} follows the Coulomb law

$$F = \frac{q_1 q_2}{4\pi\varepsilon_0 r_{12}^2} \qquad\qquad (4.41)$$

The SI system of units is used for q_1 and q_2, the amount of the two point charges.

For a charged particle at a distance r from the axis of an electrically conductive tube, the image force between the particle and wall is given by

$$F = \frac{q^2 r^2}{16\pi\varepsilon_0 r_t^2 (r_t - r)^2} \qquad\qquad (4.42)$$

Here q is the charge carried by the particle and r_t the tube radius.

The electrical migration velocity of a charged particle subject to an electrostatic force is equal to the product of the force and mechanical mobility

$$v_e = BF \qquad\qquad (4.43)$$

For plug flow (with a flat velocity profile) in a tube with grounded conductive wall, the efficiency of deposition due to image force and Brownian diffusion is (Ingham, 1981)

$$\eta = \left(\frac{q^2 t}{2\pi^2 \mu\varepsilon_0 d_p r_t^3} \right)^{1/3} \qquad\qquad (4.44)$$

The expression is valid when the residence time in the tube satisfies the following condition:

$$t << \frac{q^2 r_t}{48\pi^2 \mu \varepsilon_0 d_p D^2} \qquad (4.45)$$

As indicated in Eqs. (4.41) and (4.42), both Coulomb and image forces are proportional to the square of particle charges. The effects of these electrostatic forces on deposition in lung airways are therefore important only for highly charged particles. On the other hand, these forces probably play an important role in the collection of charged particles by hairs at the nostrils because particles are able to come very close to the hairs.

4.9 GROWTH OF HYGROSCOPIC PARTICLES

Therapeutic aerosols generally contain hygroscopic components. Many types of particles in ambient air and workplaces, such as tobacco smoke and inorganic salts, are also hygroscopic in nature. In humid air, a hygroscopic particle grows at a rate depending on relative humidity, temperature, particle size, and chemical composition of the particle.

A droplet of an aqueous solution grows in humid air as a result of condensation. It takes place when the rate at which water vapor molecules arrive at the droplet surface exceeds the rate of departure. When the two rates are equal, the droplet is in equilibrium with the vapor. At a given temperature, there is a certain vapor pressure at which the liquid and its vapor are in equilibrium. Such a vapor pressure, often called the saturation vapor pressure, is defined for a liquid with a planar surface. When the liquid has a convex surface, as in a droplet, the vapor pressure becomes higher because of the excess surface free energy associated with convex surfaces.

For a pure water droplet of diameter $d_p{}^*$, the saturation vapor pressure p_d is given by:

$$\frac{p_d}{p_s} = \exp\left(\frac{4\gamma M}{\rho_w R T d_p^*} \right) \qquad (4.46)$$

Here p_s is the saturation vapor pressure of water with a planar surface, T the absolute temperature, and R the gas constant. γ, M, and ρ_w are, respectively, the surface tension, molecular weight, and density of water. The curvature effect is called the Kelvin effect and the diameter $d_p{}^*$ the Kelvin diameter. According to Equation (4.46), the ratio p_d/p_s (termed the Kelvin ratio) is always greater than unity. At a given Kelvin ratio, all the droplets smaller than $d_p{}^*$ in diameter will evaporate while all the droplets larger than $d_p{}^*$ will grow. Only those having a diameter $d_p{}^*$ neither evaporate nor grow.

For a droplet formed from an aqueous solution, the salt dissolved in water lowers the equilibrium vapor pressure over the droplet surface. In consequence the Kelvin ratio becomes:

$$\left(\frac{p_d}{p_s}\right)_{soln} = \left(1 + \frac{6n_i m_s M}{M_s \rho_w \pi d_p^3}\right)^{-1} \left(\frac{p_d}{p_s}\right)_{water} \tag{4.47}$$

Here the subscripts soln and water indicate the Kelvin ratio for aqueous solution and pure water, respectively. $(p_d/p_s)_{water}$ is calculated from Equation (4.46). m_s and M_s are the mass and molecular weight of the dissolved salt, respectively. n_i is the number of ions each molecule of salt forms when it dissolves. For dilute solutions of strong electrolytes, the true van't Hoff factor should be used for n_i to account for the association between ions. According to equation (4.47), a trace amount of salt is sufficient to lower the Kelvin ratio to just a few percentage points above unity.

The rate of particle growth due to condensation of water vapor is given by the following equations (derivations of these equations are given in several textbooks on aerosol science and technology; see, for example, Hinds, 1999):

$$\frac{d d_p}{dt} = \frac{2M\alpha_c(p_\infty - p_d)}{\rho_w N_a (2\pi mkT)^{1/2}} \qquad \text{for } d_p < \lambda \tag{4.48}$$

$$\frac{d d_p}{dt} = \frac{4D_v M}{R\rho_w d_p}\left(\frac{p_\infty}{T_\infty} - \frac{p_d}{T_d}\right) \qquad \text{for } d_p > \lambda \tag{4.49}$$

Here N_a is the Avogadro's number, m the mass of a water vapor molecule, k the Boltzmann constant, λ the mean free path of air molecules, D_v the diffusion coefficient of water vapor molecules in air, and p the partial pressure of water vapor. The subscript ∞ and d represent, respectively, the conditions far away from the droplet and the conditions at droplet surface. In Equation (4.48), an experimentally determined value of 0.04 is commonly used for the accommodation coefficient α_c, which represents the fraction of arriving molecules that stick to the droplet surface.

In Equation (4.49), the temperature is evaluated at two different conditions, T_∞ and T_d, to account for heating of droplet due to the release of latent heat of vaporization when water vapor condenses. As the droplet temperature rises during the initial stage of condensation, heat conduction to the surrounding air also takes place. The temperature difference, $T_d - T_\infty$, reaches a steady state

when the release of the latent heat of vaporization is balanced by heat conduction to the surrounding air:

$$k_v(T_d - T_\infty) = \frac{D_v MH}{R}\left(\frac{p_\infty}{T_\infty} - \frac{p_d}{T_d}\right)$$

(4.50)

Here H is the latent heat of vaporization and k_v the thermal conductivity of air. Evaluation of the temperature elevation is needed only for conditions of rapid growth. Under conditions of sufficiently slow growth, the droplet temperature differs little from the ambient temperature.

Fuchs (1959) has proposed a correction factor, Φ, which when multiplied to the right-hand side of Equation (4.49) provides a good interpolation formula for the growth rate throughout the entire range of Kn. The factor is given by (Fuchs and Sutugin, 1971):

$$\Phi = \frac{1 + \mathrm{Kn}}{1 + 1.71\mathrm{Kn} + 1.33\mathrm{Kn}^2}$$

(4.51)

According to Eqs. (4.48) and (4.49), the rate at which particle diameter increases with time is independent of particle size for $d_p < \lambda$, but is inversely proportional to particle size for $d_p > \lambda$. It follows that small particles grow rapidly but the rate of growth drops sharply when particles grow beyond about 0.1 µm.

While absorption of water vapor molecules into a particle of high mass density increases the particle size, it may lead to decrease in particle density. As a consequence, hygroscopic growth may not give rise to a similar degree of increase in aerodynamic diameter. In the respiratory tract, hygroscopic particles are likely to grow in size, but the growth does not necessarily result in an increase in deposition rate. The particle can grow into a size that has either higher or lower deposition velocity.

4.10 SIMULTANEOUS DEPOSITION BY SEVERAL MECHANISMS

Deposition is usually a result of several mechanisms acting simultaneously. Although an expression for deposition velocity due to the combined action can be obtained by solving the equation of particle motion that includes all the forces acting on the particle, the problem is so complex that only a few special cases have been worked out.

For the problems in which deposition is dominated by a single mechanism, it is reasonable to neglect other mechanisms in calculations. When two or more

mechanisms have comparable contributions, the deposition velocity is usually estimated from empirical expressions. A widely used approach is to combine the individual deposition efficiencies as if they were independent probabilities. Take the deposition by two mechanisms, gravitational settling and Brownian diffusion, as an example. By assuming that the probability for a particle to remain airborne is equal to the product of the probabilities that the particle is not removed by the two mechanisms acting independently, the following expression for the overall efficiency of deposition can be derived:

$$\eta = 1 - (1 - \eta_s)(1 - \eta_d) = \eta_s + \eta_d - \eta_s \eta_d \qquad (4.52)$$

Here η_s and η_d are the individual efficiencies of deposition due to gravitational settling and Brownian diffusion, respectively.

Caution must be taken in using this approach, because the effects of individual mechanisms are not really independent of each other. This can be seen in a few problems that have been worked out. Following are four examples.

For deposition by gravitational settling and Brownian diffusion of particles suspended between two parallel plane surfaces, results of theoretical analysis shows that the total deposition efficiency is better approximated by the greater of the two individual deposition efficiencies rather than by combining the individual deposition efficiencies as if they were independent probabilities (Wang et al., 1968).

Theoretical analysis for simultaneous Brownian diffusion and gravitational settling of particles suspended in a circular tube shows that the combination of individual deposition efficiencies as if they were independent probabilities considerably overestimates the deposition (Goldberg et al., 1978). Taulbee (1978) has reached a similar conclusion for simultaneous Brownian diffusion and gravitational settling of aerosol particles from fully developed laminar flow in a circular tube.

For deposition by inertial impaction and gravitational settling of aerosol particles from an idealized flow (see Section 4.4) in curved tubes, the total deposition efficiency is slightly higher than those obtained by combining the individual deposition efficiencies as if they were independent probabilities (Balásházy et al., 1990).

PROBLEMS

4.1 Calculate the settling distance and root-mean-square displacement of standard density particles during transit in an airway of Generation 20 in Weibel's lung model A at a steady inspiratory flow of 0.5 L/s. Make

calculations for three different particle diameters: 0.1, 1, and 10 μm. What conclusions can be made regarding the relative contributions of gravitational settling and Brownian motion to deposition in an airway of this size?

4.2 Calculate the stop distance of standard density particles in airways of Generations 1 to 4 in Weibel's lung model A at a steady inspiratory flow of 0.5 L/s. Make calculations for two different particle diameters: 1 and 10 μm. Compare the calculated stop distances with airway diameters.

4.3 Estimate the efficiency of deposition in the trachea for standard density particles from a steady inspiratory flow of 0.5 L/s. Make calculations for two different particle diameters: 0.01 and 0.001 μm. Discuss the implication of your results with respect to potential health hazards of nanoparticles.

REFERENCES

Balásházy, I., Martonen, T.B. and Hofmann, W. (1990). Inertial impaction and gravitational deposition of aerosols in curved tubes and airway bifurcations. Aerosol Sci. Technol. 13, 308-321.

Bricard, J. and Pradel, J. (1966). Electric charge and radioactivity of naturally occurring aerosols. In: Aerosol Science, pp. 87-88 (Ed. Davies, C.N.). Academic Press, London.

Cheng, Y.S. and Wang, C.S. (1975). Inertial deposition of particles in a bend. J. Aerosol Sci. 6, 139-145.

Cheng, Y.S. and Wang, C.S. (1981). Motion of particles in bends of circular pipes. Atmos. Environ. 15, 301-306.

Cheng, Y.S., Zhou, Y. and Chen, B.T. (1999). Particle deposition in a cast of human airways. Aerosol Sci. Technol. 31, 286-300.

Cunningham, E. (1910). On the velocity of steady fall of spherical particles through fluid medium. Proc. Roy. Soc. A83, 357-365.

Davies, C.N. (1945). Definitive equation for the fluid resistance of spheres. Proc. Phys. Soc. 57, 259-270.

Einstein, A. (1905). On the kinetic molecular theory of thermal movements of particles suspended in a quiescent fluid. Ann. Physik 17, 549-560. English translation of the paper is included in: Einstein, A. (1956). Investigations on the Theory of the Brownian Movement (Ed. Furth, R.). Dover, New York.

Friedlander, S.K. (2000). Smoke, Dust, and Haze: Fundamentals of Aerosol Dynamics, Second edition. Oxford University Press, New York.

Fuchs, N.A. (1959).Evaporation and Droplet Growth in Gaseous Media. Pergamon Press, Oxford.

Fuchs, N.A. and Sutugin, A.G. (1971). High-dispersed aerosols. In: Topics in Current Aerosol Research (Eds. Hidy, G.M. and Brock, J.R.). Pergamon, New York.

Goldberg, I.S., Lam, K.Y., Bernstein, B. and Hutchens, J.O. (1978). Solutions to the Fokker-Planck equations governing simultaneous diffusion and gravitational settling of aerosol particles from a stationary gas in a horizontal circular tube. J. Aerosol Sci. 9, 209-218.

Gormley, P. and Kennedy, M. (1949). Diffusion from a stream flowing through a cylindrical tube. Proc. Roy. Irish Acad. 52A, 163-169.

Hinds, W.C. (1999). Aerosol Technology: Properties, Behavior, and Measurement of Airborne Particles, Second edition. John Wiley & Sons, New York.

Ingham, D.B. (1975). Diffusion of aerosols from a stream flowing through a cylindrical tube. J. Aerosol Sci. 6, 125-132.

Ingham, D.B. (1981). Precipitation of charged particles in human airways. J. Aerosol Sci. 12, 131-135.

Keefe, D., Nolan, P.J. and Rich, T.A. (1959). Charge equilibrium in aerosols according to the Boltzmann law. Proc. Roy. Irish Acad. 60A, 27-45.

Mercer, T.T. (1973). Aerosol Technology in Hazard Evaluation, p.83. Academic Press, New York.

Pich, J. (1972). Theory of gravitational deposition of particles from laminar flows in channels. J. Aerosol Sci. 3, 351-361.

Reist, P.C. (1993). Aerosol Science and Technology. Second edition. McGraw-Hill, New York.

Schneider, T. and Holst, E. (1983). Man-made mineral fiber size distributions utilizing unbiased and fiber length biased counting methods and the bivariate log-normal distribution. J. Aerosol Sci. 14, 139-146.

Taulbee, D.B. (1978). Simultaneous diffusion and sedimentation of aerosol particles from Poiseuille flow in a circular tube. J. Aerosol Sci. 9, 17-23.

Thomas, J.W. (1958). J. Air Pollut. Control Ass. 8, 32-34.

Vincent, J.H. (1995). Aerosol Science for Industrial Hygienists. Pergamon, Oxford, UK.

Walton, W.H. (1954). Br. J. Appl. Phys. Suppl. 3, S29-S39.

Wang, C.S., Altshuler, B. and Palmes, E.D. (1968). The distribution and deposition of particles suspended between parallel plane surfaces. J. Colloid Interface Sci. 26, 41-44.

Wang, C.S. (1975). Gravitational deposition of particles from laminar flows in inclined channels. J. Aerosol Sci. 6, 191-204.

Wells, A.C. and Chamberlain, A.C. (1967). Transport of small particles to vertical surfaces. Brit. J. Appl. Phys. 18, 1793-1799.

Willeke, K. and Baron, P.A. (2001). Aerosol Measurement: Principles, Techniques, and Applications, Second edition. Wiley-Interscience, New York.

Chapter 5

Dispersion of inhaled aerosol

Two different processes can occur to inhaled particles during transit in airways: dispersion and deposition. Dispersion refers to the spreading of particles that remain airborne as they move in and out of the lungs. Deposition represents the attachment of particles to airway walls. This chapter focuses on dispersion. Deposition will be discussed in Chapter 7.

5.1 GENERAL CONCEPTS IN AEROSOL DISPERSION

Dispersion of aerosol particles represents the process by which particles are spread out while they remain airborne. The driving forces for aerosol dispersion in lung airways are airflow and, to a lesser extent, intrinsic motion of particles. As discussed in Chapter 3, flow patterns in the respiratory tract are very complex. The axial velocity distribution differs markedly from a flat profile. Furthermore, the flow velocity profile differs between inhalation and exhalation. In consequence aerosol dispersion takes place during both respiratory phases.

Dispersion of inhaled particles is best understood by following a bolus of aerosol as it moves down a straight tube of constant cross section. Fig. 5.1 shows the movement of an aerosol bolus in a tube with two different flow velocity profiles: plug flow and fully developed laminar flow.
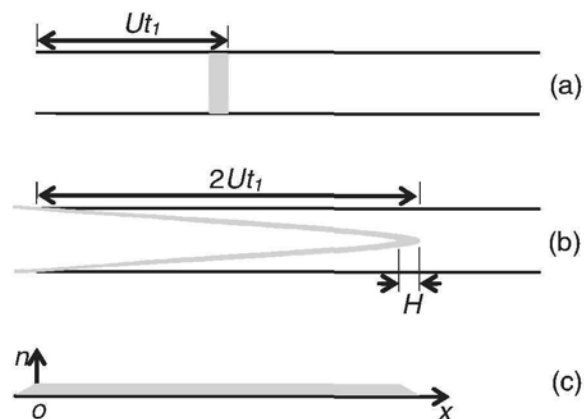
Fig. 5.1 Movement of an aerosol bolus in a tube with two different velocity profiles: (a) plug flow and (b) fully developed laminar flow. The distribution of particle concentration at time t_1 for Case (b) is shown in (c).

Fig. 5.1 (a) presents a laminar flow with a flat velocity profile. To keep the picture simple, let us assume the particles have no intrinsic motion first. In a plug flow, air moves at the same velocity U at all radial positions, and therefore aerosol bolus remains in the same shape as it moves down the tube. The bolus is simply displaced to a distance Ut_1 downstream in time t_1. No dispersion of particles takes place. If the flow reverses in direction but maintains the flat velocity profile, the particles retrace their trajectories and the bolus returns to its initial position intact at time $2t_1$ (counting from the time when the forward flow starts).

Now if we allow particles to have intrinsic motion, some particles will move out of the initial bolus boundaries. In consequence the aerosol bolus becomes wider and mixing takes place between the bolus and surrounding air as it moves down the tube. When the flow reverses its direction but maintains the same flat velocity profile, dispersion by intrinsic motion of particles continues. The bolus becomes even wider as it arrives at the tube inlet. Mixing caused by intrinsic motion is not reversible. In this case, intrinsic motion of particles is the driving force of particle dispersion as well as mixing between the aerosol bolus and surrounding air. The plug flow has no effect at all.

Depicted in Fig. 5.1 (b) is the fully developed laminar flow in a tube. Again let us assume the particles have no intrinsic motion first. The aerosol bolus moves down the tube in the shape of a parabolic shell that progressively stretches longer. At time t_1, the stretched bolus has its tip at $x = 2Ut_1$, because the velocity at the tube axis is twice the average velocity U. The particles spread out along the axial direction on both sides of the mid-point (at $x = Ut_1$). This represents particle dispersion resulting from convection. However, it is important to note that there is no mixing between the aerosol bolus and surrounding air. The bolus simply changes its shape. The dispersion of this type is reversible. If the flow reverses its direction but maintains the parabolic velocity profile, the stretched parabolic shell returns to the initial shape of bolus at the tube inlet at time $2t_1$.

It is interesting to examine the distribution of particles in the axial direction at time t_1. Except the small front section of the parabolic shell, particles are confined within an annular space at each cross section. The area of the ring is given by

$$A = \frac{\pi r_t^2 H}{2Ut_1} \qquad \text{for } 0 \le x \le 2Ut_1 - H \qquad (5.1)$$

$$A = \frac{\pi r_t^2 (x+H)}{2Ut_1} \qquad \text{for } -H \le x \le 0 \qquad (5.2)$$

Here r_t is the tube radius and H the initial width of bolus. It is assumed that the bolus is initially located between $x = -H$ and 0.

In the front section of the parabolic shell, the particles are confined within a small circle with an area

$$A = \pi\, r_t^2\left(1 - \frac{x}{2Ut_1}\right) \qquad \text{for } 2Ut_1 - H \le x \le 2Ut_1 \tag{5.3}$$

The number of particles at each cross section is proportional to the area given in the above equations. Fig. 5.1(c) shows the concentration distribution for the particles that spread out between the tube inlet and the front of the advancing bolus. The concentration is constant throughout the entire length of the stretched bolus except two short sections at the front and rear ends.

If the reverse flow has a flat velocity profile instead of a parabolic profile, the stretched parabolic shell remains in the same shape and the concentration measured as a function of time at the inlet has precisely the same profile as that shown in Fig. 5.1 (c). In other words, the dispersion seen at the inlet during reverse flow is the dispersion caused by the non-uniform velocity distribution during forward flow. Again it is important to note that there is no mixing between the bolus and surrounding air during reverse flow even though the bolus remains stretched as it returns to the inlet.

In the presence of intrinsic motion, additional dispersion takes place during both forward and reverse flows. At the end of forward flow with a parabolic velocity profile, the parabolic shell appears slightly thicker than in the absence of intrinsic motion. The bolus appearing at the inlet is broadened at the end of reverse flow with a parabolic velocity profile. If the reverse flow has a uniform velocity distribution, the particle concentration profile measured at the inlet is broader than the one shown in Fig. 5.1(c). Dispersion caused by intrinsic motion gives rise to mixing between the bolus and surrounding air. Such mixing is not reversible.

Aimed at distinguishing the roles played by flow and intrinsic motion, the discussion given above is limited to laminar flow. In turbulent flow, eddy motion also causes mixing between the bolus and surrounding air. Similar to intrinsic motion, turbulent mixing is irreversible.

Particle dispersion in air flowing in a tube is a very special case of Taylor dispersion. Strictly speaking, Taylor dispersion refers to the combined result of convection and diffusion. In his analyses of dispersion in laminar and turbulent flows in a straight tube, Taylor (1953, 1954) has assumed that the concentration of the substance under consideration is uniform at each cross section and therefore an effective axial diffusion coefficient can be used to characterize the dispersion. Aerosol particles, especially those between 0.5 and 1 μm, fail to

meet this assumption. Intrinsic motion of particles leads to only a small degree of mixing at each cross section of the tube. In consequence the particle concentration varies with the radial coordinate (and the angular coordinate as well if the velocity profile is not axisymmetric).

5.2 AEROSOL DISPERSION IN LUNG AIRWAYS

The dispersion of particles in an airway network is similar but far more complex than in a tube. When an aerosol bolus is inspired, its front splits at each bifurcation and its shell progressively becomes thinner. At the end of inhalation, the bolus spreads out to a huge but very thin sheet with numerous tips. The fingertip-shaped front advances far ahead of its tail. During exhalation, the tips of the thin aerosol sheet retreat and successively merge with each other. However, the bolus does not return to its original shape and width, because the airflow velocity profiles during exhalation are not mirror images of those during inhalation (see Chapter 3). The differences in velocity profile between the two respiratory phases broaden the bolus width as in a straight tube of constant cross section explained in Section 5.1. In addition, mixing between the aerosol bolus and surrounding air occurs in extrathoracic airways and the first few generations of the tracheobronchial region where flow is normally turbulent during inhalation. Intrinsic motion of particles also makes a small contribution to dispersion.

Broadly speaking, aerosol dispersion represents the mixing between tidal air and reserve air. The two terms, tidal air and reserve air, refer to the two portions of air separated by an imaginary boundary formed by incoming airflow. They do not refer to air molecules. In fact, there is a significant amount of air molecules crossing the imaginary boundary by diffusion. The extent to which tidal air and reserve air mix by convection during a breathing cycle has been studied experimentally using aerosol boluses containing 1-μm particles. Particles of this size have negligible intrinsic motion and, as a result, their trajectories are nearly identical to the airflow streamlines. Such particles are a useful tracer for studying airflow in lung airways.

In a bolus experiment, a subject inhales a small volume of aerosol that is preceded and followed by particle-free air. Continuous measurements of particle number concentration at the mouth as a function of inhaled or exhaled volume provide the concentration profiles illustrated in Fig. 5.2. There are two parameters that can be used to characterize an aerosol bolus: the mode and the volumetric half-width. The mode represents the volume at which the maximum particle concentration occurs. The volumetric half-width is the width of the particle concentration profile measured at the two points where the concentration is one half of the maximum. The difference in volumetric half-width between the exhaled and inhaled boluses is a measure of the degree

of aerosol dispersion in a breathing cycle. The corrected half-width, a parameter used to quantify the dispersion, is defined by the equation

$$H_{50C} = \sqrt{H_{50E}^2 - H_{50I}^2}$$
(5.4)

Here H_{50I} and H_{50E} represent the volumetric half-widths of the inhaled and exhaled boluses, respectively. One major influencing factor of aerosol dispersion is the volumetric penetration, defined as the volume of air that follows the mode of aerosol bolus into the lungs. Within the volumetric penetration range of 100-800 cm^3, the half-width of the exhaled aerosol bolus is a linear function of volumetric penetration (Heyder et al., 1988).

Another factor that influences dispersion of aerosol bolus is the volume in which the bolus is allowed to mix. Schulz, et al. (2003) have measured bolus dispersion in 32 anesthetized, mechanically ventilated dogs with total lung capacities between 1.1 and 2.5 L. Six-milliliter aerosol boluses are introduced at various time-points during inspiration to probe different volumetric lung depths. Dispersion is determined by moment analysis of particle concentrations in the expired air. The results indicate that there are linear correlations between dispersion at a given lung depth and the end-inspiratory lung volume. These data should be useful for separating the effects on bolus dispersion of altered lung volumes and altered mixing processes in diseased lungs.
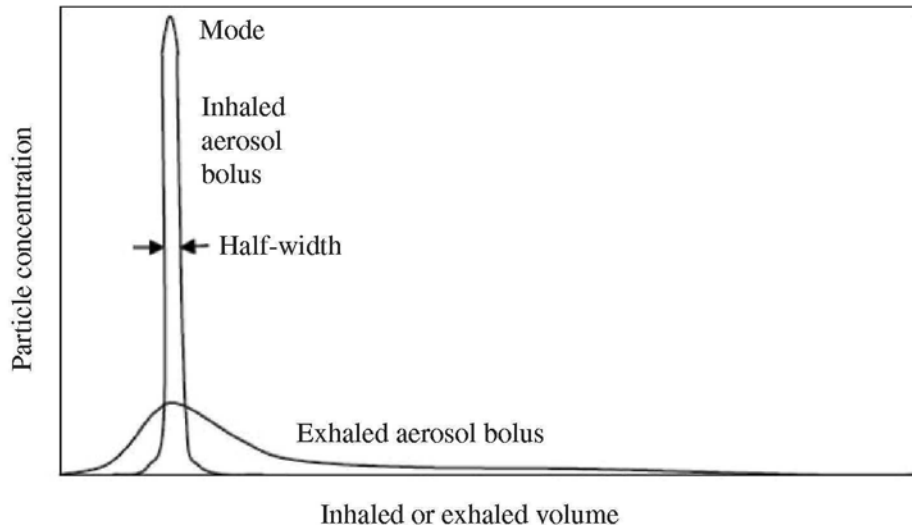
Fig. 5.2 Typical profiles of particle concentration measured at the mouth during experiments with aerosol boluses. On the *x*-axis, inhaled volume represents volumetric penetration of inhaled bolus, while exhaled volume represents the cumulative volume of exhaled air.

Dispersion of micron-sized particles represents mixing almost entirely by convection alone. Data on aerosol dispersion are therefore useful for assessing diffusion-independent mixing, or commonly termed convective mixing, that takes place during a breathing cycle. However, recent studies (Brown, et al., 1998; Darquenne, et al., 1999) suggest that the effects of asymmetry in order of sequential filling and emptying for various areas of the lungs and intrinsic motions of particles cannot be neglected. In a broader sense, sequential filling and emptying can be considered as a part of convection.

An interesting result arising from intrinsic motion is the migration of particles from tidal air to reserve air. A small displacement of a particle at the tip of an advancing front, especially in the alveolar region where the front is greatly extended, can move the particle across the interface between the tidal air and reserve air. It is not difficult to imagine that, because of the marked difference in velocity profiles between the two respiratory phases, some of these strayed particles are left far behind as the front begins to retreat during exhalation.

Incoming particles that are transferred into reserve air by various mechanisms may deposit during the current breath. Those particles that have been transferred into reserve air but remain airborne at the end of exhalation will have higher probabilities to deposit in alveoli as reserve air penetrates into the deepest part of the lungs in subsequent breaths. It is evident that mixing between tidal air and reserve air plays an important role in deposition of inhaled particles. Altshuler et al. (1959) have suggested that the intersubject variability in lung deposition arises mainly because the degree of mixing between tidal air and reserve air differs from individual to individual.

5.3 GAS MIXING IN LUNG AIRWAYS

Mixing of gases in the bronchial tree has been studied using gas tracers. Based on the concept of Taylor dispersion, the analysis assumes that the dispersion of tracer gas in the bronchial tree can be described by the one-dimensional convective diffusion equation

$$\frac{\partial n}{\partial t} + U\frac{\partial n}{\partial x} = \frac{1}{A}\frac{\partial}{\partial x}\left(D_e A \frac{\partial n}{\partial x}\right) \tag{5.5}$$

Here n is the concentration of tracer gas, t the time, x the distance from the inlet, U the average axial velocity, A the cross sectional area of the conduit, and D_e an effective axial diffusion coefficient. In the analysis, the respiratory tract is considered as a single conduit with variable cross section. The cross-sectional area is equal to the total cross-sectional area of the tubes in each generation and

therefore varies with the distance from the inlet. Use of Eq. (5.5) implies that the tracer gas is well mixed at each cross section of the trumpet-shaped conduit. The assumption is reasonable for tracer gas because gas molecules have high diffusivities and the cross section of each individual airway is small.

Scherer et al. (1975) have measured the effective axial diffusion coefficient of benzene in a symmetrical glass model of the human bronchial tree consisting of Generations 0-5 in Weibel's lung model A. The tracheal has a diameter of 3 cm. The diameter ratio of the parent and daughter tubes is proportional to the cube root of 2. The length to diameter ratio is 3 and the branching angle is 35° for each daughter tube in all bifurcations. The results show that the degree of dispersion differs between inspiration and expiration. For Reynolds number in the range of 30-2,000 (in the trachea), the effective axial diffusion coefficient is approximately a linear function of the mean axial flow velocity

$$D_e = D + 1.08 U d_t \qquad \text{for inspiration} \qquad (5.6)$$

$$D_e = D + 0.37 U d_t \qquad \text{for expiration} \qquad (5.7)$$

Here D is the molecular diffusion coefficient and d_t the tube diameter under consideration. The constant coefficients in the two expressions differ in numerical value because airflow patterns differ between the two respiratory phases.

It is important to note that mixing of gases in the bronchial tree differs from aerosol dispersion. Aerosol particles behave differently from benzene molecules because particles have markedly lower diffusivities.

PROBLEMS

5.1 Sketch a picture to show the shape of an aerosol bolus at the end of inhalation in the first five generations of airways in Weibel's lung model A. Assume the flow is laminar and fully developed in each airway segment.

5.2 Estimate the total area of the interface between an inhaled bolus and reserve air at the time when the bolus reaches the end of tubes in Generation 20 in Weibel's lung model A. Also estimate the thickness of bolus shell at that time assuming that the initial bolus is 5 cm in width. Make any assumptions as you deem necessary, but state the rationale for making them.

REFERENCES

Altshuler, B., Palmes, E.D., Yarmus, L. and Nelson, N. (1959). Intrapulmonary mixing of gases studied with aerosols. J. Appl. Physiol. 14, 321-327.

Brown, J.S., Gerrity, T.R. and Bennett, W.D. (1998). Effect of ventilation distribution on aerosol bolus dispersion and recovery. J. Appl. Physiol. 85, 2112-2117.

Darquenne, C., West, J.B. and Prisk, G.K. (1999). Dispersion of 0.5- to 2-μm aerosol in μG and hypergravity as a probe of convective inhomogeneity in the lung. J. Appl. Physiol. 86, 1402-1409.

Heyder, J., Blanchard, J.D., Feldman, H.A. and Brain, J.D. (1988). Convective mixing in Human respiratory tract: Estimates with aerosol boli. J. Appl. Physiol. 64, 1273-1278.

Scherer, P.W., Shendalman, L.H., Greene, N.M. and Bouhuys, A. (1975). Measurement of axial diffusivities in a model of the bronchial airways. J. Appl. Physiol. 38, 719-723.

Schulz, H., Eder, G. and Heyder, J. (2003). Lung volume is a determinant of aerosol bolus dispersion. J. Aerosol Med. 16, 255-262.

Taylor, G.I. (1953). Dispersion of soluble matter in solvent flowing slowly through a tube. Proc. Roy. Soc. A219, 186-203.

Taylor, G.I. (1954). The dispersion of matter in turbulent flow through a pipe.Proc. Roy. Soc. A223, 446-468.

Chapter 6

Inhalability of ambient particles

The first step for a particle in ambient air to enter the human respiratory tract is to stay in the right course as it approaches the nose or mouth. Interestingly, this does not turn out to be very easy for large particles.

When wind blows toward the face of a person, the streamlines diverge around the head except in the vicinity of the nose or mouth, the two portals of entry for air. Fig. 6.1 depicts a few streamlines in front of the face of an individual breathing through the nose and mouth simultaneously. Both the nose and mouth have thick rims, which force the air streamlines to bend considerably near the entrance. Large particles moving along these streamlines cannot negotiate the sharp turn easily and, as a result, a substantial fraction of them deposit on the rims of these two portals or other parts of the face. The fraction of ambient particles that can enter these two portals depends on particle aerodynamic diameter as well as wind velocity.

Difficulty for large particles to enter the nose or mouth arises mainly from the shapes of these two portals and their surroundings. The problem would largely disappear if particles were inhaled through a thin-walled tube inserted into the mouth. That is how it is done in administration of aerosolized drug. Breathing through a mouthpiece is also a common practice in deposition experiments.
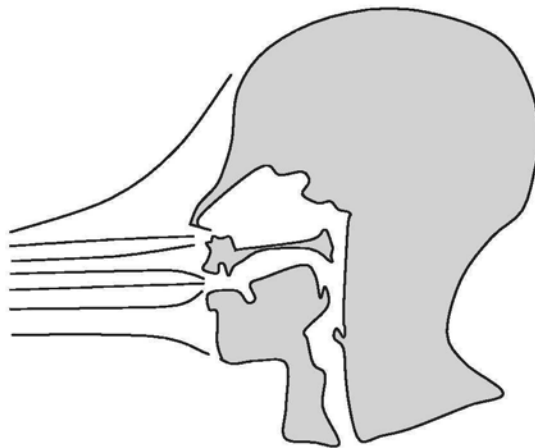
Fig. 6.1 Air streamlines approaching the face of an individual inhaling through the nose and mouth.

6.1 MOUTH INHALABILITY

Inhalable fraction has several other names. It is also known as inhalability, intake efficiency, and aspiration efficiency. Inhalability is defined as the ratio of the particle concentration in inspired air to that in ambient air. It is approximately equal to one for small particles that are able to follow air streamlines closely. For large particles, inhalability is in general less than one, but can be greater than one under unusual conditions such as when a strong wind blows directly into the nostrils or mouth.

As a parameter related to motion of large particles in flow with sharp turns, inhalability varies with particle aerodynamic diameter and ambient wind speed. The orientation of nostrils or mouth relative to the wind direction also has measurable effects on inhalability. Wind blowing towards the face gives rise to a higher inhalability than other orientations. The breathing rate affects air velocity in the vicinity of the nose or mouth, which in turn influences the inhalability to some extent.

Inhalation of ambient particles is similar to collection of particles by a blunt sampling device. The principles and experimental methods in aerosol sampling have been reviewed by Vincent (1989). Inhalability is determined experimentally using life-size mannequin heads (either with or without torso) placed in a wind tunnel (Ogden and Birkett, 1977, 1978; Armbruster and Breuer, 1982; Vincent and Mark, 1982). The test aerosol, usually consisting of particles with a narrow size distribution, enters either the mouth or nose by means of a breathing machine. Particles that have entered the mouth or nose are collected by a filter for determination of particle concentrations in inspired air. Particle concentrations in ambient air are measured from samples taken in the vicinity of the mannequin's head.

Inhalability measurements are taken with the head positioned at various angles to the wind direction. Instead of specifying an inhalable fraction for each orientation, it is a general practice to use an orientation-averaged inhalability obtained by averaging the inhalable fractions for all orientations. An orientation-averaged inhalability assumes that all orientations with respect to the wind direction are equally weighted in the average. It represents exposures when there is no dominant wind direction.

Some experiments are conducted with inhalation only, while other with inhalation through the mouth and exhalation through the nose. Results indicate that the addition of exhalation in experiments does not have detectable effect on inhalability. For the range of experimental conditions studied, breathing rate has little influence on inhalability.

At low wind speeds, the empirical equation for the orientation-averaged mouth inhalability is

$$I_o(d_a) = 0.5\left[1 + \exp(-0.06\,d_a)\right] \qquad \text{for } 1 < U_0 < 4 \text{ m/s and } d_a < 100 \text{ μm} \quad (6.1)$$

Here d_a is the particle aerodynamic diameter in μm. Eq. (6.1) is based on data obtained at wind speeds below 4 m/s in the experimental studies cited above and is adopted by the American Conference of Governmental Industrial Hygienists (ACGIH, 1985) as the sampling criterion for inhalable particulate mass (IPM). The sampling criterion specifies the desired performance of an IPM sampler in terms of collection efficiency for particles up to 100 μm in aerodynamic diameter. It is part of the criteria for health-based, size selective samplers. A comprehensive review on size-selective health hazard sampling has been given by Lippmann (1995).

When the ambient air velocity is greater than 4 m/s, the orientation-averaged mouth inhalability is given by the empirical equation (Vincent et al., 1990)

$$I_o(d_a, U_0) = 0.5\left[1 + \exp(-0.06\,d_a)\right] + 10^{-5}\,U_0^{2.75}\exp(0.055\,d_a)$$

$$\text{for } 9 > U_0 > 4 \text{ m/s and } d_a < 100 \text{ μm} \quad (6.2)$$

Here U_0 is the ambient air velocity in m/s.

There are considerable variations among experimental data on inhalability obtained in various studies. Fig. 6.2 summarizes the range of typical data for orientation averaged mouth inhalability of particles with aerodynamic diameter up to 30 μm. Inhalability levels off at about 50% for larger particles.
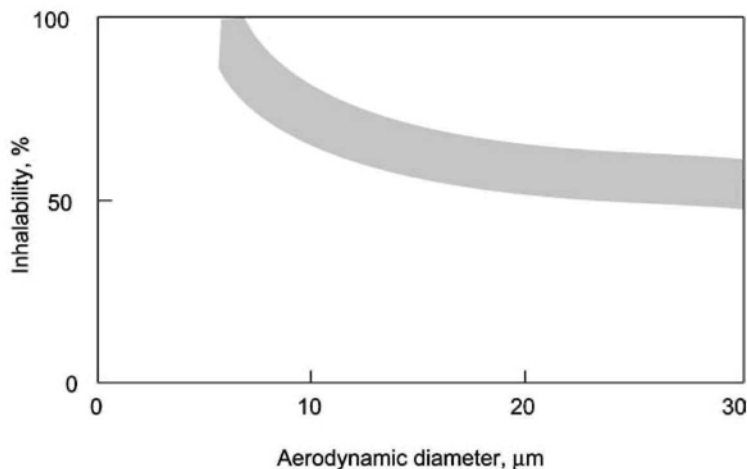
Fig. 6.2 Range of nose and mouth inhalability based on data from Ogden and Birkett (1977, 1978), Armbruster and Breuer (1982), Vincent and Mark (1982), and Vincent et al. (1990).

In earlier inhalability experiments, air velocities up to 4 m/s are considered to be representative of the wind speeds in indoor environments. Subsequent studies show that the wind speed in indoor workplaces is typically less than 0.1 m/s, except in the neighborhood of a worker's nose and mouth. Accordingly Aitken et al. (1999) have defined an environment of low air movement as one in which there is effectively no net air movement and the peak velocity is less than 0.1 m/s. To measure the inhalability in such an indoor workplace, they have conducted an experimental study using a mannequin (with head and the upper part of the body) sited in a large chamber approximately 1 m x 1 m x 3 m in dimensions. Their results show that the inhalability for oral inhalation in low air movement environments is consistently higher than the values predicted by Eq. (6.1). The largest difference occurs in the results for 20 L/min, the highest minute volume tested. In view of their results, Aitken et al. have suggested the following empirical expression for inhalability at the minute volume of 20 L/min and tidal volume of 1 L

$$I_o(d_a) = 1 - 0.0038 d_a \qquad \text{for low air movement environments} \qquad (6.3)$$

The particle aerodynamic diameter d_a is in μm.

More recently, Kennedy and Hinds (2002) have measured the inhalability of solid particles using a full-size, full-torso mannequin in a 1.6×1.6×5-m wind tunnel with three air velocities, 0.4, 1.0, and 1.6 m/s, and three minute volumes, 14.2, 20.8, and 37.3 L. Measurements are made for two types of orientation: facing-the-wind and orientation averaged. In orientation-averaged experiments, the mannequin completes one full rotation in each run.

For the ranges of conditions tested, mouth inhalability depends strongly on the orientation with respect to wind direction, but is nearly independent of wind velocity and minute volume. For particles larger than 40 μm in aerodynamic diameter, the measured values of facing-the-wind mouth inhalability are nearly twice those of orientation-averaged mouth inhalability.

Based on their data, Kennedy and Hinds have given the following empirical equation for the orientation-averaged mouth inhalability:

$$I_o(d_a) = 24.14 + 75.86 \exp(-0.00607 d_a^{1.400})$$

$$\text{for } 0.4 < U_0 < 1.6 \text{ m/s}, \ 14.2 < V_m < 37.3 \text{ L, and } d_a < 141 \text{ μm} \qquad (6.4)$$

Here V_m is the minute volume. The values given by Eq. (6.4) are higher than those given by Eq. (6.1) for particles smaller than 35 μm and lower than those given by Eq. (6.1) for larger particles. One possible explanation for the disagreements is the difference in experimental methods used for

orientation-averaged measurements. Kennedy and Hinds have employed a continuously rotating mannequin to collect, in each run, one sample that is equally representative of all orientations, whereas prior studies have taken measurements with the head positioned at various discrete angles to the wind direction, such as 0°, 45°, and 90°, and then calculated orientation-averaged inhalability as the mean of the results obtained for these discrete angles. Since measurements are made only for a limited number of discrete angles and facing-the-wind inhalability is nearly twice the orientation-averaged inhalability, the mean may have given a disproportional weight to facing-the-wind data. This would give a higher value of inhalability for large particles.

6.2 NOSE INHALABILITY

For particles smaller than 30 μm in aerodynamic diameter, results obtained from experiments with a life-size, full-torso mannequin placed in a wind tunnel show that there are few differences between the orientation averaged nose inhalability and mouth inhalability (Hinds et al., 1998). However, the nose inhalability drops below the mouth inhalability considerably for larger particles. The empirical equation for the orientation averaged nose inhalability is (Hinds, 1999)

$$I_n(d_a) = 0.035 + 0.965 \exp(-0.000113 \, d_a^{2.74}) \tag{6.5}$$

Here d_a is the particle aerodynamic diameter in μm.

PROBLEMS

6.1 Experimental measurements have shown that large particles may have inhalability higher than one when a strong wind blows directly into the nostrils or mouth. Explain why it can happen.

6.2 Estimate the fraction of ambient particles, 30 μm in aerodynamic diameter, inhaled by a mouth breather at light physical activity. Compare it with a normal nose breather.

REFERENCES

ACGIH (1985). Particle Size-Selective Sampling in the Workplace, Report of the ACGIH Technical Committee on Air Sampling Procedures. American Conference of Governmental Industrial Hygieneists, Cincinati, Ohio.

Aitken, R.J., Baldwin, P.E.J., Beaumont, G.C., Kenny, L.C. and Maynard, A.D. (1999). aerosol inhalability in low air movement environments. J. Aerosol Sci. 30, 613-626.

Armbruster, L. and Breuer, H. (1982). Investigations into defining inhalable dust. Ann. Occup.

Hyg. 26, 21-32.

Hinds, W.C., Kennedy, N.J. and Tatyan, K. (1998). Inhalability of large particles for mouth and nose breathing. J. Aerosol Sci. 29, S277-S278.

Hinds, W.C. (1999). Aerosol Technology: Properties, Behavior, and Measurement of Airborne Particles, Second edition. John Wiley & Sons, New York.

Kennedy, N.J. and Hinds, W.C. (2002). Inhalability of large solid particles. J. Aerosol Sci. 33, 237-255.

Lippmann, M. (1995). Size selective health hazard sampling. In: Air Sampling Instruments for Evaluation of Atmospheric Contaminants, 8th edition (Eds. Cohen, B.S. and Hering, S.V.). American Conference of Governmental Industrial Hygieneists, Cincinati, Ohio.

Ogden, T.L. and Birkett, J.L. (1977). The human head as a dust sampler. In; Inhaled Particles IV, Proceedings of an International Symposium Organized by the British Occupational Hygiene Society, Edinburgh, September 22-26, 1975, pp. 93-105 (Ed. Walton, W.H.). Pergamon Press, Oxford.

Ogden, T.L. and Birkett, J.L. (1978). An inhalable dust sampler for measuring the hazard from total airborne particulate. Ann. Occup. Hyg. 21, 41-50.

Vincent, J.H. and Mark, D. (1982). Application of blunt sampler theory to the definition and measurement of inhalable dust. Ann. Occup. Hyg. 26, 3-19.

Vincent, J.H. (1989). Aerosol Sampling: Science and Practice. John Wiley & Sons, Chichester, U.K.

Vincent, J.H., Mark, D., Miller, B.G., Armbruster, L. and Ogden, J.L. (1990). Aerosol inhalability at higher wind speeds. J. Aerosol Sci. 21, 577-586.

Chapter 7

Deposition of particles in the respiratory system

Deposition refers to the process by which an airborne particle during its transit or pause in an airway comes into contact with a wall surface and attaches there. This chapter focuses on general characteristics of respiratory deposition. Experimental data on regional deposition and mathematical models are covered in Chapters 8 and 9, respectively.

7.1 GENERAL CONCEPTS IN RESPIRATORY DEPOSITION

In laminar flow, the trajectory of a particle deviates slightly from a streamline because of intrinsic motion arising from particle inertia, gravity, Brownian motion, and electrostatic forces. It is mainly the intrinsic motion that leads to deposition from laminar flow. In turbulent tube flow, eddy motion provides an initial kick for particles to move from the core to a thin laminar layer next to the wall. Particles larger than about 1 µm continue to move by inertia in the thin laminar layer and may deposit if they have sufficiently high velocity normal to the surface. On the other hand, the final approach for small particles to the wall relies on Brownian motion.

Five important deposition mechanisms are related to intrinsic motion: inertial impaction, gravitational settling, Brownian motion, turbulent deposition, and electrostatic forces. The only deposition mechanism not related to intrinsic motion is interception, which occurs because particles have finite sizes. In general, deposition takes place under the combined influence of several mechanisms.

Particle properties, dimensions of airways, and breathing patterns are among the major factors influencing respiratory deposition. Particle properties that play important roles in deposition include size, density, shape, hygroscopicity, and electrical charge. Geometry and dimensions of airways depend on lung morphology and functional residual capacity. Effects of lung morphology on deposition are twofold: it defines the airway geometry for deposition and influences airflow that in turn affects particle motion. Parameters related to breathing patterns include breathing frequency, tidal volume, the nose and mouth breathing ratio, and the length of pause between inhalation and exhalation. In view of these influencing factors, it is evident that deposition characteristics differ between adults and children, and between healthy adults and patients with respiratory disease.

Many related terms have been used to express quantitative aspects of respiratory deposition. To avoid confusion, we define these terms here in a

consistent way. Some terms have been mentioned in earlier chapters, but are repeated here for easy reference.

Efficiency of deposition in an airway segment is defined as the ratio $(n_0-n_1)/n_0$, in which n_0 and n_1 denote particle concentrations at the inlet and outlet of the airway segment, respectively. Deposition efficiency is based on the concentration at the inlet of the airway segment under consideration. The term applies to either forward or reverse flow.

The term fractional deposition, or fraction of deposition, is used to represent the fraction of number or mass of inhaled particles deposited in a respiratory region or the entire respiratory tract in a breath. Deposition fraction refers to the concentration of particles in the aerosol that has entered the nose or mouth. It is important to note that the particle concentration at the inlet of the tracheobronchial or alveolar region differs from that at the inlet of the nose or mouth. The fraction of deposition in a single region of the respiratory tract is known as regional deposition. Total deposition is expressed as a fraction of inhaled particles that are not exhaled. It is the sum of the fractions of deposition in all regions of the respiratory tract. In some occasions, deposition fraction refers to the concentration of particles in ambient air. It is important to mention the reference concentration when inhalability is included in deposition fraction.

Local deposition refers to deposition over a small surface area of airway walls. The rate of local deposition is expressed in terms of the number or mass of particles deposited on a given surface area per unit time. Deposition flux represents the rate of deposition per unit surface area. Deposition velocity is the ratio of deposition flux to the particle concentration far away from the surface (the concentration in the main stream). The term areal deposition density represents the number or mass of particles deposited over a unit surface area.

7.2 TOTAL AND REGIONAL DEPOSITION

In several anatomical models discussed in Chapter 2, the respiratory tract is divided into three regions: the extrathoracic, tracheobronchial, and alveolar regions. Because of the sequential nature of these three regions, only those particles that pass through upstream regions have a chance to deposit in downstream regions. In consequence deposition fraction in a downstream region depends not only on the deposition in the region itself but also on the deposition that takes place in upstream regions. During inhalation, the particles that deposit in the alveolar region are those that have not deposited in the extrathoracic and tracheobronchial regions. From the viewpoint of preventing alveolar deposition, the extrathoracic and tracheobronchial regions provide a relatively effective defense.

Another important aspect is the sequential nature of breathing. The order in which different portions of inspired air enters the respiratory tract has marked

effect on deposition. Particles in the first portion of inspired air spend longer times in the lungs and reach smaller airways than those in later portions of inspired air and, as a consequence, have higher probabilities to deposit. Furthermore, spatial and temporal inequalities in ventilation distribution tend to increase variation in residence times and lung depths for different portions of inspired air. Aerosol dispersion due to skewed axial velocity profiles also has effects on the distribution of residence times and lung depths.

In a normal breath, the air that penetrates to the deepest part of the lungs is the residual air remaining in the dead space when the previous breath ends. The fronts of freshly inspired aerosol reach only as far as alveolar ducts. Some freshly inspired particles deposit on airway walls as they move along the respiratory tract, but none of them have a chance to deposit in alveoli because intrinsic motion is not sufficiently fast to move them into expanding alveoli. The particles that deposit in alveoli are those already in the residual air that is pushed into alveoli by freshly inspired air. It is of some interest to note that particle deposition in alveoli differs markedly from the process of gas exchange. Molecular diffusion readily takes place for freshly inspired oxygen molecules over a distance of less than one millimeter between alveolar ducts and walls of alveoli.

7.2.1 Relative Contributions of Various Mechanisms

The most important parameter influencing deposition patterns is particle size. Deposition rates for a given particle size differ from region to region mainly because deposition mechanisms are strongly size-dependent. Large particles deposit primarily by inertial impaction and gravitational settling, while deposition of small particles is predominantly due to convective Brownian diffusion. The relative importance of these three mechanisms also depends on airway diameter, flow velocity, residence time, and particle hygroscopicity. In large airways where flow velocities are high, inertial impaction and convective Brownian diffusion are the main deposition mechanisms for large and ultrafine particles, respectively. On the other hand, deposition by gravitational settling and Brownian diffusion increases with increasing residence time and decreasing airway dimension. In consequence their relative contributions are higher in small airways where flow velocities are low and airway diameters are small. For particles larger than one micrometer in diameter, gravitational settling is the main mechanism for deposition in small airways. If particles are hygroscopic, they grow rapidly after entering the respiratory tract where the relative humidity is about 99.5%. The increase in size enhances deposition by inertial impaction and gravitational settling in small airways, but reduces deposition by Brownian diffusion.

The way in which relative contributions of various mechanisms vary with respiratory flow rate and tidal volume differs from region to region. In

extrathoracic and tracheobronchial regions, inertial deposition of large particles and deposition of ultrafine particles by convective Brownian diffusion increase with increasing inspiratory flow rate. Turbulent deposition of both large and small particles also increases as the flow velocity increases. Deposition in the alveolar region is mainly a result of Brownian motion and gravitational settling and therefore varies little with respiratory flow rate. On the other hand, increase in tidal volume brings a larger proportion of tidal air into smaller airways, thereby leading to higher deposition by gravitational settling and Brownian motion.

In a given airway, the ratio of a characteristic length for a deposition mechanism to the airway diameter is a good indicator of the relative importance of that particular mechanism. The characteristic length for inertial impaction is the stop distance. For gravitational settling and Brownian diffusion, the characteristic lengths are respectively the settling distance and root-mean-square displacement during the mean residence time in an airway. The characteristics of particle deposition in various regions of the respiratory tract can be seen from the relative magnitudes of these three ratios (Hinds, 1999).

Table 7.1 compares the relative importance of inertial impaction, gravitational settling, and Brownian diffusion for deposition of standard-density spheres in selected airways at a steady inspiratory flow rate of 300 cm^3/s. As the values in Table 7.1 indicate, large particles deposit in larger airways mainly by inertial impaction and in smaller airways mainly by gravitational settling, while small particles deposit in smaller airways mainly by Brownian diffusion. It is to be noted that this table does not include convective Brownian diffusion, which is important for deposition of ultrafine particles in large airways.

Table 7.1

Comparison of inertial impaction, gravitational settling, and Brownian diffusion for standard-density spheres in selected lung airways for a steady inspiratory flow rate of 300 cm^3/s. The stop distance is based on the average flow velocity in the preceding airway, while the settling distance and root-mean-square (rms) displacement are calculated for the residence time θ in each airway that has a diameter d_t. Air is at 37°C.

Airways	d_t, cm	θ, s	Stop distance/d_t, %			Settling distance/d_t, %			rms displacement/d_t, %		
			Particle diameter, μm			Particle diameter, μm			Particle diameter, μm		
			0.1	1	10	0.1	1	10	0.1	1	10
Main bronchus	1.22	0.049	0	0.04	3.03	0	0.01	0.92	0.06	0.01	0
Terminal bronchiole	0.074	0.049	0	0.03	2.84	0.01	0.17	15.2	0.99	0.20	0.06
Alveolar duct	0.036	0.304	0	0	0.48	0.05	2.21	194	5.08	1.00	0.30

7.2.2 Alveolar Deposition during Breath-Holding

During the pause between inhalation and exhalation, deposition of particles with negligible Brownian motion is mainly a result of gravitational settling. This type of deposition is most important in the alveolar region where the distance for a particle to settle onto a surface is relatively short. The time needed for a particle to deposit onto a surface depends on its settling velocity and the distance it has to fall through.

If the airspaces are filled with a monodisperse aerosol initially, the fraction of particles remaining airborne after a pause is termed aerosol persistence. For particles depositing by gravitational settling, aerosol persistence is a function of the mean airspace dimension, settling velocity, and duration of pause.

Persistence of particles between 0.5 and 1 μm in diameter can be measured using aerosol boluses. Particles in this size range deposit in the alveolar region mainly by gravitational settling and have relatively low deposition during transit in thoracic and tracheobronchial regions. The experiments are conducted with inhalation of an aerosol bolus to the total lung capacity followed by a pause and exhalation to the residual volume. The breathing maneuver assures that all the particles remaining airborne at the end of breath-holding are exhaled and that the measured aerosol persistence corresponds to the mean airspace dimension at the lung depth reached by the bolus. The ratio of the total particle number in exhaled air to that in inhaled air is the recovery. To correct for deposition taking place during inhalation and exhalation phases, the recovery for a given breath-holding time is normalized by the recovery for zero breath-holding time. The normalization approximately cancels the deposition that occurs during the two respiratory phases.

Experiments with six subjects using aerosol boluses show that the persistence of particles during breath holding decreases with increasing depth of inhalation of the bolus (Palmes et al., 1973). The test aerosol particles are 0.5-0.6 μm in diameter. In an experimental run, a subject inhales 200-800 cm^3 of clean air, with 25 cm^3 aerosol bolus inserted at the beginning of the breath, to a lung volume slightly below the total lung capacity. After holding the breath for 0.5-20 s, a forced exhalation is made. The exhaled volume is several times the inhaled volume. The results indicate that the mean airspace dimension is smaller in the deeper part of the lungs.

Rosenthal (1989) has developed a model of aerosol recovery using the distribution of chord lengths. Because airspaces in the alveolar region consist of alveolar ducts, alveolar sacs, and alveoli, there are three possible ways for a particle in an alveolus to settle onto a surface. The particle may fall onto the wall of the alveolus; it may pass through the alveolar opening into an alveolar duct and deposit on a duct wall; or it may pass through the duct into another alveolus and deposit on the wall of that alveolus. Fig. 7.1 illustrates the three cases by three vertical lines drawn in a typical airspace in the alveolar region.
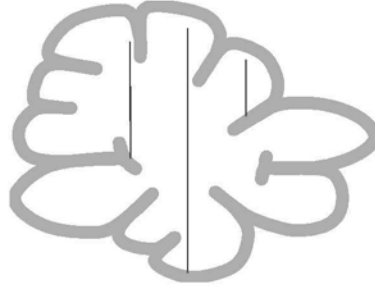
Fig. 7.1 Three possible ways for a particle in an alveolus to settle onto a surface in a typical airspace in the alveolar region.

The chord length or intercept, obtained by extending each vertical line in Fig. 7.1 to the upper wall of the alveolus, represents the maximum distance for a particle to fall before reaching a surface. Because of the enormous number of alveolar ducts, alveolar sacs, and alveoli, the chord lengths in the alveolar region approximately follow a lognormal distribution.

Rosenthal has measured aerosol recovery using dog lungs floated on a bed of saline in a Plexiglas box. The lungs expand and contract in response to oscillation of pressure in the box provided by a vacuum pump. The experiments use boluses of monodisperse aerosol consisting of di-2-ethylhexyl sebacate droplets. The mean aerodynamic diameter of particles varies from run to run, but is in the range of 0.6-0.8 μm. The bolus has a half-width of about 120 cm^3. The end inspiratory volume is near the total lung capacity and the exhaled volume is at least 1.5 times inhaled volume. The aerosol bolus is inspired deep into the lungs. Aerosol recovery is measured for breath-holding times in the range of 0-20 s. Experimental results show that the fraction of particles remaining at the end of a pause approximately fit an exponential function:

$$R_a \approx \exp(-cv_s t_h / l_m) \qquad (7.1)$$

Here l_m represents the mean chord length in the alveolar region, v_s the settling velocity, and t_h the duration of pause. The expression was first suggested by Landahl (1950) for gravitational settling in a tube during breath-holding. Using data obtained from nine dog lungs, Rosenthal has found that the equation gives the best fit when c is equal to 1.25.

It is to be noted that aerosol recovery follows the exponential form because the distance over which particles have to settle is distributed normally. One difficult problem in interpreting persistence measurements is that particles do not fill the entire airspaces evenly at the beginning of breath-holding.

Calculations for gravitational deposition from still air in a system of randomly oriented tubes show that the fraction of particles remaining airborne agrees well with the above equation for $v_s t_h / l_m < 0.5$ (Heyder, 1975). For $v_s t_h / l_m > 0.5$, the calculated results progressively fall below the values predicted by the above equation.

7.3 LOCAL DEPOSITION

Local deposition rates are required for estimating tissue doses of highly toxic particles. Deposition rates vary not only from region to region in the respiratory tract but also from site to site in an airway segment. The rate at which particles deposit at a specific site in an airway segment depends on several factors, including particle properties, geometric parameters of the airway segment, local aerodynamic characteristics, and concentration distribution of aerosol particles at the inlet cross section of the airway segment.

Local deposition has been studied using laboratory animals, physical models of lung airways, and hollow casts of various parts of the respiratory tract. These types of experiments permit detailed measurements of deposition in small surface areas. Methods for quantification of particles deposited on a small surface area include: (1) counting individual particles, (2) washing off particles for chemical analysis (such as fluorescence measurement if particles tagged with a fluorescent tracer are used), and (3) measuring the radioactivity of radio-labeled particles. Use of physical models also makes it possible to investigate the effects of various geometrical parameters of lung airways, such as branching angle, shape of carinal ridge, shape of transition zone, and orientation angle between successive bifurcations.

The materials used for construction of casts and physical models include plastics, glass, and metals. Although casts and physical models can simulate the general geometry of nose, mouth, pharynx, larynx, and tracheobronchial airways quite closely, they cannot duplicate fine structural features such as the glottal aperture, soft palate, cilia, and mucus. Nevertheless, data obtained from physical models and hollow casts represent initial deposition patterns, which are free of disturbance from clearance processes that take place continuously in the lungs. These data have proved useful for estimating local deposition rates.

Local deposition also has been investigated using theoretical analysis and numerical calculations. Recent developments in computational software have made it possible to calculate flow fields and particle trajectories in airway models with reasonably realistic geometry. These calculations are in general agreement with experimental observations.

7.3.1 Deposition in Single Bifurcations

Deposition rates are significantly higher in an airway bifurcation than in a

straight tube. During inhalation, a flow stagnation point occurs at the carinal ridge. Axial flow in the transition zone brings particles towards the flow divider at relatively high velocities. As a consequence, inertial impaction of large particles and convective Brownian diffusion of small particles lead to enhanced deposition at the carinal ridge and its vicinity. It is of interest to note that these locations of enhanced deposition, known as deposition hot spots, coincide with the sites where bronchial carcinomas occur at higher frequencies (Schlesinger and Lippmann, 1972). In addition to enhanced deposition at the carinal ridge and its vicinity, secondary flows created in each daughter tube during inhalation bring both large and small particles closer to walls and thereby give rise to slightly higher deposition along two bands, which originate at the carinal ridge and spiral around the tube in opposite directions.

Deposition during exhalation is less than during inhalation, because there is no wall surfaces directly facing the two air streams that merge in the transition zone and also because particles have already been markedly depleted in outgoing air. Nevertheless, slightly higher deposition of both large and small particles occurs on the ventral and dorsal edges that face the secondary flows created in the parent tube during exhalation (the edges are on the plane normal to the bifurcation plane).

Figure 7.2 indicates the locations where particles deposit at enhanced rates in an airway bifurcation during inhalation and exhalation. The highest deposition flux occurs at the carinal ridge and along a short section of the inner edge of each daughter tube.
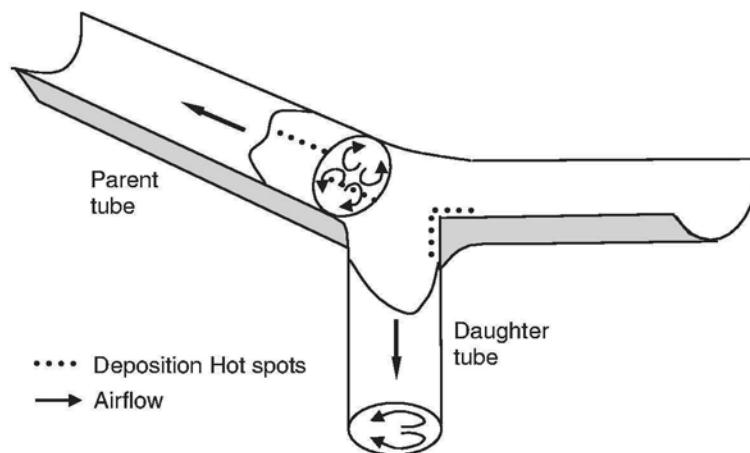
Fig. 7.2 An airway bifurcation showing deposition hot spots in the vicinity of carinal ridge during inhalation and on the ventral and dorsal edges of the parent tube during exhalation.

In gravitational deposition, no hot spots occur but the distribution of deposited particles is not uniform either. For a horizontal airway bifurcation, the wall that faces upward receives more particles than the wall that faces sideway, while the wall that faces downward receives no particles at all. Inclined airway bifurcations have deposition patterns somewhat different from a horizontal airway bifurcation. Although gravitational deposition is less sensitive to the direction of airflow, reduced particle concentrations in outgoing air also lead to lower deposition during exhalation.

Experiments with physical models have demonstrated uneven deposition in single airway bifurcations and deposition hot spots in the vicinity of carinal ridges for both large and small particles (Bell, 1970; Chua and Wang, 1972). Evidence has also been reported for slightly enhanced deposition along two spiral bands that face the two streams of secondary flow created in each daughter tube during inhalation (Yang et al., 1975; Ganatra et al., 1980).

Kim et al. (1994) have conducted deposition experiments using models of single airway bifurcations with varying geometry. The branching angle is between 30° and 45° and the diameter ratio of the daughter to parent tube ranges from 0.64 to 1. For Stokes number (based on the diameter of parent tube) greater than 0.03 and flow Reynolds number in the range of 283–3,397, deposition efficiency in the bifurcation region increases with increasing Stokes number but changes little with branching angle and diameter ratio of the daughter to parent tube. The results suggest that Stokes number is the predominant parameter that influences deposition of particles in the size range of 3-7 μm.

There are a large number of theoretical studies on deposition in single bifurcations. Bell and Friedlander (1973) have proposed a two-dimensional wedge model capable of predicting the non-uniformities of deposition along wedge walls. Cheng and Wang (1981) have made use of the similarity in flow characteristics between a bifurcation and a curved tube in their studies. Similar to a daughter tube in a bifurcation, a curved tube has a pair of secondary flows created when the flow changes its direction. Using a fully developed laminar flow proposed by Mori and Nakayama (1965), Cheng and Wang have calculated particle trajectories in a 90° bend and used limiting trajectories to compute the fraction of entering particles deposited by inertial impaction and interception. The calculations show that, for particle Reynolds number below 0.1 and curvature ratio between 4 and 30, impaction efficiency of a 90° bend is mainly a function of the Stokes number and flow Reynolds number. The results have proved useful for estimating deposition efficiency of an airway bifurcation.

Recent advances in computational software have made it possible to calculate flow fields and particle motion in airway bifurcations. Gradon and Orlicki (1990) have investigated deposition of particles from steady flow in a three-dimensional model of single airway bifurcation using numerical methods. Their results for local deposition flux show that convective diffusion of particles

can give rise to deposition hot spots at the carinal ridge.

Using a similar approach, Balásházy and Hofmann (1993a, b, and 1995) have conducted a series of numerical calculations for particle deposition by inertial impaction, gravitational settling, Brownian motion, and interception during inhalation and exhalation. For both symmetric and asymmetric models of single bifurcations, they have solved the steady-state three-dimensional Navier-Stokes equation numerically and then calculated particle trajectories using Monte Carlo techniques. Symmetric models used in the studies include a narrow and a wide bifurcation model (see Chapter 2 for details). The branching angle is 35° for both models and the bifurcation is placed horizontally. The diameter and length are both 0.5 cm for the parent tube and are 0.4 and 1.0 cm, respectively, for the daughter tubes. Two flow rates are considered: 1.25 and 4 L/min in the parent tube. The velocity profile at the inlet is either parabolic or flat. The particle diameter is in the range from 0.01 to 14 μm. Calculated spatial distribution patterns of deposition in various sections of a narrow bifurcation model are in excellent agreement with experimental results reported by Kim and Iglesias (1989) for deposition from inspiratory flow in symmetrical models of single bifurcation with branching angles between 30 and 45°. For a Stokes number (based on the radius of daughter tube) of 0.18, about 90% of deposition in the bifurcation occurs in the entrance sections of daughter tubes. Even for a Stokes number of 0.05, about 70% of deposition takes place in the entrance sections. For a given Stokes number, deposition in the narrow bifurcation tends to be higher than in the wide bifurcation. In general, deposition during exhalation is lower than during inhalation.

Patterns of enhanced deposition have been investigated for inhalation and exhalation (Balásházy and Hofmann, 1995). Calculations for inspiratory flow show that enhanced deposition occurs for both 0.01- and 10-μm particles at the carinal ridge and on the inside edge of each daughter tube. For expiratory flow, deposition hot spots occur along the ventral and dorsal edges of the parent tube for large particles, but on the ventral and dorsal edges of the transition zone for ultrafine particles. More recently, Hofmann et al. (2001) have examined the relationship between secondary flows and particle deposition patterns in three-dimensional airway bifurcations using steady inspiratory and expiratory flows. Calculations for 0.01- and 10-μm particles show that changes in the shape of transition zone, branching angle, flow rate, and inlet flow velocity profile lead to variations in secondary flow and particle deposition patterns.

Zhang et al. (1997) have computed the efficiency of deposition by inertial impaction in three-dimensional symmetric models of single bifurcations during inhalation. The results of calculations are used to derive empirical expressions for deposition efficiency as a function of Stokes number, flow Reynolds number, and bifurcation angle for a parabolic and a uniform velocity profile at the inlet. The empirical expressions are in good agreement with experimental data.

Baláshazy and Hofmann (2001) have solved the Navier-Stokes and continuity equations numerically for steady flow fields in different geometric models of airway bifurcations, which are then used to simulate the transport of particles by the Monte Carlo techniques. The inlet flow used in the calculations has a parabolic velocity profile. The geometric models studied include a narrow bifurcation, a wide bifurcation, and a physiologically realistic bifurcation. The diameters of the parent and daughter tubes correspond to those of Generations 3 and 4 in Weibel's lung model A. The simulation for particle motion takes into account particle inertia, gravitational settling, Brownian motion, and interception. To describe the uneven distribution of deposited particles, they have defined a local deposition enhancement factor as the ratio of the local deposition rate in a given surface element to the average deposition rate in the entire surface area of an airway bifurcation. For flow rates in the trachea ranging from 0.17 to 2 L/s and particle sizes ranging from 0.001 to 20 μm, the maximum enhancement factor is about 100 for a surface element of 100 x 100 μm in the physiologically realistic bifurcation model. Baláshazy and Hofmann have suggested that a surface element of this size, which corresponds to about 10 x 10 biological cells, is needed for the development of tumors.

7.3.2 Effects of Successive Bifurcations

Distribution of deposited particles in successive airway bifurcations is uneven and deposition hot spots occur in the vicinity of carinal ridges during inhalation. These deposition patterns have been observed in experimental studies using physical models and hollow casts of lung airways (Martin and Jacobi, 1972; Schlesinger and Lippmann, 1972 and 1978).

In successive bifurcations, the upstream bifurcation has marked effects on deposition in downstream bifurcations. Lee and Wang (1977) have measured deposition velocities of particles between 0.1 and 2 μm in models of two successive bifurcations. The measurements indicate that the deposition velocities in a bifurcation normal to its preceding bifurcation are considerably higher than in a bifurcation placed in the same plane as its preceding bifurcation.

Chen and Wang (1983) have calculated inertial deposition velocities in two-dimensional models of successive bifurcations. The results show that there are marked differences in deposition efficiency among channels of the same generation in both symmetric and asymmetric models. More recently, calculations by Lee et al. (1996) have indicated that, for symmetric and asymmetric three-dimensional models of successive bifurcations, the deposition efficiency of a bifurcation that is perpendicular to its preceding bifurcation is about 40% higher than the deposition efficiency of a bifurcation that is in the same plane as its preceding bifurcation. The calculations are in good agreement with experimental results reported by Lee and Wang (1977).

7.3.3 Deposition from Cyclic Flow

Inertial deposition efficiency of bronchial airways is substantially higher for cyclic flow than for constant flow. This has been demonstrated in a series of studies using hollow casts of the tracheobronchial tree with a variable-orifice larynx (Lippmann et al., 1983). Experimental studies using models of single bifurcations (Kim and Garcia, 1991a, b) have shown that cyclic flow enhances inertial deposition during both inspiratory and expiratory phases. During inhalation, the efficiency of deposition by inertial impaction from a cyclic flow is 80-200% higher than from a constant flow. The increase in deposition is about 25% during exhalation.

Using hollow casts of the human bronchial tree, Cohen et al. (1990) have measured deposition efficiency of individual airway segments for ultrafine particles from cyclic flow. The measured deposition efficiency is markedly higher than predicted from the theory of steady-state convective Brownian diffusion in a circular tube with fully developed laminar flow (see Chapter 4). The enhanced deposition efficiency has been explained as a result of differences in flow pattern between a straight tube and the transition zone of an airway bifurcation (Yu and Cohen, 1994).

Zhang et al. (2002) have carried out numerical calculations for deposition of micron-sized particles from cyclic flow in a model of triple bifurcations. Deposition efficiency is higher for cyclic flow than for steady flow. The maximal relative difference in deposition efficiency can be as high as 50% for Stokes number (based on the parent tube diameter and mean flow rate) between 0.02 and 0.12.

Theoretical analysis (Kojic and Tsuda, 2004) have shown that flow oscillation may have marked effects on the site of gravitational deposition from laminar flow in a straight tube, when the time for gravitational settling is appreciable relative to the time for flow oscillation.

7.3.4 Deposition of Fibers in Single Bifurcations

Deposition of glass fibers from steady and cyclic flow have been investigated using a brass model of single bifurcation (Myojo, 1987, 1989, and 1990). The diameters of parent and daughter tubes of the bifurcation model correspond to the tubes in Generations 3 and 4 in Weibel's lung model A. The length of the parent tube is 15 cm. The bifurcation is symmetric, with a branching angle of 45°. Before entering the bifurcation model, the test aerosol passes through a neutralizer containing [85]Kr to reduce particle charges to the Boltzmann equilibrium distribution.

Using an expression for the drag force on a rod given by Harris and Fraser (1976), Myojo has defined the Stokes number for randomly oriented fibers as

$$\text{Stk}_f = \frac{\rho \, d_f^2 U \sin\theta}{8\mu d_t \left[\dfrac{0.385}{\ln(2l_f / d_f) - 0.5} + \dfrac{1.230}{\ln(2l_f / d_f) + 0.5} \right]}$$

(7.2)

Here d_f and l_f are the fiber diameter and length, respectively, ρ the mass density of the fiber, U the mean flow velocity in a daughter tube, θ the branching angle, μ the air viscosity, and d_t the diameter of a daughter tube. Two flow rates are used in the tests for deposition from steady flow: 15.6 and 31.2 cm³/s in a daughter tube. At these flow rates, the average deposition efficiency for fibers 1-2 μm in diameter is in the range of 6.1×10^{-4} to 8.8×10^{-3}. Deposition increases with increasing Stokes number and fiber length. At small Stokes number, the deposition of fibers depends strongly on their length, indicating that it is mainly a result of interception. Fibers deposited on wall surfaces are oriented in the flow direction and enhanced deposition takes place at the carinal ridge. Data obtained using cyclic flow at 30 breaths per minute indicate that the deposition efficiencies are 1.4-1.7 times those measured using steady flow at the same average flow rate (Myojo, 1989).

Monte Carlo simulations have been conducted for deposition of rigid fibers from steady flow in three-dimensional bifurcation models (Ahmed et al., 1997). The simulation takes into consideration inertial impaction, gravitational settling, Brownian motion, and interception. At the inlet to the airway model, the flow velocity profile is parabolic and the starting points of particle trajectories are selected randomly according to the velocity distribution. Calculated efficiencies of deposition from inspiratory flow for the fibers that enter the airway model with random orientations are in fair agreement with experimental data reported by Myojo (1987). Interceptive deposition of long fibers leads to an enhanced dose at the transition zone because of the sudden change in flow direction. Deposition hot spots occur in the vicinity of the carinal ridge during inhalation and at the ventral and dorsal edges of the parent tube that face the secondary flow during exhalation.

PROBLEMS

7.1 If a physiologically realistic model of two successive bifurcations is constructed using the method described by Heistracher and Hofmann (1995), what deposition patterns can be expected for large and small particles in bifurcations of the second generation.

7.2 Calculate the root-mean-square displacement in one second for 0.01-μm particles and compare it with the diameter of an alveolar duct.

REFERENCES

Ahmed, M., Hofmann, W., Baláshazy, I. and Heistracher, T. (1997). Deposition of rigid fibers in three-dimensional airway bifurcation models. J. Aerosol Sci. 28, Suppl. 1, S429-S430.

Baláshazy, I. and Hofmann, W. (1993a). Particle deposition in airway bifurcations – I. Inspiratory flow. J. Aerosol Sci. 24, 745-772.

Baláshazy, I. and Hofmann, W. (1993b). Particle deposition in airway bifurcations – II. Expiratory flow. J. Aerosol Sci. 24, 773-786.

Baláshazy, I. and Hofmann, W. (1995). Deposition of aerosol in asymmetric airway bifurcations. J. Aerosol Sci. 26, 273-292.

Baláshazy, I. and Hofmann, W. (2001). Fluid dynamics and related particle deposition patterns in human airway bifurcations. In: Medical Applications of Computer Modeling: The Respiratory System, pp. 83-108 (Ed. Martonen, T.B.). WIT Press, Southampton, UK.

Bell, K.A. (1970). Theory of Particle Deposition by Inertial Forces at Bifurcations in the Human Respiratory Tract. M.S. Thesis. California Institute of Technology, Pasadena, CA.

Bell, K.A. and Friedlander, S.K. (1973). Aerosol deposition in models of a human lung bifurcation. Staub Reinhalt Luft 33, 178-182.

Chen, H. and Wang, C.S. (1983). Particle deposition in models of successive bifurcations. J. Chin. Inst. Chem. Eng. 14, 191-203.

Cheng, Y.S. and Wang, C.S. (1981). Motion of particles in bends of circular pipes. Atmos. Environ. 15, 301-306.

Chua, J.H. and Wang, C.S. (1972). Deposition of submicron particles from steady flows in a branched tube. J. Res. Assoc. Powder Tech., Japan 9 (Special issue), 37-45.

Cohen, B.S., Sussman, R.G., and Lippmann, M. (1990). Ultrafine particle deposition in a human tracheobronchial cast. Aerosol Sci. Technol. 12, 1082-1091.

Ganatra, C.P., Gebreyes, K. and Wang, C.S. (1980). Deposition of saline droplets in a model of the human bronchial tree. Chem. Eng. Commun. 4, 523-529.

Gradon, L and Orlicki, D. (1990). Deposition of inhaled aerosol particles in a generation of the tracheobronchial tree. J. Aerosol Sci. 21, 3-19.

Harris, R.L. and Fraser, D.A. (1976). A model for deposition of fibers in the human respiratory system. Am. Ind. Hyg. Assoc. J. 37, 73-89.

Heistracher, T. and Hofmann, W. (1995). Physiologically realistic models of bronchial airway bifurcations. J. Aerosol Sci. 26, 497-509.

Heyder, J. (1975). Gravitational deposition of aerosol particles within a system of randomly oriented tubes. J. Aerosol Sci. 6, 133-137.

Hinds, W.C. (1999). Aerosol Technology: Properties, Behavior, and Measurement of Airborne Particles, Second edition. John Wiley & Sons, New York.

Hofmann, W., Baláshazy, I. and Heistracher, T. (2001). The relationship between secondary flows and particle deposition patterns in airway bifurcations. Aerosol Sci. Technol. 35, 958-968.

Kim, C.S. and Iglesias, A.J. (1989). Deposition of inhaled particles in bifurcating airway models: I. Inspiratory deposition. J. Aerosol Med. 2, 1-14.

Kim, C.S. and Garcia, L. (1991a). Particle deposition in cyclic bifurcating tube flow. Aerosol Sci. Tecnnol. 14, 302-315.

Kim. C.S. and Garcia, L. (1991b). Particle deposition in cyclic converging tube flow. Aerosol Sci. Technol. 14, 322-330.

Kim, C.S., Fisher, D.M., Lutz, D.J. and Gerrity, T.R. (1994). Particle deposition in bifurcating airway models with varying airway geometry. J. Aerosol Sci. 25, 567-581.

Kojic, M. and Tsuda, A. (2004). A simple model for gravitational deposition of non-diffusing particles in oscillatory laminar pipe flow and its application to small airways. J. Aerosol Sci. 35, 245-261.

Landahl, H.D. (1950). On the removal of air-borne droplets by the human respiratory tract. I. The lung. Bull. Math. Biophys. 12, 43-56.

Lee, J.W., Goo, J.H. and Chung, M.K. (1996). Characteristics of inertial deposition in a Double bifurcation. J. Aerosol Sci. 27, 119-138.

Lee, W.C. and Wang, C.S. (1977). Particle deposition in systems of repeatedly bifurcating tubes. In: Inhaled Particles IV, Proceedings of an International Symposium Organized by the British Occupational Hygiene Society, Edinburgh, September 22-26, 1975, pp. 49-60 (Ed. Walton, W.H.). Pergamon Press, Oxford.

Lippmann, M., Gurman, J. and Schlesinger, R. (1983). Role of particle deposition in occupational lung disease. In: Aerosols in the Mining and Industrial Work Environments, Vol. I, pp. 119-183 (Eds. Marple, V.A. and Liu, B.Y.H.). Ann Arbor Science, Ann Arbor, Michigan, USA.,

Martin, D. and Jacobi, W. (1972). Diffusion deposition of small-sized particles in the bronchial tree. Health Physics 23, 23-29.

Mori, Y. and Nakayama, W. (1965). Study on forced convective heat transfer in curved pipes: I. Laminar region. Int. J. Heat Mass Transfer 8, 67-72.

Myojo, T. (1987). Deposition of fibrous aerosol in model bifurcating tubes. J. Aerosol Sci. 18, 337-347.

Myojo, T. (1989). Deposition of fibrous aerosol in a model of a human lung bifurcation under cyclic flow conditions. J. Aerosol Res. (Japan) 4, 198-205.

Myojo, T. (1990). The effect of length and diameter on the deposition of fibrous aerosol in a model lung bifurcation. J. Aerosol Sci. 21, 651-659.

Palmes, E.D., Wang, C.S., Goldring, R.M. and Altshuler, B. (1973). Effect of depth of inhalation on aerosol persistence. J. Appl. Physiol. 34, 356-360.

Rosenthal, F.S. (1989). Aerosol recovery following breathholding derived from the distribution of chordlengths in pulmonary tissue. J. Aerosol Sci. 20, 267-277.

Schlesinger, R.B. and Lippmann, M. (1972). Particle deposition in casts of the human upper tracheobronchial tree. Am. Ind. Hyg. Assoc. J. 33, 237-251.

Schlesinger, R.B., Lippmann, M. (1978). Selective particle deposition and bronchogenic carcinoma. Environ. Res. 15, 424-431.

Yang, Y.M., Lee, W.C. and Wang, C.S. (1975). Deposition of half-micron particles from steady flows in models of human bronchial airways. AIChE Symposium Series, No. 147, Vol. 71, Air: I. Pollution Control and Clean Energy, pp. 33-37.

Yu, C.P. and Cohen, B.S. (1994). Tracheobronchial airway deposition of ultrafine particles. In: Inhaled Particles VII, Proceedings of an International Symposium on Inhaled Particles Organized by the British Occupational Hygiene Society, September 16-22, 1991 (Eds. Dodgson, J. and McCallum, R.L.). Ann. Occup. Hyg. 38, Suppl. 1, 83-89.

Zhang, L., Asgharian, B. and Anjilvel, S. (1997). Inertial deposition of particles in the human upper airway bifurcations. Aerosol Sci. Technol. 26, 97-110.

Zhang, Z., Kleinstreuer, C. and Kim, C.S. (2002). Cyclic micron-size particle inhalation and deposition in a triple bifurcation lung airway model. J. Aerosol Sci. 33, 257-281.

Chapter 8

Experimental studies on total and regional deposition

Over past decades, experimental studies with human subjects have provided consistent data on total and regional deposition. These results have led to a better understanding of the influences of particle properties, lung volume, tidal volume, and breathing frequency. This chapter focuses on deposition data obtained mainly with normal adults. An individual with obstructive lung disease can have a markedly different deposition pattern, with enhanced local deposition in some parts of the respiratory tract.

Since clearance mechanisms and tissue response to deposited particles differ from region to region, data on deposition in a specific respiratory region are useful for assessing the effect of inhaled particles. Regional deposition data also have applications in designing devices and procedures for delivery of aerosolized pharmaceutical agents.

Because of the sequential nature of respiratory regions, an upstream region has profound effects on the deposition pattern in a downstream region. It is important to distinguish deposition fraction from deposition efficiency of a downstream region. These terms have been defined in Chapter 7.

8.1 EXPERIMENTAL METHODS

There are several ways to conduct inhalation experiments with human subjects and the results differ accordingly. In single-breath experiments, a subject inhales from functional residual capacity and then exhales to residual volume. The data thus obtained represent deposition of particles inhaled in the current breath.

If the subject breathes at a given tidal volume, some particles do not deposit during the current breath. They simply move into reserve air and deposit in subsequent breaths. Particle concentration in reserve air reaches a steady state after the subject has inhaled a test aerosol for several breaths. To study lung deposition under steady-state conditions, it is important to let a subject breathe continuously under controlled conditions for several breaths before taking measurements of particle concentration in exhaled air.

Respiratory deposition depends on both physical and biological factors. The biological factors include anatomical and inhalation parameters. Most studies are conducted with subjects breathing spontaneously at specified frequency and tidal volume. In some studies, the subject breathes at constant flow rates. Another important parameter to control is the lung volume from which a subject begins to inhale aerosols. The functional residual capacity has been used as a reference point in most studies. In studies with special objectives, inhalation of

aerosols begins at a volume other than the functional residual capacity. A critical part of deposition experiments is to train the subject to breathe at specified lung volume, tidal volume, breathing frequency, and the length of pause between inhalation and exhalation. Even under close control of inhalation parameters, considerable intersubject variability still can occur in deposition data. Differences arise mainly from variability in anatomical parameters among individuals.

Inhalation of insoluble particles tagged with low level radioactive materials facilitates external counting of gamma activity in the thorax. In a series of studies, Lippmann and his associates have used monodisperse aerosols consisting of insoluble iron oxide particles (Lippmann, 1977; Chan and Lippmann, 1980). The particles, tagged with either ^{99m}Tc (half-life of 6 h, photopeak at 143 keV) or ^{198}Au (half-life of 2.8 d, photopeak at 410 keV), have a density of 2.56 g/cm^3. Before inhalation, the aerosols are passed through a neutralizer to attain the Boltzmann equilibrium charge distribution. Gamma activity from particles deposited in the thorax is measured using an array of four collimated NaI(Tl) scintillation detectors in a low background gamma counting chamber. A collimator, which works like a lens, confines the field of detection to a small region.

Stahlhofen and his associates have also used insoluble iron oxide particles labeled with ^{198}Au in their studies of regional deposition (Stahlhofen et al., 1980, 1981a, 1981b, 1983). The average particle density is 3.2 g/cm^3. In the preparation of aqueous Fe$_2$O$_3$-colloid for atomization, FeCl$_3$ is hydrolyzed and the resulting aqueous Fe$_2$O$_3$-colloid thoroughly dialyzed to remove the residual chloride. Without a thorough dialysis, particles with a small amount of hygroscopic chloride tend to grow when inspired into the lungs.

Other radiotracers used in deposition studies include ^{99m}Tc-labeled polystyrene particles and ^{111}In-labelled Teflon particles.

8.1.1 Experimental Methods for Extrathoracic Deposition

Deposition in the mouth, pharynx, and larynx has been measured using radio-labeled particles. The subject breathes the test aerosol through a mouthpiece. Immediately after inhalation, particles deposited in the mouth are washed off for gamma counting. Activity in the pharynx and larynx is measured externally. Because some deposited particles are swallowed during the inhalation experiment, activity in the stomach should be included as part of extrathoracic deposition (Stahlhofen et al., 1980).

Nasal deposition can be determined using non-radioactive particles. Data on total deposition in the respiratory tract are obtained with four different breathing maneuvers in inhalation and exhalation: (1) nose-in and nose-out, (2) nose-in and mouth-out, (3) mouth-in and nose-out, and (4) mouth-in and mouth-out. A mouthpiece is used in experiments with mouth breathing. By using all four

breathing maneuvers and assuming that oral deposition is negligible when breathing through a tube, it is possible to determine the deposition efficiency of nasal airways separately for the two respiratory phases (Heyder and Rudolf, 1977).

$$\eta_{In} = 1 - \left[\frac{(1 - E_{nn})(1 - E_{no})}{(1 - E_{oo})(1 - E_{on})} \right]^{1/2} \tag{8.1}$$

$$\eta_{En} = 1 - \left[\frac{(1 - E_{nn})(1 - E_{on})}{(1 - E_{oo})(1 - E_{no})} \right]^{1/2} \tag{8.2}$$

Here E_{nn}, E_{no}, E_{on}, and E_{oo} are the measured total deposition fractions for nose-in nose-out, nose-in mouth-out, mouth-in nose-out, and mouth-in mouth-out breathing, respectively. These two expressions can be derived using the concept of compartments-in-series model to be described in Chapter 9.

Hollow casts and physical models of extrathoracic airways have been used extensively for studies of particle deposition. The casts and models are usually prepared from airways of cadavers or based on airway dimensions obtained from magnetic resonance imaging (MRI) scans. It is relatively simple to measure particles deposited in a cast using either radiometric counting or chemical analysis. Experiments with casts can also avoid swallowing problems. However, this approach has limitations in duplicating the geometry and fine surface structures of extrathoracic airways, especially the glottal aperture and the positions of tongue and soft palate. Difficult problems also arise in simulating oscillatory flow to obtain velocity and concentration boundary layers similar to those in human airways.

8.1.2 Experimental Methods for Thoracic Deposition

Results of earlier studies (Albert and Arnett, 1955; Albert et al., 1973) indicate that clearance of particles deposited in the tracheobronchial tree is essentially completed within 24 hours. By making use of this clearance pattern, it is possible to separate the tracheobronchial and alveolar deposition. This approach has been used in studies conducted by several research groups.

In the studies carried out by Lippmann and his associates (Lippmann, 1977; Chan and Lippmann, 1980), the subject breathes spontaneously through a mouthpiece at a frequency of 14 breaths/min and a tidal volume of approximately 1,000 cm^3. Measurements of gamma activity are made 5 minutes and 24 hours after exposure. The fraction of initial deposition cleared in the first 24 hours is considered to be the tracheobronchial deposition.
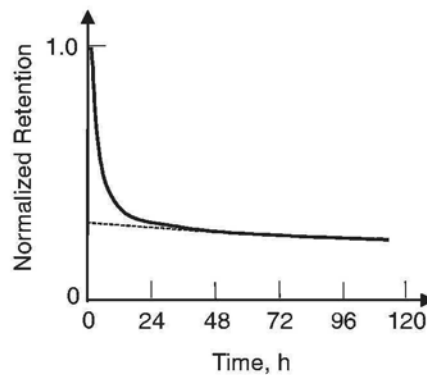
Fig. 8.1 Normalized retention as a function of clearance time.

In the investigations conducted by Stahlhofen and his associates (Stahlhofen et al., 1980, 1981a, 1981b, 1983), the subject breathes through a cylindrical mouthpiece, 16 mm in inner diameter, at constant flow rates of 250 and 750 cm^3/s. The gamma activity from particles deposited in the thorax is measured within 2 minutes after inhalation and followed for several days. The results indicate that clearance of deposited particles consists of a fast phase and a slow phase. If the thoracic activity data measured at various times after completion of the tracheobronchial clearance are normalized by the activity measured immediately after inhalation and fitted by a linear or exponential function of clearance time, the function can be extrapolated back to the beginning of clearance (or the end of exposure). The intercept thus obtained represents the slow-cleared fraction and the balance of the initial deposition the fast-cleared fraction (see Fig. 8.1). Values of the intercept determined with linear and exponential functions are nearly identical. For the purposes of comparison, it is usually assumed that the fast- and slow-cleared fractions thus evaluated correspond to deposition fractions in the tracheobronchial and alveolar regions, respectively. The results obtained by this method differ slightly from tracheobronchial and alveolar deposition fractions determined using the 24-hour clearance cutoff point.

Aerosol boluses have been used as a probe to measure deposition fraction for inhalation to a given volumetric depth of the lungs. In this type of experiments, the subject inhales filtered air from the functional residual capacity to a prescribed inspiratory volume and then exhales to the residual volume, with an aerosol bolus injected at a specified volumetric depth of the lungs during inhalation. The result thus obtained represents deposition for the aerosol bolus that has reached the specified lung depth. Such data differ from those obtained using an entire breath of aerosol, because in the latter case different portions of aerosol reach different lung depths and spend different lengths of time in the

respiratory tract. However, it is quite difficult to relate lung depths to anatomical regions because of spatial and temporal inequalities in ventilation distribution.

8.1.3 Experimental Methods for Total Deposition

Total deposition can be measured using non-radioactive particles. During an inhalation experiment, particle concentration and flow rate are continuously measured at suitable locations outside the mouth by a photometer and a Fleisch tube, respectively. Integrating the product of particle concentration and flow rate with respect to time during inhalation and exhalation gives, respectively, the total number of particles inhaled and exhaled. Alternatively, the number of particles in inspired and expired air can be counted near the mouth. The ratio of the total number of particles in expired air to that in inspired air is the total deposition. Because the subject breathes through a mouthpiece, the result thus obtained does not include extrathoracic deposition.

8.2 DEPOSITION IN HEAD AIRWAYS

In the nose, nasal hairs and bends remove large particles effectively by inertial impaction and turbulent deposition. Under conditions of light exercise and nose breathing, approximately 80% of inhaled 5-μm particles deposit in the nose. Most of the deposition takes place near the transition from the anterior to posterior nasal passages. Deposition by inertial impaction in head airways increases with increasing particle diameter.

Because of high diffusion coefficients and flow velocities, ultrafine particles also have high deposition rates in head airways. Deposition by convective Brownian diffusion increases with decreasing particle diameter.

As a results of inertial impaction and convective Brownian diffusion, the fractional deposition curve of head airways is U-shaped, with the minimum at about 0.1 μm. Increase in respiratory flow rate promotes extrathoracic deposition by inertial impaction as well as convective Brownian diffusion.

8.2.1 Data from Human Subjects

Data obtained with human subjects show large variations arising from intersubject variability in anatomical parameters as well as differences in experimental designs. Earlier data have been reviewed and analyzed by Yu et al. (1981).

As discussed in Chapter 4, deposition by inertial impaction is mainly a function of Stokes number, while deposition by convective Brownian diffusion primarily depends on Schmidt and flow Reynolds numbers. Using experimental data obtained with human subjects, Rudolf et al. (1986) have derived the following empirical expression for inertial deposition efficiency of nasal airways during inhalation:

$$\eta_n = 1 - \frac{1}{1 + 0.0003 d_a^2 Q} \qquad \text{for inertial deposition} \qquad (8.3)$$

Here d_a is the aerodynamic diameter in μm and Q the volumetric flow rate in cm^3/s.

During natural mouth breathing, deposition in the mouth varies with the position of tongue and the extent to which the mouth is open. When a mouthpiece is used, inertial deposition in the extrathoracic region occurs mostly in the larynx (Stahlhofen et al., 1980; Emmett and Aitken, 1982). Flow in the larynx is turbulent. There are jets, secondary flows, and recirculation downstream of the ventricular and vocal folds. These flow patterns give rise to high deposition rates. Furthermore, deposition in the larynx varies with flow rate and tidal volume because of changes in the glottal aperture. Statistical analysis of data obtained with mouthpiece breathing gives the following empirical expression for inertial deposition efficiency of oral airways and larynx during inhalation (Rudolf et al., 1990):

$$\eta_o = 1 - \frac{1}{1 + 0.00011(d_a^2 Q^{0.6} V_t^{-0.2})^{1.4}} \qquad \text{for inertial deposition} \qquad (8.4)$$

Here d_a is the aerodynamic diameter in μm, Q the volumetric flow rate in cm^3/s, and V_t the tidal volume in cm^3. The group, $d_a^2 Q^{0.6} V_t^{-0.2}$, is termed impaction parameter.

Fig. 8.2 displays experimentally determined deposition fraction as a function of impaction parameter for head airways during mouthpiece breathing. It is important to note that the data plotted in the figure are deposition fraction for a complete breath.

8.2.2 Data from Casts

Recent studies on deposition in casts of extrathoracic airways have focused on small particles. Data from casts exhibit a smaller degree of scatter, because only a few casts have been constructed and the same casts are used in most experiments. Using data obtained from replicate casts of the human naso-oropharyngeal passage and larynx, Swift et al. (1992) have derived the following empirical expression for the diffusional deposition efficiency during inhalation:

$$\eta_{In} = 1 - \exp(-18 D^{1/2} Q^{-1/8}) \qquad \text{for diffusional deposition} \qquad (8.5)$$

Here D is the particle diffusion coefficient in cm^2/s and Q the volumetric flow rate in cm^3/s.

Making use of deposition data from human volunteers and casts, Cheng (2003) has combined the expressions for efficiency of deposition due to inertial impaction and convective Brownian diffusion into a single equation. Since the deposition data for inhalation and exhalation do not differ significantly, a single regression equation is given for either phase of a breathing cycle. For an adult, Cheng has obtained the following empirical expressions for deposition efficiency of the nasal and oral airways, respectively

$$\eta_n = 1 - \exp(-0.000185\ d_a^2 Q - 36.5 D^{0.50} Q^{-0.28}) \qquad (8.6)$$
$$\text{for inertial and diffusional deposition}$$

$$\eta_o = 1 - \exp(-0.0000166\ d_a^2 Q - 48.8 D^{0.66} Q^{-0.31}) \qquad (8.7)$$
$$\text{for inertial and diffusional deposition}$$

Here d_a is the aerodynamic diameter in μm, Q the flow rate in cm^3/s, and D the particle diffusion coefficient in cm^2/s. The exponential functions in the above two equations contain two terms: the first term for inertial impaction and the second for convective Brownian diffusion. The equations apply to either phase of a breathing cycle.
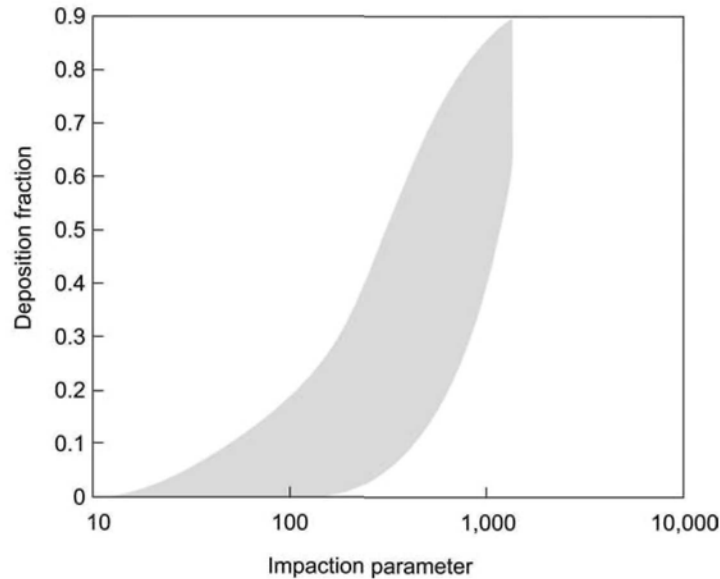
Fig. 8.2 Extrathoracic deposition fraction during mouthpiece breathing. The band covers the data from Lippmann (1977), Chan and Lippmann (1980), and Stahlhofen et al. (1980, 1981a, and 1983). Impaction parameter: $d_a^2 Q^{0.6} V_t^{-0.2}$ (adapted from ICRP, 1994).

In addition, Cheng has incorporated characteristic airway dimensions in nasal deposition equations. For inertial deposition, the Stokes number is defined in terms of the smallest cross-sectional area of nasal airways. The inertial deposition efficiency during inhalation or exhalation is given by:

$$\eta_n = 1 - \exp(-110\,\text{Stk}_n) \qquad \text{for inertial deposition} \qquad (8.8)$$

$$\text{Stk}_n = \frac{\pi^{0.5} d_a^2 Q}{18\mu A_m^{1.5}} \qquad (8.9)$$

Here μ is the air viscosity in g/cm·s, Q the flow rate in cm³/s, d_a the aerodynamic diameter in cm, and A_m the minimum cross-sectional area of nasal airways in cm².

For diffusional deposition, the characteristic airway dimension is related to the surface area of the turbinate region. Results of analysis give the following empirical expression for diffusional deposition efficiency of nasal airways during inhalation or exhalation:

$$\eta_n = 1 - \exp(-0.78\,S_f^{4.14} D^{0.5} Q^{-0.28}) \qquad \text{for diffusional deposition} \qquad (8.10)$$

Here S_f is the average airway shape factor of the turbinate region, D the particle diffusion coefficient in cm²/s, and Q the flow rate in cm³/s.

The average airway shape factor of the turbinate region is defined as the average value of the ratio of airway perimeter to a reference perimeter. Using magnetic resonance imaging (MRI) scans of the nasal airways from 10 adult male volunteers, Cheng et al. (1996) have obtained 1.28 to 3.10 cm² for A_m and 2.09 to 2.90 for S_f.

Eqs. (8.8) to (8.10) can be used to predict nasal deposition for subjects with different airway dimensions.

8.3 DEPOSITION IN THE TRACHEOBRONCHIAL REGION

In the tracheobronchial region, deposition of large particles takes place primarily by inertial impaction in larger airways and by gravitational settling in smaller airways. For ultrafine particles, the predominant mechanism for deposition is convective Brownian diffusion. There are many experimental studies on regional deposition. A comprehensive review of earlier studies on regional deposition has been given by Lippmann (1977).

The study by Chan and Lippmann (1980), which has extended the earlier studies of Lippmann and Albert (1969) and Lippmann (1977) to smaller

particles, includes 26 healthy non-smokers. The monodisperse aerosols used in the study consist of insoluble iron oxide particles tagged with either ^{99m}Tc or [198]Au. Particle size ranges from 0.2 μm (mass median diameter) to 7 μm (mass median aerodynamic diameter). The subject breathes through a mouthpiece at a frequency of 14 breaths/min and a tidal volume of about 1,000 cm³. The subject follows audible signals for the breathing maneuver.

In a series of studies, Stahlhofen et al. (1980, 1981a, 1981b, 1983) have measured regional deposition using constant flow rates of 250 and 750 cm³/s. The tidal volume ranges from 250 to 1500 cm³. The monodisperse aerosols used in the study consist of insoluble iron oxide particles labeled with [198]Au. Particle size ranges from 1 to 14 μm in aerodynamic diameter.

Foord et al. (1978) have measured total and regional deposition of inhaled particles in 15 healthy male non-smokers using monodisperse aerosols containing ^{99m}Tc-labeled polystyrene particles. The study includes three different particle sizes, 2.5, 5.0, and 7.5 μm. The subject breathes through the mouth with several different breathing patterns: the tidal volume ranging from 0.5 to 2.0 L and the breathing frequency from 10 to 25 breaths/min. The activity cleared from the lungs in the first 24 hours after inhalation of the radio-labeled particles is used to calculate fractional deposition in the tracheobronchial region.

Emmett and Aitken (1982) have reported data on total and regional deposition in 12 healthy subjects breathing through the mouth. The study uses monodisperse aerosols containing radioactively labeled polystyrene particles between 3.5 and 10 μm in aerodynamic diameter.

Fig. 8.3 shows experimentally determined deposition fraction for the tracheobronchial region. There are considerable variations among the data reported by various research groups. The band covers the data reported by the four groups mentioned above. The smallest particle size used in these studies is about 0.15 μm.

Because most particles larger than 8 μm have been removed by inertial impaction in extrathoracic airways and particles between 0.1 and 1 μm have relatively low deposition rates, the curve of deposition fraction for the tracheobronchial region has a peak in the size range from 1 to 8 μm. The peak is closer to 8 μm, indicating the dominant role played by inertial impaction.

Results of calculations using ICRP and NCRP deposition models (see Chapter 9) show that the tracheobronchial deposition curve has another maximum in the particle size range below 0.1 μm. This is again a result arising from the sequential nature of respiratory regions. Because deposition by convective Brownian diffusion increases with decreasing particle size, the head airways become an increasingly effective collector for particles smaller than 0.005 μm. In consequence a peak appears between 0.001 and 0.01 μm in the tracheobronchial deposition curve.
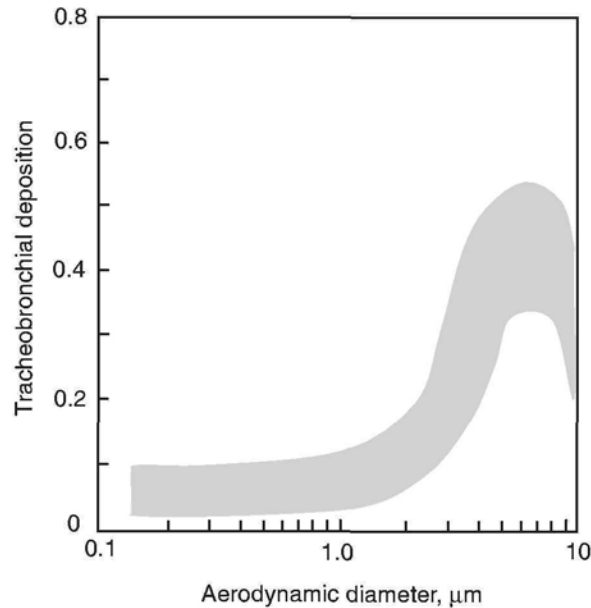
Fig. 8.3 Deposition fraction in the tracheobronchial region during mouthpiece inhalation as a function of aerodynamic diameter, except below 0.5 μm where geometric diameter is used. The band covers data from Lippmann (1977), Chan and Lippmann (1980), Stahlhofen et al. (1980, 1981a, and 1983), Foord et al. (1978), and Emmett and Aitken (1982).

In head airways, collection of large particles by inertial impaction is more effective than collection of small particles by convective Brownian diffusion. As a result, the fractional deposition of large particles in head airways is about one order of magnitude higher than in the tracheobronchial region, while the deposition fractions of small particles are comparable in the two regions.

Deposition patterns differ to some extent between men and women. Kim and Hu (1998) have investigated deposition patterns in healthy adult subjects (11 men and 11 women) using aerosol boluses as a probe. The monodisperse aerosols consist of di-2-ethylhexyl sebacate particles. Three different particle diameters, 1, 3, and 5 μm, are used in the study. As described in Section 8.1.2, the method of bolus probe involves inhalation of filtered air from the functional residual capacity to a prescribed inspiratory volume (500 cm^3) and exhalation to the residual volume, with an aerosol bolus injected at a specified volumetric depth of the lungs during inhalation. The aerosol bolus is 40 cm^3 in volume and the lung depth ranges from 100 to 500 cm^3 with a 50-cm^3 increment. The subject breathes through the mouth at a constant flow rate. At all lung depths tested, deposition fraction tends to be higher in women than in men for 1-μm particles. For 3- and 5-μm particles, deposition fractions in women are markedly higher

than those of men at lung depths less than 200 cm^3 but are comparable to or lower than those of men in lung depths larger than 200 cm^3. For the three flow rates (150, 250, and 500 ml/s) used in the study, total lung deposition is comparable between men and women for 1-μm particles but is 9 to 31% higher in women than in men for 3- and 5-μm particles. The results indicate that women have higher inertial deposition rates in extrathoracic and tracheobronchial regions. These airways could be potential sites for the development of tumors when women are exposed to toxic particles of high concentrations.

8.4 DEPOSITION IN THE ALVEOLAR REGION

In the alveolar region, deposition takes place mainly by Brownian diffusion and gravitational settling. Low flow velocities and small airway dimensions in this region favor deposition by these two mechanisms. As the last region in the respiratory tract, its fractional deposition curve has a strong influence from the two upstream regions. Fig. 8.4 displays experimentally determined deposition fraction in the alveolar region for particles between 0.1 and 10 μm during mouth breathing. The deposition curve has a maximum between 1 and 4 μm of particle aerodynamic diameter, a result arising from the sequential nature of respiratory regions. Position of the peak depends on the route of inhalation. It occurs at about 3 μm with a deposition fraction of about 0.5 for mouth breathing and at about 2 μm with a deposition fraction of about 0.2 for nose breathing. The peak for nose breathing is lower and appears at a smaller particle size because the nose is a more effective collector for large particles.

The fractional deposition curve for the alveolar region is similar in shape to that for the tracheobronchial region. Results of calculations using ICRP and NCRP deposition models show that it also has a second peak, again reflecting the sequential nature of respiratory regions. The second peak generally appears in the size range from 0.01 to 0.1 μm.

For particles between 0.1 and 1 μm, fractional deposition in the alveolar region is nearly independent of particle size. The deposition data are obtained from experiments with steady-state breathing. Particles in this size range are not able to deposit within the time span of one breath in the alveolar region, because gravitational settling and Brownian motion are not sufficiently rapid. The particles simply transfer from inspired air to the reserve air in the current breath and then deposit in subsequent breaths. The determining factor for deposition is therefore the rate at which particles are transferred from tidal air to the reserve air.

To investigate the effect of bronchoconstriction, Svartengren et al. (1987) have measured regional deposition in eight healthy nonsmokers using ^{111}In-labelled Teflon particles with an aerodynamic diameter of 2.5 μm. The

breathing maneuver involves inhalation at 0.5 L/sec to the total lung capacity. The experiments consist of a provocation and a control series. In the provocation experiment, the subject inhales a methacholine bromide aerosol to induce bronchoconstriction before inhaling Teflon particles. In the control experiment, inhalation of Teflon particles precedes the methacholine bromide aerosol. Total deposition differs only slightly between the two series, 83 ± 6% (mean ± SD) for the control series and 84 ± 5% for the provocation series. In contrast, alveolar deposition, estimated as the percentage retention 24 h after inhalation, differs markedly between the two series. They are 42 ± 10% and 77 ± 12%, respectively, for the provocation and control experiments. The results indicate that nearly half of the deposition of 2.5-μm particles has been shifted from the alveolar region to the tracheobronchial region as a result of bronchoconstriction.

8.5 SUMMARY OF REGIONAL DEPOSITION

Table 8.1 summarizes the effects of particle size, flow rate, and tidal volume on deposition fractions in the three respiratory regions for male adults under levels of physical activity ranging from resting to heavy exercise. Parameter values included in the table are particle size between 1 to 10 μm, flow rate between 250-1000 cm^3/s, and tidal volume between 500 to 2000 cm^3. The effects of these three parameters vary from region to region, reflecting the complex relationships between influencing parameters and regional deposition.
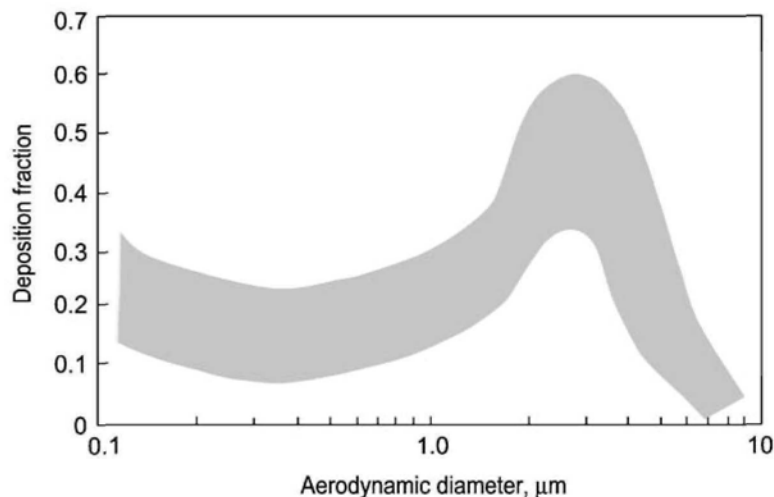
Fig. 8.4 Deposition fraction in the alveolar region for mouth breathing. Geometric diameter is used for particles smaller than 0.5 μm. The band covers data from Lippmann (1977), Chan and Lippmann (1980), Stahlhofen et al. (1980, 1981a, and 1983), Foord et al. (1978), and Emmett and Aitken (1982).

Table 8.1
Variations of regional deposition fractions with particle size, flow rate, and tidal volume for male adults under levels of physical activity ranging from resting to heavy exercise.

	Particle size 1-10 μm	Flow Rate 250-1000 cm³/s	Tidal Volume 500-2000 cm³
Extrathoracic Region	Deposition fraction increases with increasing particle size	Deposition fraction increases with increasing flow rate for both nose and mouth breathing	Deposition fraction decreases slightly with increasing tidal volume for mouth breathing
Tracheobronchial Region	Deposition fraction changes slightly with particle size	Deposition fraction changes slightly with flow rate for both nose and mouth breathing	Deposition fraction increases slightly with increasing tidal volume for mouth breathing
Alveolar Region	Deposition fraction is a unimodal function of particle diameter in this size range	Deposition fraction decreases with increasing flow rate for both nose and mouth breathing	Deposition fraction increases with increasing tidal volume for mouth breathing

8.6 TOTAL DEPOSITION

The parameters that influence total deposition include particle property, airway dimension, flow rate, and inhalation route. Total deposition represents the combined deposition of particles in all regions of the respiratory tract and, as a consequence, its relationships with influencing parameters are more complex than those seen in regional deposition.

Total deposition data are useful for assessment of the health risk of highly soluble particles, because dissolution of these particles and subsequent absorption into bloodstreams take place rapidly in all regions of the respiratory tract except the anterior nasal passages. Measurements on total deposition also have been used to validate mathematical models.

8.6.1 Deposition of Nonhygroscopic Particles

Fig. 8.5 shows the total deposition fraction for nonhygroscopic particles during mouthpiece breathing. The band covers the data reported by Lippmann (1977), Chan and Lippmann (1980), Stahlhofen et al. (1980, 1981a, and 1983), Foord et al. (1978), Emmett and Aitken (1982), Heyder et al. (1982), and Schiller et al. (1986). The data from Schiller et al. (1986) for silver particles between 5 and 200 nm have been corrected for the effects of instrumental dead space (Gebhart et al., 1989).
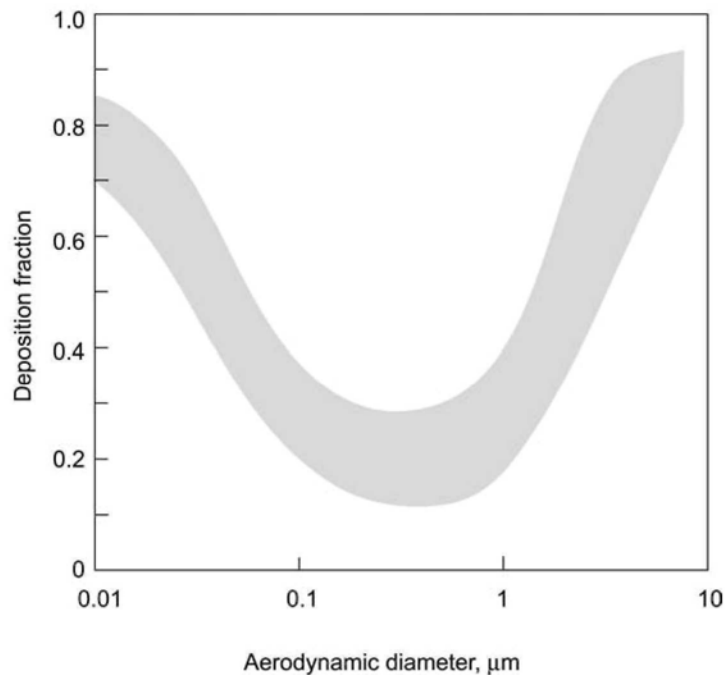
Fig. 8.5 Total respiratory deposition during mouthpiece inhalation as a function of aerodynamic diameter, except below 0.5 μm where geometric diameter is used. The band covers data from Lippmann (1977), Chan and Lippmann (1980), Stahlhofen et al. (1980, 1981a, and 1983), Foord et al. (1978), Emmett and Aitken (1982), Heyder et al. (1982), and Schiller et al. (1986).

Total deposition is higher for nose breathing because the smaller nose passageway is a better filter than the month. For either nose or mouth breathing, the total deposition curve has a minimum between 0.2 and 0.5 μm. It is a result of relatively small contributions by inertial impaction and convective Brownian diffusion to deposition of particles in this size range. For particles outside this size range, deposition by inertial impaction increases with increasing particle aerodynamic diameter, while deposition by convective Brownian diffusion increases with decreasing particle size.

Low breathing frequency favors gravitational settling of large particles and Brownian diffusion of small particles, while high breathing frequency favors inertial impaction of large particles and convective Brownian diffusion of small particle. As a result, the total respiratory deposition has a minimum at about 15-20 breaths/min when it is plotted as a function of breathing frequency. Regional deposition fractions in the tracheobronchial and alveolar regions do not follow this pattern.

Total deposition is less sensitive to change in flow rate. Even though the

levels of exercise have marked influences on tidal volume and breathing frequency, their effects on total deposition are smaller than intersubject variability.

As mentioned earlier, some experiments are conducted with controlled breathing pattern in which the subject breathes at constant inspiratory and expiratory flow rates. In a study of 20 subjects (Heyder et al., 1982), the mean total deposition fractions obtained with controlled and spontaneous mouth-breathing patterns are almost identical, even though the spontaneous breathing experiments have a larger range of flow rates and thereby a larger range of deposition fractions. Both breathing patterns have a marked intersubject variability in deposition. It is to be noted that the same total deposition may have different ratios of the tracheobronchial and alveolar deposition fractions.

Some data are available on total deposition in children (Becquemin et al., 1991; Schiller-Scotland et al., 1992, 1994a, 1994b). At the same tidal volume and flow rate, the measured total deposition in children is higher by an average factor of 1.5 than that in adult males for all particle sizes. However, regional deposition does not vary in the same pattern among the three respiratory regions. Musante and Martonen (2000) have calculated regional depositions in children of four different ages: 7, 22, 48, and 98 months. The results indicate that fractional deposition in the tracheobronchial airways decreases with age for sedentary and heavy activity levels. However, fractional deposition in the alveolar region is highest in 4-year children under resting conditions but increases with age under heavy activity conditions.

8.6.2 Deposition of Hygroscopic Particles

There are a few experimental measurements on total deposition of hygroscopic particles (Hänel and Heyder, 1980; Blanchard and Willeke, 1984; Tu and Knutson, 1984). Experimental results show that sodium chloride particles have a minimum total deposition at the dry-particle size of 0.08 μm. Because the minimum occurs at about 0.5 μm for nonhygroscopic particles, the findings indicate that sodium chloride particles have a growth factor of about 6 in human lungs.

8.6.3 Deposition of Highly Charged Particles

Experimental results show that total deposition increases significantly when particles carry high levels of charges (Melandri et al., 1977; Tarroni et al., 1980; Melandri et al., 1983). The increment in total deposition due to particle charges can be defined as $(E - E_0)/(1 - E_0)$, where E and E_0 represent total deposition of charged and uncharged particles, respectively. For monodisperse aerosol consisting of carnauba wax particles (density between 0.99 and 1.01 g/cm^3) in the size range of 0.3 to 1 μm, the increment in total deposition due to particle charges is found to increase linearly with $(q - q_c)$, where q_c is a threshold charge

level below which the effect of charges on deposition is negligible. The increment in total deposition is about 7% for 0.3-μm particles carrying 30 elementary charges, 14% for 0.6-μm particles carrying 80 elementary charges, and 16% for 1.0-μm particles carrying 135 elementary charges. For the submicron particles used in these experiments, most of the deposition takes place in the alveolar region. Uncharged particles in this size range have relatively low deposition. As a result, the increase in deposition by image forces is quite significant.

Yu (1985) has shown that, for particle concentrations lower than 10^5 particles/cm^3, the electrostatic repulsive force between particles carrying charges of like sign is not important because the particles are relatively far apart. Increase in deposition of charged particles is mainly due to image force. The following expression proposed by Yu for the efficiency of deposition by image force is in good agreement with the data.

$$\eta = \left(\frac{8Bl_t}{\pi\varepsilon_0 d_t^3 U} \right)^{1/2} (q - q_c) \qquad \text{for deposition by image force} \qquad (8.11)$$

Here B is the mechanical mobility of the particle, l_t the tube length, ε_0 (= 8.85 x 10^{-12} C^2/N·m^2) the permittivity of a vacuum, d_t the tube diameter, and U the mean flow velocity. The threshold charge varies with particle size, airway diameter, and the residence time of particles in an airway segment. In the alveolar region, q_c is estimated to be 54 elementary charges for 1-μm particles of standard density.

Experiments using a hollow cast of the human larynx-tracheobronchial tree show that most of the enhancement in deposition of highly charged particles (2-7 μm in mass median aerodynamic diameter) occurs in the larynx and the trachea (Chan et al., 1978). Deposition hot spots also appear downstream of the larynx where an air jet forms and flow separation takes place. The experiments are conducted with monodisperse aerosol consisting of ^{99m}Tc tagged Fe_2O_3 particles (density = 2.56 g/cm^3). Each particle carries 360 to 1,100 negative elementary charges.

PROBLEMS

8.1 Explain why, at the same flow rate, a larger tidal volume leads to a higher deposition fraction in the alveolar region.

8.2 Explain why the particle size for the second peak (in the larger size range) in the alveolar deposition curve decreases with increasing flow rate but

increases with increasing respiratory frequency.

8.3 Discuss how the total deposition curve is changed by growth of hygroscopic particles when it is plotted as a function of dry particle size.

REFERENCES

Albert, R.E. and Arnett, L.C. (1955). Clearance of radioactive dust from the lung. Arch. Ind. Health 12, 99-106.

Albert, R.E., Lippmann, M. Peterson, H., Berger, J., Sanborn, K. and Bohning, D. (1973). Bronchial deposition and clearance of aerosols. Arch. Ind. Med. 131, 115-127.

Becquemin, M.H., Yu, C.P., Roy, M. and Bouchikhi, A. (1991). Total deposition of inhaled particles related to age: Comparison with age-dependent model calculations. Radiat. Prot. Dosim. 38, 23-28.

Blanchard, J.D. and Willeke, K. (1984). Total deposition of ultrafine sodium chloride particles in human lungs. J. Appl. Physiol. 57, 1850-1856.

Chan, T.L., Lippmann, M., Cohen, V.R. and Schlesinger, R.B. (1978). Effect of electrostatic charges on particle deposition in a hollow cast of human larynx-tracheobronchial tree. J. Aerosol Sci. 9, 463-468.

Chan, T.L. and Lippmann, M. (1980). Experimental measurements and empirical modeling of the regional deposition of inhaled particles in humans. Am. Ind. Hyg. Assoc. J. 41, 399-409.

Cheng, K.H., Cheng, Y.S., Yeh, H.C., Guilmette, R.A., Simpson, S.Q., Yang, S.Q. and Swift, D.L. (1996). In vivo measurements of nasal airway dimensions and ultrafine aerosol depositing in human nasal and oral airways. J. Aerosol Sci. 27, 785-801.

Cheng, Y.S. (2003). Aerosol deposition in the extrathoracic region. Aerosol Sci. Technol. 37, 659-671.

Emmett, P.C. and Aitken, R.J. (1982). Measurements of the total and regional deposition of inhaled particles in the human respiratory tract. J. Aerosol Sci. 13, 549-560.

Foord, N., Black, A. and Walsh, M. (1978). Regional deposition of 2.5-7.5 μm diameter inhaled particles in healthy male non-smokers. J. Aerosol Sci. 9, 343-357.

Gebhart, J., Schiller-Scotland, C.F., Eagan, M.J. and Nixon, W. (1989). On the relationship between experimental data for total deposition and model calculations. Part I: Effect of instrumental dead space. J. Aerosol Sci. 20, 141-147.

Hänel, G. and Heyder, J. (1980). Deposition of hygroscopic atmospheric aerosol particles in the human respiratory tract. Staub-Reinhalt. Luft 40, 9-13.

Heyder, J. and Rudolf, G. (1977). Deposition of aerosol particles in the human nose. In: Inhaled Particles IV, Proceedings of an International Symposium Organized by the British Occupational Hygiene Society, Edinburgh, September 22-26, 1975, pp. 107-126 (Ed. Walton, W.H.). Pergamon Press, Oxford, United Kingdom.

Heyder, J., Gebhart, J., Stahlhofen, W. and Stuck, B. (1982). Biological variability of particle deposition in the human respiratory tract during controlled and spontaneous mouth-breathing. In: Inhaled Particles V, Proceedings of an International Symposium on Inhaled Particles Organized by the British Occupational Hygiene Society, Cardiff, September 8-12, 1980. (Eds. Walton, W.H., Critchlow, A. and Coppock, S.M.). Ann. Occup. Hyg. 26, 137-147.

International Commission on Radiological Protection (1994). Human Respiratory Tract Model for Radiological Protection, Annals of the ICRP, Publication 66. Elsevier Science,

Tarrytown, NY.

Kim, C.S. and Hu, S.C. (1998). Regional deposition of inhaled particles in human lungs: Comparison between men and women. J. Appl. Physiol. 84, 1834-1844.

Lippmann, M. and Albert, R.E. (1969). The effect of particle size on the regional deposition of inhaled aerosols in the human respiratory tract. Am. Ind. Hyg. Assoc. J. 30, 357-375.

Lippmann, M. (1977). Regional deposition of particles in the human respiratory tract. In: Handbook of Physiology, Section 9: Reactions to Environmental Agents, pp. 213-232 (Eds. Lee, D.H.K., Falk, H.L., Murphy, S.D. and Geiger, S.R.). The American Physiological Society, Bethesda, MD.

Melandri, C., Prodi, V., Tarroni, G., Formignani, M., De Zaiacomo, T., Bompane, G.F. and Maestri, G. (1977). On the deposition of unipolarly charged particles in the human respiratory tract. In: Inhaled Particles IV, Proceedings of an International Symposium Organized by the British Occupational Hygiene Society, Edinburgh, September 22-26, 1975, pp. 193-201 (Ed. Walton, W.H.). Pergamon Press, Oxford.

Melandri, C., Tarroni, G., Prodi, V., De Zaiacomo, T., Formignani, M. and Lombardi, C.C. (1983). Deposition of charged particles in the human airways. J. Aerosol Sci. 14, 657-669.

Musante, C.J. and Martonen, T.B. (2000). Computer simulations of particle deposition in the developing human lung. J. Air & Waste Manage. Assoc. 50, 1426-1432.

Rudolf, G, Gebhart, J., Heyder, J., Schiller, C.F. and Stahlhofen, W. (1986). An empirical formula describing aerosol deposition in man for any particle size. J. Aerosol Sci. 17, 350-355.

Rudolf, G, Köbrich, R. and Stahlhofen, W. (1990) Modeling and algebraic formulation of regional aerosol deposition in man. J. Aerosol Sci. 21 (Suppl. 1), S403-S406.

Schiller, C.F., Gebhart, J., Heyder, J. Rudolf, G, and Stahlhofen, W. (1986). Factors influencing total deposition of ultrafine aerosol particles in the human respiratory tract. J. Aerosol Sci. 17, 328-332.

Schiller-Scotland, C.F., Hlawa, R., Gebhart, J., Wönne, R. and Heyder, J. (1992). Total deposition of aerosol particles in the respiratory tract of children during spontaneous and controlled mouth breathing. J. Aerosol Sci. 23 (Suppl. 1), S457-S460.

Schiller-Scotland, C.F., Hlawa, R., Gebhart, J., Heyder, J., Roth, C. and Wönne, R. (1994a). Particle deposition in the respiratory tract of children during spontaneous and controlled mouth breathing. In: Inhaled Particles VII, Proceedings of an International Symposium on Inhaled Particles Organized by the British Occupational Hygiene Society, September 16-22, 1991 (Eds. Dodgson, J. and McCallum, R.L.). Ann. Occup. Hyg. 38, Suppl. 1, 117-125.

Schiller-Scotland, C.F., Hlawa, R. and Gebhart, J. (1994b). Experimental data for total deposition in the respiratory tract of children. Toxicol Lett. 72, 137-144.

Stahlhofen, W., Gebhart, J. and Heyder, J. (1980). Experimental determination of the regional deposition of aerosol particles in the human respiratory tract. Am. Ind. Hyg. Assoc. J. 41, 385-398.

Stahlhofen, W., Gebhart, J. and Heyder, J. (1981a). Biological variability of regional deposition of aerosol particles in the human respiratory tract. Am. Ind. Hyg. Assoc. J. 42, 348-352.

Stahlhofen, W., Gebhart, J., Heyder, J., Philipson, K. and Camner, P. (1981b). Intercomparison of regional deposition of aerosol particles in the human respiratory tract and their long-term elimination. Exp. Lung Res. 2, 131-139.

Stahlhofen, W., Gebhart, J., Heyder, J. and Scheuch, G. (1983). New regional deposition data of the human respiratory tract. J. Aerosol Sci. 14, 186-188.

Svartengren, M., Linnman, L., Philipson, K. and Camner, P. (1987). Regional deposition in

human lung of 2.5 μm particles. Exp. Lung Res. 12, 265-279.

Swift, D.L., Montassier, N., Hopke, P.K., Karpen-Hayes, K., Cheng, Y.S., Su, Y.F., Yeh, H.C. and Strong, J.C. (1992). Inspiratory deposition of ultrafine particles in human nasal replicate cast. J. Aerosol Sci. 23, 65-72.

Tarroni, G., Melandri, C., Prodi, V., De Zaiacomo, T., Formignani, M. and Bassi, P. (1980). An indication on the biological variability of aerosol total deposition in the humans. Am. Ind. Hyg. Assoc. J. 41, 826-831.

Tu, K.W. and Knutson, E.O. (1984). Total deposition of ultrafine hydrophobic and hygroscopic aerosols in the human respiratory system. Aerosol Sci. Technol. 3, 453-463.

Yu, C.P., Diu, C.K. and Soong, T.T. (1981). Statistical analyses of aerosol deposition in nose and mouth. Am. Ind. Hyg. Assoc. J. 42, 726-733.

Yu, C.P. (1985). Theories of electrostatic lung deposition of inhaled aerosols. Ann. Occup. Hyg. 29, 219-227.

Chapter 9

Deposition models

Mathematical models of particle deposition are useful for interpreting experimental data as well as making predictions for the conditions not covered by experiments. Many mathematical models have been developed in past decades. All models make simplifying assumptions on lung morphometry and use theoretical or empirical equations for deposition efficiency of airway segments. These models have different degrees of complexity and give somewhat different estimates. Despite considerable variations in regional deposition predicted by these models, calculated total deposition differs only slightly among various predictions.

There are two basic types of deposition models: continuous and compartments-in-series models. Continuous models consider the respiratory tract as a continuous conduit of variable cross section and use a set of partial differential equations to describe transport of particles in the conduit. Solution of transport equations generally entails numerical methods. By contrast, compartments-in-series models treat the respiratory tract as a series of compartments and use only algebraic expressions for deposition efficiency of each compartment.

9.1 CONTINUOUS MODELS

In continuous models, the respiratory tract is treated as a filter bed or a tube of variable cross sections. The deposition model proposed by Altshuler (1959) considers the respiratory tract as a continuous filter bed, while the trumpet model developed by Yu and his associates (Taulbee and Yu, 1975; Yu, 1978) uses a trumpet-shaped conduit to represent the respiratory tract.

The trumpet model assumes that the axial flow velocity and particle concentration are uniform at each cross section of the conduit (Taulbee and Yu, 1975). In other words, these two variables depend only on the axial coordinate and time. A mass balance for particles over a short section of the respiratory tract gives the following transport equation

$$A_T \frac{\partial n}{\partial t} = -A_A U \frac{\partial n}{\partial x} + \frac{\partial}{\partial x}\left(A_A D_e \frac{\partial n}{\partial x}\right) - L_d \tag{9.1}$$

Here $n(x, t)$ is the mean particle concentration at the axial coordinate x and time t, $A_A(x)$ the cross-sectional area of the conduit obtained by summing over all
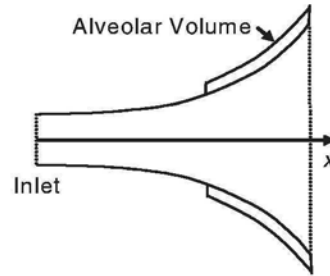
Fig. 9.1 A trumpet airway model.

airways at distance x from the trachea inlet, $U(x)$ the average axial velocity of airflow, $D_e(x)$ the apparent axial diffusion coefficient, and $L_d(x, t)$ the deposition rate per unit length of the conduit. $A_T(x, t)$ is the total cross-sectional area that, in the alveolar region, includes the additional cross-sectional area due to the alveolar volume (see Fig. 9.1). The product, $l_t(A_T - A_A)$, is the alveolar volume associated with an airway generation of length l_t. In the calculations, the alveolar volume is assumed to expand and contract uniformly during breathing. Taulbee and Yu have also derived the expressions of $L_d(x, t)$ for their calculations. In subsequent studies, the transport equation has been slightly revised (Yu, 1978; Yu and Diu, 1983).

According to Taulbee and Yu, the distributions of airway length and diameter in each generation give rise to a distribution of flow velocities in these airways, which in turn leads to the apparent axial diffusion of aerosol particles in the conduit. By assuming that the flow velocities in various airways in a generation follow a normal distribution with a standard deviation of 0.6, Taulbee and Yu have obtained the following expression for apparent axial diffusion coefficient:

$$D_e = 0.3 U l_t \tag{9.2}$$

The continuous model developed by Egan and Nixon (1985) also uses Eq. (9.1) for calculations. It differs from the model proposed by Taulbee and Yu in the expressions of apparent axial diffusion coefficient and particle deposition efficiencies. For the values of D_e, Nixon and Egan use the expressions of effective axial diffusion coefficient proposed by Scherer et al. (1975) for mixing of gases in a glass model of bronchial airways.

The effective axial diffusion coefficients for gas transport have been discussed in Chapter 5. They are given by Eqs. (5.6) and (5.7):

$$D_e = D + 1.08 U d_t \qquad \text{for inspiration} \tag{5.6}$$

$$D_e = D + 0.37 U d_t \qquad \text{for expiration} \qquad (5.7)$$

Here D is the molecular diffusion coefficient and d_t the tube diameter under consideration. For applications in particle transport, the particle diffusion coefficient is used for D in the above equations. It is important to note that the diffusion coefficient of particles is orders of magnitude smaller than that of gas molecules. In consequence the apparent axial diffusion coefficient of aerosol particles calculated from Eqs. (5.6) and (5.7) mainly comes from the second terms. The constant coefficients in the above two expressions differ in numerical value because airflow patterns differ between the two respiratory phases.

The variables, n, U, A_A, A_T, D_e, and L_d, in Eq. (9.1) are considered as functions of time and axial distance in the deposition model developed by Nixon and Eagan. Furthermore, the model assumes that the cross-sectional areas of bronchial, bronchiolar, and alveolated airways vary according to a sinusoidal function of time. The transport equation is solved numerically for $n(x, t)$ until a steady-state deposition rate is obtained. It takes several breaths to reach such a steady state. Results of calculations using constant flow rates are in general agreement with experimental data reported by Heyder et al. (1986) for various particle sizes under controlled breathing conditions.

Instead of using the Eulerian approach to calculate particle concentrations as described above, one can employ the Lagrangian approach to follow each inhaled particle in a typical airway path. In this approach, the equation of motion is used to calculate the trajectory of each inspired particle with a given initial position at the inlet to the nose or mouth. By following the trajectory of each inspired particle in a complete breath, it is possible to find out whether the particle deposits in the airway path or remains airborne at the end of exhalation. The fate of an inhaled particle and, if it deposits, the site of deposition depend on the initial position at the inlet. By simulating the movement of tens of thousands of particles, one can obtain statistical mean values for deposition rate in an airway path of a given length. If the respiratory tract is assumed to contain a number of airway paths of various lengths, calculations can be repeated for different airway paths. The values for deposition in pathways of various lengths can be weighted using the path length distribution of the respiratory tract and then summed to give the average values for total and regional deposition. Such a deposition model, termed randomly distributed paths model, is conceptually simple. It takes into account the variations in dimensions of airways in the same generation through the use of different airway paths. The main drawback of the model is the enormous amounts of computing time and memory capacity needed for calculations.

9.2 COMPARMENTS-IN-SERIES MODELS

In a compartments-in-series model, the respiratory tract is considered as a system containing a number of compartments connected in series. Accordingly, inspired aerosol can be divided into a number of portions, each of which reaches a certain compartment during inhalation. As shown in Fig. 9.2, the first portion of inspired aerosol sequentially goes through Compartments *1, 2, ..., f*, where *f* represents the most distal compartment reached by this portion of inspired aerosol. The second portion of inspired aerosol reaches Compartment *f-1*, etc. Because some particles deposit in each compartment during transit, the particle concentration decreases in the forward direction from compartment to compartment.

When the direction of flow reverses during exhalation, the portion of inspired aerosol that reaches Compartment *f* has to go backwards through Compartments *f-1, f-2,···, 1* in sequence.

The residual air is pushed by the advancing tidal air into deeper parts of the lungs during inhalation, but trails behind the retreating tidal air during exhalation. If it is assumed that no mixing takes place between tidal air and residual air (that is, no residual air remains in Compartments *1, 2, ···, f-1*), the tidal volume and the volumes of all the compartments reached by tidal air have the following relationship:

$$V_t = V_1 + V_2 + ... + \tilde{V}_f \tag{9.3}$$

Here V_t is the tidal volume, V_i the volume of Compartment *i*, and $\tilde{V}_f$ the volume of the portion of tidal air that arrives in Compartment *f*. Eq. (9.3) implies that Compartment *f* contains some residual air. Because each compartment keeps a portion of tidal air, a successively smaller volume of tidal air goes to the next compartment. The assumption of no mixing between tidal air and residual air leads to an underestimate of the lung depth reached by tidal air. In reality, a certain degree of mixing takes place between these two parts of air and, as a result, the first portion of tidal air goes beyond the final compartment that is reached when there is no mixing.
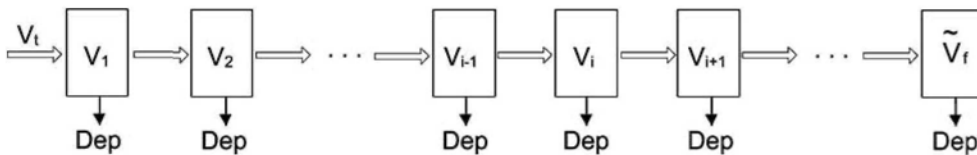
Fig. 9.2 A compartments-in-series model of the respiratory tract. Dep: deposition.

The compartments-in-series model takes into account the deposition occurring in each compartment during inhalation and exhalation phases. Because of the sequential nature of the system, the particles that deposit in Compartment i during inhalation come from two parts of inhaled aerosol: (1) all the portions that have passed through Compartment i and entered into subsequent compartments and (2) the portion that has just reached this compartment. The first part has a volume of $(V_{i+1}+V_{i+2}+\cdots+\tilde{V}_f)$, while the second part has a volume of V_i. For both parts, the particle concentration is less than that in inspired aerosol because of deposition during passage form Compartment 1 to Compartment i. If η_{Ii} represents the efficiency of deposition in Compartment i during inhalation, then the particle concentration in the aerosol reaching Compartment i is equal to the concentration in inspired aerosol multiplied by the factor $(1-\eta_{I1})(1-\eta_{I2})\cdots(1-\eta_{Ii-1})$. The fractional deposition in Compartment i during inhalation is given by:

$$E_{Ii} = (1 - \eta_{I1})(1 - \eta_{I2})...(1 - \eta_{I,i-1})\left[\eta_{Ii}\left(V_{i+1} + V_{i+2} + \cdots + \tilde{V}_f \right) + \alpha_{Ii}\eta_{Ii}V_i \right]\cdot\left(\frac{1}{V_t}\right)$$

$$(9.4)$$

Here E_{Ii} is the fractional deposition based on the total particle number in inspired air. The weighting factor α_{Ii} is a function of the residence time of particles in Compartment i during inhalation. It is usually assumed to be 0.5 in calculations.

The particles that deposit in Compartment i during exhalation come from each portion of inhaled aerosol that has passed through Compartment i and entered into a subsequent compartment during inhalation as well as the portion that has just reached Compartment i at the end of inhalation. Because each of these portions has gone through different numbers of compartments before it arrives in Compartment i during exhalation, it is easier to consider the deposition from each portion one at a time. If η_{Ei} represents the efficiency of deposition in Compartment i during exhalation, the particles remaining airborne in Compartment i at the end of inhalation have the following fractional deposition in Compartment i during exhalation:

$$E_{Ei,i} = (1 - \eta_{I1})(1 - \eta_{I2})\cdots(1 - \eta_{I,i-1})(1 - \alpha_{Ii}\eta_{Ii})\ \alpha_{Ei}\eta_{Ei}V_i \cdot\left(\frac{1}{V_t}\right)$$

$$(9.5)$$

Here $E_{Ei,i}$ is the fractional deposition based on the total particle number in inspired air. The weighting factor α_{Ei} is a function of the residence time of

particles in Compartment i during exhalation. It is usually assumed to be 0.5 in calculations.

The particles remaining airborne in Compartment $i+1$ at the end of inhalation have the following fractional deposition in Compartment i during exhalation:

$$E_{Ei,i+1} = (1 - \eta_{Ii})(1 - \eta_{I2}) \cdots (1 - \eta_{Ii})(1 - \alpha_{I,i+1}\eta_{I,i+1})(1 - \alpha_{E,i+1}\eta_{E,i+1})$$

$$\cdot \eta_{Ei} V_{i+1} \cdot \left(\frac{1}{V_t}\right) \tag{9.6}$$

The particles remaining airborne in Compartments $i+2, \cdots, f\text{-}1$ at the end of inhalation have expressions similar to Eq. (9.6) for fractional deposition in Compartment i during exhalation. The particles remaining airborne in Compartment f at the end of inhalation have the following fractional deposition in Compartment i during exhalation:

$$E_{Ei,f} = (1 - \eta_{Ii})(1 - \eta_{I2}) \cdots (1 - \eta_{If-1})(1 - \alpha_{If}\eta_{If})$$

$$\cdot (1 - \eta_{E,i+1})(1 - \eta_{E,i+2}) \cdots (1 - \eta_{E,f-1})(1 - \alpha_{Ef}\eta_{Ef}) \cdot \eta_{Ei} \tilde{V}_f \cdot \left(\frac{1}{V_t}\right) \tag{9.7}$$

The fractional deposition in Compartment i during the entire exhalation phase is the sum of $E_{Ei,i}, E_{Ei,i+1}, \ldots, E_{Ei,f}$:

$$E_{Ei} = \left[\prod_{j=1}^{i-1}(1 - \eta_{Ij})\right] \cdot (1 - \alpha_{Ii}\eta_{Ii})\alpha_{Ei}\eta_{Ei}\frac{V_i}{V_t} + \left[\prod_{j=1}^{i}(1 - \eta_{Ij})\right] \cdot \eta_{Ei}$$

$$\cdot \sum_{j=i+1}^{f}\left[\prod_{k=i+1}^{j-1}(1 - \eta_{Ek})(1 - \eta_{Ik})\right] \cdot (1 - \alpha_{Ij}\eta_{Ij})(1 - \alpha_{Ej}\eta_{Ej})\left(\frac{V_j}{V_t}\right) \tag{9.8}$$

Adding E_{Ei} to E_{Ii} gives the fractional deposition in Compartment i during one breath:

$$E_i = E_{Ii} + E_{Ei} \tag{9.9}$$

The sum of E_i over all compartments is the total deposition in the entire respiratory tract. The derivations given above clearly show the filtration effect of preceding compartments.

9.2.1 Typical Path Deposition Models

The first multi-compartment model for particle deposition was developed by Findeisen (1935). The lung model used in his calculations consists of nine compartments, with airway diameter and length specified for each compartment. Such an anatomical model is known as a typical path lung model. Many later deposition models have made various degrees of refinement in lung anatomy, airflow pattern, and equations for deposition efficiency, but the respiratory tract remains to be represented by typical path lung models. These include those developed by Landahl (1950), Beeckmans (1965), ICRP (International Commission on Radiological Protection, 1994), and NCRP (National Council on Radiation Protection and Measurements, 1997).

Both ICRP and NCRP models estimate regional and total deposition for a wide range of particle sizes and breathing conditions. With the objectives of estimating the dose to organs and tissue receiving from inhalation of radioactive particles, these two models also consider clearance and transport of deposited particles between regions. In addition, they include parameters that can be applied to individuals in various population groups such as males and females of different ages. To facilitate the fairly complicated calculations, computer programs have been developed for the ICRP model (Birchall et al., 1991; Jarvis, et al., 1994) and the NCRP model (Chang et al., 1991). These two models will be discussed in more details in Sections 9.3 and 9.4.

9.2.2 Single Path with Statistically Distributed Airway Dimensions

Another type of compartments-in-Series model is the stochastic model proposed by Hofmann et al. (2001). Instead of using a typical path lung model, they assume that each inspired particle passes through a single path with statistically distributed airway dimensions. The model retains the concept of airway generations but permits the diameters and lengths of airways in each generation to be randomly distributed. In other words, the dimensions of airways are described by probability density functions, with constraints by correlations between some parameters. At each bifurcation, a Monte Carlo method is employed to determine the dimensions of the daughter tube into which the particle under consideration enters. Deposition in each airway segment and alveolus is calculated using the expressions for efficiency of deposition by convective Brownian diffusion, inertial impaction, and gravitational settling. Clearly, each particle goes through a path with different airway dimensions. By simulating the movement of tens of thousands of particles, it is possible to obtain statistical mean values for total, regional, and local (in an airway segment) deposition. The model has the advantage of taking into account the variations in diameter, length, and branching angle among airways of the same generation. Furthermore, it is capable of providing three-dimensional deposition patterns, because the coordinates of each airway is known. By comparing with

SPECT (Single Photon Emission Computed Tomography) data, the three-dimensional deposition patterns allow validation of the model. Results of calculations for distribution of deposited particles per voxel among hemispherical shells of the lungs are in fair agreement with SPECT measurements reported by Fleming et al. (1996). The measurements are made using controlled breathing conditions and ^{99m}Tc-tagged particles between 1.41 and 6.28 μm in mass median aerodynamic diameter.

More recently, Goo and Kim (2003) have used the same basic concept to develop a computational scheme for tracing the movement of inspired aerosol in the respiratory tract. By dividing the tidal volume into a number of small volume elements, the scheme employs a Monte Carlo method to determine the dimensions of airways for each volume element to pass through. It assumes a normal distribution for each of the four morphological parameters: the length, diameter, branching angle, and inclination angle relative to gravity of the airway segments in each generation. Selected values for each parameter are discarded if they fall outside prescribed ranges. Dimensional correlations between the parent and daughter tubes are allowed to have variable values, instead of fixed mean values. This is considered to be more realistic because airway dimensions are normally distributed. The computational scheme takes into account the expansion and contraction of airways and assumes that the flow division at each bifurcation is symmetric. Deposition in each airway segment is calculated using the expressions for efficiency of deposition by convective Brownian diffusion, inertial impaction, and gravitational settling. For the purpose of comparison, Goo and Kim have also calculated the deposition fraction in each airway generation of a typical path lung model by the same computational scheme without making a random selection of airway dimensions for inspired particles. The results of the Monte Carlo method are in good agreement with those calculated for a typical lung model, except that the Monte Carlo method gives higher deposition fractions in larger conducting airways for larger particles at higher flow rates. Goo and Kim have suggested that the Monte Carlo method is more sensitive to parameters related to inertial deposition.

9.2.3 Tubes-and-Bifurcations-in-Series

In a mathematical model developed for predicting deposition of fibers in the respiratory tract, Asgharian and Yu (1989) have assumed that deposition takes place by convective Brownian diffusion and gravitational settling in straight airway segments and by inertial impaction and interception in the transition zones of airway bifurcations. This represents a deposition model of tubes-and bifurcations-in-series.

Subsequently, Yu et al. (1994) have modified the deposition model by incorporating the expressions for deposition efficiency derived by Chen (1992). The modified model has been used to calculate the size distributions of

refractory ceramic fibers deposited in the pulmonary region of the accessory lobe of rats. The results are in good agreement with experimental data. According to the calculations, only fibers smaller than 3 μm in diameter and shorter than 30 μm can reach the tracheobronchial and alveolar regions of rats.

9.3 THE ICRP DEPOSITION MODEL

Over the past 45 years, the International Commission on Radiological Protection has developed three mathematical models for calculating deposition and retention of inhaled radioactive particles. They appear in ICRP Publication 2 (ICRP, 1960), Publication 30 (ICRP, 1979), and Publication 66 (ICRP, 1994), respectively. The second model, developed and published by an ICRP Task Group on Lung Dynamics in 1966 (TGLD, 1966), has incorporated all technical information available at that time and has been widely used since its publication. The third model represents an improved version.

9.3.1 Respiratory Tract Morphometry

The characteristics of the respiratory tract used in the ICRP model are described in Chapter 2. It can be considered as a composite airway structure adapted from several lung models. The ICRP morphometric model has adopted its own numbering system for airway generations, which differ to some extent from Weibel's lung model A. Based on deposition and clearance patterns, the respiratory tract is divided into five regions: (1) the anterior nasal passages, (2) the posterior nasal passages, pharynx, and larynx, (3) the first nine generations of the conducting airways (the trachea and bronchi), (4) the last seven generations of the conducting airways (the bronchioles), and (5) the alveolar region. The ICRP model treats the alveolar region as one single region in calculations of deposition fraction, but divides it into three compartments for consideration of particle clearance.

In calculations for regional deposition, the ICRP model considers each respiratory region as a filter and gives a set of algebraic expressions for filtration efficiency of each region. The efficiency expressions are given separately for inhalation and exhalation phases.

To account for differences arising from physical activity levels, gender, age, and ethnic characteristics, the ICRP model provides anatomical and physiological parameters for scaling. The algebraic expressions for regional deposition efficiency are first developed for the reference adult male and then extended to subjects of different body sizes using a scaling factor. The scaling factor differs from region to region. For most regions, it is defined as the ratio of a representative airway dimension between the subject under consideration and the reference adult male. The ratio of the tracheal diameter is used for extrathoracic and bronchial regions, while the diameter ratio of the 16th

generation airway is used for the alveolar region. For the bronchiolar region, it is the diameter ratio of the 9th generation airway for deposition by convective Brownian diffusion, but the mean residence time for deposition by gravitational settling and inertial impaction.

9.3.2 Inhalability

The following equation is used in the ICRP model for inhalable fraction at any wind speed up to 10 m/s

$$I_o = 1 - 0.5\left(1 - \frac{1}{1 + 0.00076 d_p^{2.8}}\right) + 10^{-5} U^{2.75} \exp(0.055 d_p) \tag{9.10}$$

The expression differs slightly in form from Eqs. (6.1) and (6.2) in Chapter 6, but the numerical values calculated from this equation are within the range of data shown in Fig. 6.2. In the ICRP model, inhalability is assumed to be independent of inhalation route (nose or mouth breathing), age, gender and ethnicity.

9.3.3 Deposition in Extrathoracic Regions

Because inertial impaction and gravitational settling are deposition processes related to aerodynamics, the ICRP model combines the effects of these two processes to give the overall efficiency of aerodynamic deposition processes. It is calculated by combining the individual deposition efficiencies as if they were independent probabilities:

$$\eta_a = 1 - (1 - \eta_i)(1 - \eta_s) \tag{9.11}$$

Here the subscripts a, i, and s indicate aerodynamic processes, inertial impaction, and gravitational settling, respectively.

For extrathoracic regions, the ICRP model employs empirical equations to calculate filtration efficiencies for aerodynamic processes and convective Brownian diffusion separately. The following form is used for the efficiency of deposition due to aerodynamic processes:

$$\eta_a = b\left(1 - \frac{1}{1 + cX^p}\right) \qquad \text{for deposition by aerodynamic processes} \tag{9.12}$$

The factor b is equal to 0.5 and 1 for the first and second extrathoracic regions, respectively. The group X is defined as $d_a^2 Q$, where the aerodynamic diameter d_a is in μm and the volumetric flow rate Q in cm^3/s. The values of constants c and p

differ between the two extrathoracic regions and are obtained by fitting experimental data. The expressions for deposition efficiency are identical for inhalation and exhalation.

For deposition due to convective Brownian diffusion, the following form is used:

$$\eta_d = b[1 - \exp(-cX^p)] \qquad \text{for diffusional deposition} \qquad (9.13)$$

Here the subscript d denotes convective Brownian diffusion. Again the factor b is equal to 0.5 and 1 for the first and second extrathoracic regions, respectively. For convective Brownian diffusion, the group X is defined as $D/Q^{1/4}$, where the particle diffusion coefficient D is in cm^2/s and the volumetric flow rate Q in cm^3/s. The values of constants c and p differ between the two extrathoracic regions and are determined by fitting experimental data. The expressions for deposition efficiency are identical for inhalation and exhalation.

The combined deposition efficiency of convective Brownian diffusion and aerodynamic processes is approximated by the root sum of squares of the individual efficiencies:

$$\eta = (\eta_d^2 + \eta_a^2)^{1/2} \qquad \text{for } \eta < 0.3 \qquad (9.14)$$

The ICRP model takes into account the division of inspired air between the nose and mouth for mouth breathers and normal nose breathers. For normal nose breathers, 100% of inspired air goes through the nose at all physical activity levels except heavy exercise at which inspired air splits evenly between the nose and mouth. For a mouth breather, the fraction of total inspiratory flow passing through the mouth is 30% at sleep and rest, but increases to 60 and 70% at the levels of light and heavy exercise, respectively. These values are based on a review given by Miller et al. (1988).

9.3.4 Deposition in Thoracic Regions

For the three thoracic regions, the equations for deposition efficiency due to aerodynamic processes and convective Brownian diffusion are both in the same form as the equation for convective Brownian diffusion shown in Eq. (9.13). This functional form is taken from a series of empirical expressions developed by Rudolf et al. (1983, 1986, and 1990). The constant b is equal to 1 for all thoracic regions. The expressions for X differ between aerodynamic processes and convective Brownian diffusion. For aerodynamic processes, X is proportional to $d_a^2 Q$ for the bronchial region, but is related to the residence time and aerodynamic diameter in the bronchiolar and alveolar regions. For convective Brownian diffusion, X is equal to the product of diffusion coefficient

and residence time in all three thoracic regions. The values of the two constants, c and p, are given for deposition by aerodynamic processes and convective Brownian diffusion, respectively, for each region. Their values are derived by a parameter optimization procedure using the deposition efficiency calculated from the theoretical model of Egan et al. (1989).

At this point it is useful to note that the ICRP algebraic model for particle deposition is based on the concept of compartments in series, while the theoretical analysis given by Egan et al. considers the respiratory tract as a continuous conduit. The ICRP algebraic model only uses the analysis given by Egan et al. to derive values of constants c and p.

To obtain the values of constants in the algebraic equations for deposition efficiency, the anatomical model of the respiratory tract recommended by the ICRP is used in the theoretical analysis of Egan et al. to calculate deposition fractions in each respiratory region. In the calculations, expressions for inertial impaction in larger bronchial airways are based on the experimental results obtained with cyclic inspiratory flow in replicate casts of the human upper tracheobronchial tree (Gurman et al., 1984). For deposition by gravitational settling and convective Brownian diffusion, the calculations make use of the theoretical expressions derived by Pich (1972) and Ingham (1975) respectively. These two expressions are discussed in Chapter 4.

As mentioned before, enhanced deposition by convective Brownian diffusion takes place in the vicinity of carinal ridge in bronchial airways because of turning streamlines. To account for this effect, the ICRP model incorporates an enhancement factor β in the constant c in Eq. (9.13). The following expression for enhancement factor is derived using the experimental results obtained with realistic flow conditions in a tracheobronchial cast (Cohen et al., 1990) and the analysis made by Yu and Cohen (1994):

$$\beta = 1 + 100 \exp\{-[\log_{10}(100 + 10 d_d^{-0.9})]^2\} \tag{9.15}$$

Here d_d is the equivalent diffusion diameter in μm. Named thermodynamic diameter in the ICRP model, the equivalent diffusion diameter is defined as the diameter of a sphere that has the same value of diffusion coefficient as the particle under consideration.

In making comparison between calculations and experimental data on regional deposition, the ICRP model takes into account the slow clearance phase for particles deposited in the bronchial and bronchiolar regions (see Chapter 10). For some particle sizes, the agreement with experimental data is better when calculated fractional deposition in these two thoracic regions is reduced by an amount representing the particles that have deposited in these regions but not cleared in 24 hours.

9.3.5 Deposition of Hygroscopic Particles

For hygroscopic particles, the change in particle diameter due to growth is taken into consideration in the ICRP model. The size of a hygroscopic particle is considered to be a function of its residence time in the humid lung air at 37°C and relative humidity of 99.5%. The following two equations are used to estimate the aerodynamic diameter and diffusion coefficient of particles, respectively:

$$d_a(t) = d_a(\infty) - [d_a(\infty) - d_a(0)]\exp\left[\frac{-2.13t^{0.55}}{d_a(0)}\right] \tag{9.16}$$

$$D(t) = D(0) - [D(0) - D(\infty)]\frac{d_a(t) - d_a(0)}{d_a(\infty) - d_a(0)} \tag{9.17}$$

Here 0 represents the values in ambient air and the symbol ∞ the values at equilibrium. The residence time, t, is measured from the time a particle enters the nose or mouth. The equilibrium diameter is calculated using the method described by Ferron (1977). It takes a relatively short time for the tidal air to adjust its temperature and relative humidity to the values of lung air. The effect of this short relaxation time can be accounted for by assuming that hygroscopic growth does not start until 0.1 s after the tidal air has entered the nose (Ferron et al., 1988).

9.3.6 Empirical Equations for Regional Deposition

For each of the three regions of the respiratory tract (the head airways, tracheobronchial tree, and alveolar region), Hinds (1999) has given a simplified equation for calculating fractional deposition of spherical particles, 1 g/cm^3 in density, during one complete breath. The three simplified equations, obtained by curve-fitting procedures, are capable of giving deposition fractions within ±0.03 of the predictions by the ICRP model for particles in the size range from 0.001 to 100 μm. The deposition fractions calculated from these simplified equations represent averaged values for males and females at three levels of physical activity: sitting, light exercise, and heavy exercise. In the equations given below, the particle diameter d_p is in μm. These simplified deposition equations are applicable to nonspherical particles if the particle diameter is replaced by the aerodynamic diameter for particles larger than 0.5 μm and by the equivalent volume diameter for particles smaller than 0.5 μm.

The deposition fraction for the head region is

$$E_h = \frac{I_o}{1 + \exp(6.84 + 1.183 \ln d_p)} + \frac{I_o}{1 + \exp(0.924 - 1.885 \ln d_p)} \tag{9.18}$$

The inhalable fraction, I_o, is included in the above expression to account for the effect of inhalability. It can be calculated from Eq. (9.10).

For the tracheobronchial region, the deposition fraction is

$$E_t = \frac{0.00352}{d_p} \{\exp[-0.234(\ln d_p + 3.40)^2] + 63.9 \exp[-0.819(\ln d_p - 1.61)^2]\} \tag{9.19}$$

The fractional deposition for the alveolar region is

$$E_a = \frac{0.0155}{d_p} \{\exp[-0.416(\ln d_p + 2.84)^2] + 19.11 \exp[-0.482(\ln d_p - 1.362)^2]\} \tag{9.20}$$

The fractional deposition for the entire respiratory tract is the sum of the three regional depositions. Even though Eqs. (9.19) and (9.20) do not contain inhalable fraction I_o explicitly, they have taken the inhalability into consideration. The fractional depositions thus calculated are relative to the particle concentration in ambient air.

9.4 THE NCRP DEPOSITION MODEL

The NCRP model is officially published in 1997 (NCRP, 1997). The anatomical model of the respiratory tract used in the NCRP model is identical to the one proposed by Yeh and Schum (1980). The characteristics of this lung model are discussed in Chapter 2.

Based on the patterns of particle deposition and clearance, the respiratory tract is divided into four regions: Naso-oro-pharyngo-laryngeal region (NOPL), tracheobronchial region (TB), pulmonary region (P), and thoracic lymphatic system (LN). The lymphatic system provides an important clearance mode by which deposited particles are brought into contact with lymphoid cells. It is not included in deposition calculations.

Using the concept of airway generations, the NCRP model considers deposition with more subdivisions of the respiratory tract. It estimates deposition in the nose and throat by empirical equations and deposition in each generation of the respiratory tract by theoretical and empirical equations. The model includes parameters that can be applied to individual in various groups

such as males and females of different ages, smokers, and patients with respiratory diseases.

The NCRP model uses Eq. (6.1) for calculations of inhalability. Its computational scheme for particle deposition is essentially based on the deposition model developed by Yeh and Schum (1980).

9.4.1 Deposition in the Extrathoracic Region

For the nose and mouth, the efficiencies of deposition for particles larger than 0.2 μm in diameter are given by:

$$\eta_{In} = \frac{1}{1 + (0.000217 \rho d_p^2 Q)^{-0.94}} \qquad \text{for } d_a > 0.2 \text{ μm} \qquad (9.21)$$

$$\eta_{En} = \frac{1}{1 + (0.000435 \rho d_p^2 Q)^{-1.01}} \qquad \text{for } d_a > 0.2 \text{ μm} \qquad (9.22)$$

$$\eta_{Io} = \frac{1}{1 + (0.0000333 \rho d_p^2 Q)^{-1.37}} \qquad \text{for } d_a > 0.2 \text{ μm} \qquad (9.23)$$

$$\eta_{Eo} = \eta_{Io} \qquad \text{(if there is no other information)} \qquad (9.24)$$

The subscripts n and o denote nose and mouth respectively, while the subscripts I and E indicate inhalation and exhalation respectively. The impaction parameter, $\rho d_p^2 Q$, is proportional to the Stokes number defined in Eq. (4.19). The particle density ρ is in the units of g/cm^3, the particle diameter d_p in μm, and the flow rate Q in cm^3/s. These empirical expressions are derived from an extensive amount of experimental data that have been summarized by Yu et al. (1981).

For particles smaller than 0.2 μm in diameter, the following expressions are derived from measurements using human nasal and oral casts (Cheng et al., 1988, 1990, 1993; Swift et al., 1992; Yamada et al., 1988):

$$\eta_{In} = 1 - \exp(-18.2 D^{1/2} Q^{-1/8}) \qquad \text{for } d_p < 0.2 \text{ μm} \qquad (9.25)$$

$$\eta_{En} = 1 - \exp(-21.3 D^{1/2} Q^{-1/8}) \qquad \text{for } d_p < 0.2 \text{ μm} \qquad (9.26)$$

$$\eta_{Io} = 1 - \exp(-14.6 D^{1/2} Q^{-1/8}) \qquad \text{for } d_p < 0.2 \text{ μm} \qquad (9.27)$$

$$\eta_{Eo} = 1 - \exp(-12.1 D^{1/2} Q^{-1/8}) \qquad \text{for } d_p < 0.2 \text{ μm} \qquad (9.28)$$

Here D is the diffusion coefficient of particles in cm^2/s and Q the volumetric flow rate in cm^3/s. The last two equations apply only to spontaneous oral breathing. There is almost no deposition in the mouth when it is widely open such as in heavy exercise or when a mouth tube is used.

When the nose and mouth are both used in breathing, the efficiency of deposition in both channels is

$$\eta_{Ino} = \alpha_I \eta_{In} + (1 - \alpha_I)\eta_{Io} \qquad (9.29)$$

$$\eta_{Eno} = \alpha_E \eta_{En} + (1 - \alpha_E)\eta_{Eo} \qquad (9.30)$$

Here α_I and α_E are, respectively, the fractions of air inspired and expired through the nose.

The overall efficiency of deposition due to several mechanisms is calculated by combining the individual deposition efficiencies as if they were independent probabilities.

9.4.2 Deposition in Thoracic Regions

The efficiency of deposition by diffusion from turbulent flow in a straight tube is calculated using the following approximate expression (Landahl, 1963):

$$\eta_{td} = 3.544\mu_t^{1/2} - 1.395\mu_t \qquad \text{for diffusion from turbulent flow} \quad (9.31)$$

$$\mu_t = \frac{D l_t}{Q} \qquad (4.32)$$

Here D is the diffusion coefficient of particles, l_t the tube length, and Q the volumetric flow rate of the aerosol.

The following approximate expression, proposed by Beeckmans (1965), is employed to calculate the efficiency of deposition by Brownian diffusion during a pause between inhalation and exhalation,

$$\eta_d = 1 - \exp(-7.712 kTC_c t_h / \pi\mu d_p d_t^2) \qquad \text{for deposition during a pause} \quad (9.32)$$

Here k is the Boltzmann constant, T the absolute temperature, C_c the slip correction factor, t_h the duration of pause, μ the air viscosity, d_p the particle diameter, and d_t the tube diameter.

The NCRP model uses the expression derived by Ingham (1975) to calculate the deposition efficiency due to convective Brownian diffusion from laminar flow in a straight tube. The expression is discussed in Chapter 4. Enhanced

deposition by convective Brownian diffusion in the vicinity of a carinal ridge is calculated using the following expression (Yeh, 1974):

$$\eta_e = 1 - (1 - \eta_{ld})^{f_e} \tag{9.33}$$

$$f_e = 1 + \frac{2\theta}{\pi}\left(13 - \frac{12\theta}{\pi}\right)\frac{d_t}{l_t} \qquad \text{for } l_t/d_t > 5 \tag{9.34}$$

Here θ is the branching angle in radians and η_{ld} the efficiency of deposition by convective Brownian diffusion from laminar flow in a straight tube.

The following equation is used to calculate the efficiency of deposition due to gravitational settling:

$$\eta_s = 1 - \exp\left(-\frac{2gC_c\rho d_p^2 l_t \sin\phi}{9\pi\mu d_t U}\right) \tag{9.35}$$

Here g is the gravitational acceleration, ρ the particle density, U the average flow velocity, and ϕ the inclination angle relative to gravity ($\phi = 90°$ for horizontal tube). This is an approximate expression given by Beeckmans (1965).

For deposition by gravitational settling during a pause between inhalation and exhalation, the efficiency of deposition is calculated by the above equation with l_t/U replaced by the duration of pause.

To calculate the efficiency of deposition by inertial impaction, the NCRP model employs the following equations

$$\eta_i = 1 - \frac{2}{\pi}\arccos(\theta\,\text{Stk}) + \frac{1}{\pi}\sin[2\arccos(\theta\,\text{Stk})] \qquad \text{for } \theta\,\text{Stk} < 1 \tag{9.36}$$

$$\eta_i = 1 \qquad \text{for } \theta\,\text{Stk} \geq 1 \tag{9.37}$$

$$\text{Stk} = \frac{\rho d_p^2 U C_c}{18\,\mu d_t} \tag{9.38}$$

Here Stk is the Stokes number. Eqs. (9.36) and (9.37) are approximate expressions derived by Yeh (1974).

In the calculations, the airway dimensions are adjusted to the functional residual capacity plus one-half of the tidal volume. The functional residual capacity is either based on the actual value or taken to be 0.4 times the total lung capacity. The conducting airway diameters are assumed to vary according to the

square root of the lung volume, while both the diameters and lengths of airways in the alveolar region are considered to be proportional to the cube root of the lung volume.

9.5 COMPARISON OF THE ICRP AND NCRP MODELS

The ICRP and NCRP models differ mainly in the morphometric parameters of the lungs and the deposition equations used in calculations. The ICRP employs a hybrid model of the respiratory tract consisting of five regions, while the NCRP uses the typical path lung model proposed by Yeh and Schum (1980).

In the ICRP model, the equations used to calculate deposition efficiency of each region are mainly empirical expressions obtained from curve fitting procedures using either experimental data or results of theoretical calculations (the theory itself uses either analytical or empirical expressions for deposition loss and the results of calculations have been validated with experimental data). On the other hand, the NCRP model employs empirical deposition equations for the head airways, but uses either analytical or empirical expressions to make generation-by-generation calculations for deposition in the tracheobronchial and alveolar regions.

The expressions for inhalability differ slightly between the ICRP and NCRP models. The two models also differ in interpretation of the two phases that appear in clearance of particles deposited in the tracheobronchial region. The ICRP model takes into account a slow-cleared fraction for particles deposited in the bronchial and bronchiolar regions. The NCRP model follows the traditional approach by dividing the fast-cleared and slow-cleared fractions between the tracheobronchial and alveolar regions. It does not take into account the slow clearance phase for particles deposited in the bronchial and bronchiolar regions.

Yeh et al. (1996) have used the ICRP and NCRP models to make deposition calculations for the same particle size distribution, lung volume, and breathing conditions. It is to be noted that the calculations had been made before the NCRP model was officially published. The expressions Yeh et al. used for convective Brownian diffusion in oral airways differ from the final forms adopted in the NCRP model, but the numerical results are not expected to differ much. Calculations are made for nose breathing with the following conditions:

Tidal volume = 770 cm^3
Breathing frequency = 13 breaths/min
Functional residual capacity = 3 L
Particle density = 1 g/cm^3
Particle size = 0.001 – 10 μm, with two particle size distributions: (1) a monodisperse aerosol and (2) a lognormally distributed aerosol with a geometric standard deviation of 2.5.

Because the ICRP model has two extrathoracic regions and two tracheobronchial regions, the results calculated from the ICRP model are combined for comparison with the NCRP model for corresponding regions. The results of calculations indicate that, while the deposition fractions in head airways are very similar for the full range of particle size from 0.001 to 10 μm, those in the tracheobronchial and alveolar regions differ for particles smaller than 0.1 μm. The NCRP model predicts a somewhat higher deposition in the tracheobronchial tree and therefore a lower deposition in the alveolar region. Yeh et al. have suggested that the difference probably arises from the fact that the two models use different expressions to account for enhanced deposition due to convective Brownian diffusion in the vicinity of carinal ridges.

9.6 CONCLUDING REMARKS

In principle, it is possible to predict the fate of an inhaled particle from transport equations. This requires solving continuity and Navier-Stakes equations for the flow field in a completely specified respiratory tract and then using it to calculate particle trajectories from the equation of motion. However, flow distribution to various parts of the lungs depends on the morphometry and elastic properties of airways. Current knowledge of lung morphometry and compliance is insufficient to carry out detailed calculations for flow fields in lung airways. Even if a complete set of information on lung morphometry and airway properties is available, the size of computer and the time needed for such calculations would be enormous. At present we can only opt for a mathematical model that makes simplifying assumptions on lung morphometry and particle motion, but incorporates all we know about lung deposition.

In recent years, significant advances have been made in numerical calculations for flow fields and particle deposition in relatively realistic airway models, including extrathoracic airways, bifurcations, and alveolated ducts. The results of these calculations have been used mainly to describe local deposition. It would be useful to incorporate these results in models of respiratory deposition.

PROBLEMS

9.1 As discussed in Chapter 8, nasal deposition can be determined from Eqs. (8.1) and (8.2) using total deposition data obtained from four different breathing maneuvers in inhalation and exhalation. Use the concept of compartments-in-series model to derive these two equations.

9.2 Deposition fraction of a lognormally distributed aerosol in each region of the respiratory tract can be calculated using a compartments-in-series model.

Propose a scheme for making such calculations.

REFERENCES

Altshuler, B. (1959). Calculation of regional deposition of aerosol in the respiratory tract. Bull. Math. Biophys. 21, 257-270.

Asgharian, B . and Yu, C.P. (1989). Deposition of fibers in the rat lung. J. Aerosol Sci. 20, 355-366.

Beeckmans, J.M. 1965. The deposition of aerosols in the respiratory tract – I. Mathematical analysis and comparison with experimental data. Can. J. Physiol. Pharmacol. 43, 157-172.

Birchall, A., Bailey, M.R. and James, A.C. (1991). LUDEP: A lung dose evaluation program. Radiat. Prot. Dosim. 38(1-3), 167-174.

Chang, I.Y., Griffith, W.C., Shyr, L.J., Yeh, H.C., Cuddihy, R.G. and Seiler, F.A. (1991). Software for the draft NCRP respiratory tract dosimetry model. Radiat. Prot. Dos. 38, 193-199.

Chen, Y.K. (1992). Dynamics of charged fibers and application to lung deposition. Ph.D. dissertation, Mechanical and Aerospace Engineering, State University of New York at Buffalo.

Cheng, Y.S., Yamada, Y., Yeh, H.C. and Swift, D.L. (1988). Diffusional deposition of ultrafine aerosols in a human nasal cast. J. Aerosol Sci. 19, 741-751.

Cheng, Y.S., Yamada, Y., Yeh, H.C. and Swift, D.L. (1990). Deposition of ultrafine aerosols in a human oral cast. Aerosol Sci. Technol. 12, 1075-1081.

Cheng, Y.S., Yamada, Y., Yeh, H.C. and Swift, D.L. (1993). Deposition of thoron progeny in human head airways. Aerosol Sci. Technol. 18, 359-375.

Cohen, B.S., Sussman, R.G., and Lippmann, M. (1990). Ultrafine particle deposition in a human tracheobronchial cast. Aerosol Sci. Technol. 12, 1082-1091.

Egan, M.J. and Nixon, W. (1985). A model of aerosol deposition in the lung for use in inhalation dose assessments. Radiat. Prot. Dosim. 11, 5-17.

Egan, M.J., Nixon, W., Robinson, N.I., James, A.C. and Phalen, R.F. (1989). Inhaled aerosol transport and deposition calculations for the ICRP task group. J. Aerosol Sci. 20, 1301-1304.

Ferron, G.A. (1977). The size of soluble aerosol particles as a function of the humidity of the air. Application to the human respiratory tract. J. Aerosol Sci. 8, 251-267.

Ferron, G.A., Haider, B. and Kreyling, W.G. (1988). Inhalation of salt aerosol particles-I. Estimation of the temperature and relative humidity of the air in the human upper airways. J. Aerosol Sci. 19, 343-363.

Findeisen, W. (1935). Über das absetzen kleiner, in der luft suspendierter teilchen in der menschlichen lunge bei der atmung. Pflügers Archiv für gesamte Physiologie des Menschen und der Tiere 236, 367-379.

Fleming, J.S., Hashish, A.H., Conway, J.H., Nassim, M.A., Holgate, S.T., Halson, P., Moore, E., Bailey, A.G. and Martonen, T.B. (1996). Assessment of deposition of inhaled aerosol in the respiratory tract of man using three-dimensional multimodality imaging and mathematical modeling. J. Aerosol Med. 9, 317-327.

Goo, J.H. and Kim, C.S. (2003). Theoretical analysis of particle deposition in human lungs considering stochastic variations of airway morphology. J. Aerosol Sci. 34, 585-602.

Gurman, J.L., Lippmann, M. and Schlesinger, R.B. (1984). Particle deposition in replicate casts of the human upper tracheobronchial tree under constant and cyclic inspiratory flow. I. Experimental. Aerosol Sci. Technol. 3, 245-252.

Heyder, J., Gebhart, J., Rudolf, G., Schiller, C.F. and Stahlhofen, W. (1986). Deposition of particles in the human respiratory tract in the size range 0.005–15 µm. J. Aerosl Sci. 17, 811-825.

Hinds, W.C. (1999). Aerosol Technology: Properties, Behavior, and Measurement of Airborne Particles, Second edition, pp. 244-245. John Wiley & Sons, New York.

Hofmann, W., Koblinger, L. and Bergmann, R. (2001). Stochastic modeling of particle deposition in the human lung. In: Medical Applications of Computer Modeling: The Respiratory System, pp. 109-129 (Ed. Martonen, T.B.). WIT Press, Southampton, UK.

Ingham, D.B. (1975). Diffusion of aerosols from a stream flowing through a cylindrical tube. J. Aerosol Sci. 6, 125-132.

International Commission on Radiological Protection (1960). Recommendations of the International Commission on Radiological Protection Report of Committee II on Permissible Dose for Internal Radiation (1959). ICRP Publication 2. Pergamon Press, Elmsford, New York.

International Commission on Radiological Protection (1979). Limits for Intakes of Radionuclides by Workers. ICRP Publication 30. Part 1. Pergamon Press, Elmsford, New York.

International Commission on Radiological Protection (1994). Human Respiratory Tract Model for Radiological Protection, Annals of the ICRP, Publication 66. Elsevier Science, Tarrytown, NY.

Jarvis, N.S., Birchall, A., James, A.C., Bailey, M.R. and Dorrian, M.-D. (1994). LUDEP 1.1 Personal computer program for calculating internal doses using the new ICRP respiratory tract model, NRPB-SR264. National Radiological Protection Board, Chilton, Didcot, Oxon OX11 0RQ, UK.

Landahl, H.D. (1950). On the removal of air-borne droplets by the human respiratory tract – I. The lung. Bull. Math. Biophys. 12, 43-56.

Landahl, H.D. (1963). Particle removal by the respiratory system. Note on the removal of airborne particulates by the human respiratory tract with particular reference to the role of diffusion. Bull. Math. Biophys. 25, 29-39.

Miller, F.J., Martonen, T.B., Ménache, M.G., Graham, R.C., Spektor, D.M.and Lippmann, M. (1988). Influence of breathing mode and activity level on the regional deposition of inhaled particles and implications for regulatory standards. In: Inhaled Particles VI, Proceedings of an International Symposium and Workshop on Lung Dosimetry Organized by the British Occupational Hygiene Society in Co-operation with the Commission of the European Communities, Cambridge, September 2-6, 1985 (Eds. Dodgson, J., McCallum, R.I., Bailey, M.R. and Fisher, D.R.). Ann. Occup. Hyg. 32 (Suppl. 1), 3-10.

National Council on Radiation Protection and Measurements (1997). Deposition, Retention and Dosimetry of Inhaled Radioactive Substances, NCRP Report 125. NCRP, Bethesda, Maryland.

Pich, J. (1972). Theory of gravitational deposition of particles from laminar flow in channels. J. Aerosol Sci. 3, 351-361.

Rudolf, G, Gebhart, J., Heyder, J., Scheuch, G.. and Stahlhofen, W. (1983). Modeling the deposition of aerosol particles in the human respiratory tract. J. Aerosol Sci. 14, 188-192.

Rudolf, G, Gebhart, J., Heyder, J., Schiller, C.F. and Stahlhofen, W. (1986). An empirical formula describing aerosol deposition in man for any particle size. J. Aerosol Sci. 17, 350-355.

Rudolf, G, Köbrich, R. and Stahlhofen, W. (1990) Modeling and algebraic formulation of regional aerosol deposition in man. J. Aerosol Sci. 21 (Suppl. 1), S403-S406.

Scherer, P.W., Shendalman, L.H., Greene, N.M. and Bouhuys, A. (1975). Measurement of

axial diffusivities in a model of the bronchial airways. J. Appl. Physiol. 38, 719-723.

Swift, D.L., Montassier, N., Hopke, P.K., Karpen-Hayes, K., Cheng, Y.S., Su, Y.F., Yeh, H.C. and Strong, J.C. (1992). Inspiratory deposition of ultrafine particles in human nasal replicate cast. J. Aerosol Sci. 23, 65-72.

TGLD (ICRP Task Group on Lung Dynamics) (1966). Deposition and retention models for Internal dosimetry of the human respiratory tract. Health Phys. 12, 173-207.

Taulbee, D.B. and Yu, C.P. (1975). A theory of aerosol deposition in the human respiratory tract. J. Appl. Physiol. 38, 77-85.

Yamada, Y., Cheng, Y.S., Yeh, H.C. and Swift, D.L. (1988). Inspiratory and expiratory deposition of ultrafine particles in a human nasal cast. Inhal. Toxicol. 1, 1-11.

Yeh, H.C. (1974). Use of a heat transfer analogy for a mathematical model of respiratory tract deposition. Bull. Math. Biol. 36, 105-116.

Yeh, H.C. and Schum, G.M. (1980). Models of human lung airways and their application to inhaled particle deposition. Bull. Math. Biol. 42, 461-480.

Yeh, H.C., Cuddihy, R.G., Phalen, R.F. and Chang, I.Y. (1996). Comparisons of calculated respiratory tract deposition of particles based on the proposed NCRP model and the new ICRP66 model. Aerosol Sci. Technol. 25, 134-140.

Yu, C.P. (1978). Exact analysis of aerosol deposition during steady breathing. Powder Technology 21, 55-62.

Yu, C.P., Diu, C.K. and Soong, T.T. (1981). Statistical analyses of aerosol deposition in nose and mouth. Am. Ind. Hyg. Assoc. J. 42, 726-733.

Yu, C.P. and Diu, C.K. (1983). Total and regional deposition of inhaled aerosols in humans. J. Aerosol Sci. 14, 599-609.

Yu, C.P. and Cohen, B.S. (1994). Tracheobronchial airway deposition of ultrafine particles. In: Inhaled Particles VII, Proceedings of an International Symposium on Inhaled Particles Organized by the British Occupational Hygiene Society, September 16-22, 1991 (Eds. Dodgson, J. and McCallum, R.L.). Ann. Occup. Hyg. 38, Suppl. 1, 83-89.

Yu, C.P., Zhang, L., Oberdörster, G., Mast, R.W., Glass, L.R. and Utell, M.J. (1994). Deposition modeling of refractory ceramic fibers in the rat lung. J. Aerosol Sci. 25, 407-417.

Chapter 10

Fate of deposited particles

Traditionally, removal from the respiratory tract, or lung clearance, has been the focus of attention on the fate of deposited particles. Clearance, implying complete elimination from the respiratory tract, is only part of a sequence of interplays between inhaled particles and the host. The interplays include deposition, transport, dissolution, translocation, accumulation in the respiratory tract or other organs, biotransformation, interaction with cells, and excretion. The initial deposition pattern is the starting point for all subsequent interactions.

The term retention refers to the amount of deposited particles remaining in the respiratory tract. Because clearance processes take place continuously, retention is a function of clearance time.

10.1 MECHANISMS OF PARTICLE CLEARNCE

In contrast to deposition, which is a physical process, lung clearance is a biological process involving several alternative pathways. There are four major mechanisms by which deposited particles clear from the respiratory tract: (1) transport by mucociliary escalators to the pharynx followed by entry into the gastrointestinal (GI) tract, and (2) incorporation by alveolar macrophages followed by transport to mucociliary escalators or lymph nodes, (3) entry into regional lymph nodes via lymphatic vessels, and (4) dissolution followed by absorption into blood circulation.

10.1.1 Mucociliary Transport

A thin layer of mucus covers nearly all airway surfaces in the extrathoracic and tracheobronchial regions. The average thickness of the mucus layer is 15 µm in the extrathoracic region, 5 µm in bronchial airways, and 2 µm in bronchiolar airways. Except for the anterior nasal passages, the epithelium in these two regions is ciliated. Because of repeated beating by underlying cilia, the mucus continuously moves towards the pharynx at velocities varying from site to site. This moving system, known as mucociliary escalator, is capable of carrying deposited particles, macrophages, and dissolved materials to the GI tract via the pharynx.

Clearance efficiency of mucociliary escalators increases with increasing particle size (Scheuch et al., 1996). It also depends on many other factors, including particle loading, irritants, age, and disease. Chemical agents such as cigarette smoke, sulfuric acid droplets, nitrogen dioxide, and ozone may have

marked effects on mucociliary transport rates. Their effects have been reviewed by Lippmann and Schlesinger (1984).

10.1.2 Phagocytosis

Alveolar macrophages are free phagocytic cells. Normally found in serous fluid that covers the alveolar epithelium, these phagocytic cells can engulf and transport deposited particles to the mucus layer in tracheobronchial airways. There are about 5 billion alveolar macrophages in a healthy adult.

Alveolar macrophages move in a pattern resembling an amoeba. They contact deposited particles either by chance or by oriented motion in response to chemical agents in particles.

How alveolar macrophages move to mucociliary escalators is not fully understood. They may simply move in a random manner or move by surface tension gradients. When particle loading is low, alveolar macrophages can quite efficiently engulf deposited particles and move them to mucociliary escalators. At higher particle loadings, increasingly more free deposited particles enter the lymphatic system directly.

10.1.3 Entry into Lymphatic System

As a part of the immune system, the lymphatic system consists of lymph nodes and lymphatics (the small vessels that link the lymph nodes). Lymphatic vessels form a special circulatory system that carries lymph, a clear fluid containing mainly lymphocytes.

Operating in close partnership with blood circulation, the lymphatic system scavenges fluids and proteins that have escaped from cells or tissues and returns them to bloodstreams. Fluids in the interstitial connective tissue drain into lymph capillaries and then flow through lymphatic vessels into lymph nodes.

All three regions of the respiratory tract contain lymphatic tissue. The lymphatic system provides a major clearance pathway for deposited particles. Free deposited particles as well as particle-laden macrophages can enter lymphatic vessels and then move to lymph nodes, where they can remain for a long period of time. The rates at which particles clear via the lymphatic system are relatively slow in comparison with other pathways.

10.1.4 Absorption into Blood Circulation

Absorption is the most effective mechanism to clear soluble particles from the respiratory tract. Toxicants absorbed into bloodstreams may be delivered to target organs if they are not detoxified through biotransformation. On the other hand, absorption is the pathway for systemic delivery of aerosolized drugs. Dissolved material can continue to interact with airway tissues before it is

absorbed. It can even bind with tissue components and remain in the tissue for prolonged periods of time.

Absorption into bloodstreams is a two-stage process. A soluble particle, or soluble substance in a highly insoluble particle, first dissolves into surrounding fluids and then diffuses through the epithelium into bloodstreams. Particle properties that affect the dissolution rate include solubility, surface characteristics, and particle size. Chemicals adsorbed on particles may have effects on the rate of dissolution. As a particle dissolves, its physical and chemical properties can vary with time, which in turn may change the dissolution rate.

Dissolution of soluble material and subsequent absorption into bloodstreams takes place in all regions of the respiratory tract except the anterior nasal passages. Dissolved material can penetrate through epithelial cells or pass between them. The rate of absorption differs from region to region depending mainly on the thickness of epithelial cells. Absorption through the alveolar epithelium is two-fold faster than through the tracheobronchial epithelium.

Other factors that influence absorption rates include acidity, lipophilicity, and molecular weight. Acidity has effects on weak acids and bases. Weak acids have higher absorption rates at lower pH values, while weak bases have higher absorption rates at higher pH values. The absorption rate of an organic compound strongly depends on its lipophilicity (Bond et al., 1985). The lipophilicity is measured in terms of the octanol/water partition coefficient. A lipid soluble compound has a higher absorption rate. The rate at which molecules of lipid-insoluble compounds pass through the membrane is inversely proportional to the molecular weight.

There are other minor routes for particles to enter blood circulation. Dissolved material may pass through lymphatic vessels before entering bloodstreams. Very small particles may enter blood vessels without dissolving (Stradling et al., 1978a; 1978b).

10.2 PARTICLE CLEARANCE IN VARIOUS AIRWAY REGIONS

Deposited particles remain in the respiratory tract for various lengths of time depending on particle properties, sites of deposition, and clearance rates. In the respiratory tract, there are four distinct regions in which deposited particles clear at different rates by different pathways: (1) anterior nasal airways, (2) remaining parts of the extrathoracic region including posterior nasal airways, oral cavity, pharynx, and larynx, (3) the tracheobronchial region, and (4) the alveolar region. Fig. 10.1 depicts the major clearance pathways for these four regions.
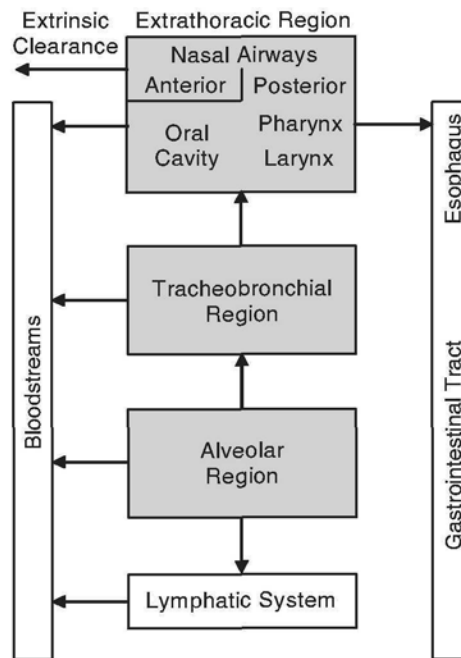
Fig. 10.1 Major clearance pathways for various airway regions.

10.2.1 Extrathoracic Regions

In the anterior nasal airways, mucus moves outwards because the nares are not ciliated. Particles deposited in this part of extrathoracic region are removed by wiping, sneezing, or nose blowing.

In the remaining part of extrathoracic region, particles clear by mucociliary transport to the GI tract via the pharynx. The particle clearance velocity is approximately 6 mm/min in posterior nasal airways. It takes about 10 minutes to move deposited particles from nasal airways to the GI tract. Particles deposited in the mouth clear rapidly through swallowing. For soluble particles, an effective clearance pathway is dissolution followed by absorption into blood streams.

10.2.2 Tracheobronchial Region

In the tracheobronchial region, the mucociliary escalator clears deposited particles to the gastrointestinal tract via the pharynx. Particle-laden macrophages arriving from the alveolar region also clear by the same pathway. Soluble particles deposited in tracheobronchial airways are simultaneously subject to mucociliary transport and dissolution with subsequent absorption into blood circulation.

The velocity of mucus flow in this region decreases with increasing generation number. It is approximately in inverse proportion to the total perimeter of all airways in each generation. In consequence mucus flow has a linear velocity of about 5.5 mm/min in the trachea but drops to about 1 μm/min in terminal bronchioles. This is necessary lest the converging of mucus flow from distal to proximal airways might give rise to fluid pooling. Mucus flow may slow down around the carinal ridge of an airway bifurcation because of the absence of cilia. On average the time needed for clearance of deposited particles ranges from less than an hour to about 2 days in the region.

The rates at which particles clear by mucociliary transport from this region have been measured using radio-labeled insoluble particles. These measurements are expressed in terms of fractional retention as a function of time. Particle retention depends strongly on the distribution of deposited particles in large and small ciliated airways, which in turn is determined by breathing conditions and particle properties. Particles deposited in proximal airways clear faster because of shorter distances to the pharynx and higher mucus velocities.

For insoluble Fe_2O_3 particles between 1 and 10 μm in aerodynamic diameter inhaled at constant flow rates through a mouthpiece, Stahlhofen et al. (1980) have found that the tracheobronchial clearance is completed within 30 to 40 h for quiet breathing conditions (at a tidal volume of 1,000 cm^3 and a breathing frequency of 7.5 breaths/min) and within 24 h for breathing under working conditions (at a tidal volume of 1,500 cm^3 and a breathing frequency of 15 breaths/min).

While most of the particles deposited in larger ciliated airways in the tracheobronchial region of healthy, nonsmoking adults clear within 24 h (Albert and Arnett, 1955; Albert et al., 1967; Albert et al., 1969), there is evidence that a considerable fraction of insoluble particles deposited in small ciliated airways remain well beyond this time span. In terminal bronchioles, the mucus-secreting cells and ciliated cells do not completely cover wall surfaces. In consequence particles deposited on these surfaces do not clear promptly through mucociliary escalators. It is likely that some of these particles are taken up by macrophages inside the mucus in these smaller airways. This route of particle removal is probably responsible for the slow clearance of some insoluble particles from the tracheobronchial tree.

Camner and Philipson (1978) have measured deposition and clearance of particles inhaled to the total lung capacity at a flow rate of 500 cm^3/s. The test aerosol consists of 4-μm Teflon particles tagged with [111]In. Measurements of radioactivity in the lungs show that particle retention decreases markedly in the first 24 h after inhalation. During the following three days, the retention remains

nearly constant but differs considerably (by a factor of 2) among the 10 healthy men studied.

In a study conducted by Stahlhofen et al. (1986), the subject inhales aerosol boluses containing [198]Au-labeled, 3-μm iron oxide particles. Inhalation begins from expiratory reserve volume at a constant flow rate of 250 cm^3/s. The tidal volume is 1000 cm^3. The bolus, which has a mean volumetric half width of 50 cm^3, is injected at various points during inhalation to give a range of front depths (the volumetric distance between the bolus front and the larynx at end inhalation). The subject holds the breath for about 15 seconds at end inhalation to increase the amount of deposition. The results for normal male nonsmokers indicate that about 40% of deposited particles do not clear within six days even for front depths of just about 50 cm^3.

More recently, Falk et al. (1997) have studied clearance of ^{111}In-labeled, 6.2-μm Teflon particles from small ciliated airways. In their study, 8 healthy subjects inhale test aerosols at two different flow rates: 450 and 45 cm^3/s. The use of these two flow rates is based on theoretical calculations that 6.2-μm particles deposit mainly in large bronchi and the alveolar region at 450 cm^3/s, but mainly in small ciliated airways at 45 cm^3/s. According to the retention data, about 50% of deposited particles clear in the first 24 hours for both modes of inhalation, but the patterns of clearance for remaining particles differ between the two modes. These results suggest that the slow-cleared fraction of particles deposited in small ciliated airways clear in a pattern different from that in the alveolar region.

Bennett et al. (1998) have studied deposition and retention of ^{99m}Tc-labeled iron oxide particles in bronchial airways using aerosol boluses. The particles have a mass median aerodynamic diameter of 3.5 μm. The subject inhales a 40-cm^3 aerosol bolus to a volumetric front depth of 40-cm^3. At end inhalation, the lung volume is at 70% total lung capacity. The results show that the retention at 24 hours after inhalation is 27 ± 5%, of which a significant portion appears in large bronchial airways.

10.2.3 Alveolar Region

Fig. 10.2 depicts major clearance pathways for particles deposited in the alveolar region. For insoluble particles, the main clearance pathway is incorporation into alveolar macrophages followed by movement of particle-laden macrophages to mucociliary escalators or lymphatic vessels. Particles can also penetrate into tissue and then pass through lymphatic vessels into lymph nodes. Soluble particles are more likely to dissolve into lung fluids followed by absorption into bloodstreams. Highly soluble particles may dissolve within minutes after deposition.
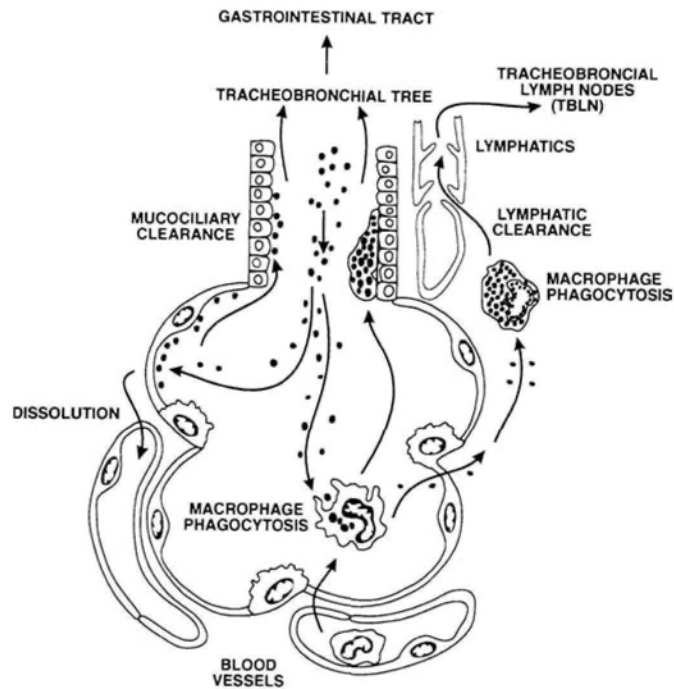
Fig. 10.2 Major clearance pathways in the alveolar region. Reprinted with permission from National Council on Radiation Protection and Measurements (1997).

The rate at which macrophage-mediated transport clears deposited particles is relatively slow. In consequence insoluble particles may remain in the alveolar region for hundreds of days or longer. Particles that penetrate into tissue may remain in the interstitium indefinitely. Similarly, material dissolved in lung fluid may bind with tissue components and remain in the tissue for prolonged periods of time.

Fibers longer than 5 μm clear very slowly because they are too large for alveolar macrophages to engulf. Clearance of these elongated particles generally relies on dissolution with absorption into bloodstreams. They can also penetrate toward the lung pleura.

The alveolar-lymphatic retention of insoluble Fe_2O_3 particles has a half-life of about 50 to 70 days (Albert et al., 1967; Stahlhofen et al., 1980). Clearance rates have been measured for a few other types of particles including polystyrene (Bohning et al., 1982), Teflon (Philipson et al., 1985), and fused aluminosilicate (Bailey et al., 1988). The NCRP model has given the following expression for the rate at which insoluble particles are clear by alveolar macrophages (NCRP, 1997).

$$f(t) = 0.005\exp(-0.02t) + 0.001 \tag{10.1}$$

Here $F(t)$ is the fraction of deposited particles cleared per day and t the time measured in days.

The rate of particle clearance varies form individual to individual. It also changes with aging, respiratory disease, environmental exposure, and physiological conditions. Particle over-loading may slow down clearance processes. On the other hand, low doses of irritating gases or particles may lead to increase in clearance rates.

In view of the relatively high speeds at which deposited particles are cleared by mucociliary escalator, the tracheobronchial tree indeed provides an effective defense line for the alveolar region. The tracheobronchial airways not only collect particles as they pass by during inhalation, but also help remove deposited particles that have been carried up by macrophages from the alveolar region. In this respect, it is useful to view the tracheobronchial and alveolar regions as two distinct parts. The fractions of deposition in these two regions have markedly different health implications. The ratio of deposition fraction in the alveolar region to that in the tracheobronchial tree is a good indicator for the potential health hazards of particulate toxicants to the pulmonary region.

10.3 PARTICLE ACCUMULATION IN RESPIRATORY AIRWAYS

Retention of deposited particles in the respiratory tract is the net result of two opposing processes: deposition and clearance. Continuous exposure to low concentrations may not lead to accumulation if the rate of clearance exceeds the rate of deposition. The doses to tissues in the respiratory tract and other organs depend on many factors including the rates of deposition, transport, dissolution, absorption, and translocation.

Some particles are retained, or sequestered, in the tissues of airway walls in the respiratory tract. Tests with laboratory animals indicate that a small fraction of deposited particles in the tracheobronchial region may penetrate into the epithelium and remain there for a prolonged period of time (Gore and Patrick, 1978). Churg and his associates (Churg and Wright, 1988; Churg et al., 1990) have demonstrated that particle retention in the airway walls occurs in the entire tracheobronchial tree as well as respiratory bronchioles.

Particles initially deposited in the respiratory tract may move to other parts of the body, possibly a result of transport by lymph, blood, or macrophages (via the GI tract). A known example is the transport of deposited asbestos fibers from the respiratory tract to pleural surfaces.

PROBLEMS

10.1 Explain why particles deposited at higher volumetric flow rates in the tracheobronchial region clear faster.

10.2 Discuss how spatial inequality in ventilation distribution can affect clearance patterns of deposited particles.

REFERENCES

Albert, R.E. and Arnett, L.C. (1955). Clearance of radioactive dust from the lung. Arch. Ind. Health 12, 99-106.

Albert, R.E., Lippmann, M., Spiegelman, J., Strehlow, C., Briscoe, W., Wolfson, P. and Nelson, N. (1967). The clearance of radioactive particles from the human lung. In: Inhaled Particles and Vapors II, pp. 361-377 (Ed. Davies, C.N.). Pergamon Press, Oxford.

Albert, R.E., Lippmann, M. and Briscoe, W. (1969). The characteristics of bronchial clearance in humans and the effects of cigarette smoking. Arch. Environ. Health 18, 738-755.

Bailey, M.R., Kreyling, W.G., Andre, S. et al. (1988). An interspecies comparison of the translocation of material from lung to blood. Ann. Occup. Hyg. 32, 975-985.

Bennett, W.D., Scheuch, G., Zeman, K.L., Brown, J.S., Kim, C. Heyder, J. and Stahlhofen, W. (1998). Bronchial airway deposition and retention of particles in inhaled boluses: effect of anatomic dead space. J. Appl. Physiol. 85, 685-694.

Bohning, D.E., Atkins, H.L. and Cohn, S.H. (1982). Long-term particle clearance in man: Normal and impaired. Ann Occup. Hyg. 26, 259-271.

Bond, J.A., Baker, S.M. and Bechtold, W.E. (1985). Correlation of the octanol/water partition coefficient with clearance haft-times of intratracheally instilled aromatic hydrocarbons in rats. Toxicology 36, 285-295.

Camner, P. and Philipson, K. (1978). Human alveolar deposition of 4 μm Teflon particles. Arch. Environ. Health 33, 181-185.

Churg, A. and Wright, J.L. (1988). Mineral particles in airway walls in the lungs of long-term chrysotile miners. In: Inhaled Particles VI, Proceedings of an International Symposium and Workshop on Lung Dosimetry Organized by the British Occupational Hygiene Society in Co-operation with the Commission of the European Communities, Cambridge, September 2-6, 1985 (Eds. Dodgson, J., McCallum, R.I., Bailey, M.R. and Fisher, D.R.). Ann. Occup. Hyg. 32 (Suppl. 1), 173-180.

Churg, A., Wright, J.L. and Stevens, B. (1990). Exogenous mineral particles in the human bronchial mucosa and lung parenchyma. I. Nonsmokers in the general population. Exp. Lung Res. 16, 159-175.

Falk, R., Philipson, K., Svartengren, M., Jarvis, N., Bailey, M. and Camner, P. (1997). Clearance of particles from small ciliated airways. Exp. Lung Res. 23, 495-515.

Gore, D.J. and Patrick, G. (1978). The distribution and clearance of inhaled UO_2 particles on the first bifurcation and trachea of rats. Phys. Med. Biol. 23, 730-737.

Lippmann, M. and Schlesinger, R.B. (1984). Interspecies comparisons of particle deposition and mucociliary clearance in tracheobronchial airways. J. Toxicol. Environ. Health 13, 441-469.

National Council on Radiation Protection and Measurements (1997). Deposition, Retention and Dosimetry of Inhaled Radioactive Substances, NCRP Report 125. NCRP, Bethesda, Maryland.

Philipson, K., Falk, R. and Camner, P. (1985). Long-term lung clearance in humans studied with Teflon particles labeled with chromium-51. Exp. Lung Res. 9, 31-42.

Scheuch, G., Stahlhofen, W. and Heyder, J. (1996). An approach to deposition and clearance measurements in human airways. J. Aerosol Med. 9, 35-41.

Stahlhofen, W., Gebhart, J. and Heyder, J. (1980). Experimental determination of the regional deposition of aerosol particles in the human respiratory tract. Am. Ind. Hyg. Assoc. J. 41, 385-398.

Stahlhofen, W., Gebhart, J., Rudolf, G. and Scheuch, G. (1986). Measurement of lung clearance with pulses of radioactively-labeled aerosols. J. Aerosol Sci. 17, 333-336.

Stradling, G.N., Ham, G.J., Smith, H., and Breadmore, S.E. (1978a). The mobility of americium dioxide in the rat. Radiat. Res. 76, 549-560.

Stradling, G.N., Ham, G.J., Smith, H., Cooper, J. and Breadmore, S.E. (1978b). Factors affecting the mobility of plutonium-238 dioxide in the rat. Int. J. Radiat. Biol. 34, 37-47.

Chapter 11

Health effects

There are beneficial as well as harmful aerosols. According to their nature, harmful particles can be classified into three categories: chemically toxic, infectious, and radioactive. In general, there is a relationship between the response and the dose received.

A biochemically active particle may contain only a small amount of active agents. In this respect, an inhaled particle simply acts as a carrier that facilitates delivery of deleterious or beneficial components to specific surface areas of lung airways. In view of the tortuous narrow passageways and sharp turns they have to go through, aerosol particles are an effective carrier. As an indication of their effectiveness, about one half of all 3-μm particles inhaled through the mouth deposit in the alveolar region.

11.1 ADVERSE HEALTH EFFECTS

In addition to respiratory disease, some types of deposited particles can cause systemic diseases following their dissolution and absorption.

The period between first exposure to an agent and the appearance of symptoms varies depending on the characteristics of the agent and disease. Some symptoms appear within hours from an acute exposure, whereas others may have latency periods as long as 20 years.

Synergistic or antagonistic effects play an important role. Synergism represents the interaction of two or more agents that produces an adverse effect greater than the sum of the effects resulting from exposure to each agent separately. Antagonism is an interaction between two or more agents that results in a reduction in adverse effect of each agent.

Host factors have a strong influence on biological responses to harmful particles. The main host factors include state of health, genetic trait, immunological status, and psychological state such as anxiety and stress.

11.1.1 Chemical Toxicants

Inhalation of particulate toxicants can lead to various types of responses including fibrotic, systemic, irritant, allergic, mutagenic, teratogenic, and carcinogenic responses. Injury of tissues may result from the inhaled compound or its metabolic products. Effects may differ considerably between direct exposure of epithelial cells to toxicants and exposure to the toxicants after phagocytosis. Toxicity also depends on particle size and physicochemical

properties of the agent. Concentration of the agent and duration of exposure are two important factors influencing response. Acute and chronic exposure may result in different adverse effects.

Pneumoconioses, characterized by scars due to increase in interstitial fibrous tissue, are diseases resulting from retention of certain types of particles in the alveolar region. Different types of dusts may produce different patterns of fibrotic lesions. For example, crystalline free silica found in mines, foundries, blasting operations, and glass manufacturing can give rise to a nodular type of fibrosis (silicosis). On the other hand, asbestos fibers can cause a diffuse fibrosis (asbestosis) if they exceed 2 μm in length and 0.1 μm in width (Lippmann, 1990). Coal workers' pneumoconiosis has a complicated form. Most pneumoconioses result in shortness of breath and chronic cough, but pneumoconioses from certain types of dust, such as iron oxide, may have no evidence of functional impairment.

Systemic response arises from chemical toxicants that affect certain organs or tissues. Target sites include respiratory tract, gastrointestinal tract, hematopoietic system, liver, kidney, bones, endocrine system, and nervous system. Herbicides, pesticides and heavy elements such as mercury, lead, cadmium, arsenic, molybdenum, and selenium are known systemic toxicants. An example of systemic response is metal fume fever, an acute flu-like illness with symptoms of throat irritation and dry cough. The symptoms appear within hours following heavy exposure to fumes of metal oxides.

Irritant response generally results from inhalation of particulate sulfates, pesticides, and droplets of sulfuric acid or other strong acids. They cause inflammation in affected regions such as rhinitis, pharyngitis, laryngitis, bronchitis, pulmonary edema, and pneumonia.

Allergic response involves sensitization by initial exposure and reaction to subsequent exposure. Such response can lead to bronchial asthma. Examples of allergens include nickel, cobalt, arsenic, chromium, organic dusts, herbicides, and insecticides.

Inhalation is a route of entry for airborne mutagens (agents that produce changes in DNA), teratogens (agents that cause developmental malformations), and carcinogens. Among known or suspected chemical mutagens are DDT, sodium arsenate, cadmium sulfate, and some lead salts. Examples of known or suspected chemical teratogens include dioxin, organic mercury, cadmium sulfate, and sodium arsenate.

There is a broad variety of chemical carcinogens including cigarette smoke, soot, asbestos, arsenic, chromates, and certain petroleum products. Changes in lung tissues can begin when an individual is exposed to a cancer-causing substance. A few abnormal cells may appear in the lining of bronchi. If

exposure to the carcinogen continues, more abnormal cells can appear and lead to formation of a tumor.

In addition to asbestosis, asbestos fibers can cause bronchial cancer and mesothelioma. The latency period is 20 years or longer. To have chronic toxicity, inhaled asbestos fibers must exceed the following critical length limits: 5 μm for mesothelioma and 10 μm for lung cancer. In addition, fiber width must be less than 0.1 μm to induce mesothelioma and larger than this limit to cause lung cancer (Lippmann, 1990).

Cigarette smoke, containing particles and vapors, has been identified to be the cause of a plethora of diseases. In addition to cancers of the lungs, larynx, esophagus, bladder, cervix, kidney, pancreas, and stomach, smoking can give rise to emphysema, chronic bronchitis, pneumonia, chronic heart and cardiovascular diseases, abdominal aortic aneurysms, acute myeloid leukemia, cataracts, and gum disease. Central bronchial airways are the most common sites for lung cancer in cigarette smokers (Schlesinger and Lippmann, 1978).

11.1.2 Ambient Particles

The diseases resulting from exposure to ambient aerosols include pulmonary emphysema, bronchitis, and, perhaps, lung cancer. Asthmatics are particularly susceptible to the adverse effects of aerosol acidity in ambient air.

Emphysema is a condition of over-inflation of structures in the alveolar region. The over-inflation arises from a breakdown of alveolar walls. Early symptoms of emphysema include shortness of breath and cough. The primary cause of emphysema is cigarette smoking. There is also an inherited form of emphysema due to deficiency of a protein called alpha 1-antitrypsin.

Bronchitis is an inflammation of the lining of bronchial airways. When bronchial airways are inflamed, less air is able to flow to and from the alveolar region and a heavy mucus or phlegm is coughed up. Cigarette smoking is the number one cause of chronic bronchitis. Dusts and fumes in ambient air and workplaces are other common causes of this disease. Higher rates of chronic bronchitis are found among workers exposed to particles of high concentrations, such as coal miners, grain handlers, and metal molders.

Emphysema and chronic bronchitis in combination comprise chronic obstructive pulmonary disease (COPD). A COPD patient has difficulty breathing because (1) the airways lose their elasticity and therefore cannot keep open properly; (2) some alveolar walls are destroyed; (3) airway walls are inflamed; and (4) cells in airways make more mucus than usual, which tends to clog the airways.

Ambient aerosol is a mixture containing numerous chemical species of natural and anthropogenic origins. These particles are either directly emitted into the atmosphere from many different types of sources or formed in air by

gas-to-particle conversion processes. Harmful components identified in highly polluted air include acid sulfate species, heavy metals, reactive organic compounds, and peroxides. At sufficiently high doses these components can produce local respiratory diseases or systemic disorders. However, none of the harmful components mentioned above exists in ambient particles at sufficiently high concentration levels to cause a specific disease.

Ambient particles are harmful when their concentration exceeds a certain limit; epidemiological studies have indicated a strong association of increases in human morbidity and mortality rates with increased concentrations of ambient particles in a certain size fraction (Wilson and Spengler, 1996; Vedal, 1997). Complexity in chemical characteristics of ambient particles has led to considerable difficulty in identifying the components responsible for adverse health effects. Thus, it remains largely unclear which specific components are responsible. Concentration alone cannot explain the causal relationship. According to the threshold limit values recommended by American Conference of Governmental Industrial Hygienists, a worker can be exposed to nuisance or inert dust at the concentration of 5 mg/m^3 in the respirable fraction without measurable injury.

Questions have been raised whether ambient particles are a carrier of short-lived, difficult-to-quantify, but harmful compounds. Friedlander and Yeh (1998) have provided supporting evidence for the involvement of peroxides in the adverse health effects of particulate pollutants. Reactive oxygen species (ROS) in particles also have been shown to play an important role. Highly reactive oxygen-containing species, such as hydroxyl radical and hydrogen peroxide, are collectively described as ROS. In ambient air, photochemical reactions involving reactive organic gases can produce ROS, which are distributed in the gas and particulate phases. Combustion aerosols, such as vehicular exhaust, also contain relatively high concentrations of ROS. Hung and Wang (2001) have reported that the concentrations of particulate ROS in ambient air are strongly associated with photochemical activities. There is a good correlation between the concentrations of ambient ozone and ROS in submicron particles, especially in the ultrafine fraction that are freshly produced by either photochemical reactions in ambient air or combustion processes in vehicular engines.

Aerosol particles can serve as an effective carrier for ambient peroxides and reactive oxygen species to reach the alveolar region. In the absence of particles, inhaled peroxides and ROS mainly deposit in tracheobronchial airways because of their high solubility and diffusivity. When these reactive species are adsorbed on particle surfaces, they can easily reach the alveolar region and thereby lead to an adverse effect greater than in tracheobronchial airways.

Because of their small sizes and surface characteristics, ultrafine particles appear to be more toxic than larger particles. Respiratory effects are shown to

be associated with the number of ultrafine particles (Peters et al., 1997). A recent study indicates that ultrafine particulate pollutants are capable of inducing oxidative stress and mitochondrial damage (Li et al., 2003).

Pulmonary effects of ultrafine particles have been reviewed by Oberdörster (2001). Studies on rodents indicate that ultrafine particles administered to the lungs cause a greater inflammatory response than larger particles of the same total particle mass do. Surface chemistry appears to be an important contributing factor of their high toxicity. Furthermore, it appears that deposited ultrafine particles largely escape capture by alveolar macrophage and therefore have higher probabilities to enter the pulmonary interstitium. These results lend support to the hypothesis that ultrafine particles are causally involved in adverse responses seen in susceptible groups of the population. The need for further studies on ultrafine particles has been stressed in a couple of recent reports (National Research Council, 1998; Friedlander and Pui, 2003).

11.1.3 Bacteria and Viruses

Inhalation is an important route of entry for bacterial and viral pathogens. Single bacterial particles can remain airborne for a long time and therefore have high probabilities to be transmitted through air. Viruses in droplets generated by sneezing and coughing of a patient can survive for hours and gain access to another host while they are airborne.

Droplet size plays an important role in determining the atmospheric spread of infectious diseases. Sneezing and coughing can produce droplets of various sizes. The distance to which a droplet can be transported depends on the rate at which the droplet evaporates. Large droplets settle out of air quickly and, even if they are inhaled, may not reach the pulmonary region. For many pulmonary diseases, the susceptible part is the alveolar region of the respiratory tract. However, smaller droplets can evaporate rapidly to less than 10 μm in diameter. It is mainly these residual particles, named droplet nuclei (Wells, 1934), that can spread the diseases.

Tuberculosis and bacterial pneumonia are two common respiratory diseases caused by bacteria. Symptoms of tuberculosis include feeling tired, loss of appetite, fever, coughing up blood, and night sweats. Pneumonia is a serious infection of the lungs. When the lungs are infected, the alveoli fill with pus and other liquid, thereby greatly reducing the ability to transfer oxygen to the bloodstream.

Legionnaires' disease is a form of bacterial pneumonia. It has acquired its name, because the first known outbreak occurred in the Bellevue Stratford Hotel in Philadelphia where a convention of the Pennsylvania Department of the American Legion was held. In that outbreak, over 200 people contracted this previously unknown type of pneumonia as a result of exposure to mist from

contaminated water that was used to cool the air in the hotel's air conditioning system. The disease can also be contracted by inhaling mist from water sources such as whirlpool baths and showers that are contaminated with Legionella bacteria.

Anthrax is a disease caused by Bacillus anthracis, a spore-forming bacterium. Its symptoms are similar to a common cold initially, but progress to severe breathing problems and shock in a few hours to a few days. To contract the pulmonary form of Anthrax, it requires inhalation of 8 to 20 thousand spores into the alveolar region of the lungs. Droplets that deposit in the nose are not likely to cause the disease.

Examples of diseases due to viruses include influenza, common cold, viral pneumonia, and severe acute respiratory syndrome (SARS). When a person is infected by influenza virus, the tissues of respiratory tract become swollen and inflamed. Prominent symptoms of flu are high fever, muscle aches, severe headache, dry cough, and sore throat. Patients with common colds have milder fever, stuffy nose, sneezing, coughing, and also sore throat. Flu and common colds mostly spread through transfer of virus-containing droplets by inhalation or hand-to-hand contact.

SARS is a respiratory disease due to a type of coronavirus. First reported in Asia in February 2003, its symptoms include high fever (temperature higher than 38.0°C), shortness of breath, headache, coughing, diarrhea, and malaise. Most SARS patients develop pneumonia. According to the World Health Organization, a total of 8,098 people worldwide were infected during the 2003 outbreak. Of these, 774 died. A probable transmission route of the SARS virus is the spread of droplets produced by the cough or sneeze of a patient. Infection can occur if these droplets deposit on the mucous membranes of the mouth, nose, or eyes of persons who are nearby.

11.1.4 Radioactive Particles

The most common radioactive particles in ambient air are radon daughters. After release from soil, radon gas continues to decay and generate a series of radioactive products. These radon daughters easily attach to ambient particles and become a source of radiation exposure for the general population. Occupational exposure to radioactive particles mainly occurs in uranium, tin, and hematite mines.

The primary health effect from inhalation of radioactive particles is cancer. Damage caused by ionizing radiation at the cellular or molecular level can give rise to uncontrolled growth of cells. This is a stochastic effect resulting from long-term, low-level exposure to radiation. Increased doses lead to increase in probability of occurrence. All regions of the respiratory tract are susceptible, but

the frequency of incidence differs from region to region. The types of radiogenic tumors and target tissues have been reviewed by ICRP (1994).

Soluble radionuclides in deposited particles can be absorbed into bloodstreams. Depending on their metabolic behavior, these radionuclides can be retained in various organs for different periods of time.

11.2 THERAPEUTIC AGENTS

A broad variety of pharmaceutical agents can be effectively delivered through inhalation to treat respiratory and systemic diseases. Examples of aerosolized agents for treating respiratory disorders include bronchodilators and mucolytics. Antibacterial and antiviral agents have been used in aerosol form for treating pulmonary infections. For aerosol therapy of systemic illnesses, various degrees of success have been achieved with hormones, vaccines, antibiotics, and cardiovascular drugs. Among the agents tested for systemic medication, aerosolized insulin and heparin appear to be very promising.

Two proven classes of aerosolized drugs for treatment of asthma and chronic obstructive pulmonary disease are β_2-adrenergic agonists and glucocorticoids. Inhalation of β_2-adrenergic agonists can relax bronchial smooth muscle, stimulate skeletal muscle, and inhibit release of inflammatory mediators. Short-acting β_2-adrenergic agonists can provide bronchodilation within minutes of inhalation. Glucocorticoids are useful for treatment of inflammation.

Anticholinergics are among other common agents for treatment of asthma and chronic obstructive pulmonary disease. As bronchodilators, anticholinergics agent have a slower onset but a comparable duration of action as β_2-adrenergic agonists.

Aerosolized formulations of corticosteroids have become commonly used agents in treating respiratory diseases such as asthma, cystic fibrosis, and obstructive lung disorders. These formulations are able to influence existing inflammation.

Mucolytics such as N-acetylcysteine can give rise to rapid liquefaction of viscid mucus. When administered in aerosol form, they can help maintain adequate mucus viscosity in patients with chronic obstructive airway disease.

PROBLEMS

11.1 A review of the SARS epidemic in 2003 indicates that, in some countries, a majority of cases were caused by nosocomial infection. Discuss possible transmission routes of the SARS coronavirus in hospitals.

11.2 A potential terrorist weapon is the release of plant and animal pathogens in aerosol form. These pathogens can have devastating effects on agriculture if they are released at points where they can spread out rapidly. What strategies can be used to protect agriculture from such terrorist attacks?

REFERENCES

Friedlander, S.K. and Yeh, E.K. (1998). The submicron atmospheric aerosol as a carrier of reactive chemical species: Case of peroxides. Appl. Occup. Environ. Hyg. 13, 416-420.

Friedlander, S.K. and Pui, D.Y.H. (Workshop Chair and Co-Chair) (2003). Emerging Issues in Nanoparticle Aerosol Science and Technology (NAST), Report of a National Science Foundation Workshop, University of California, Los Angeles, June 27-28, 2003. This report is available at http://dalton.chemeng.hosted.ats.ucla.edu/nanoaerosol_workshop/report.pdf

Hung, H.F. and Wang, C.S. (2001). Experimental determination of reactive oxygen species in Taipei aerosols. J. Aerosol Sci. 32, 1201-1211.

International Commission on Radiological Protection (1994). Human Respiratory Tract Model for Radiological Protection, Annals of the ICRP, Publication 66. Elsevier Science, Tarrytown, NY.

Li, N., Sioutas, C., Froines, J.R., Cho, A., Misra, C. and Nel, A. (2003). Ultrafine particulate pollutants induce oxidative stress and mitochondrial damage. Environ. Health Perspect. 111, 455-460.

Lippmann, M. (1990). Effects of fiber characteristics on lung deposition, retention, and disease. Environ Health Perspect. 88, 311-317.

National Research Council (1998). Research Priorities for Airborne Particulate Matter. I. Immediate Priorities and a Long-Range Research Portfolio. National Academy Press, Washington, D.C.

Oberdörster, G. (2001). Pulmonary effects of inhaled ultrafine particles. Int. Arch. Occup. Environ. Health 74, 1-8.

Peters, A., Wichmann, H.E., Tuch, T., Heinrich, J. and Heyder, J. (1997). Respiratory effects are associated with the number of ultrafine particles. Am. J. Respir. Crit. Care Med. 155, 1376-1383.

Schlesinger, R.B., Lippmann, M. (1978). Selective particle deposition and bronchogenic carcinoma. Environ. Res. 15, 424-431.

Vedal, S. (1997). Ambient particles and health: Lines that divide. J. Air Waste Manage. Assoc. 47, 551-581.

Wells, W.F. (1934). On air-borne infection; II. Droplets and droplet nuclei. Am. J. Hyg. 20, 611.

Wilson, R. and Spengler, J.D. (Eds) (1996). Particles in Our Air: Concentrations and Health Effects. Harvard University Press, Cambridge, Mass.

Chapter 12

Applications

Particle transport in the respiratory tract has been a subject of intensive studies, because it has applications in health risk assessment of particulate pollutants, development of diagnostic procedures, and design of respiratory delivery devices and methodology for therapeutic agents. Advances in these applications as well as development of new applications can be expected as our understanding of inhaled particles improves.

12.1 HEALTH RISK ASSESSMENT

Deposition models have been used to evaluate doses to target tissues of the respiratory tract for both chemical toxicants and radioactive particles. These applications have proved useful in setting standards and guidelines for protection of workers as well as the general population.

Although local deposition patterns provide only the initial dose, the data are useful as a starting point for development of a comprehensive dosimetry model that includes subsequent translocation and biotransformation of deposited particles. To evaluate the dose-response relationship of an inhaled agent, it is important to express the effective dose at the site of action. Both dose and tissue sensitivity varies with site. Dose is higher in the vicinity of carinal ridges because of higher deposition and slower clearance rates at these sites. Tissues in some groups of airways are particularly sensitive to toxic materials. For example, segmental and subsegmental bronchi are preferential sites for the development of carcinomas. Symmetric lung models have been used for calculations of dose per airway generation. However, such calculations may not provide accurate information on effective doses at the site of action because lung airways are asymmetric in nature. Asymmetric lung models would be a better choice for this purpose.

Particle properties such as size, shape, surface area, solubility, and chemical composition should be taken into consideration in dose calculations. Rates of clearance and absorption into bloodstreams depend on these properties. For some chemicals, the toxicity arises from their metabolites. Direct exposure of tissues to toxic particles and exposure to the toxicants after phagocytosis may have very different consequences. Exposure conditions such as particle loading and simultaneous exposure to several toxicants also have marked influence on biological responses.

Particle dose can be expressed in terms of particle number or mass per unit volume of tissues. It also can be expressed in terms of areal density, that is, particle number or mass per unit surface area of tissues. The dose per unit volume of tissues is appropriate for assessing the effects of radioactive substances that emit long-range radiation and for highly soluble chemical toxicants that deposit relatively evenly in the lungs. On the other hand, particle doses per unit surface area of tissues are more suitable for assessing the effects of radioactive species that emit short-range radiation and for insoluble particles with active chemicals on their surfaces.

Dose parameters may differ for different types of particles. For radioactive substances, the important dose parameters are time-integrated total energy deposition and energy deposition rate in tissue. For chemical toxicants, the important dose parameters may be the peak concentration, time-integrated concentration, duration of exposure, and concentrations of potential metabolic products.

Both the International Commission on Radiological Protection (ICRP, 1994) and the National Council on Radiation Protection and Measurements (NCRP, 1997) have developed models for calculating doses from inhalation of radionuclides. In order to take a coherent international approach to radiation protection, the NCRP has adopted the ICRP recommendations on exposure calculations for radiation workers and the public. Nevertheless, the NCRP model represents a valuable alternative approach to the ICRP model.

12.2 AEROSOL DIAGNOSIS

Aerosols have been used in assessment of regional ventilation, airway obstruction, responses to pharmaceutical agents, pulmonary epithelial permeability, mucociliary transport, and airway responsiveness to sensitizing and non-sensitizing stimuli. These applications have been reviewed by Dolovich et al. (1993).

The aerosol ventilation test has been successfully applied in the evaluation of pulmonary embolism. Compared to radioactive gases, submicron-sized radioactive particles can provide regional ventilation scans with excellent resolution. In the assessment of airway obstruction, measurements on deposition and clearance of 3-μm radioactive particles in large and small airways are utilized to detect early airway abnormalities.

Radio-labeled drug particles have been employed to study correlation between deposition and airway response. The results have proved useful for adjusting doses, evaluating performance of aerosol delivery devices, and assessing new formulations. Pulmonary epithelial permeability can be assessed using submicron-sized radioactive particles of low-molecular-weight,

hydrophilic materials. Submicron-sized particles deposited in the alveolar region diffuse rapidly across the pulmonary epithelium and capillary endothelium into the vascular space. The rate at which these radioactive particles leave the alveolar region represents a measure of epithelial permeability.

A number of respiratory diseases have marked influence on the rate of mucociliary transport. Radioactive particles have been used to measure mucociliary clearance rates as discussed in Chapter 8. On the other hand, movement of inert or radioactive particles on the tracheal mucus can be directly observed using a bronchoscope or a gamma camera.

Airway responsiveness to stimuli is measured using inhalation provocation tests. For non-sensitizing chemicals such as histamine, the test is relatively easy and safe. Provocation tests for responsiveness to allergens or chemical sensitizers are more complex and risky. They should be performed under direct physician supervision.

The following discussion focuses on two recently developed diagnostic procedures: aerosol bolus dispersion test and aerosol-derived airway morphometry.

12.2.1 Aerosol Bolus Dispersion Test

As described in Chapter 5, aerosol dispersion reflects the flow patterns in lung airways. In an aerosol bolus dispersion test, the breathing maneuver consists of two steps: (1) inhaling, at a constant flow rate, particle-free air from the functional residual capacity to a given fraction of the total lung capacity, with an aerosol bolus inserted into the air stream at a predetermined volumetric lung depth, and (2) exhaling until the particle concentration in exhaled air is no longer detectable or when the residual volume is reached.

To establish reference values for possible clinical applications of this technique, Brand et al. (1997) have used it to study aerosol bolus dispersion in 79 healthy subjects. The test aerosol consists of monodisperse di-2-ethylhexyl sebacate droplets approximately 0.84 μm in diameter. The droplets are non-hygroscopic and have a settling velocity of 23 μm/s. Aerosol boluses, 20 cm^3 in volume, are injected at volumetric lung depths of 20- 800 cm^3. The volumetric lung depth refers to the air volume between the volume at which the maximum particle concentration is measured and the end-inspiratory volume. The results show that aerosol bolus dispersion increases with increasing total lung capacity, but on average does not vary with flow rate and the level of lung inflation. The corrected half-width, H_{50C}, is approximately a power function of the volumetric lung depth, V_p.

$$H_{50C} = 12V_p^{0.57} \qquad\qquad (12.1)$$

Aerosol bolus dispersion is sensitive to changes in distribution of lung ventilation. Because diseased lungs tend to increase dispersion, the technique of aerosol bolus dispersion is capable of detecting early lung impairment caused by cigarette smoking (Brand, 1994).

12.2.2 Aerosol-derived Airway Morphometry

Aerosol-derived airway morphometry measures airspace dimensions in the respiratory tract using the relationship between intrapulmonary airspace dimension and fraction of monodisperse aerosol particles deposited by gravitational settling. To establish reference values for clinical applications of this technique, Brand et al. (1995) have used it to study airspace dimensions in 79 healthy subjects. The breathing maneuver for the measurement includes four steps: (1) exhaling to the midpoint of expiratory reserve volume, (2) inhaling, at a constant flow rate of 250 cm^3/s, a monodisperse aerosol up to a fraction (0.5-0.85) of the total lung capacity, (3) holding the breath for a predetermined time, and (4) exhaling at the same constant flow rate to below the functional residual capacity. As discussed in Chapter 7, the fraction of particles deposited by gravitational settling during breath-holding depends on the settling velocity v_s of particles, breath-holding duration t_h, and effective airspace dimension l_m. The test aerosol contains monodisperse di-2-ethylhexyl sebacate droplets about 0.84 μm in diameter. The droplets are non-hygroscopic and have a settling velocity of 23 μm/s. The breath-holding duration ranges from 2 to 18 s.

If the inhaled aerosol volume is considered to be composed of a sequence of boluses, the particles in the bolus that reaches a region with smaller l_m have a shorter distance to settle before depositing onto a wall surface and thereby have a higher deposition fraction. The number concentration of particles is recorded as a function of respired volume. The particle recovery (R_a), defined as the ratio of the particle number concentration in the portion of expired air from a given lung depth to the concentration in inhaled aerosol, is a function of breath holding time and volumetric lung depth. By plotting the particle recovery against the breath holding time on a semi-log graph, a straight line is obtained for each volumetric lung depth. The straight line fits the following empirical equation

$$R_a = \exp(-1.27 v_s t_h / l_m) \qquad\qquad (12.2)$$

This equation has the same form as Eq. (7.1). Depending on the volumetric lung depth reached by the portion of aerosol (the aerosol bolus), the value of l_m

calculated from this equation gives an estimate of either the mean airway diameter in the conductive region or the mean chord length in the alveolar region. To compare the mean airspace dimension, the volumetric lung depth reached by the aerosol bolus is normalized by the end-inspiratory lung volume at which the breath is held.

Pulmonary emphysema is a disease characterized by enlargement of air spaces distal to terminal bronchioles and destruction of alveolar walls. Aerosol-derived airway morphometry (ADAM) and aerosol bolus dispersion test (ABD) are useful for detecting macroscopic pulmonary emphysema. The sensitivity and specificity of these two tests are comparable to the parameters obtained by high-resolution computed tomography for in vivo diagnosis of macroscopic emphysema. Because ADAM and ABD are noninvasive and easy to perform, they are suitable for screening macroscopic emphysema in occupational studies (Kohlhäufl et al., 1999).

By applying aerosol-derived airway morphometry and aerosol bolus dispersion tests, it is possible to distinguish the morphometric changes caused by emphysema from those caused by fibrosis with high sensitivity and specificity (Brand et al., 1999). Patients with pulmonary emphysema show an increase in aerosol bolus dispersion, but patients with interstitial pulmonary fibrosis have normal results in the ABD test. Furthermore, the pattern of increased airspace dimensions shown in ADAM tests differs between the two patient groups. While patients with pulmonary emphysema show enlarged airspace dimensions in all lung depths, patients with interstitial pulmonary fibrosis show enlarged airspace dimensions only in the lung periphery.

The increase in aerosol bolus dispersion in patients with pulmonary emphysema is likely a consequence of lung destruction that increases collateral ventilation, pendelluft, and airway closure during exhalation. Collateral ventilation is the ventilation of alveolar region through channels that bypass the normal airways. In emphysema patients, peripheral airways become obstructed, thereby causing air to flow preferentially through collateral pathways to provide for more even distribution of ventilation. Pendelluft is the transient movement of air out of some alveoli and into others when flow has just stopped at the end of each respiratory phase. It occurs when regions of the lungs differ in compliance and airway resistance so that the time constants of their filling or emptying in response to a change of transpulmonary pressure are not the same.

12.3 AEROSOL THERAPY

Inhalation offers a number of advantages over other routes for drug delivery. In the treatment of certain respiratory diseases, pulmonary delivery has the advantages of minimizing systemic side effects and reducing the time of

delivery to the site of action. Inhalation is also an attractive alternative for medication of systemic illnesses, because soluble particles deposited in the alveolar region are readily dissolved and absorbed into the bloodstream. Even large molecules such as insulin, growth hormone, interferon-β, and calcitonin can easily enter the capillary network through the alveolar epithelium.

Gene therapy by aerosol inhalation appears to be a promising approach for treating cystic fibrosis (Rochat and Morris, 2002). Recent clinical trials with aerosols in cystic fibrosis patients have revealed that gene transfer from the lumen to respiratory epithelium can be achieved in vivo, although the transfer efficiency still needs improvement.

Compared to injection and oral administration of pharmaceutical agents, the dose delivered by inhalation varies from individual to individual, depending on breathing characteristics and respiratory tract anatomy. It is important to distinguish inhaled doses from deposited doses.

In addition to the site and rate of deposition, the pharmacokinetics of an inhaled drug depend on the rates of several subsequent processes including mucociliary transport, pulmonary endocytosis, dissolution, absorption, and metabolism. The efficacy of aerosol therapy can be improved through proper design of drug formulations, delivery devices, and breathing maneuvers for targeting. The principles of inhaled particles are useful for making better selections in these three aspects of aerosol therapy.

12.3.1 Drug Formulations

The rate at which an active agent in a deposited drug particle is absorbed into the bloodstream depends on particle size, deposition site, dissolution rate, and the rate at which the particle is cleared from its deposition site. Slow dissolution rate is more desirable for topical treatment because of the need to maintain an effective drug concentration at the site of action. Control of release rate can help achieve maximum pulmonary targeting.

In contrast to ambient particles that are inhaled as they are, aerosolized drugs can be designed to maximize therapeutic effects. In principle, it is possible to optimize the absorption rate of an active agent by properly selecting the physicochemical properties of particles, including size, shape, density, hygroscopicity, solubility, and electric charge. Solubility, stability and safety are three important issues in inhalation formulations. Refinement in formulation of therapeutic agents can lead to significant improvements in the efficacy of aerosol therapy.

12.3.2 Delivery Devices

Devices commonly used to deliver aerosolized therapeutic agents include nebulizers, metered-dose inhalers, and dry powder inhalers. Basic principles

and design of these devices have been reviewed in a couple of recent books (Bisgaard, 2002; Hickey, 2003).

There are two general ways to disintegrate a liquid into small droplets: ultrasonic waves and air jets. In an ultrasonic nebulizer, droplets are generated at the liquid surface where ultrasonic waves are created by vibration of a ceramic piezoelectric crystal. Hand-held ultrasonic nebulizers have been developed using microelectronics, but they are not as portable as metered-dose inhalers and dry powder inhalers. An air-jet nebulizer works by the Bernoulli principle. When compressed air passes through an orifice, the resulting high flow velocity creates a low pressure area. Liquid drawn into the area is atomized when it mixes with the air jet. Because of the need to supply compressed air, air-jet nebulizers are less convenient than ultrasonic nebulizers.

A metered-dose inhaler comprises four basic parts: the base formulation, container, metering valve, and actuator. The base formulation, consisting of the medication and volatile propellants, is pressurized in the container. The actuator is used to depress a valve stem in the metering chamber, which in turn deliver a metered portion of the liquid phase of the formulation. The liquid spray leaves the inhaler at very high speeds, usually resulting in significant deposition at the back of the mouth

Dry powder inhalers come in two variations: single and multiple doses. Several designs are available for dispensing single doses, but basically they all fill the drug mixture in a hard capsule. The drug capsule, loaded in the inhaler, is pierced or broken open just before inhalation. In a multiple-dose device, the drug contained in a reservoir is dispensed into a dosing chamber before each use. Dry powder inhalers are inspiratory flow driven. In consequence there is no need for a patient to carefully coordinate breathing with hand actuation as is required with metered-dose inhalers.

Dry powder particles tend to adhere to each other. For better deagglomeration of adhered particles, dry powder inhalers are usually used with high inhalation flow rates. Significant deposition of particles may occur on the back of the mouth as a result of impingement of the jet from the inhaler outlet. For the same inspiratory flow rate, deposition in the mouth increases with decreasing outlet diameter of the dry powder inhaler. Numerical calculations for an idealized mouth model with small circular inlets of various diameters show that, at a flow rate of 32.9 L/min, the fraction of 5-μm particles deposited on the back of the mouth is 70% and 42%, respectively, for 3- and 5-mm inlets (Matida et al., 2003).

12.3.3 Breathing Maneuvers for Targeting

It is usually desirable to deliver drug to specific sites or regions of the respiratory tract. The distribution of certain receptors is uneven in the lungs

(Karlsson et al., 1988). Some tend to concentrate at carinal ridges. On the other hand, the regions where medication is needed depend on conditions of disease. Targeting has the purposes of delivering a drug to the areas of lungs where the agent can provide its maximum therapeutic effect and avoiding the areas where the worst side effect occurs. By selecting an appropriate set of tidal volume, respiratory frequency, breathing maneuver, posture, particle size, and particle density, it is possible to preferentially deposit particles in a target site or region. However, it is important to bear in mind that subsequent transport and biotransformation are additional factors that play important roles in determining the effective doses.

Heyder and Svartengren (2002) have shown that, if extrathoracic airways, trachea, and bronchi are combined as one region and the remaining lung airways combined as another region, the particle size distribution has little effect on targeting efficiency. For example, both monodisperse and log-normally distributed aerosol particles (with a geometric standard deviation of 2) of standard density (1 g/cm^3) and identical mass median aerodynamic diameters have a targeting efficiency of over 90% for each of these two combined regions. These conclusions are obtained from calculations for the following two sets of breathing patterns and particle sizes: (a) tidal volume = 180 cm^3, respiratory period = 0.6 s, and mass median aerodynamic diameter = 8 μm, and (b) tidal volume = 1,000 cm^3, respiratory period = 20 s, and mass median aerodynamic diameter = 2 μm.

Most therapeutic particles contain hydrophilic salts and therefore can grow substantially during transport in the respiratory tract. The major effects of particle growth take place in the bronchioles and alveolar region. Hygroscopic growth of therapeutic particles, which are generally in the micron-size range, can lead to change in deposition patterns as well as increase in deposition rates. Surfactants applied on droplet surfaces are capable of delaying hygroscopic growth (Otani and Wang, 1984). It might be possible to use this technique to target deposition of therapeutic particles at specific lung depths.

Bennett et al. (2002) have reviewed aerosolized drug treatment with regards to targeting specific areas of the lungs. Targeting can be divided into two categories: serial and parallel. Serial targeting aims to deliver particles to either the conducting airways or the alveolar region, while parallel targeting aims at specific lobes.

For serial targeting, delivery of an aerosol bolus to shallow lung depths under slow inhalation favor deposition in conducting airways, while slow and deep inhalations followed by breath-holding enhance deposition in the alveolar region. Breath-holds following inhalation of aerosol boluses facilitate deposition in the regions where they have reached. The optimal particle size for targeting the alveolar region is about 3 μm.
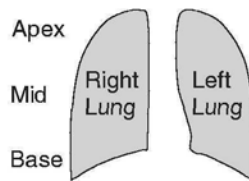
Fig. 12.1 Schematic diagram of the lungs showing various parts for targeting.

Diseased areas of the lungs need parallel targeting, because in a spontaneous breath air and particles have difficulty reaching the most diseased and poorly ventilated areas. By reviewing earlier studies on the distribution of inspired gas, Bennett et al. have suggested that parallel targeting can be achieved by varying body position or inspiratory muscle groups together with properly selecting the injection point of aerosol boluses in the tidal air. The following regional ventilation patterns are useful for parallel targeting:

(1) Early in a vital capacity inhalation more air goes to the apical part than the basal part of the lungs (see Fig. 12.1).
(2) In an inhalation near the total lung capacity, air preferentially distributes to the basal part of the lungs.
(3) Early in an inspiratory capacity breath, higher flow rates favor distribution of air to the apical part of the lungs.
(4) For all flow rates, the ratio of apical to basal distribution is lower in an upright posture than in a supine position (Sybrecht, et al., 1976).
(5) In an upright posture, the bolus inhaled at functional residual capacity tends to distribute preferentially to the basal part of the lungs with an abdominal inspiration, while it tends to distribute evenly (or preferentially to apical regions) with intercostal inspirations (Roussos et al., 1977).

PROBLEMS

12.1 Discuss potential advantages in using aerosols of elongated particles for drug delivery and design a device for delivering such particles to lung airways.

12.2 Surfactants applied on droplet surfaces are capable of delaying hygroscopic growth. Design a strategy to use this technique for targeting therapeutic particles at the alveolar region.

REFERENCES

Bennett, W.D., Brown, J.S., Zeman, K.L., Hu, S.C., Scheuch, G. and Sommerer, K. (2002). Targeting delivery of aerosols to different lung regions. J. Aerosol Med. 15, 179-188.

Bisgaard, H., O'Callaghan, C. and Smaldone, G.C. (Eds.) (2002). Drug Delivery to the Lung. Marcel Dekker, Inc., New York.

Brand, P., Tuch, T., Manuwald, O. et al. (1994). Detection of early lung impairment with aerosol bolus dispersion. Eur. Respir. J. 7, 1830-1836.

Brand, P., Rieger, C., Beinert, T. and Heyder, J. (1995). Aerosol-derived airway morphometry in healthy subjects. Eur. Respir. J. 8, 1639-1646.

Brand, P., Rieger, C., Schulz, H., Beinert, T. and Heyder, J. (1997). Aerosol bolus dispersion in healthy subjects. Eur. Respir. J. 10, 460-467.

Brand, P., Kohlhäufl, M., Meyer, T., Selzer, T., Heyder, J. and Häußinger, K. (1999). Aerosol-derived airway morphometry and aerosol bolus dispersion in patients with lung fibrosis and lung emphysema. Chest 116, 543-548.

Dolovich, M.B., Cockcroft, D.W. and Coates, G. (1993). Aerosols in diagnosis: ventilation, airway penetrance, epithelial permeability, mucociliary transport and airway responsiveness. In: Aerosols in Medicine: Principles, Diagnosis and Therapy, Second edition, Chapter 7 (Eds. Morén, F., Dolovich, M.B., Newhouse, M.T. and Newman, S.P.). Elsevier Science, Amsterdam.

Heyder, J. and Svartengren, M.U. (2002). Basic principles of particle behavior in the human respiratory tract. In: Drug Delivery to the Lung, p.42 (Eds. Bisgaard, H., O'Callaghan, C. and Smaldone, G.C.). Marcel Dekker, New York.

Hickey, A.J. (Ed.) (2003). Pharmaceutical Inhalation Aerosol Technology. Second edition. Marcel Dekker, Inc., New York.

International Commission on Radiological Protection (1994). Human Respiratory Tract Model for Radiological Protection, Annals of the ICRP, Publication 66. Elsevier Science, Tarrytown, NY.

Karlsson, J.A., Sant'Ambrogio, G., and Widdicombe, J. (1988). Afferent neural pathways in cough and reflex bronchoconstriction. J. Appl. Physiol. 65, 1007-1023.

Kohlhäufl, M., Brand, P., Rock, C., et al. (1999). Noninvasive diagnosis of emphysema: Aerosol morphometry and aerosol bolus dispersion in comparison to HRCT. Am. J. Respir. Crit. Care Med. 160, 913-918.

Matida, E.A., DeHaan, W.H., Finlay, W.H. and Lange, C.F. (2003). Simulation of particle deposition in an idealized mouth with different small diameter inlets. Aerosol Sci. Technol. 37, 924-932.

National Council on Radiation Protection and Measurements (1997). Deposition, Retention and Dosimetry of Inhaled Radioactive Substances, NCRP Report 125. NCRP, Bethesda, MD.

Otani, Y. and Wang, C.S. (1984). Growth and deposition of saline droplets covered with a monolayer of surfactant. Aerosol Sci. Technol. 3, 155-166.

Rochat, T. and Morris, M.A. (2002). Gene therapy for cystic fibrosis by means of aerosol. J. Aerosol Med. 15, 229-235.

Roussos, C.S., Fixley, M., Genest, J., Cosio, M., Kelly, S., Martin, R.R. and Engel, L.A. (1977). Voluntary factors influencing the distribution of inspired gas. Am. Rev. Respir. Dis. 116, 457-467.

Sybrecht, G., Landau, L., Murphy, B.G., Engel, L.A., Martin, R.R. and Macklem, P.T. (1976). Influence of posture on flow dependence of distribution of inhaled ^{133}Xe boli. J. Appl. Physiol. 41, 489-496.

Appendices

Appendix A1. Frequently Used Physical Constants

Boltzmann's constant	k	1.381×10^{-16} dyn·cm/K
Avogadro's number	N_a	6.022×10^{23} molecules/mol
Gas constant	R	8.314×10^7 dyn·cm/mol·K,
		82.06 cm³·atm/mol·K
Elementary charge	e	1.602×10^{-19} C,
		4.803×10^{-10} statC
Permittivity of a vacuum	ε_0	8.854×10^{-12} C²/N·m²
Gravitational acceleration	g	980.7 cm/s²

Appendix A2. Conversion Factors

Length
1 micrometer (μm) = 10^{-6} m = 10^{-4} cm = 10^{-3} mm = 10^3 nm = 10^4 Å
1 nanometer (nm) = 10^{-3} μm = 10^{-9} m
1 Ångstrom (Å) = 10^{-4} μm = 10^{-10} m

Volume
1 μm³ = 10^{-15} L = 10^{-18} m³
1 liter (L) = 10^{15} μm³ = 10^{-3} m³
1 m³ = 10^{18} μm³ = 10^3 L

Force
1 dyne (dyn) = 10^{-5} N = 1.021×10^{-3} g force
1 Newton (N) = 10^5 dyn = 102 g force
1 gram (g) force = 980.7 dyn = 9.807×10^{-3} N

Temperature
degree Celsius (°C) = $K - 273.16$

Pressure
1 atmosphere (atm) = 1.013×10^6 dyn/cm² = 1.013×10^5 N/m² = 760 mmHg
$\qquad\qquad\qquad = 1.013 \times 10^5$ Pa = 101.3 kPa
1 dyn/cm² = 9.869×10^{-7} atm = 0.1 N/m² = 7.501×10^{-4} mmHg
1 mm of mercury (mmHg) (at 0°C) = 1.316×10^{-3} atm = 1.333×10^3 dyn/cm²
$\qquad\qquad\qquad = 1.333 \times 10^2$ N/m²
1 Pascal (Pa) = 10 dyn/cm² = 1 N/m²
1 torr = 1 mmHg

Viscosity
1 poise (P) = 1 g/cm s = 1 dyn·s/cm² = 0.1 Pa·s

Electrical Units
1 ampere (amp) = 2.998×10^9 statamp
1 statampere (statamp) = 3.336×10^{-10} amp

1 volt (V) = 3.336×10^{-3} statV
1 statvolt (statV) = 299.8 V
1 farad (F) = 10^6 μF = 8.988×10^{11} statF
1 statfarad (statF) = 1.113×10^{-12} F
1 ohm = 1.113×10^{-12} statohm
1 statohm = 8.988×10^{11} ohm

Appendix A3. SI Prefixes

10^{-12}	pico	p
10^{-9}	nano	n
10^{-6}	micro	μ
10^{-3}	milli	m
10^{-2}	centi	c
10^3	kilo	k
10^6	mega	M
10^9	giga	G
10^{12}	tera	T

Appendix A4 (a). Properties of Air at 20°C and 1 atm

Density	ρ	1.20×10^{-3} g/cm^3 = 1.20 g/L
Viscosity	μ	1.81×10^{-4} P = 1.81×10^{-5} Pa·s
Mean free path	λ	0.066 μm
Diffusion coefficient	D	0.20 cm^2/s
Average molecular weight	$\overline{M}$	29.0 g/mol

Appendix A4 (b). Properties of Air at 37°C and 1 atm

Density	ρ	1.13×10^{-3} g/cm^3 = 1.13 g/L
Viscosity	μ	1.89×10^{-4} P = 1.89×10^{-5} Pa·s
Mean free path	λ	0.07 μm
Diffusion coefficient	D	0.22 cm^2/s

Appendix A5 (a). Properties of Aerosol Particles at 20°C and 1 atm.

Particle Diameter (μm)	Slip Correction Factor	Settling Velocity (cm/s)	Diffusion Coefficient (cm^2/s)	Mechanical Mobility (cm/s dyn)
1.00E-03	2.19E+02	6.60E-07	5.20E-02	1.29E+12
2.00E-03	1.10E+02	1.32E-06	1.30E-02	3.22E+11
5.00E-03	4.43E+01	3.34E-06	2.10E-03	5.19E+10
1.00E-02	2.24E+01	6.76E-06	5.32E-04	1.32E+10
2.00E-02	1.15E+01	1.39E-05	1.37E-04	3.38E+09
5.00E-02	5.01E+00	3.77E-05	2.38E-05	5.88E+08
1.00E-01	2.89E+00	8.70E-05	6.85E-06	1.69E+08
2.00E-01	1.88E+00	2.26E-04	2.23E-06	5.51E+07
5.00E-01	1.33E+00	1.00E-03	6.32E-07	1.56E+07
1.00E-00	1.17E+00	3.51E-03	2.76E-07	6.83E+06
2.00E-00	1.08E+00	1.30E-02	1.28E-07	3.17E+06
5.00E-00	1.03E+00	7.78E-02	4.90E-08	1.21E+06
1.00E+01	1.02E+00	3.06E-01	2.41E-08	5.96E+05
2.00E+01	1.01E+00	1.21E+00	1.19E-08	2.96E+05
5.00E+01	1.00E+00	7.55E+00	4.76E-09	1.18E+05
1.00E+02	1.00E+00	3.02E+01	2.37E-09	5.87E+04

Appendix A5 (b). Properties of Aerosol Particles at 37°C and 1 atm.

Particle Diameter (μm)	Slip Correction Factor	Settling Velocity (cm/s)	Diffusion Coefficient (cm^2/s)	Mechanical Mobility (cm/s dyn)
1.00E-03	2.32E+02	6.70E-07	5.58E-02	1.30E+12
2.00E-03	1.16E+02	1.34E-06	1.40E-02	3.27E+11
5.00E-03	4.69E+01	3.38E-06	2.25E-03	5.27E+10
1.00E-02	2.38E+01	6.85E-06	5.71E-04	1.33E+10
2.00E-02	1.22E+01	1.41E-05	1.46E-04	3.42E+09
5.00E-02	5.27E+00	3.80E-05	2.53E-05	5.92E+08
1.00E-01	3.01E+00	8.69E-05	7.24E-06	1.69E+08
2.00E-01	1.94E+00	2.24E-04	2.33E-06	5.44E+07
5.00E-01	1.35E+00	9.76E-04	6.51E-07	1.52E+07
1.00E-00	1.18E+00	3.39E-03	2.82E-07	6.60E+06
2.00E-00	1.09E+00	1.26E-02	1.31E-07	3.05E+06
5.00E-00	1.04E+00	7.46E-02	4.97E-08	1.16E+06
1.00E+01	1.02E+00	2.93E-01	2.44E-08	5.71E+05
2.00E+01	1.01E+00	1.16E-00	1.21E-08	2.83E+05
5.00E+01	1.00E+00	7.24E-00	4.82E-09	1.13E+05
1.00E+02	1.00E+00	2.89E+01	2.41E-09	5.62E+04

Index

This page is intentionally left blank